

REPUBLIQUE DU CAMEROUN

UNIVERSITE DE YAOUNDE I

FACULTE DES SCIENCES

CENTRE DE RECHERCHE ET DE
FORMATION DOCTORALE EN
SCIENCES TECHNOLOGIE ET
GEOSCIENCES

UNITE DE RECHERCHE ET DE
FORMATION DOCTORALE EN
PHYSIQUES ET APPLICATIONS

B.P 812 Yaoundé

Email : crfd_stg@uy1.uninet.cm



REPUBLIC OF CAMEROON

THE UNIVERSITY OF YAOUNDE I

FACULTY OF SCIENCES

POST GRADUATE SCHOOL OF
SCIENCES, TECHNOLOGY
GEOSCIENCES

DOCTORAL RESEARCH UNIT AND
TRAINING IN PHYSICS AND
APPLICATIONS

B.P 812 Yaoundé

Email : crfd_stg@uy1.uninet.cm

LABORATOIRE DE MECANIQUE, MATERIAUX ET STRUCTURES
LABORATORY OF MECHANICS, MATERIALS AND STRUCTURES

MODULATION INSTABILITY AND LOCALIZED WAVES PATTERNS IN NONLINEAR TRANSMISSION LINE WITH JOSEPHSON JUNCTION

Thesis submitted and defended in partial fulfillment of the requirements for the award of the
degree of Doctor of Philosophy (Ph.D) in Physics
speciality

Fundamental Mechanics and Complex Systems,

by

HAMADOU HALIDOU

Registration number **09W1319**

Master's degree in Physics,

Under the supervision of

BOUETOU BOUETOU Thomas

Professor-UY 1



Thesis defended in front of the following jury:

President: KOFANE Timoléon Crépin, *Professor, University of Yaoundé 1 ;*

Reporter: BOUETOU BOUETOU Thomas, *Professor, University of Yaoundé 1 ;*

Members: NJAKA Jean-Marie Bienvenu, *Professor, University of Yaoundé 1 ;*

TCHOFFO Martin, *Professor, University of Dschang, Cameroon ;*

DJUIDJE KENMOE Germaine, *Professor, University of Yaoundé 1 ;*

KUETCHE KAMGANG Victor, *Associate Professor, University of Yaoundé 1.*

Year 2023



DÉPARTEMENT DE PHYSIQUE
DEPARTMENT OF PHYSICS

ATTESTATION DE CORRECTION DE LA THÈSE DE DOCTORAT/Ph.D

Nous, Professeur **DJUIDJE KENMOE Germaine** et Professeur **KOFANE Timoléon Crépin**, respectivement Examineur et Président du jury de la Thèse de Doctorat/Ph.D de Monsieur **HAMADOU HALIDOU**, Matricule **09W1319**, préparée sous la direction du Professeur **BOUETOU BOUETOU Thomas**, intitulée : « **Modulation instability and localized waves patterns in nonlinear transmission line with josephson junction** », soutenue le **Vendredi, 28 Juillet 2023**, en vue de l'obtention du grade de **Docteur/Ph.D** en Physique, Spécialité **Mécanique Matériaux et Structures**, Option **Mécanique Fondamentale et Systèmes Complexes**, attestons que toutes les corrections demandées par le jury de soutenance ont été effectuées.

En foi de quoi, la présente attestation lui est délivrée pour servir et valoir ce que de droit.

Fait à Yaoundé le... **05 OCT 2023**

Examineur

Pr DJUIDJE KENMOE
Germaine



Le Chef de Département de Physique

Pr NDJAKA Jean-Marie
Bienvenu

Le Président du jury

Pr KOFANE
Timoléon Crépin

Dedication

To my parents :

- **HALIDOU DAOUDA** may their soul remains in peace and **HOUREY HAMAN**.

Acknowledgments

First of all, let us give thanks to **Almighty God** who gave me the strength, patience and wisdom to complete this work.

Writing the acknowledgement page of a thesis is an opportunity to measure what the work accomplished due to others. Beyond the traditional exercise, I would like to underline the accompaniment, the collaborations, the help and the support that I have received.

- I would like to thank **Professor Thomas BOUETOU BOUETOU** of the University of Yaounde 1, who directed this work and with whom I have been working since the master's degree. This achievement was only made possible through his scientific contributions, his advice, his support, his unfailing patience, his total availability and all the actions he accomplished for the realization of this work. I will be eternally grateful to him.
- I would also like to thank **Doctor SOULEYMANOU ABBAGARI** of the University of Maroua, for his implication at all levels in the realization of this work, in particular in the using of formal calculation tools. Indeed, although being in the shadow since my master thesis, he has been my mentor in research.
- I would also like to thank **Doctor Alphonse HOUWE** from the University of Buea, who introduced me to the modeling of transmission lines. He was also like a mentor for me, who permitted a reorientation of my subject.
- Let me now thank my teachers of the Department of Physics of the University of Yaoundé 1, at the head of which **Professor NDJAKA Jean-Marie Bienvenu**, Head of the Department of Physics of the Faculty of Science of the University of Yaoundé 1. For the teachings, advice and encouragement they gave us during this training.

- I would also like to thank the members of the jury for the honor they gave me by accepting to evaluate this work.
President :**Professor Timoléon Crépin KOFANE** of the University of Yaounde;
Reporter :**Professor Thomas BOUETOU BOUETOU** of the University of Yaounde;
Members :**Professor Jean-Marie Bienvenu NDJAKA** of the University of Yaounde;
Professor Martin TCHOFFO of the University of Dschang;
Professor Germaine DJUIDJE KENMOE of the University of Yaounde;
Professor Victor KUETCHE KAMGANG of the University of Yaounde;
- I would like to thank **Doctor Michel NTI MBALLA** and **Doctor GRAM SHOU Jean Paul** for reviewing the French and English version of this work.
- I sincerely thank all my classmates, especially **Doctor KAMGA FOUALENG Arnaud Samuel**, **Doctor NGOUNOU Armel**, **KAMDOUM KUITCHE Alex** for their constant and unconditional help during this work.
- I also thank my elders of the Laboratory of Physics-Mathematics of the **NATIONAL POLYTECHNIC HIGH SCHOOL** for their multiform and very decisive support for this work.
- I thank all my family from near and far including the **family HALIDOU DAOUDA**, **family DAIROU DAWAI**, **family SADOU BABBA LAOUANE**, **Monsieur BOUBA AOUSSINE**, **Monsieur HAMIDOU NOUHOU**, **Monsieur AYOUBA DAMBA** for their moral supports during the development of this dissertation.
- I thank my friends **Bernadette NAMAN SIMO** , **Bastos BAZLNA** and **Robert HAMAN** for their multiform and very decisive support throughout this adventure.
- I can not forget my colleagues of the **GBHS MBANKOMO** for their encouragement.
- I can't forget the members of my didactic laboratory name Interdisciplinary Didactics Laboratory **LARIDI** for their help.
- I can't forget my friends in the ENSPT neighborhood (Vladi Solidarity).

Contents

Dedication	i
Acknowledgments	ii
Abbreviation	vii
Abstract	xv
Résumé	xvi
General Introduction	1
Chapter 1 Literature Review	7
1.1 Introduction	7
1.2 Generalities on Electrical Transmission Line	8
1.2.1 Basic concept on electrical transmission line	8
1.2.2 Modelisation of electrical transmission line	13
1.2.3 Elements of nonlinearity in the electrical transmission line	16
1.2.4 Electromagnetic wave equation of nonlinear electrical transmission line	22
1.3 Localized waves in nonlinear transmission line	33
1.3.1 Solitary waves concept	33
1.3.2 Type of soliton	34
1.3.3 Localized waves patterns solution of nonlinear transmission line model	40
1.4 Applications	42
1.5 Conclusion	43
Chapter 2 Model and Methodology	45

2.1	Introduction	45
2.2	Overview of the two methods of fractionnal derivative	46
2.2.1	The new extended direct algebraic method	46
2.2.2	The new sub-ODE method	51
2.3	Description of model	59
2.3.1	Description of physical model and justification	59
2.3.2	Analytical treatment	60
2.3.3	Linear analysis: Linear dispersion and group velocity	63
2.3.4	2.2.2.3 Nonlinear analysis: NLS equation and soliton solution	65
2.4	Modulation instability	68
2.4.1	Definition	69
2.4.2	Some examples of modulation instability	69
2.4.3	Modulation instability of our system	78
2.5	Conclusion	79
Chapter 3 Results and Discussions		81
3.1	Introduction	81
3.2	Application of the methods	82
3.2.1	On solving the nonlinear differential governing low-pass electrical transmission lines by using the new extended direct algebraic method	83
3.2.2	On solving the nonlinear differential governing low-pass electrical transmission lines by using the new sub-ODE equation	94
3.3	Physical interpretation	97
3.4	Linear stability analysis and rogue waves	98
3.4.1	Modulation instability in the NETL with the Josephson junction	98
3.4.2	Peregrine soliton	103
3.4.3	Super rogues waves soliton	107
3.5	Envelope soliton : Bright and dark	111
3.6	Numerical simulation	113
3.6.1	Localized waves in NETL with JJ	113
3.6.2	Modulated waves patterns in NETL with JJ	115

3.7 Conclusion	116
General Conclusion	120
Appendix	124
3.8 Deduction of the discrete transmission line equation	124
3.9 How the junction works as a SQUID magnetic field sensor	125
Bibliography	128
List of Publications	145

List of Sigles and Abbreviations

- NLSE** : Nonlinear Schrödinger equation
TL : Transmission Line
NETL : Nonlinear Transmission Line
SQUID : Superconducting Quantum Interference Device
RSFQ : Rapid Single Quantum Flux
JTL : Transmission Line with Josephson Junction
RCSJ : Resistively Capacitively Shunted Junction
RLGC : Resistance inductance conductance capacitance
IO : Integer derivative
FO : Fractional derivative
KdV : Korteweg-de Vries
NLSE : Nonlinear Schrödinger Equation
CGLE : Complex Ginzburg Landau Equation
PDE : Partial Differential Equation
CCGL : Complex Coupled Ginzburg Landau Equation
LLG : Landau-Lifshitz-Gilbert
RW : Rogue Wave
SRW : Super Rogue Wave
PS : Peregrine Soliton
SG : Sine Gordon
LHTL : Left-Handed Transmission Line
RHTL : Right-handed Transmission Line
LTC : Lightwave Transmitter Modulator

FFT : Fast Fourier Transform

FFT : Conjugate Complex

DSP : Digital Signal Processing

MI : Modulation Instability

BEC : Bose Einstein Condensate

DNA : Desoxyribo Nucleic Acid

PBD : Peyard-Bishop-Dauxois

HFSC : Heisenberg Ferromagnetic Spin Chain

ODE : Ordinary Differential Equation

MMFES : Mass Excitation and Eddy Current Spectrogram

LC : Inductance-Capacitance

List of Figures

Figure 1	Straight pairs [3]	10
Figure 2	Twisted pairs [3]	11
Figure 3	Coaxial line [3]	12
Figure 4	Parallel plates lines [3]	12
Figure 5	Coplanar lines [3]	12
Figure 6	Transmission line	14
Figure 7	Model of electrical transmission line with loss	15
Figure 8	Model of lossless electrical transmission line	16
Figure 9	Principle of the Josephson effect. [80]	19
Figure 10	RCSJ approach of equivalent circuit for a Josephson junction. [80]	21
Figure 11	Bright soliton	34
Figure 12	Super rogue wave	36
Figure 13	Peregrine soliton	38
Figure 14	Kink soliton shape	38
Figure 15	Dark soliton shape	39
Figure 16	Schematic representation of the nonlinear electrical transmission line with Josephson junction	61
Figure 17	(a) is the plot of the dispersion relation versus wave number and (b) the group velocity versus wave number at $J = 200nA$, $L_1 = 480\mu H$, $C_1 = 1pF$, $C_2 = 2pF$	65
Figure 18	(a) is the plot of the dispersion coefficient and (b) nonlinearity coefficient at $J = 200nA$, $L_1 = 480\mu H$, $C_1 = 1pF$, $C_2 = 2pF$	66

Figure 19 Illustration of the bright ($6.3 \times 10^8 kHz < f < 6.655 \times 10^8 kHz$) and dark ($6.656 \times 10^8 kHz < f < 6.8 \times 10^8 kHz$) formation areas depending on the sign of the product (PQ) versus angular frequency at $J_0 = 200nA$, $L_1 = 480\mu H$, $C_1 = 1pF$, $C_2 = 2pF$ 67

Figure 20 (Color online) Growth rate versus the wavenumber of the perturbation Q for $q = \frac{\pi}{8}$, $\omega_b = 1$, $S = 2.5 \times 10^{-12} eV$, $D = 0.05 eV$ and $b = 0.35 \times 10^{10}$. This has been plotted for three values of the anharmonic stacking coupling constant ρ . Note also that the carrier wave with $q = \frac{\pi}{8}$ and $\rho = 0$ is unstable to perturbation of any wavenumber. 71

Figure 21 (Color online) Growth rate versus the wavenumber of the perturbation Q for $q = 0$, $\omega_b = 1$, $S = 2.5 \times 10^{-12}$, $D = 0.05 eV$ and $b = 0.35 \times 10^{10}$. This has been plotted for three values of the anharmonic stacking coupling constant ρ . Note also that the carrier wave with $q = \frac{\pi}{8}$ and $\rho = 0$ is unstable to perturbation of any wavenumber (blue line). 71

Figure 22 Gain spectra of modulation instability (growth rate) Eq.(2.44) for three values of the nonlinear length with $\gamma = 3$; $P_0 = (0,2; 0,4; 0,5)$; $k_1 = (0,85; 0,5; 0,2)$; $\delta = (0,8; 0,8; 0,9)$; $\mu = (1,7; 0,2; 2)$; $\alpha = (0,8; 2; 1)$: 74

Figure 23 Gain spectra of modulation instability (growth rate) Eq.(2.44) for three values of the nonlinear length with $\gamma = 3$; $P_0 = (10; 15; 20)$; $k_1 = (0,85; 0,5; 0,2)$; $\delta = (0,8; 0,8; 0,9)$; $\mu = (1,7; 0,2; 2)$; $\alpha = (0,8; 2; 1)$: 75

Figure 24 Gain spectra of modulation instability (growth rate) Eq.(55) for three values of the nonlinear length with $\gamma = 3$; $P_0 = (0,2; 0,4; 0,5)$; $k_1 = (0,85; 0,5; 0,2)$; $\delta = (0,8; 0,8; 0,9)$; $\mu = (1,7; 0,2; 2)$; $\alpha = (0,8; 2; 1)$ 77

Figure 25 Gain spectra of modulation instability (growth rate) Eq.(55) for three values of the nonlinear length with $\gamma = 3$; $P_0 = (10; 15; 20)$; $k_1 = (0,85; 0,5; 0,2)$; $\delta = (0,8; 0,8; 0,9)$; $\mu = (1,7; 0,2; 2)$; $\alpha = (0,8; 2; 1)$: 77

Figure 26 Spatiotemporal plot evolution and contour plot of dark solitons $|u_{21}(x, t)|^2$ at $\alpha = 1$, $A_1 = e$, $k_1 = -k_2 = 3.840$, $g_0 = 0.001, g_1 = 0.018$, $\lambda = -0.312$, $\sigma = -0.0185$ 85

Figure 27 Spatiotemporal plot evolution of kink-like solitons $|u_{21}(x, t)|^2$ at $\alpha = 0.75$, $\alpha = 0.85$, $\alpha = 0.95$ and $\alpha = 1$, $A = e$, $k_1 = -k_2 = 25.840$, $g_0 = 0.001, g_1 = -0.18$, $\mu = -0.015$, $\lambda = -0.0312$, $\sigma = -2.000185$ respectively 86

Figure 28 Spatiotemporal plot evolution of 2D of kink-like solitons $|u_{23}(x, t)|^2$ at $\alpha = 0.95$, $A = e$, $k_1 = -k_2 = 20.840$, $g_0 = -0.001, g_1 = 0.18$, $\mu = -0.015$, $\lambda = -0.0312$, $\sigma = -10.000185$ 86

Figure 29 Spatiotemporal plot evolution of the W-shape bright soliton of $|\mathfrak{S}u_{43}(x, t)|^2$ for (a) $[\alpha = 0.52, \alpha = 0.54, \alpha = 0.56]$ (b) $[\alpha = 0.45, \alpha = 0.46, \alpha = 0.47]$ at $A = e$, $k_1 = 10.75$, $k_2 = 2.15$, $u_0 = 0.2$, $g_0 = 3.33$, $g_0 = 0.75$, $p = q = 1$, $\mu = 0$, $\lambda = -0.5$, $\sigma = 0.02$, $p = 0.8$, $q = 0.5$ 88

Figure 30 Contour plot evolution of the W-shape bright soliton of $|\mathfrak{S}u_{43}(x, t)|^2$ for (c) $[\alpha = 0.5, \alpha = 0.47]$ (d) $[\alpha = 0.48, \alpha = 0.49]$ at $A = e$, $k_1 = 10.75$, $k_2 = 2.15$, $u_0 = 0.2$, $g_0 = 3.33$, $g_0 = 0.75$, $p = q = 1$, $\mu = 0$, $\lambda = -0.5$, $\sigma = 0.02$, $p = 0.8$, $q = 0.75$ 89

Figure 31 Spatiotemporal plot evolution of the dark soliton of $|\mathfrak{R}u_{43}(x, t)|^2$ for (T) $[\alpha = 0.45, \alpha = 0.47, \alpha = 0.49]$ (R) $[\alpha = 0.55, \alpha = 0.57, \alpha = 0.59]$ at $A = e$, $k_1 = 10.75$, $k_2 = 2.15$, $u_0 = 0.2$, $g_0 = 3.33$, $g_0 = 0.75$, $p = 0.71$, $q = 0.95$, $\mu = 0$, $\lambda = -0.5$, $\sigma = 0.02$ 89

Figure 32 Plot evolution of $|\mathfrak{S}u_{43}(x, t)|^2$ for $\alpha = 0.48$, $A = e$, $k_1 = 20.75$, $k_2 = 2.15$, $u_0 = 0.2$, $g_0 = 3.33$, $g_0 = 0.75$, $p = 0.71$, $q = 0.95$, $\mu = 0$, $\lambda = -0.5$, $\sigma = 0.02$ 90

Figure 33 Plot evolution of breather corresponding to $|\mathfrak{S}u_{43}(x, t)|^2$ for $\alpha = 0.48$, $A = e$, $k_1 = 25.75$, $k_2 = 18.54$, $u_0 = 0.72$, $g_0 = 3.33$, $g_0 = 0.75$, $p = 0.8$, $q = 0.4$, $\mu = 0$, $\lambda = -0.5$, $\sigma = 0.02$ 90

Figure 34 Plot evolution of of the bright soliton $|\mathfrak{S}u_{43}(x, t)|^2$ for $\alpha = 0.48$, $A = e$, $k_1 = 25.75$, $k_2 = -18.54$, $u_0 = -0.72$, $g_0 = 3.33$, $g_0 = 0.75$, $p = 0.8$, $q = 0.4$, $\mu = 0$, $\lambda = -0.5$, $\sigma = 0.02$ 91

Figure 35 Spatiotemporal Plot evolution of bright $|u_{53}(x, t)|^2$ at $A = e$, $k_1 = -k_2 = 20.40$, $g_0 = -5.001, g_1 = -10.18$, $\lambda = -0.002$ 92

Figure 36 Spatiotemporal plot of dark solitons $|u_{61}(x, t)|^2$ at $\alpha = 0.85, \alpha = 0.90, \alpha = 0.95, \alpha = 1$, respectively and $g_1 = -1.04, A = e, k_1 = -4.84, k_2 = -0.90, u_0 = 5.125, \sigma = -1.185$ 92

Figure 37 Illustration of the ratio bright (Q/P) versus angular frequency with the effect of plasma frequency (m) $\omega_j = 3.044 \times 10^{16} rad.s^{-1}, \omega_j = 3.0442 \times 10^{16} rad.s^{-1}, C_1 = 1pF, C_1 = 2pF$ and (n) the effect of the capacitor at $C_1 = 20pF, J_0 = 200nA, L_1 = 480\mu H$ 99

Figure 38 Illustration of the growth rate of MI in terms of wave number and critical wave number with the effect of plasma frequency (s_1) 3D, (s_2) contour plot and (s_3) 2D plot at $\omega_j = 3.044 \times 10^9 rad.s^{-1}, C_1 = 1pF, C_2 = 400pF$ at $J_0 = 200nA, L_1 = 780\mu H$ 100

Figure 39 Illustration of the growth rate of MI in terms of wave number and critical wave number with the effect of plasma frequency (s_4) contour plot and (s_5) 2D plot at $\omega_j = 3.044 \times 10^8 rad.s^{-1}, C_1 = 0.1pF, C_2 = 20pF$ at $J_0 = 200nA, L_1 = 780\mu H$ 101

Figure 40 Illustration of the growth rate of MI in terms of wave number and critical wave number with the effect of plasma frequency (s_6) 3D and (s_7) contour plot at $\omega_j = 7.6104 \times 10^{15} rad.s^{-1}, C_1 = 40pF, C_2 = 200pF$ at $J_0 = 200nA, L_1 = 780\mu H$ 102

Figure 41 Illustration of the growth rate of MI in terms of wave number and critical wave number with the effect of plasma frequency (s_6) 3D and (s_7) contour plot at $\omega_j = 6.7618 \times 10^3 rad.s^{-1}, C_2 = 2C_1$ (blue line) and $C_1 = 2C_2$ (red line) at $J_0 = 200 nA, L_1 = 480 \mu H$ 103

Figure 42 The comparison of the growth rate of MI under the influence of the capacitors C1 and C2 and fixed value of the critical wave number (s_9)[$\omega_j = 6.06 \times 10^3 rd.s^{-1} rad.s^{-1}$], (s_{10})[$\omega_j = 4 \times 10^3 rd.s^{-1} rad.s^{-1}$], (s_{11})[$\omega_j = 3.20 \times 10^3 rd.s^{-1} rad.s^{-1}$], (s_{12})[$\omega_j = 6.761 \times 10^3 rad.s^{-1}$] at $J_0=200nA, L_1 = 780\mu H$ 104

Figure 43 (S_8) is the 2D plot of the Peregrine rogue wave and (S_9) the 3D spatiotemporal evolution of the Peregrine rogue wave at $C_1 = 2pF$, $C_2 = 470pF$ at $J_0 = 200nA$, $L_1 = 480\mu H$ 105

Figure 44 (s_{10}) is the contour plot of the Peregrine solitons and (s_{11}) the 2D spatiotemporal evolution of the Peregrine rogue wave at $C_1 = 20pF$, $C_2 = 470pF$ at $J_0 = 200nA$, $L_1 = 480\mu H$ 105

Figure 45 Spatiotemporal plot evolution of the Peregrine solitons at $\tau = 0 ms$, $\tau = 5 ms$, $\tau = 10 ms$, $\tau = 15 ms$, $\tau = 20 ms$ for $C_1 = 420 pF$, $C_2 = 480 pF$ at $J_0 = 200 nA$, $L_1 = 480 \mu H$ 106

Figure 46 Spatiotemporal plot evolution of the Peregrine solitons $\tau = 0 ms$, $\tau = 5 ms$, $\tau = 10 ms$, $\tau = 15 ms$, $\tau = 20 ms$ for $C_2 = 2C_1$ (blue line) and $C_1 = 2C_2$ (red line) at $J_0 = 200 nA$, $L_1 = 480 \mu H$ 106

Figure 47 (C_1) Spatiotemporal plot evolution and (C_2) plot 2D of the SRWs at $C_2 = 210C_1$ at $J_0 = 200 nA$, $L_1 = 480 \mu H$ 108

Figure 48 (R_1) Spatiotemporal plot evolution and (R_2) contour plot of the SRWs at $C_1 < C_2$ and $J_0 = 200 nA$, $L_1 = 480 \mu H$ 108

Figure 49 Spatiotemporal plot evolution of the SRWs at (g_1) $\tau = 0 ms$, (g_2) $\tau = 5 ms$, (g_3) $\tau = 10 ms$, (g_4) $\tau = 15 ms$, (g_5) $\tau = 20 ms$ for $C_1 < C_2$ and $J_0 = 200 nA$, $L_1 = 480 \mu H$ 109

Figure 50 (q_1) Spatiotemporal plot evolution of the SRWs (q_2) and contour plot evolution at $C_2 = 18.75C_1$ and $J_0 = 200nA nA$, $L_1 = 480 \mu H$, $\phi_0 = 2.064 \times 10^{-10}$ 109

Figure 51 Spatiotemporal plot evolution of the bright soliton with (t=0) as initial condition at $C_1 = 50pF$, $C_2 = 750pF$, $\omega_j = 0.034$, $\omega = 0.0026$, and $J_0 = 200nA$, $L_1 = 240 \mu H$, $\phi_0 = 2.064 \times 10^{-10}$ 112

Figure 52 Spatiotemporal plot evolution of the dark soliton at $C_1 = 50pF$, $C_2 = 750pF$, $\omega_j = 0.034$, $\omega = 0.0026$, and $J_0 = 200nA$, $L_1 = 240 \mu H$, $\phi_0 = 2.064 \times 10^{-10}$ 112

Figure 53 Localized waves like rogue waves at specific time of propagation with the values of the plasma frequencies (a) $\omega_j = 6,06 \times 10^3 rad/s$; (b) $\omega_j = 3,20 \times 10^3 rad/s$. The other parameter is $J_0 = 200 nA$, $L_1 = 780 \mu H$ 117

Figure 54 Localized modes close to rogue wave (a-b) are respectively the variation of the excitation wave vector k. (a) $k = 0,5$ and $k = 1,4$. The other parameter are $C_1 = 400 pF$, $C_2 = 700 pF$ and $J_0 = 200 nA$ 117

Figure 55 The propagation of the bright soliton at different time for the cell index $n = 150$, given for $C_1 = 400,2 pF$ witch correspond to $\omega_j = 6,06 \times 10^3 rad/s$. and $J_0 = 200 nA$, $L_1 = 240 \mu H$, $\phi_0 = 2.064 \times 10^{-10}$ 118

Figure 56 The propagation of the modulated wave pattern has fulfilled with breather behavior, with the value of the $\omega_j = 3,20 \times 10^3 rad/s$ and varying the wave vector k. For $k = 0,1$, Increasing strong enough the wave vector to $k = 0,5$ and $k = 0,75$ and other parameters $J_0 = 200 nA$, $L_1 = 240 \mu H$ $\phi_0 = 2.064 \times 10^{-10}$ 118

Figure 57 The propagation of dark soliton with $C_1 = 960 pF$, $C_2 = 420 pF$ and $k = 0,75$. When we have increase the wave vector to $k = 1,25$ and it is shown that the dark soliton tends to expand preserves its shape. 119

Figure 58 Schematic representation of the nonlinear electrical transmission line with Josephson junction 125

Abstract

This research work consists in building a nonlinear electrical transmission line model, capable of generating different localized wave envelopes at very high frequencies. From the literature review, it appears that the weakness of the nonlinearity arising from the line components limits the formation of a wide variety of localized wave profiles. Consequently, we believe that the incorporation of Josephson junctions at very low temperatures will increase the non-linearity of the line. This, in turn, will facilitate very high-frequency propagation of the various localized wave patterns. To verify this research hypothesis, we first demonstrated the possibility of formation of different wave patterns using the fractional derivative applied to a simple line. Next, a nonlinear transmission line was realized as an initial model of a parallel Josephson junction network. A discrete equation is deduced from Kirchhoff's laws. By applying the semi-discrete perturbation method to the equation, the dispersion relation, the group velocity and the nonlinear Schrödinger equation of the flux envelope were derived from the model. As results obtained, the propagation of bright and dark solitons for two frequency regimes of the infrared order. What's more, the plasma frequency ω_j behaves like an oscillator in the system, as it decreases, the instability gain decreases while cancelling out the envelope amplitude. As it increases, so does the instability, leading to the formation of localized waves, notably peregrines and super-rogue waves. Numerical simulation of the discrete line equation has enabled us to confirm the propagation in the line of bright and dark solitons, and others localized wave patterns as obtained analytically.

Keywords: Josephson junction, plasma frequency, Schrödinger equation, perturbation method, localized wave, modulation instability.

Résumé

Ce travail de recherche consiste à construire un modèle de ligne de transmission électrique non linéaire, capable de générer différentes enveloppes d'ondes localisées à très haute fréquence. De la revue de littérature, il ressort que la faiblesse de la non linéarité issue des composants de la ligne, limite la formation d'une grande diversité de profils d'ondes localisées. En conséquence, nous pensons que l'incorporation des jonctions Josephson à très basse température augmentera la non-linéarité de la ligne. Ce faisant, il y aura la facilitation de la propagation à très haute fréquence des différents modèles d'ondes localisées. Pour vérifier cette hypothèse de recherche, nous avons d'abord montré à l'aide de la dérivée fractionnaire appliquée à une ligne simple, la possibilité de formation des différents modèles d'ondes. Ensuite nous avons réalisé une ligne de transmission non linéaire en tant que modèle initial d'un réseau de jonction Josephson parallèle. Des lois de Kirchhoff est déduite une équation discrète. En appliquant la méthode de perturbation semi-discrète à l'équation, la relation de dispersion, la vitesse de groupe et l'équation de Schrödinger non linéaire de l'enveloppe du flux ont été dérivées du modèle. Comme résultats obtenus, la propagation des solitons brillants et sombres pour deux régimes de fréquences de l'ordre de l'infrarouge. Bien plus, la fréquence plasma ω_j se comporte comme un oscillateur du système, lorsqu'elle diminue le gain d'instabilité diminue tout en annulant l'amplitude de l'enveloppe. Lorsqu'elle augmente, l'instabilité augmente aussi, ce qui entraîne la formation des ondes localisées, notamment les pérégrines et les super rogue waves. La simulation numérique de l'équation discrète de la ligne nous a permis de confirmer la propagation dans les lignes des soliton bright et dark, et les modèles d'ondes localisées tel que obtenus analytiquement.

Mots clés: Jonction de Josephson, fréquence plasma, équation de Schrödinger, méthode de perturbation, onde localisée, instabilité de modulation.

General Introduction

The generation of superconducting states in materials (metals) has attracted a great deal of interest from physics and mathematics researchers in recent years, following Brian David Josephson's discovery of the Josephson effect in 1962 [1]. The incorporation of the Josephson junction into a conducting metal allows, at very low temperatures, the generation, control and protection of a superconducting state in that metal [2]. Non-linear electrical transmission lines thus offer a real advantage for the study of this phenomenon, both for their importance in data transport and for the ease they offer in terms of modeling.

Indeed, a transmission line is a structure that serves as a support and guide for electromagnetic waves [3]. It can also be defined as a combination of passive components used to transport a signal from a source (or transmitter) to a load (or receiver). As such, transmission lines are used to carry various types of signals (electromagnetic, telephone, digital or analog) between a transmitting source and a receiving load, or vice versa. The distance being transmitted, the bandwidth of the signal and the technology used depend on the type of information. Each line has a specific transport capacity, which depends on the nature of the material it is fabricated from, and the characteristics of the signal to be transported. The physical modeling of the transmission line by the localized element approach has led to the replacement of the physical structure by a series of components made up largely of capacitors, inductors and recently of JJ whose response to current and voltage respectively is highly nonlinear. Since these are nonlinear and dispersive media, modifying the characteristics of these components easily allows the synthesis of different types of nonlinear media [4]. This modeling process follows the theory of transmission lines (TL), which is a well-known theoretical tool for the analysis and design of materials for electromagnetic (EM) applications, including the study of the EM properties of non-linear electrical transmission lines (NETL). Therefore, a NETL model is

identified a number of characteristic constants, including its impedance, its damping constant (which specifies the losses in the line), and the signal travel speed (depending on the material used). As dispersion is standard, since it comes from the structural periodicity between successive cells, a variety of transmission lines have been experimented with different nonlinear elements [5–20]. This succession of numerical and analytical work has given great satisfaction, especially on the dynamics of modulated waves in NETLs. Thus, the analysis of various nonlinear excitations in these low nonlinearity models has allowed the resolution of problems in quantum mechanics, in plasma media, in the control of medical systems, in signal transport and of course in communication support by NETLs [21–25]. Traveling wave solutions are usually obtained by reducing the discrete nonlinear evolution equations into associated ordinary differential equations. Thus, a plethora of nonlinear differential equations have been derived to describe a variety of nonlinear wave phenomena in many areas of physics such as quantum mechanics, plasma physics, fiber optics, metamaterials, condensed matter physics, field theory, fluid dynamics, to name a few [26–35]. The literature at our disposal shows that in electronics, the modeling of phenomena leads mainly to three known nonlinear differential equations such as: the Korteweg-de Vries equation (KdV), the nonlinear Schrödinger equation (NLS) or the complex Ginzburg Landau equation (CGL) with periodically varying dispersion and nonlinearity coefficients [36]. For example, some electrical systems have a potential dependent capacitance with a non integer power law, which has memory or transient effects [37–39]. In the last decades, countless integration patterns have been proposed to construct exact analytical solutions and approximate numerical solutions to the obtained nonlinear differential equations, including the subequation method, the Sinh-Gordon expansion method, the new extended direct algebraic method, the $\exp^{(-\psi(\xi))}$ expansion method, the rational hyperbolic method, the generalized auxiliary equations technique, the generalized Kudryashov method (GK), the fractional and variational iteration algorithm I, the improved variational iteration algorithm II, the efficient method without local mesh, the collocation method without local mesh, a new generalized Jacobi elliptic function method, the extended tanh method, the rational hyperbolic function method, the rational exponential function method, the tanh-coth method, just to name a few [40–43].

However, recent studies have shown that at very high frequencies, new phenomena appear that cannot be taken into account by integer-order nonlinear partial differential equations, as is the case at low frequencies. This situation has led on the one hand to the use of nonlinear differential equations with fractional derivatives to model these nonlinear power lines, in order to obtain solution profiles of the rational type [44]. However, for very high frequencies, this solution seems limited. This is why several researchers have recently developed very high-frequency superconducting power lines using the Josephson junction, in order to reduce ohmic losses and take into account the memory effect thanks to its high non-linearity. In practical terms, the Josephson junction is the basis for the design of the SQUID, a femto-Tesla sensitive magnetometer with numerous applications in medicine, geophysics and biology. In addition, RSFQ logic using the Josephson junction as a building block enables circuit speeds on the order of hundreds of GHz [45], while featuring negligible power consumption and reduced architectural complexity [46]. For this reason, Abdoukary et al. [47] studied envelope solitons in a nonlinear left-handed transmission line with a Josephson junction. They started from a unit circuit model representing a left-hand transmission line to establish the nonlinear Schrödinger equation (NLSE) using the reductive perturbation method. They obtained a nonlinear Schrödinger model that is well known to admit solitary wave solutions. Thus, they realized that depending on whether the PQ product is positive or negative, two frequency regimes form around 10 GHz, where bright and dark solitons form. More recently, Houwe et al [48] have incorporated a high-nonlinearity Josephson junction into a left-hand line so that it supports many types of solitons compared with previous studies. Applying the generalized Riccati method, they obtained, in addition to bright and dark solitons, the kink soliton.

Nevertheless, we believe that previous work has been limited to metamaterials, and the frequencies obtained are below those expected by theory in this field. What about conventional materials? Could we reach frequencies in the infrared range, which corresponds to the vibrational frequency of lattice phonons?

As a general hypothesis of this research, we believe that an electrical transmission line model consisting of a network of parallel Josephson junctions, taking into account parasitic capacitive effects in the line, will facilitate the propagation of different wave profiles localized at frequen-

cies in the infrared range.

From this general hypothesis we formulate the following specific objectives:

- Demonstrate, with the aid of fractional derivatives, the possibility of propagation in nonlinear transmission lines of rational solitons such as brilliant W-form solitons;
- Construct a nonlinear transmission line model based on a compact parallel Josephson junction network capable of taking into account all the effects involved in the detection of a very high-frequency signal;
- Use the reductive perturbation method in the semi-discrete approximation to construct the nonlinear Schrödinger equation (1-NLSE) representing the mathematical model of the line;
- Show analytically the possibility of dark and bright soliton propagation, and other localized waveforms using modulation instability studies;
- Confirm the propagation of the various localized wave profiles above using numerical simulation.

This work is structured around three chapters as follow :

Chapter I is devoted to the literature review and preliminaries of this work. To this end, in the first section we present generalities on nonlinear power lines, including basic concepts, the modeling process, types of nonlinear components and the resulting integer or fractional order differential equations. Then, in the second section, we present the concept of the localized wave, in particular the soliton and its evolution, the types of soliton propagated in power lines and the investigation methods used, the concept of modulation instability, and finally the applications of the various localized wave models. The aim of this approach is to identify the structural and functional limits of existing lines and the models and equation solutions to which they lead, and then to propose a new, more efficient system.

Chapter II is reserved for the presentation of our line model and the method we will use in this study. We first present the two methods of fractionnal order derivative for investigating the soliton solution, namely: the new extended direct algebraic method and the new sub-ODE method. Next, we model our NETL and apply Kirchoff's laws to a unit cell and derive the discrete Sine-Gordon equation that serves as the mathematical model for our line. In addition, because the amplitudes of the wave are sufficiently small, we perform a limited sinusoidal development and a semi-discrete approximation of the initial wave, which we subject to a slight transverse perturbation. By calculating the algebraic equations and cancelling the third-order coefficients, we obtain the nonlinear Schrödinger equation governing the envelope dynamics. This operation will enable us to highlight the essential parameters of the line, such as the dispersion relation, group velocity, dispersion coefficients and nonlinearity. At the end of this operation, we will present some of the modulation instability analysis methods used in different fields of physics, and we will introduce the method we have chosen for our study. This mathematical tool will enable us to establish the zone of wave propagation stability, identify the key parameters of our line's stability and generate other localized wave models. moreover, the Schrödinger equation obtained has already been the subject of several studies and possesses analytical solutions that are already known, including bright and dark solitons, peregrines and super-scure waves. We simply need to associate the dispersion (P) and non-linearity (Q) parameters obtained from the analytical study of the line with these solutions, in order to represent and verify the characteristics of the evolution of these waves in the line. Consequently, in order to verify the validity of our analytical approach and determine the evolution of the system taking into account the instability zone. We carried out numerical simulations using the MATLAB ODE45 solver, setting the number of cells to $N=1001$ for the discrete equation of motion with a given perturbed initial condition.

Chapter III is devoted to results and discussion, and is divided into five sections. In the first section, we study the different types of soliton solutions for the fractional nonlinear differential equation conforming to NETL using, on the one hand, the new extended direct algebraic method and, on the other hand, the new Sub-ODE equation. In Section 2, we

perform a stability analysis of our model, and note that there is indeed a stable and an unstable wave propagation zone. In Section 3, we study the analytical propagation of bright and dark solitons for two cutoff frequency regimes. We represent the soliton at different times and appreciate the evolution and profile of the soliton during its evolution. Section 4 also presents analytical solitons, in particular peregrines and super rogue waves. In Section 5, numerical analysis confirms the propagation of the various modulated wave profiles obtained analytically. What's more, this numerical analysis has enabled us to appreciate the wave profile after a certain time, which is not the case with the analytical method.

Chapter 1

Literature Review

1.1 Introduction

Over the past four decades, the advent of the Internet has led to an exponential increase in telecommunications requirements, including interconnection devices such as : telephone lines, power lines, waveguides for high frequency signals and fiber optics. The increase of the frequency to 60 GHz in the millimeter frequency band, which should allow higher data rates of the order of 5 to 7 Gb/s, was the answer to the growing requirements of broadband telecommunication systems. This increase needs the realization of more integrated and more efficient active or passive circuits. However, if optical fibers are to progressively replace the TL for long-distance and transcontinental telecommunication links, the latter must continue to be used in various fields, including electronic circuits, local communications, and electric power transmission. This is why their study is essential, in order to use them correctly, especially at high frequencies where propagation times become relatively appreciable, but also for new applications of the latter. This requires a perpetual adaptation of electronic systems to a very high integration of components and transmission systems. This is to overcome the problem of the increasing congestion of the allocated bands and the significant increase of the required data rates [49]. After the discovery of Maxwell's equations that made possible the propagation of electromagnetic waves, the scientific world is looking for a long distance and lossless energy transport system based on the exploitation of electromagnetic propagation on a material support. From a structural point of view, several material supports serving as electromagnetic waveguides have been tested.

Among the most used supports, we have bifilar cables, coaxial cables and microstrip cables, each having its advantages and disadvantages. However, all these supports have a common difficulty for very high frequency signals, the losses that are manifested by the degradation of the transported signal or the fires due to the Joule effect. Thus, the soliton as it was discovered by John Scott Russel with amazing properties such as its ability to keep intact its shape and speed during its propagation has interested the community of researchers in electronics, to overcome the previous difficulties related to the losses of the transported electrical energy. In this sense, several studies on the modeling of NETLs have been conducted [6, 50, 51]. In this regard, the mathematical modeling of nonlinear electric transmission lines has led mainly to three types of nonlinear differential equations such as: the Korteweg and De Vries equation, the Ginsburg-Landau equation and the nonlinear Schrodinger equation, representing the dynamics of voltage or potential along a line, in the approximation of the slowly varying envelope [7]. However, recent studies have shown that at very high frequencies, new phenomena appear and cannot be modeled by the nonlinear partial differential equations of integer order. This situation is due to the weakness of the nonlinearity brought by the components of the transmission line. We ask ourselves the question, if the increase of the nonlinearity of the network by a Josephson junction will not allow to propagate the energy without loss at very high frequency? In order to identify the diversity of concepts and theoretical frameworks belonging to various fields and disciplines in this work, a conceptual clarification, a review of methods and solutions in NETLs is necessary to get the most relevant picture of the situation. Thus in this chapter, we will identify the theoretical framework that will allow us to carry out this research, namely: transmission lines, the Josephson junction, the different types of localized waves propagated in NETLs and the modulation instability used.

1.2 Generalities on Electrical Transmission Line

1.2.1 Basic concept on electrical transmission line

1.2.1.1 Line

A line is a geometric shape, considered as extended in length, but of negligible width (thickness). The use here of this mathematical concept refers to the relationship between the dimensions of

the structure studied, in particular the length considered here as infinitely large compared to the thickness of the structure. This generally cylindrical shape is said to be homogeneous when its section is linearly constant.

1.2.1.2 Transmission Line

A transmission line is a structure used to conduct electromagnetic waves [3]. It can also be defined as a combination of conductive components used to carry an signal from a source (or transmitter) to a load (or receiver). A transmission line is identified by its characteristic impedance, its damping constant (which specifies the losses in the line), and the speed of signal traveling (depending on the material used). They are used to transport various signals such as electrical, telephonic, digital or analog, between a transmitting source and a receiving load, or vice versa. Therefore, the distance to be transmitted, the bandwidth of the signals and the technology used depend on the type of information. Each line has a specific transport capacity, which depends on the nature of the material it is made of and the characteristics of the signal to be transported. Moreover, this capacity depends on the structural configuration of the cable. Indeed, these transmission lines known as cables are generally composed of one or more conductive lines, each surrounded by a layer of insulation called dielectric. Thus, we find coaxial cables, bifilar lines (straight pair, twisted pair or shielded pair), coplanar lines or microstrip lines, etc.

1.2.1.3 Electrical Transmission Line

A power transmission line is a device usually consisting of two or more parallel conductors designed to transmit or guide electromagnetic energy from one point to another. Power lines are used in two main areas, covering a wide range of frequencies and powers :

- The transmission of electrical energy for lighting and powering machinery and other devices in general (they use base frequencies up to 50Hz).
- The transmission of information in the form of low power, low voltage electrical signals at frequencies covering a wide spectrum (they use very high frequencies going beyond 10MHz), in the field of communications, electronics, etc.

Below we present the most common transmission line and their specific characteristics.

1.2.1.4 Type of electrical transmission line

Materially and structurally, transmission lines are available in various forms, each of them with

its advantages and inconveniences. Among the most widely used and known we have :

- **The two-wire line**

These are lines with two identical, parallel copper conductors, each covered with a solid dielectric and both held in close proximity by insulating separators. An example is the ordinary electrical cable used as an extension cord in the home. However, these bi-filar cables are being used less and less for energy transmission, although they are inexpensive but have limited losses. At high frequencies, a two-wire line with small diameter conductors $2a$ in front of their separation $2d$. Around each conductor, the electric field is practically radial, and the current penetration practically uniform around the circumference. The linear resistance of the line increases as the square root of the frequency of the propagating wave. At very low frequencies, the resistance reduces to that of direct current. The consequence of these different effects is the overall increase in losses due to wire resistance and dielectric losses. There are several types of two-wire lines:

Straight pairs: This kind cable uses two parallel conductors separated by a layer that maintains a gap between them. Compared to other two-wire lines, this cable has the following disadvantage : high losses, low bandwidth and high sensitivity to noise.



Figure 1: Straight pairs [3]

Twisted pairs: In this type of cable, the two wires are twisted together and are also separated by a layer that maintains the spacing between them. It has a characteristic impedance of 600 Ohms [54], and is used to carry telephone, digital or analog signals. This two-wire cable is widely used in the telecommunications and computer industries and has the advantage over other cables of being less sensitive to noise.

Shielded Twisted Pairs: In this type of two-wire cable, the two wires are twisted and are also separated by a layer that provides spacing between the two, with the exception that it is



Figure 2: Twisted pairs [3]

surrounded by a conductive foil which serves as noise immunization contrary to two-wire cable. It is used in the computing industry as a 10 and 100 Mbps network cable.

- **Coaxial line:**

The coaxial line, also called coaxial cable, is the most common transmission line. Because it can carry different frequencies up to 3 GHz. Structurally, coaxial cable consists of two metallic conductors: an axial cylindrical conductor, and a peripheral cylindrical conductor used to block internal losses and stray radiation from the line. Figure 3 shows the structure of a coaxial line. The center conductor is shown here as braided strands, but is often a solid wire. The dielectric is usually solid polyethylene, but sometimes it is a polyethylene wire wrapped around the center conductor with a large helix pitch, or a polyethylene foam to achieve lower permittivity (lower linear capacitance) and higher propagation speed. The shield is made of fine braided wire, but aluminum foil wrapped around the dielectric is often used. The envelope or sheath is also made of various materials that are more or less resistant to environmental conditions, polyethylene, polyvinyl chloride, etc. In this respect, the losses depend strongly on the quality of the dielectric used. The bandwidth is important. At high frequencies, the current flows over the surface of the facing conductors, and the linear resistance increases as the square root of the frequency. The use of coaxial cable extends to any application where a signal must undergo a minimum of distortion and attenuation, or where the elimination of external interference is paramount. Coaxial cables are used in the following areas: Telecommunication, aerospace, radio/television, computer etc.

For example, for a coaxial line with a central conductor of radius $a = 2mm$ and a screen of internal radius $b = 6mm$ spaced by a solid dielectric of relative permittivity equal to 2,2. When the losses are negligible, we evaluate its characteristic impedance at $Z_o = 44,4ohms$ and the propagation speed of a signal in this cable at $u = 2,02.10^8m/s$.

- **Printed line**



Figure 3: Coaxial line [3]

Parallel plates : Parallel plates lines are rarely used in practice, but they can be used to simplify the analysis of more complex waveguides. The figure below gives an example.

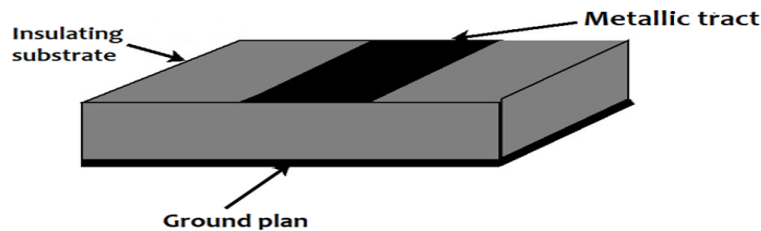


Figure 4: Parallel plates lines [3]

Coplanar lines : The coplanar line is a waveguide often used in integrated circuits. It is similar to the microstrip line [54], except that the grounds are placed on each side of the conductor, as in figure 5. In the high frequency range, above a few 100 MHz, special lines are used on circuits to connect "chips" or components together. They are cheap because they use printed circuit technology. The different existing geometries are presented in the following. The electrical characteristics of the lines depend on the dimensions of the metallizations and the characteristics of the materials used (metals and dielectrics).

- It has no loss at any frequency ;

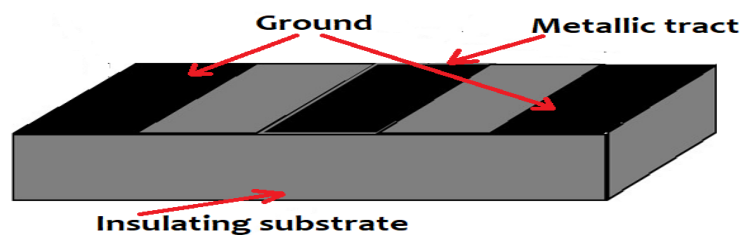


Figure 5: Coplanar lines [3]

- It resists high voltage overloads.
- It has stable characteristics (characteristic impedance, damping constant and speed of signal traveling);
- It is compatible in terms of size with the standard chords we have in stock.

All these phenomena must be modeled for their eventual mathematical analysis and control.

1.2.2 Modelisation of electrical transmission line

There are two approaches to modeling a transmission line, modeling by Maxwell's equations (where the structure of the transmission line depends on the characteristics and dimensions of the dielectric substrate, as well as the propagation of the electromagnetic field in this substrate), or modeling by localized elements (where the transmission line is represented by electrical components, such as capacitors, inductors, and resistors where appropriate). In this study, we use the electrical circuit or localized element approach. Like the theory of electrical circuits from which it is derived, the theory of transmission lines adopts the same vocabulary and the same notation convention. As such, the modeling of a transmission line is not totally different from the modeling of a simple circuit, it is a serial duplication of this circuit. The simple circuit or unit cell represents a small section dx of the line, while the serial duplication of the cell represents the entire line. The choice of this section is dictated by the order of magnitude of the wavelength of the input signal which is the voltage. Thus, for very high frequencies the wavelength or the section must be very small, because the wavelength is inversely proportional to the frequency. It is therefore necessary to choose a section less than or equal to the wavelength of the signal. From a physical point of view, this choice is justified by the need to control the behavior of the line parameters, because some physical phenomena whose effects could be neglected at low frequency, can not be at high frequency. Thus, the modeling of transmission lines for high frequency signals uses very small cross-sections modeled by parameters familiar from circuit analysis such as line resistance, line inductance and line capacitance. Moreover, for high frequencies these terms are more dependent on Maxwell's equations, including the use of electric and magnetic fields.

1.2.2.1 Modeling an electrical transmission line with loss

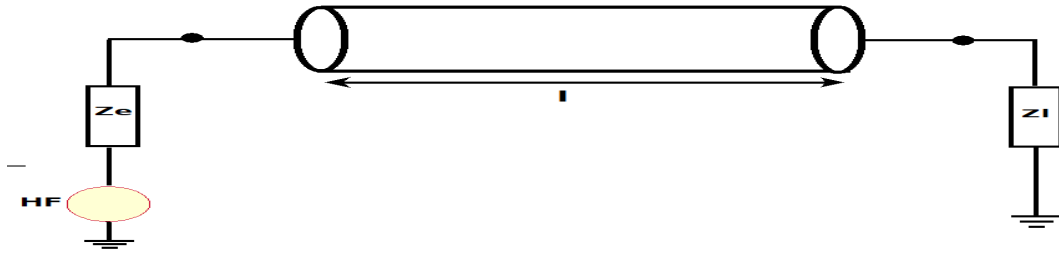


Figure 6: Transmission line

Modeling a lossy transmission line means representing it by the essential elements, which correspond to its response to the input current or voltage, in the form of propagation constants. It is said to be lossy when it takes into account all the energy losses by Joule effect during the propagation of the voltage. Indeed, starting from the fact that the speed of propagation of the electric voltage is not instantaneous in the line, but depends on the characteristics of the material used. A specific study of the evolution of the intensity and the voltage in the line was carried out. Thus, by considering the source as the spatial and temporal origin and each point of the line L , corresponds to a couple of magnitude of voltage and intensity (V, I) . This allowed us to see that these two quantities are functions of the position x and time t : $V(x, t)$ and $I(x, t)$. By choosing a section dx of the line such that v and $v+dv$ are the voltages at the input and output of the element, and i and $i+di$ are the corresponding currents. It can be seen that, for each section dx of the line, the following effects must be taken into account, as soon as we are in the variable voltage regime :

- **resistive effect** of each of the two conductors, because the conductors are not perfect (non-zero resistivity) and the skin effect must be taken into account (decreasing current density as the conductor is inserted). This effect results in a Joule effect, corresponding to an energy consumption, which can be represented by an electrical resistance of value Rdx ;
- **conductive effect of the insulator** which separates the two conductors, because the insulator is not perfect (non-zero conductivity) and thus also causes a consumption of energy by Joule effect, which one can model by an electric conductance of value Gdx ;
- **inductive effect** translating the self-induction effect of the conductive segment on itself, tending to slow down the current variations (Lenz's law), this effect is represented by an induc-

tance of value Ldx ;

- **capacitive effect** highlighted by the system composed of the two conductors separated by the insulator, translating the mutual dependence of the variation of charge on each of the two conductors tending to slow down the variations of voltage. This effect is represented by a capacitor of value Cdx , hence the following local model (see figure 7).

These quantities R , L , C and G are called the primary constants of the line. The orders of magnitude of L and C are however variable depending on the geometry of the line. However, the current values are, for L between 50 and 500 nH/m, for C between 20 and 100 pF/m.

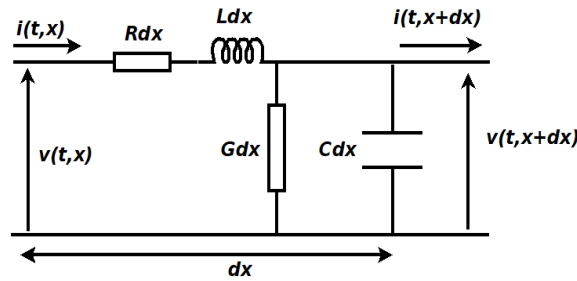


Figure 7: Model of electrical transmission line with loss

1.2.2.2 Modeling a lossless electrical transmission line

Still called ideal line, the transmission lines without losses are lines for which the losses by Joule effect are negligible. This type of line will be modeled as the previous line but considering the zero resistive effects ($R=0$) and the zero conductive effects of the insulator ($G=0$). So here we have to find a type of material (metal) with zero resistance and an insulator with infinite resistance. In reality, such a type of material does not exist at room temperature, and even less so an insulator of infinite resistance, which at high frequency always becomes a conductor (see Figure 8).

NB: The above line is also called the conventional line or straight hand line. However, when we swap the position of the capacitor with that of the inductor, and duplicate to n -order, we obtain a line called the left-hand transmission line, which models a material called the metamaterial. The concept of metamaterials was mentioned for the first time in the field of optics in 1968, by the Russian physicist Victor Veselago [56]. Several other forms of modeling are given in the literature depending on the effects that we want to take into account and the form of the signal

that we want to obtain.

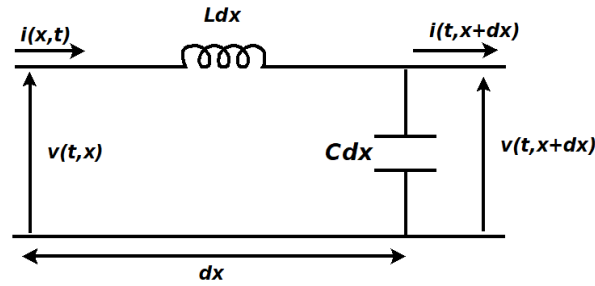


Figure 8: Model of lossless electrical transmission line

1.2.3 Elements of nonlinearity in the electrical transmission line

Electrical transmission lines are said to be nonlinear if they contain in their models nonlinear electrical components, such as the capacitor, the coil, the nonlinear resistor or a Josephson junction. We already know that, in a transmission line, the dispersion comes from the structural periodicity between the successive meshes. The combination of nonlinearity and dispersion in the line leads to nonlinear differential equations responsible for the phenomenon of voltage propagation in the form of a progressive wave of soliton type. This non-linearity is concretely manifested in the line by the variation of the primary parameters of the line according to the frequency of the voltage at the terminals of the line, such as: capacitor, chokes, Josephson junction, and in some cases the resistance. The most commonly used nonlinear component is the capacitor with capacity that varies with the applied voltage. Thus, depending on the environment that we want to model, we will choose the appropriate nonlinear component(s), which we will place on the branches in series or in parallel. In recent years, the Josephson junction has been sufficiently solicited for its strong nonlinearity. The first non-linear transmission line was realized by Hirota and Suzuki, with a variable capacitance depending on the voltage. In the rest of this work, we have chosen two non-linear components which are the capacitor and the Josephson junction that we will explain below.

1.2.3.1 Nonlinear capacitor

When the nonlinear element is a capacitor, which means that it has a capacitance that varies with the voltage applied across it. This is a variable capacitor, most commonly used for radio

tuning, which allows the amount of electrical charge it can hold to change over a certain range, measured in a unit called farads. Nonlinear capacitors come in the form of reverse biased varactor diodes (variable capacitance diode), more commonly known as varicap, is a semiconductor electronic device very closely related to a standard diode but with certain capacitances similar to a capacitor. The varactor diode is used in place of a variable capacitor which is a more expensive and difficult device to install. On the other hand, due to the shortcomings presented by nonlinear chokes and resistors, most of the work on nonlinear power lines is conducted by considering capacitors as nonlinear elements, but with different types of nonlinearity relationship between voltage and capacitance [57]. In this study, the nonlinear capacitor in this network is a varicap diode that admits that the capacitance varies with the applied voltage.

1.2.3.2 Nonlinear Josephson junction

- **The Josephson effects and applications**

The Josephson effect is the passage of paired electrons called Cooper pair through a thin insulating dielectric barrier placed between two superconductors. This pair of electrons crosses the insulating layer by tunneling effect [58], without any resistance from the metal. This is one of the remarkable effects of superconductivity, called a macroscopic quantum phenomenon that appears at very low temperatures in some metals. As a consequence, there is no voltage drop as long as the current remains below a specific level, called critical current. Indeed, the voltage positive initial constant of disturbance of electrons maintained indefinitely. All of these effects were predicted by Brian D. Josephson in the early 1960s. This effect can be controlled by applying a magnetic field which reduces the intensity of a supercurrent through the barrier. Indeed, magnetic fields cannot penetrate inside the Josephson junction through fractional vortices. Thus, the current strength increases and decreases at different locations as the magnetic field strength changes, allowing for controlled signal flow and switching. Furthermore, when superconductors are exposed to a direct current, electron pairs pass through the barrier releasing electromagnetic waves, resulting in the production of small amounts of light instead of heat.

In recent years, transporting a signal without losing the initial quality has always been the major concern of mankind in many fields such as telecommunications, electronics and many others. Thus, since the discovery of the Josephson effect, many researchers have invested to

develop new technologies that will be able to transport signals while limiting losses. On a practical level, the realization of passive circuits is much more important than that required for active elements. The Josephson effect can also be applied to radio electronics used in extreme cold conditions, as a Josephson junction can function as a sensor of electromagnetic oscillations. Moreover, the study of the JJ is very topical in the technological race in order to determine the successor to silicon. Indeed, carbon nanotubes, spintronics, optronics, all tracks are beaten in this technological hunt to determine the most efficient and cost-effective solution for tomorrow. Because that circuits based on this junction can also store data and can be manufactured in small spaces thanks to their efficiency, so their use in computers is possible. RSFQ (Rapid Single Flux Quantum) logic, which uses the Josephson junction as a building block, allows circuit speeds of the order of hundreds of GHz to be achieved, while maintaining negligible power consumption and reduced complexity of architectures [15]. The Josephson effect occurs at very low temperatures and is most effective at temperatures near zero degrees Kelvin (about $-460^{\circ}F$).

- **Importance of the Josephon Junction in a circuit**

A Josephson junction is a voltage-controlled oscillator capable to generate very high frequencies, up to the bandgap frequency of the superconductor (typically up to 1000 GHz). This by introducing a relationship that links classical mechanics to quantum mechanics, in particular between frequency and voltage $V = \frac{\hbar}{2e}\omega_j$, where \hbar is Planck's constant, ω_j is the Josephson angular frequency and e is the charge of electrons. Systems using this effect can be connected to measure very low magnetic fields, down to the femto tesla. The Josephson junction, thanks to its high sensitivity and its ability to operate even at zero voltage, has revolutionized metrology. Instruments incorporating Josephson junctions use the Josephson effect to make precise dimensional measurements, amplify electromagnetic signals, and drive fast computers. For example, the Josephson junction is a key component of SQUIDs (Superconductive Quantum Interferometer Device), which is a magnetometer with a sensitivity in the femto tesla range. This tool has important applications in the fields of geophysics, biology and medicine R59, R60. They can also excite low power levels in generators that can be designed to be switched over multiple frequencies. A JJ switches signals faster than any other solid-state switch. Such a system can

operate at DC or microwave frequencies. Superconductors can therefore be used at very good temperature with JJ.

- **The Josephson junction model**

In order to model a Josephson junction, we present the approach that led to the modeling of the Josephson effect. Let us observe the diagram below which presents the principle of the Josephson effect. Let φ be the phase difference between superconductors 1 and 2, which generates the Cooper pair current I_s crossing the insulating barrier by tunneling effect. Let us suppose that a non dissipative current can flow between the two superconducting electrodes. This so-called Josephson current results from the coherent transfer of Cooper pairs between the two superconductors, due to the existence of a phase difference $\varphi = \varphi_2 - \varphi_1$ between the two superconductors. The charge carriers in a metal superconductor with Josephson junction are quantum objects described by a complex wave function (we neglect here the interactions between carriers and the spin effects).

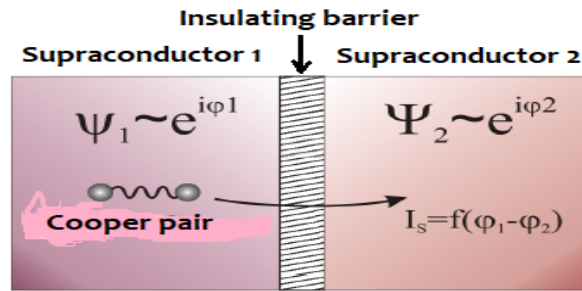


Figure 9: Principle of the Josephson effect. [80]

$$\Psi = |\Psi| \exp(i\varphi) \quad (1.1)$$

Where:

- $|\Psi|^2$ is the particle density
- Ψ is the wave function
- φ Represents the phase of the wave which is itself a function of space and time (r ; t).

Josephson showed that a supercurrent I_s can cross the insulating barrier even at zero voltage ; this current is a function of the phase difference $\varphi = \varphi_2 - \varphi_1$ between the wave functions of the two superconductors between the wave functions of the two superconductors:

$$I_s = I_c \sin \varphi \quad (1.2)$$

Where I_c is the critical current corresponding to the maximum non-dissipative current that the superconducting tunnel junction can withstand before it transitions to the normal state. This current depends significantly on the geometrical factors of the barrier, the material properties, and the operating temperature.

So far, we have only considered simple circuits that can be described by localized passive circuit elements. We will now deal with high-frequency coupling schemes that are better characterized by distributed circuit elements, i.e., microwave transmission lines and cavity resonators. When we consider the previous circuit as the SQUID (Superconducting QUantum Interference Device) elementary brick of the RSFQ logic. It has the property of having several stable states of operation which allow to realize a memory effect. There are several possible configurations of SQUID; we study here the one constituted by two Josephson junctions in a superconducting loop. This is called a "dc SQUID", because the junctions can be biased with a direct current and the following phase difference [61]:

$$\varphi = \varphi_2 - \varphi_1 = 2\pi \frac{\phi_n}{\phi_0} \quad (1.3)$$

with $\phi_n = n \frac{\hbar}{2e} = n\phi_0$.

In RSFQ logic the information about the flux state is transmitted from one superconducting loop to the other, using the fact that a phase change of 2π on a junction corresponds to the passage of a flux quantum through the junction itself [59]. The JTL (Josephson Transmission Line), based on this principle, allows the transmission of flux quanta through the RSFQ circuit with practically no attenuation of the signal; if Josephson junctions with progressively larger critical currents are used, it is even possible to amplify the output signal.

The quasi-particle transport and the capacitance between the electrodes are treated as finite elements in parallel to the ideal junction, through which only a current of Cooper pairs flows. The voltage at the terminals of the circuit follows the second relation demonstrated by Josephson,

which links the phase difference $\Delta\varphi$ to the electrodynamic properties of the junction :

$$\frac{d\varphi}{dt} = \frac{2eV}{\hbar} \quad (1.4)$$

This relation does not take into account any approximation, and considers only fundamental physical quantities. It is always valid, except in particular cases in which the equilibrium of the stationary state of the electrodes is broken by parasitic currents, for example in the vicinity of normal currents or in the presence of a heat flux [59]. The Josephson effect can be classified into two different regimes depending on whether φ is constant or varies with time $\Delta\varphi(t)$. In the second case which concerns us, where φ varies with time, we speak rather of an alternating Josephson effect. The term Josephson current I_c which passes between the electrodes is not sufficient to describe the behavior of the junction in variable regime. The model of the Josephson junction proposed by the RCSJ approach is a relatively simple equivalent circuit that uses finite elements. The following figure shows this equivalent circuit for the case where the junction is current biased.

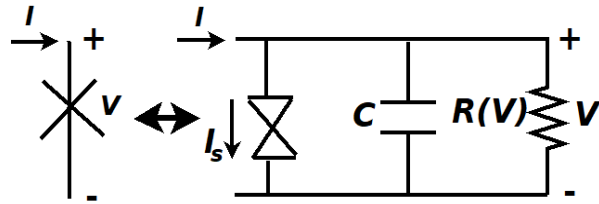


Figure 10: RCSJ approach of equivalent circuit for a Josephson junction. [80]

Using the superconducting RCSJ model, the quasiparticle transport I_N and the interelectrode capacitance I_C , are treated as finite elements in parallel to the ideal junction, through which a current of Cooper pairs of Cooper pairs I_s . The voltage across the junction obeys the law of equation 1.4.

Applying Kirchhoff's law in the circuit of Figure 10, we obtain :

$$\begin{aligned} I &= I_s + I_N + I_C = I_c \sin \varphi + \frac{V}{R_N} + C \frac{dV}{dt} \\ &= I_c \sin \varphi + \frac{1}{R_N} \frac{\hbar}{2e} \frac{d\varphi}{dt} + C \frac{\hbar}{2e} \frac{d^2\varphi}{dt^2} \end{aligned} \quad (1.5)$$

Here R_N is the resistance in the junction that the normal electrons see (the quasiparticle resistance). This is the so-called RCSJ model (the resistively shunted junction model). This

simple model has turned out to be adequate in predicting the principal behavior of Josephson junctions. It is very useful for the design of superconducting electronics. However in the framework of our study, we will consider, the electrical transport is dominated just by Cooper pairs, and the quasiparticles (electron) present activated by thermal fluctuations are negligible. The normal resistivity R_N is therefore very large and tends to infinity in this regime. The field of investigation of superconductors is extremely vast given the complexity of this type of material. They represent a certain economic and strategic stake on an international scale. And this, in view of its multiple applications. Superconductors are generated and controlled by Josephson junctions, which are themselves integrated into transmission lines.

1.2.4 Electromagnetic wave equation of nonlinear electrical transmission line

1.5.1.1 Telegrapher's equation [62]

The telegrapher's equations are a system of two partial linear differential equations that describe the evolution of voltage and current on a power line as a function of distance and time. Oliver Heaviside developed the power line model that leads to these equations in the 1880s. It applies to any power line, regardless of frequency, and covers transmission and reflection phenomena on a transmission line, whether it is used for telegraph, telephone, or any other purpose, as well as on power grid distribution lines.

An element of length dx of a two-conductor line can be assimilated to a quadrupole made up of elements derived from the parameters R , L , C and G . Let us consider the simplified representation of the lossy line (figure 7), which allows us to simplify the derivation of the propagation equations. Let us now apply the laws of electrical networks to this section. By applying the mesh law to the cell of rank n :

$$dv(x, t) - Ri(x, t)dx - L\frac{\partial i(x, t)}{\partial t}dx = 0 \quad (1.6)$$

$$di(x, t) - Gv(x, t)dx - C\frac{\partial v(x, t)}{\partial t}dx \quad (1.7)$$

Dividing both members by dx, we get the following two equations:

$$\frac{\partial v(x, t)}{\partial x} = Ri(x, t) + L \frac{\partial i(x, t)}{\partial t} \quad (1.8)$$

$$\frac{\partial i(x, t)}{\partial x} = Gv(x, t) + C \frac{\partial v(x, t)}{\partial t} \quad (1.9)$$

We obtain a system of two linear partial differential equations whose solutions are the current $i(x, t)$ and the voltage $v(x, t)$ which crosses the line at all points and at all times. By deriving the two members of the first one with respect to x , we have :

$$\frac{\partial^2 v(x, t)}{\partial x^2} = -R \frac{\partial i(x, t)}{\partial t} - L \frac{\partial}{\partial t} \left(\frac{\partial i(x, t)}{\partial x} \right) \quad (1.10)$$

Let us now carry equation (1.10) in the latter and group the terms. We obtain the following linear differential equation still called equation of the telegraphers :

$$\frac{\partial^2 v(x, t)}{\partial x^2} = LC \frac{\partial^2 v(x, t)}{\partial t^2} + (LC + RG) \frac{\partial v(x, t)}{\partial t} + RGv(x, t) \quad (1.11)$$

In the same way, we would obtain for the current :

$$\frac{\partial^2 i(x, t)}{\partial x^2} = LC \frac{\partial^2 i(x, t)}{\partial t^2} + (LC + RG) \frac{di(x, t)}{dt} + RGi(x, t) \quad (1.12)$$

These are two linear differential equations of the second order with partial derivatives, are wave equations. We will now examine the special case of lines where the linear resistance and conductance can be considered negligible. These are called lossless lines. In this case R and G are zero, the previous equations become :

$$\frac{\partial^2 v(x, t)}{\partial x^2} = LC \frac{\partial^2 v(x, t)}{\partial t^2} \quad (1.13)$$

$$\frac{\partial^2 i(x, t)}{\partial x^2} = LC \frac{\partial^2 i(x, t)}{\partial t^2} \quad (1.14)$$

If we assume that the propagation regime is sinusoidal, equations (1.13) and (1.14) become :

$$\frac{\partial^2 v(x, t)}{\partial^2 x} = (R + jLw)(G + jCw)v(x, t) = 0 \quad (1.15)$$

$$\frac{\partial^2 i(x, t)}{\partial^2 x} = (R + jLw)(G + jCw)i(x, t) = 0 \quad (1.16)$$

we pose the following constant :

$$\gamma = \sqrt{(R + jLw)(G + jCw)} \quad (1.17)$$

Where γ is the propagation constant of the line (complex quantity), which can be put in the form: $\gamma = \alpha + j\beta$

α , the real part, is an attenuation parameter expressed in (Np/m). This coefficient is a function of several parameters: losses in the conductor losses in the dielectric substrate, and radiation losses. The imaginary part is a phase parameter expressed in (rad/m). We obtain by identification from equation (1.15) the following expressions of α and β :

$$\alpha = \sqrt{\frac{1}{2}(R^2 + L^2\omega^2)(G^2 + C^2\omega^2) + (LG - RC\omega^2)} \quad (1.18)$$

$$\beta = \sqrt{\frac{1}{2}(R^2 + L^2\omega^2)(G^2 + C^2\omega^2) - (LG - RC\omega^2)} \quad (1.19)$$

Equations (1.15) and (1.16) admit solutions of the form :

$$v(z) = V_i \exp(-\gamma z) + V_r \exp(\gamma z) \quad (1.20)$$

$$i(z) = I_i \exp(-\gamma z) + I_r \exp(\gamma z) \quad (1.21)$$

Where V_i , I_i , V_r and I_r are integration constants, the ratio of impedance constants gives the following constant which is homogeneous to an impedance :

$$\frac{V_i}{I_i} = -\frac{V_r}{I_r} = \sqrt{\frac{R + jL\omega}{G + jC\omega}} \quad (1.22)$$

This constant determined by the ratio $\frac{V_i}{I_i}$ is called the characteristic impedance Z_c of the line :

$$Z_c = \sqrt{\frac{R + jL\omega}{G + jC\omega}} \quad (1.23)$$

NB: generally for the cable of televisor it is 50 ohm or 75 ohm.

For lossless lines we have: $R = G = 0$, $\alpha = 0$, $\gamma = j\beta = j\omega\sqrt{LC}$. The characteristic impedance in these conditions is real, their value is given by :

$$Z_c = \sqrt{\frac{L}{C}} \quad (1.24)$$

We have $\beta = \omega\sqrt{\mu\varepsilon}$, so: $LC = \mu\varepsilon$ Where μ and ε are respectively the effective permeability and the effective permittivity of the materials. The propagation velocity for a lossless line is given by the relation :

$$u = \frac{1}{\sqrt{LC}} \quad (1.25)$$

At relatively high frequencies, the phase velocity tends to a limit essentially determined by the distributed capacitance and inductance, independent of losses.

1.5.1.2 Partial differential equation for nonlinear transmission line

A nonlinear electric transmission line (NETL) is a system of repeating inductors, capacitors, or Josephson junctions, where the inductors, capacitors, junctions, or all three are nonlinear in their response to current and voltage, respectively. In reality, many components used in power lines are nonlinear components, so the primary parameters R , L , and C are not necessarily all constant. For this reason, NETLs are very convenient tools for modeling nonlinear dispersive media and even for modeling exotic properties of new systems. The mathematical model of nonlinear electrical transmission lines automatically leads to nonlinear partial differential equations (PDE). Generally, researchers usually transform the equation governing the dynamics of waves in nonlinear electrical lines to a well-known nonlinear differential equation. The literature at our disposal shows that the corresponding mathematical models often obtained are the Korteweg-de Vries equation (KdV), the NLS equation or the complex Ginzburg-Landau equation (CGL) with periodically varying dispersion and nonlinear coefficients [36]. Indeed, the NETL is one of the most popular physical models in electronics, and is governed by classical integer and fractional order PDEs. Thus, when we take into account the nonlinear components of the line, which can be either the capacitor, the coil or the Josephson junction, we obtain, after applying the mesh law, a system of N coupled nonlinear differential equations that cannot be solved without using approximations. However, by using the continuous medium approximation, and a multiscale perturbation, these equations reduce to a nonlinear differential equation. The first equation thus obtained was obtained by a fourth-order approximation which led to the modified Boussinesq nonlinear differential equation [63]. This is very similar to the one obtained by Boussinesq in 1895 for shallow water hydrodynamic waves, although there is an important difference which lies in the nonlinear term which involves here a temporal and not a spatial derivative. Although this modified Boussinesq equation is not fully integrable, it describes the properties of the electric chain well and has the potential to be easily manipulated experimentally on a power line. Nevertheless, this equation is much less easy to use than the KdV equation, because there are far fewer mathematical tools available. Thus, additional approximations were used to move from the modified Boussinesq equation to the KdV equation. The error in switching from a

KdV-type description is of the order of magnitude of the experimental error when measuring electrical chains, but the gain is significant because we have the important mathematical tools that KdV theory provides. Furthermore, Scott [63] has shown that the KdV equation describes weakly nonlinear waves in a nonlinear LC transmission line containing a finite number of cells, which consist of a linear inductance in the series branch and a nonlinear capacitor in the shunt branch. If the nonlinearity is shifted from the capacitor parallel to the shunt branch of the line to a capacitor parallel to the series branch, the NLS equation is obtained instead [64, 65].

It has been proved by many physics researchers that the best governing mathematical model capable of describing the electrical propagation in NETLs reduces to different types of NLS equations or to a pair of coupled nonlinear Ginzburg-Landau Schrödinger equations [25, 66]. Indeed, using the reductive perturbation approach in the semi-discrete approximation, several authors have shown that the modulated wave dynamics in NLTLs can be described, with a good approximation, by the well-known NLS equations [67, 68]. A few years ago, we presented a model for wave propagation on a discrete NLTL based on the NLS equation complex expansion on the governing nonlinear equations [69]. In our recent work on NLTLs, we have shown that the modulated lattice wave dynamics can be governed either by an NLS equation with a linear external potential or by a generalized Chen-Lee-Liu equation [70], which appears as a cubic NLS equation with an additional cubic derivative term. Kengne et al [71] modeled an RLC transmission line with variable capacitance capacitor by the complex coupled Ginzburg Landau equations (CCGL). Kuek et al [10] modeled a cascaded LC section chain consisting of nonlinear inductors in series and linear capacitors in parallel using a simplified form of the Landau-Lifshitz-Gilbert (LLG) equation.

1.5.1.3 Fractional order derivative in non-linear transmission line

- **Historical context of the introduction of the fractional derivative**

The history of the theory of fractional derivation goes back to the end of the 17th century. All scholars agree to place its beginning at the end of 1695, when Hospital asked Leibniz a question about the meaning of $\frac{d^n y}{dx^n}$ when $n = \frac{1}{2}$ [72]. Indeed, in his prophetic answer, Leibniz predicted a possible non-integer derivation theory, stating that: "this would lead to a paradox from which useful consequences will be drawn one day". Euler (1730) was the first to attempt

to theorize this problem when he studied the simple case of fractional integrals of monomials of arbitrary real order in the heuristic mode of the time. Subsequently, Fourier (1822) [73] proposed an integral representation to define the derivative, and his version can be considered the first definition of the derivative of arbitrary (positive) order. Abel (1826) solved an integral equation associated with the tautochron problem, which is considered the first application of the fractional derivative. But the first real serious attempt to give a logical definition of the fractional derivative is due to Liouville who published nine papers on this subject between 1832 and 1837. In 1832 [74] he proposed a definition based on the differentiation formula for the exponential function, and the other formula is presented in terms of an integral and is now called Liouville's version for non-integer order integration. However, the most important paper was published by Riemann [75], ten years after Liouville. Furthermore, Grűnwald [76] and Letnikov [77], independently, developed an approach to non-integer order derivatives in terms of a convenient convergent series, in contrast to the Riemann-Liouville approach, which is given by an integral. Letnikov showed that his definition coincides with the versions formulated by Liouville, for particular values of the order, and by Riemann, under a convenient interpretation of the so-called non-integer order difference. Hadamard (1892) [73] published a paper where the non-integer order derivative of an analytic function must be done in terms of its Taylor series. A few years later, the fractional derivative underwent a dazzling development, in the formulation of certain problems considered as complex. For this purpose, other definitions appeared. Weyl [78] introduced a derivative in order to get around a problem involving a particular class of functions, the periodic functions. Riesz [79,80] proved the mean value theorem for fractional integrals and introduced another formulation which is associated with the Fourier transform. Marchaud (1927) [81,82] introduced a new definition of the non-integer order of derivatives. Nevertheless, it was Caputo (1967) [83] who formulated a definition, admittedly more restrictive than the Riemann-Liouville one, but more appropriate for discussing problems involving a fractional differential equation with initial conditions [84,85]. Because of the importance of Caputo's version, we will compare this approach with the Riemann-Liouville formulation. The definition as proposed by Caputo reverses the order of the integral and derivative operators with the non-integer order derivative of Riemann-Liouville. We summarize the difference between these two formulations. In Caputo's formula: first we compute the derivative of integer order and then we

compute the integral of non-integer order. In the Riemann-Liouville formula: first we compute the non-integer order integral and then we compute the integer order derivative. It is important to mention that the Caputo derivative is useful to face problems where the initial conditions are made in the function and in the respective derivatives of integer order. After the first conference at the University of New Haven in 1974, CF has developed and several applications have appeared in many areas of scientific knowledge. As a result, distinct approaches to solving problems involving the derivative have been proposed and distinct definitions of the fractional derivative are available in the literature. From the 1900's the "useful consequences" of this mathematical model are visible with the fractional differential equations which appeared in the modeling of several phenomena in fields such as physics, biology, engineering, etc. [86–88].

However, some definitions of fractional order derivatives introduced in the transmission lines have shown limitations in their mathematical formalism, especially the derivative of a product or fraction of a function. Indeed, this derivative generalizes the formalism of the derivative of integer order to the fractional order, which is not the case until now with the Riemann-Liouville derivative and the Caputo derivative. The ambiguity of these definitions of fractional order derivatives, whose properties sometimes exclude them from applications in circuit theory, has motivated other researchers. Another type of non-classical derivative is the so-called conformable derivative which was introduced by Khalil et al [89]. This interesting fractional derivative is based on a limit form as in the classical derivative and has similar properties to the classical derivative. The new conformal fractional derivative is now of great interest and is the subject of several articles concerning boundary value problems, see [90,91]. One of the essential mathematical tools of this fractional calculus is the fractional derivation operator D^α . The problem is thus to define an operator D^α for real values of α , such that when α takes an integer value n , we find the usual n -th derivation for $n > 0$ or the iterated integration $|n|$ times for $n < 0$. There are many approaches to fractional derivation, we will highlight the approaches that are frequently used approaches in applications.

- **The Riemann-Liouville approach**

Definition 1 : Let $p > 0$; the Riemann-Liouville fractional derivative of order p of a

function $f \in \mathcal{C}((a; \infty), \mathbb{R})$ is defined by

$$D_{a^+}^{(p)} f(t) = \frac{1}{\Gamma(n-p)} \frac{d^n}{dt^n} \int_a^t (t-s)^{n-p-1} f(s) ds \tag{1.26}$$

where $n = [p] + 1$, provided the right side is pointwise defined on $(a; \infty)$:

• **Approche de Caputo**

Définition 2 : Let $p > 0$ and $n = [p] + 1$; the Caputo's fractional derivative of a function $f \in ([a; b]; \mathbb{R})$ is defined by

$$D_{a^+}^{(p)} f(t) = \frac{1}{\Gamma(p-n)} \frac{d^n}{dt^n} \int_a^t (t-s)^{n-p-1} f^n(s) ds \tag{1.27}$$

Suppose $p > 0$ and $n = [p] + 1$; then the relation between Riemman-Liouville, Caputo fractional derivatives and Riemann Liouville integral can be expressed by the theorem below.

Theorem : Set $D = \frac{d}{dt}$; then we have for $p, q > 0$:

$$D_{a^+}^{(p)} f(t) = {}^C D_{a^+}^{(p)} f(t) + \sum_{k=0}^{n-1} \frac{f^k(a)(t-a)^{k-p}}{\Gamma(k-p+1)} \tag{1.28}$$

In mathematical modeling the use of fractional derivatives in the Riemann-Liouville sense leads to initial conditions containing the boundary values of fractional derivatives in the lower bound $t = a$. A certain solution of this problem has been proposed by M.Caputo.

Let $p \geq 0$ (with $n - 1 \leq p < n$ and $n \in \mathbb{N}^*$) f is a function such that $frac{d^n}{dt^n} f \in L_1[a, b]$.

The fractional derivative of order p of f in the sense of Caputo is defined by :

$$D_t^{(p)} f(t) = \frac{1}{\Gamma(n-p)} \int_a^t (t-\tau)^{n-p-1} f^{(n)}(\tau) d\tau \tag{1.29}$$

$$= I_t^{(n-p)} \left(\frac{d^n}{dt^n} f(t) \right) \tag{1.30}$$

• **Conformable Fractional Derivative**

All definitions of fractional derivatives satisfy the linearity property. However, properties, such as the product rule, quotient rule, chain rule, Rolle's theorem, mean value theorem, and composition rule, are missing from almost all fractional derivatives. These and other inconsistencies

have raised many problems in real applications and have limited the possibilities of exploring these fractional calculations. To avoid these difficulties, Khalil et al, [89] proposed an interesting idea that extends the definitions of ordinary limits of derivatives of a function called the conformal fractional derivative. This definition allows many extensions of some classical theorems of calculus for which applications are essential in fractional differential models that existing definitions do not allow. This conformal derivative has attracted the interest of researchers because it seems to satisfy all the requirements of the standard derivative. The basic concepts about conformable derivative are as follows : Given a function $h : \alpha \in (0, 1) \rightarrow \mathfrak{R}$ Then the "conformable fractional derivative" of h of order α is defined by

$$\frac{d^\alpha h(t)}{dt^\alpha} = \lim_{\varsigma \rightarrow +\infty} \frac{h(t + \varsigma t^{1-\alpha}) - h(t)}{\varsigma}. \quad (1.31)$$

for all $t > 0$, $\alpha \in (0, 1)$. If f is α -differentiable in some $(0, a)$, $a > 0$, and $\lim_{t \rightarrow 0^+} h^{(\alpha)}(t)$ exists, then define $h^{(\alpha)}(0) = \lim_{t \rightarrow 0^+} h^{(\alpha)}(t)$

Theorem : Let $\alpha \in (0, 1]$ and $f = f(t)$, $g = g(t)$ be α -conformable differentiable at $t < 0$.

Hence,

- $D_t^\alpha (af + bg) = aD_t^\alpha f + bD_t^\alpha g$, and $a, b \in \mathbb{R}$.
- $D_t^\alpha (t^\beta) = \beta t^{\beta-\alpha}$ and $\beta \in \mathbb{R}$.
- $D_t^\alpha (fg) = fD_t^\alpha (g) + gD_t^\alpha (f)$.
- $D_t^\alpha \left(\frac{f}{g} \right) = \frac{gD_t^\alpha (f) - fD_t^\alpha (g)}{g^2}$.

1.4.3.3 Some fractional differential equation for nonlinear transmission line

In many fields and particularly in electricity, the introduction of new mathematical tools, in particular the fractional derivative, has allowed to better model electrical phenomena. Indeed, we are often confronted with a problem such as: how to describe a particular phenomenon in a precise and simple way? As new phenomena will surface, the existing tools will become obsolete to better model. However, the implementation of fractional derivatives must not contradict the laws of physics (the mathematical equations). For example, Ampere's and Faraday's laws, the dependence between the coil voltage and the coupled alternating magnetic flux, the Maxwellian distribution laws, even if these will be refined by the Lorentz transformation for high speeds.

Moreover, each model must be confirmed by one or more relevant experiments. The main reason for the application of FO derivatives in the modeling of the elements of an electric circuit lies in its non-local properties compared to the classical definition of IO derivatives. Indeed, unlike integer order derivatives, fractional order derivatives include a memory of all previous states of the considered circuit element (the time domain history) in the calculations. In addition, in the process of designing the components of an electrical circuit, the derivative FO brings additional degrees of freedom to the system, which allows for design flexibility and optimization freedom [91, 92]. With respect to circuit components, in FO models of transmission lines, the FO inductance can be useful in modeling the skin effect while the FO capacitance is capable of modeling various non-idealities of the dielectric medium characteristics (e.g., the accumulation of electric charge along the line and memory effects in the dielectric polarization). As demonstrated in several experimental works [74, 75, 92, 93], the FO transmission line model allows for more compact and accurate analytical modeling over a wide frequency band compared to traditional IO modeling. Some definitions of FO derivatives are well established and have already been applied in circuit theory, while other definitions have only recently been introduced. With respect to the propagation of waves in power lines, Ryszard Sikora [92] has shown that relatively simple mathematical models containing fractional order derivatives can be a convenient and "flexible" tool for approximating frequency characteristics when the multifrequency MMFES method is applied. Houwe et al. [62] modeled by the nonlinear fractional differential equation a low-pass electrical transmission line, consisting of a number of LC connected with negligible dissipative effect. This allowed to obtain an ordinary differential equation, with the fractional complex time assumption: [93]. Aydin, B. Samanci, and S. Ozoguz showed that the fractional order characterization allows the derivation of an effective model that incorporates the transmission line loss over a wide frequency range of 1-6 GHz, which is useful in high bandwidth applications such as the 5G system [94, 129]. Y. Shang et al. worked on metamaterial T-lines, they showed that in a circuit with RLGC electrical parameters, the integer order model is insufficient to describe the characteristics of T-lines for millimeter waves. First, because the loss term in the T-line is difficult to model (distributed dispersion loss and non-quasi-static effects) [96], requiring a large number of RLGC components to fit the entire millimeter-wave frequency region [62, 97]; second, the metamaterial T-line has more complex coupling structures

such as the metamaterial load on the host T-line. Nevertheless, the fractional order model has recently shown to be a promising candidate for compact T-line modeling in the millimeter-wave frequency region. It has been used to calibrate the capacitor (C) and inductor (L) components in the conventional RLGC T-line model in the high-frequency region. By properly choosing the values of the fractional order parameters, a compact equivalent circuit model can be constructed for any T-line to fit a high frequency, broadband region. In this paper, we have developed a FO of RLGC model for metamaterial T-lines in the wave frequency region, with the following advantages. First, the fractional order RLGC model of the line can have a compact description of the distributed dispersion components. Second, the FO of RLGC model can accurately model the coupling effect in resonant-type metamaterial T-lines. The proposed FO of RLGC model is verified using S-parameter measurement results (up to 325 GHz) for metamaterial T-lines fabricated in 65 nm. Compared to the conventional IO of RLGC model, the proposed FO of RLGC model demonstrates better accuracy in the compact form of the equivalent circuit models. Some aspects of fractional differential equations, such as stability, existence and uniqueness of solutions, have been the subject of much research. Due to the inclusion of frequency-dependent losses and non-quasi-static effects, good agreement of the characteristic impedance is observed between the FO model for frequencies up to 110 GHz. In contrast, the traditional IO of RLGC model provides agreement between the model and measurements only up to 10 GHz. E. Fendzi-Donfack et al. [98], used fractional partial differential equations to model a fractional NETL and the fractional perturbation of the nonlinear Schrodinger equation (NLS) with the Kerr law nonlinearity term. They showed that the fractional complex transformation can be considered as a soft method to convert the fractional differential equation into an ODE using the conformal fractional derivative. In fact, by using the fractional derivative where the fractal index appears as a useful tool to easily change the fractional differential equation into a partial differential equation, we can describe the discontinuity of the medium without any difficulty.

1.3 Localized waves in nonlinear transmission line

1.3.1 Solitary waves concept

The soliton is a solitary wave, spatially localized, whose stability properties are spectacular. The soliton, also called solitary wave, was observed for the first time by the Scottish engineer and mathematician, John Scott Russel in 1834, however it was not until about ten years later that his observations were reported in the scientific literature [98]. John Scott Russel, was struck by the propagation of a hydrodynamic wave in the Hermiston canal, near the Riccarton Heriot-Watt University located in Edinburgh, by noting that its shape and its speed remained unchanged during its propagation. It is from this empirical observation that the need for a mathematical interpretation of the phenomenon was born, and then eventually its applications. This necessarily requires a modeling of the phenomenon, from numerical simulation to the construction of an exact mathematical solution, through different models. Several researchers have conducted investigations to understand this phenomenon, but it remained without mathematical interpretation until 1871, the year Joseph Valentin Boussinesq proposed an approximate equation of the phenomenon [99]. The equation that correctly modeled the propagation of a solitary wave on the surface of a narrow and shallow channel was that of Korteweg - de Vries in 1894-1895 [100]. However, it is the construction of the soliton solutions of the "Korteweg-de Vries" equation by Zabusky and Kruskal [54] that the existence of a "solitary wave" will be definitively established. After this important discovery of the hydrodynamic soliton, many researchers turned to this new era of research: nonlinear physics. Thus, since the beginning of the 70's, many equations describing nonlinear systems are known and the solitons themselves have been observed directly or indirectly in various media R36. However, due to the difficulties of experimentation, there are only a few systems where solitons are easily and directly observed in controlled laboratory experiments. In this respect, nonlinear electrical transmission lines are good examples, as they are easily amenable to experimental [101, 102]. Several types of soliton have been propagated in NETLs, with different applications in real life. In this section we present the different types of soliton propagated in NETLs, in particular the W-shape soliton which is the subject of our contribution and which is propagated for the first time in power lines with several concrete application perspectives.

1.3.2 Type of soliton

The soliton can propagate in any dispersive and nonlinear medium such as air, water or solids. Thus, according to the energy state of the propagation medium before and after the passage of the wave, they are classified into two categories: non-topological solitons and topological solitons [63].

1.3.2.1 Non-topological soliton

A soliton is non-topological when the propagation medium is in the same energy state before and after the passage of the wave. These solitons are those observed in hydrodynamics (although some are observed in solid mechanics). Non-topological solitons are dynamical structures that propagate locally while maintaining their shape and velocity, but which cannot exist at rest. The non-topological soliton in a hydrodynamic environment for example, can be described by the KdV equation or the NSL equation, which are nonlinear and dispersive partial differential equations for a function of two real variables x and t . As non-topological soliton we can note for example: the envelope soliton, the optical light soliton, the peregrine soliton, the rogue wave, the W-shape bright soliton and others [103–106].

- **Bright soliton**

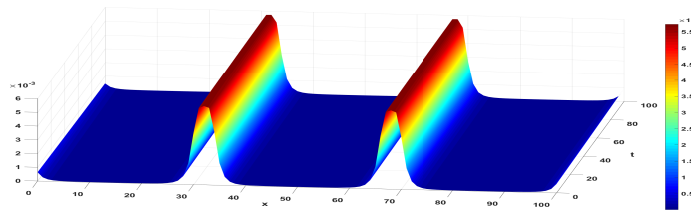


Figure 11: Bright soliton

Bright solitons are known as bell-shaped solitons or non-topological solitons [63]. The bright soliton is considered as a localized peak of light intensity above a background of continuous waves. These types of soliton waves are usually modeled by the sech function. Indeed, in the context of nonlinear optics, solitons are classified as either temporal or spatial, depending on whether the confinement of light occurs in time or in space during the propagation of the wave.

Both types of solitons evolve from a nonlinear change in the refractive index of an optical material induced by light intensity: a phenomenon known as the optical Kerr effect in the field of nonlinear optics. Several forms of bright solitons have been propagated in other media than the optical medium, notably nonlinear transmission lines.

- **Rogue wave soliton**

Rogue waves (RW) are also known as freak waves, monster waves, killer waves, giant waves, huge waves, super waves, gigantic waves, or extreme waves, etc. All these and similar names have been the subject of several recent publications related to the unique giant waves appearing in the ocean, which Akhmediev and al. [107] describes as "waves that appear from nowhere and disappear without a trace". It is a very rare and extremely giant type of wave that possesses powerful concentrated energy and strong nonlinearity. Indeed, the physical mechanisms of the rogue wave have attracted a lot of attention as more and more maritime accidents are due to this extreme wave, causing devastating damage to ships and offshore structures and even causing significant damage to shipboard personnel and valuable property. Although, we do not have a complete understanding of this phenomenon due to the difficult and risky observation conditions, studies on the mechanisms of rogue waves are therefore of great importance for the design and operation of ships and platforms. Some possible mechanisms have been summarized in review articles [108–110]. The most common mathematical description of these waves is based on certain rational solutions of the NLS equation. Today we have many family of rogue wave, such as the peregrine and super rogue wave. The well-known prototype of the RW in a (1+1)-dimensional equation is the first-order RW solution of the NLS equation, also called Peregrine solution (PS) [111]. The super rogue wave (SRW) is also a rational solution to the NLS equation, a higher order than the standard RW. Therefore, it has higher energy and causes more serious disasters. Since SRWs have caused many marine disasters, these waves are also very dangerous to transmission lines and understanding them is a necessity.

- **Peregrine soliton**

The PS, which was first discovered in 1983 by Peregrine [111], is a rational function of second degree, representing a double spatiotemporal localization on a finite continuous background,

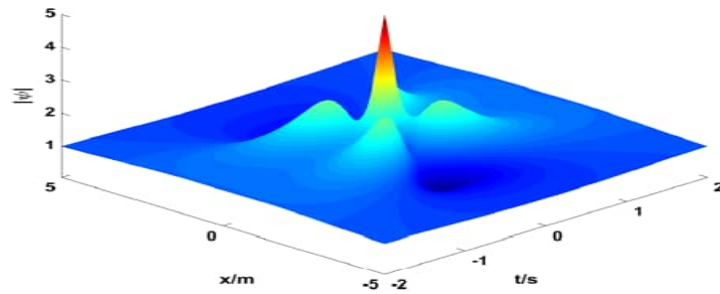


Figure 12: Super rogue wave

used in the modeling extreme wave events in various scientific areas, from oceanography and hydrodynamics to NETLs through nonlinear optics. The PS, is a particular form of solitary wave, also known as rational solution, "isolated Ma soliton", "explosion-decay solitary wave", "rational mode of growth and decay", "algebraic blast" or "fundamental solution of rogue wave". Unlike other classes of solitons, it is thus localized both in time and space : it emerges from nowhere and extracts its energy from a continuous wave, to reach a very high intensity before disappearing as suddenly as it appeared and returning to its initial state. Therefore, from a small fluctuation on a continuous background, the PS expands, its temporal duration decreasing and its amplitude increasing. At the point of maximum compression, its amplitude reaches three times the amplitude of the surrounding continuous background (if we reason in intensity as it is the case in optics, it is a factor nine (9) which separates the peak of the soliton from the surrounding background). After this point of maximum compression, the wave sees its amplitude decrease and widen to finally disappear, this behavior of the PS corresponds to the criteria usually used to qualify a rogue wave. The PS is a mathematical solution of the NLS equation, or the Gross-Pitaevskii equation. This solution was established in 1983 by Howell Peregrine, researcher at the Department of Mathematics of the University of Bristol [111]. This soliton solution was obtained by searching for a limit behavior of the solutions of breathers of the focusing NLS equation. These breather solutions belong to the families of solitons on a constant and non fading background, where the continuous wave envelope serves as a pedestal. Thus, the rational PS presents itself as a limiting behavior of the other two types of breathing solitons, i.e. the Kuznetsov-Ma breather and the Akhmediev soliton [112]. Although with a phase shift, the latter becomes a nonlinear extension of the homoclinic orbit

waveform corresponding to an unstable mode in the modulation instability phenomenon. For this reason, this wave was observed for the first time in the context of modulation instability of plane waves. The modulational instability that produces the PS in an experiment requires a careful choice of initial conditions, but its dynamics has now been observed in a number of careful studies in different systems, first in nonlinear optical fibers, then in hydrodynamic wave reservoirs, plasmas, in irregular oceanic seas, and recently in nonlinear power lines. Recent mathematical studies have shown that the PS solution actually appears more generally in the nonlinear localization of high-power pulses in the semiclassical (zero dispersion) limit of the focusing NLS equation. The first experimental observation of the PS in a water wave tank was recently documented by Chabchoub et al. [113] while in optics it has been observed by Kibler et al. [88]. This observation was later supported by numerical experiments and within the framework of exact 2D potential theory. This fundamental solution has a large peak whose height is three times that of the asymptotic background, surrounded by two deep troughs. The PS is the well-known prototype of the RW in a (1+1)-dimensional equation also consider as the first-order RW solution of the NLS equation. These rogue waves are localized both in space and in time. More precisely, they emerge from the background at a very early stage of the evolution, then reach the main peak (or amplitude maximum) of the fundamental model or the strong interaction zone of the other models mentioned above, and eventually retreat back into the same background. However, experimental studies conducted on the PS structure have been limited to the plane wave modulation instability regime. The characteristics of the first-order rogue wave call PS can be summarized as follows:

- (i) (quasi-) rational solution (or equivalent solution modulus);
- (ii) dual localization in time and space;
- (iii) large amplitude (the peak has a height at least three times that of the background) with a hole on each side.

1.3.2.2 Topological soliton

Topological solitons are those that are seen more in the field of solid mechanics. They are called topological when the propagation medium is in different energy states before and after the passage of the wave. Unlike non-topological solitons, they are dynamic structures that propagate locally while maintaining their shape and velocity and can be at rest. The soliton

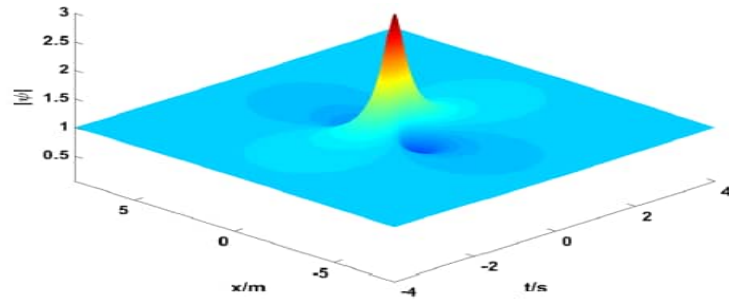


Figure 13: Peregrine soliton

can be described in this state by the Sine Gordon equation.

- **Kink soliton**

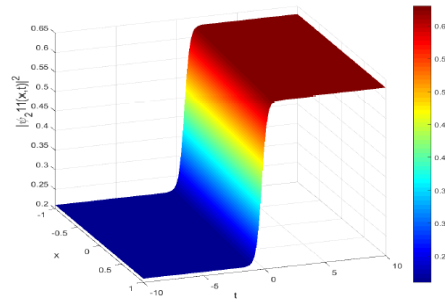


Figure 14: Kink soliton shape

Kink-solitons are generally one-dimensional topological solitons [106]. They represent a twist in the value of a solution and cause a transition from one value to another. This soliton contains two extremes, a minima and a maxima, it is the existence of these two extremes that induces an additional topological constraint. In reality, the kink are quasi-solitons, which correspond indeed to a fast variation of the variable. These quasi-solitons do not emerge unchanged from collisions with other kinks. The Sine Gordon (SG) equation which has a sinusoidal potential is the only one that leads to a fully integrable system possessing kink soliton solutions. The solutions of the SG equation are called kink or anti-kink solitons, and the velocity does not depend on the amplitude of the wave. The kinks then describe fundamental excitations of the system having a very important contribution to the statistical thermodynamics. This model can also describe topological defects in polymers like polyacetylene. In field theory, it has been

proposed as a simple model of stable states different from the "vacuum" state. A good physical example of a kink solution is a Bloch wall between two magnetic domains in a ferromagnet. The magnetic spins rotate, for example, from spin down in one domain to spin up in the adjacent domain. The transition region between spin down and spin up is called the Bloch wall. Under the influence of an applied magnetic field, the Bloch wall can propagate according to the Sine-Gordon equation.

- **Dark soliton**

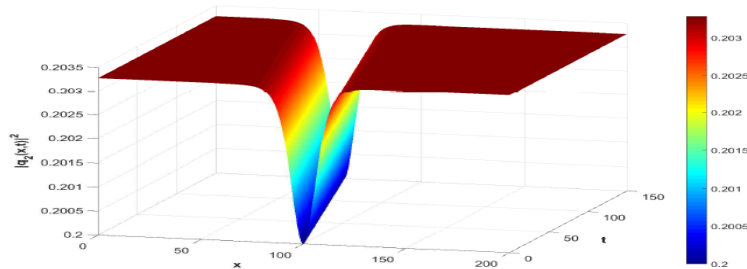


Figure 15: Dark soliton shape

Transmission of stationary nonlinear optical pulses in dispersive dielectric fibers. I. Anomalous dispersion Dark solitons are also known as topological solitons or simply topological defects. The dark soliton is characterized by a localized decrease in intensity associated with a more intense continuous wave background. In the context of optical fibers, the generation of dark solitons in the normal dispersion regime has been predicted by many researchers [103,120], and demonstrated experimentally [121]. They are observed as localized intensity dips on a continuous wave background with a non-trivial phase profile. Dark solitons have a number of interesting properties. For example, these solitons have been shown to be more robust to perturbations than their bright counterparts, including perturbations due to loss and amplified spontaneous emission noise. In addition, dark solitons can be created without a threshold value in the input pulse power. As applications, it has been shown that various types of all-optical switches can be "written" using structures created during the propagation and interaction of dark spatial solitons. As previously demonstrated for bright solitons, these induced structures can guide a weak probe beam of a different frequency or polarization, thus acting as light-induced structured waveguides. These types of devices have very interesting properties, for example, they

can retain the transverse velocity. The key feature used in switching dark space solitons, even in the presence of two-photon absorption. The effect that can have a dramatic destructive influence on bright space solitons. Experimental observations of a holey soliton in a nonlinear electrical network, with nonlinear capacitances, were made by Muroya et al [122]. They showed that the holey soliton generated from an initial wave propagates stably in the circuit, and that the modulation width and depth of this soliton were in agreement with theoretical predictions based on the NLS model.

1.3.3 Localized waves patterns solution of nonlinear transmission line model

In electronics, NETLs are a major tool for modeling a nonlinear dispersive medium, in order to study the propagation of voltage or potential waves in this medium, in the form of electrical solitons [123]. Thus, by changing the characteristics of NETLs components, one can model different states and conditions in the medium. In general, researchers transform the equation governing the dynamics of voltage or potential waves in nonlinear power lines into a well-known differential equation such as the KdV equation, NLSE [36], CGLE, before searching for solutions. The first study of soliton wave propagation was carried out by Hirota and Suzuki [5], who first physically explained some fundamental properties of solitons in terms of nonlinear properties of the LC lattice, and then mathematically demonstrated by establishing analytical expressions as a solution of soliton in a particular LC lattice. Nagashima and Amagishi [124] were the first to simulate the propagation of analogous solitons in the Toda atomic lattice [125]. Following this pioneering work, many other scientists around the world have turned to the study of soliton-like wave propagation with NETLs as a support [20–25, 126]. Among these, we have the study of the dynamics of nonlinear and modulated waves, bright and dark soliton pulses [127, 128], and intrinsic localized modes also called breathers [129, 130]. Propagation of pulses with frequencies beyond the called allowed band has revealed the gap solitons corresponding to supertransmission [25, 131–133]. The collision of solitons in NETLs has also been studied [124, 134, 135]. In the same time classical NETLs have been treated analytically by several authors and have allowed the exploration of certain soliton solutions of kink, anti-kink, bell, anti-bell, singular, periodic and periodic singular type [123, 131, 136, 137]. Some characteristics of solitons have also

been observed experimentally in NETLs, notably the interactions between solitons [138, 139], the recurrence phenomenon [140] and the networks [141, 142]. Some potential applications of NETLs such as harmonic generation [143], pulse shaping [6], and pulse compression [144] have been studied. Some left-handed transmission lines, such as the composite right/left-handed transmission line with voltage-dependent shunt capacitors have been used to propagate bright and dark solitons [127]. Fabien II et al. studied the analytical and numerical effects of nearest-neighbor couplings on the propagation of skywave signals in a nonlinear electrical transmission line. Thus, NETLs can support several types of soliton solutions including: dark, bright, bent, pulse, envelope, peregrine, rogue, kink, and anti-kink, and others. In recent years, one of the most important objectives of research in NETLs is the generation at very high frequency of solitons with rational pulse profile. However, at very high frequency, new uncontrolled phenomena appear in the lines, such as the memory effect, the skin effect, which must be taken into account in the propagation of solitons in NETLs. Indeed, the nonlinearity produced until now by the capacitor or the coil, whose capacitance or inductance changes with the applied voltage, seems to be inoperative for this purpose, since it presents both a frequency and spatial dispersion. In order to overcome these difficulties with NETLs, several researchers have started to use fractional models for its non-local properties on the one hand, and the use of superconducting components such as the Josephson junction on the other hand. Thus, many experimental works have shown that the transmission line model with a fractional order derivative allows to obtain soliton solutions with rational profile and more over a wide frequency band compared to the traditional modeling with the integer order derivative. Among these works, that of kumar and al [66], used the conformal derivative to model the propagation of rational solitons of form W, M and U in a nonlinear transmission line. The NETL model used in this study consists of a nonlinear network with several coupled nonlinear LC dispersive transmission lines. Also, the JJs was used to replace the varactors, in order to increase the nonlinearity and produce a better solution profile and frequency. Recently, Houwe et al have shown that the highly nonlinear nature of the JJ arrays incorporated in the JLHTL structure can support many types of solitons such as dark solitons, bright solitons, bent solitons, and anti-bent solitons at very high frequencies. Moreover, these analytical results are in agreement with numerical simulations. Some work has been devoted to the possibility of existence and

dynamics of rational solitons, in particular the alpha-form in LH nonlinear transmission lines, but there is little work on RH nonlinear transmission lines. Moreover, there is also no work to our knowledge on the propagation of rational solitons, in a NETL model with JJ. Thus, we have realized a RHNETL with JJ to propagate different localized waves as : PS, SRWs, breathers in addition to the classical bright and dark solitons, for very high frequencies than the previous results.

1.4 Applications

. The Josephson junction as an electronic component has several applications [59, 60], notably in nonlinear transmission lines such as :

- Signal shaping and enhancement in data transmission for high speed digital circuits. Indeed, RSFQ logic, using the JJ as a basic element, allows to reach operating speeds of circuits of the order of hundreds of GHz, while maintaining negligible power consumption and reduced architecture complexity.
- Reduction of pulse rise and fall times, in high-speed sampling oscilloscopes and other instruments for microwave systems. A recent experimental study demonstrated the use of NLTL with JJ in an electrical soliton oscillator, as a single port system, which itself generates soliton pulses from ambient noise. An amplifier was used in the realization of this soliton oscillator to compensate for losses and stabilize the oscillations.
- The miniaturization of components: physically small but electrically large components such as antennas with a reduced size of $\frac{1}{10}$ (at least) having performances equal or superior to conventional antennas.
- The realization of the supercomputer, currently being considered by the army and major research centers.
- The use in a wide range of optical applications: very high resolution imaging systems.

- The development of broadband, moderate intensity Terahertz (THz) sources, accessible to many applications: from condensed matter physics to biomedical, manufacturing and other techniques.
- The development of superconducting electronics with the realization of a 50 GHz LTC microprocessor with one million logic gates, memories, inputs/outputs and packaging.
- The realization of analog-to-digital converter circuits with RSFQ technology, which constitute the real limit of mobile and radio communications. In particular, very high speed switches, and in signal processing, for example the DSP4 for real-time FFT. The conversion of imaging systems (reading) into writing systems using higher density photonic and electronic components.
- The realization of quantum mechanical circuits such as SQUID. In particular, the revolution in metrology, introducing a fundamental relationship between frequency and voltage, the use of digital and programmable volt values, the design of sampling oscilloscopes, spectrum analyzers with a very wide bandwidth. It can be defined as meta-surfaces whose geometry controls the propagation of surface waves. Indeed, the Josephson junction is the basis of SQUIDS, magnetometers with a sensitivity in the order of femtotesla at 1Hz which find a wide application in medicine, geophysics and biology.

1.5 Conclusion

This chapter is devoted to the review of the literature on TLs and localized waves. In the first section, the generalities on TLs were presented. This presentation allowed us first to clarify the basic concepts used in TLs, in particular the types of lines, their advantages and disadvantages. Then to present the modeling approach used and the different elements of non linearity. Finally we present the different nonlinear equations to which the TLs models lead. It appears from this first section that firstly the printed lines are the ones that behave better at very high frequencies, secondly the nonlinear elements used are very limited to produce some localized wave profiles, and thirdly the Schrödinger equation is the most appropriate for the transport of high frequency signals in transmission lines. In section two, we present the literature review

on localized waves in NETLs. Thus, we presented the conceptual evolution of the solitary wave from its first observation to its current conceptualization. Then, we present the different types of localized wave profiles such as: bright and dark solitons, the kink, the SRW, the PS, and the SRWs. Finally, we review recent work that has allowed the propagation of different localized wave profiles, including the different types of propagated solitons and their applications. From this work, it appears that several types of localized waves have been propagated in power lines. However, few works have allowed the propagation of SRW, PS and other exotic forms of very high frequency localized waves in LTs, while they have several applications in daily life.

Chapter 2

Model and Methodology

2.1 Introduction

The study of propagation in very high frequency power lines of localized waves has been the subject of research in recent years, particularly because of the ease it offers for experimentation [6, 50, 51, 55]. Indeed, a large number of researches have been devoted to the study of short pulses in NETLs with different types of nonlinearities [8–20, 57]. In this context, different types of models and methods have been used to study wave propagation in these NETLs. These different models have led to nonlinear differential equations and mainly to the nonlinear Schrödinger equation (NLS). Several efficient techniques to study analytically the nonlinear Schrödinger equation (NLS) describing solitary waves have been used. Thus, these different works have allowed the propagation of several localized wave profiles at different frequency ranges. Several mathematical techniques have been used to verify the modulation instability of these waves. However, recent studies have shown that at very high frequencies, new phenomena appear and cannot be taken into account by the complete differential nonlinear equations as at low frequencies. This situation has led on the one hand to the use of fractional order which has led to nonlinear differential equations with fractional derivative to model these nonlinear power lines and on the other hand to the incorporation of new components with high nonlinearity. Indeed, by using the fractional derivative, the fractal index appears as a useful tool to easily transform the fractional differential equation into a partial differential equation, we can describe the discontinuity of the medium without any difficulty . Thus, effective methods

have been developed to obtain some exact and numerical solutions of fractional differential equations [145–159]. However, the fractional method has certainly made it possible to obtain rational profiles of localized waves, but has not solved the problem related to the frequency. To overcome this problem, several researchers have realized very high frequency and superconducting power lines using the Josephson junction, which is able to reduce ohmic losses and can take into account the memory effect due to its strong nonlinearity. In this sense, Abdoukary et al. [47] have studied the envelope solitons in a left-handed nonlinear transmission line with Josephson junction. For this purpose, they made a unit circuit model representing a left-handed transmission line to establish the nonlinear Schrödinger equation (NLSE) using the reductive perturbation method. They obtained a nonlinear Schrödinger model that is well known to admit solitary wave solutions. Thus, they realized that depending on the behavior of the PQ product, two different regimes are obtained: low and high frequency regimes where bright and dark solitons are formed. More recently, Houwe et al. [48] have incorporated a Josephson junction with high nonlinearity in a left-handed line so that it supports at very high frequency many types of solitons. As results, by applying the generalized Riccati method, they obtained exact solutions of the traveler's curvature solitons and the envelope solitons (dark soliton and bright soliton). In this chapter, we will first model the conventional left hand line with JJ which will be considered here as our model. Then we will use the perturbation method to deduce the key parameters of the propagation, notably the NLS equation. Finally we will determine by the method of modulation instability, the conditions of propagation and modulation instability of the localized waves obtained. This work will end with a numerical study that will confirm the analytical results obtained previously. Moreover, powerful mathematical and computational tools such as Maple and Matlab will be used.

2.2 Overview of the two methods of fractionnal derivative

2.2.1 The new extended direct algebraic method

The fundamental of the new extended direct algebraic method is given by the following steps [160–165].

Step 1: Adopting the partial differential equation (PDE) in the following form

$$H(u, D_t^\alpha u, D_x^\alpha u, D_y^\alpha u, D_t^{2\alpha} u, D_t^\alpha D_x^\beta u, \dots) = 0, \quad 0 < \alpha, \beta < 1, \quad (2.1)$$

where $u(x, t)$ is an unknown function and H is a polynomial of u .

Surmise the traveling-wave hypothesis as follows and then adopting $u(x, t) = U(\xi)$

$$\xi = \frac{k_1}{\Gamma(1 + \alpha)} t^\alpha + \frac{k_2}{\Gamma(1 + \alpha)} x^\alpha \quad (2.2)$$

while k_1, k_2 are constants to be determined, and $k_1, k_2 \neq 0$. Thus, the PDE can turn into ordinary differential equation

$$F(U, k_1 U', k_1 k_2 U'', k_1^3 U''', \dots) = 0, \quad (2.3)$$

and prime denotes the derivative with respect to ξ .

Step 2: Considering that Eq.(2.3) has the solution in the following expression

$$U(\xi) = \sum_{j=0}^N g_j Q^j(\xi), \quad g_n \neq 0. \quad (2.4)$$

where $g_j (0 \leq j \leq N)$ are constants to be determined later and $Q(\xi)$ satisfies the following ODE

$$Q'(\xi) = Ln(A)(\lambda + \mu Q(\xi) + \sigma Q^2(\xi)), \quad (2.5)$$

and $A \neq 0, 1$. The solutions of ODE Eq.(2.5) are:

Case 1: $\mu^2 - 4\lambda\sigma < 0$ and $\sigma \neq 0$

$$Q_1(\xi) = -\frac{\mu}{2\sigma} + \frac{\sqrt{-(\mu^2 - 4\lambda\sigma)}}{2\sigma} \tan_A \left(\frac{\sqrt{-(\mu^2 - 4\lambda\sigma)}}{2} \xi \right), \quad (2.6)$$

$$Q_2(\xi) = -\frac{\mu}{2\sigma} + \frac{\sqrt{-(\mu^2 - 4\lambda\sigma)}}{2\sigma} \cot_A \left(\frac{\sqrt{-(\mu^2 - 4\lambda\sigma)}}{2} \xi \right), \quad (2.7)$$

$$Q_3(\xi) = -\frac{\mu}{2\sigma} + \frac{\sqrt{-(\mu^2 - 4\lambda\sigma)}}{2\sigma} \tan_A \left(\sqrt{-(\mu^2 - 4\lambda\sigma)} \xi \right) \\ \pm \frac{\sqrt{-pq(\mu^2 - 4\lambda\sigma)}}{2\sigma} \sec_A \left(\sqrt{-(\mu^2 - 4\lambda\sigma)} \xi \right), \quad (2.8)$$

$$Q_4(\xi) = -\frac{\mu}{2\sigma} - \frac{\sqrt{-(\mu^2 - 4\lambda\sigma)}}{2\sigma} \cot_A \left(\sqrt{-(\mu^2 - 4\lambda\sigma)} \xi \right) \\ \pm \frac{\sqrt{-pq(\mu^2 - 4\lambda\sigma)}}{2\sigma} \csc_A \left(\sqrt{-(\mu^2 - 4\lambda\sigma)} \xi \right), \quad (2.9)$$

$$Q_5(\xi) = -\frac{\mu}{2\sigma} - \frac{\sqrt{-(\mu^2 - 4\lambda\sigma)}}{2\sigma} \tan_A \left(\frac{\sqrt{-(\mu^2 - 4\lambda\sigma)}}{4} \xi \right) - \frac{\sqrt{-(\mu^2 - 4\lambda\sigma)}}{2\sigma} \cot_A \left(\frac{\sqrt{-(\mu^2 - 4\lambda\sigma)}}{4} \xi \right), \quad (2.10)$$

Case 2: $\mu^2 - 4\lambda\sigma > 0$ and $\sigma \neq 0$

$$Q_6(\xi) = -\frac{\mu}{2\sigma} + \frac{\sqrt{(\mu^2 - 4\lambda\sigma)}}{2\sigma} \tanh_A \left(\frac{\sqrt{(\mu^2 - 4\lambda\sigma)}}{2} \xi \right), \quad (2.11)$$

$$Q_7(\xi) = -\frac{\mu}{2\sigma} + \frac{\sqrt{(\mu^2 - 4\lambda\sigma)}}{2\sigma} \coth_A \left(\frac{\sqrt{(\mu^2 - 4\lambda\sigma)}}{2} \xi \right), \quad (2.12)$$

$$Q_8(\xi) = -\frac{\mu}{2\sigma} + \frac{\sqrt{(\mu^2 - 4\lambda\sigma)}}{2\sigma} \tanh_A \left(\sqrt{(\mu^2 - 4\lambda\sigma)} \xi \right) \pm i \frac{\sqrt{pq(\mu^2 - 4\lambda\sigma)}}{2\sigma} \operatorname{sech}_A \left(\sqrt{(\mu^2 - 4\lambda\sigma)} \xi \right), \quad (2.13)$$

$$Q_9(\xi) = -\frac{\mu}{2\sigma} - \frac{\sqrt{(\mu^2 - 4\lambda\sigma)}}{2\sigma} \coth_A \left(\sqrt{(\mu^2 - 4\lambda\sigma)} \xi \right) \pm \frac{\sqrt{pq(\mu^2 - 4\lambda\sigma)}}{2\sigma} \operatorname{csch}_A \left(\sqrt{(\mu^2 - 4\lambda\sigma)} \xi \right), \quad (2.14)$$

$$Q_{10}(\xi) = -\frac{\mu}{2\sigma} - \frac{\sqrt{-(\mu^2 - 4\lambda\sigma)}}{4\sigma} \tanh_A \left(\frac{\sqrt{(\mu^2 - 4\lambda\sigma)}}{4} \xi \right) - \frac{\sqrt{(\mu^2 - 4\lambda\sigma)}}{4\sigma} \coth_A \left(\frac{\sqrt{(\mu^2 - 4\lambda\sigma)}}{4} \xi \right), \quad (2.15)$$

Case 3: $\lambda\sigma > 0$ and $\mu = 0$

$$Q_{11}(\xi) = \sqrt{\frac{\lambda}{\sigma}} \tan_A \left(\sqrt{\lambda\sigma} \xi \right), \quad (2.16)$$

$$Q_{12}(\xi) = -\sqrt{\frac{\lambda}{\sigma}} \cot_A \left(\sqrt{\lambda\sigma} \xi \right), \quad (2.17)$$

$$Q_{13}(\xi) = \sqrt{\frac{\lambda}{\sigma}} \tan_A \left(\sqrt{2\lambda\sigma} \xi \right) \pm \sqrt{pq \frac{\lambda}{\sigma}} \operatorname{sec}_A \left(\sqrt{2\lambda\sigma} \xi \right), \quad (2.18)$$

$$Q_{14}(\xi) = -\sqrt{\frac{\lambda}{\sigma}} \cot_A \left(\sqrt{2\lambda\sigma}\xi \right) \pm \sqrt{pq\frac{\lambda}{\sigma}} \csc_A \left(\sqrt{2\lambda\sigma}\xi \right), \quad (2.19)$$

$$Q_{15}(\xi) = \frac{1}{2} \sqrt{\frac{\lambda}{\sigma}} \left(\tan_A \left(\frac{\sqrt{\lambda\sigma}}{2}\xi \right) - \sqrt{\frac{\lambda}{\sigma}} \cot_A \left(\frac{\sqrt{\lambda\sigma}}{2}\xi \right) \right). \quad (2.20)$$

Case 4: $\lambda\sigma < 0$ and $\mu = 0$

$$Q_{16}(\xi) = -\sqrt{\frac{-\lambda}{\sigma}} \tanh_A \left(\sqrt{-\lambda\sigma}\xi \right), \quad (2.21)$$

$$Q_{17}(\xi) = -\sqrt{\frac{-\lambda}{\sigma}} \coth_A \left(\sqrt{-\lambda\sigma}\xi \right), \quad (2.22)$$

$$Q_{18}(\xi) = -\sqrt{\frac{-\lambda}{\sigma}} \tanh_A \left(\sqrt{2\lambda\sigma}\xi \right) \pm i\sqrt{pq\frac{-pq\lambda}{\sigma}} \operatorname{sech}_A \left(2\sqrt{-\lambda\sigma}\xi \right), \quad (2.23)$$

$$Q_{19}(\xi) = -\sqrt{\frac{-\lambda}{\sigma}} \coth_A \left(2\sqrt{-\lambda\sigma}\xi \right) \pm \sqrt{-pq\frac{\lambda}{\sigma}} \operatorname{csch}_A \left(2\sqrt{-\lambda\sigma}\xi \right), \quad (2.24)$$

$$Q_{20}(\xi) = -\frac{1}{2} \left(\sqrt{\frac{-\lambda}{\sigma}} \tanh_A \left(\frac{\sqrt{-\lambda\sigma}}{2}\xi \right) + \sqrt{\frac{-\lambda}{\sigma}} \coth_A \left(\frac{\sqrt{-\lambda\sigma}}{2}\xi \right) \right), \quad (2.25)$$

Case 5: $\mu = 0$ and $\lambda = \sigma$

$$Q_{21}(\xi) = \tan_A(\lambda\xi), \quad (2.26)$$

$$Q_{22}(\xi) = -\cot_A(\lambda\xi), \quad (2.27)$$

$$Q_{23}(\xi) = \tan_A(2\lambda\xi) \pm \sqrt{pq} \sec_A(2\lambda\xi), \quad (2.28)$$

$$Q_{24}(\xi) = -\cot_A(2\lambda\xi) \pm \sqrt{pq} \csc_A(2\lambda\xi), \quad (2.29)$$

$$Q_{25}(\xi) = \frac{1}{2} \left(\tan_A\left(\frac{\lambda}{2}\xi\right) - \cot_A\left(\frac{\lambda}{2}\xi\right) \right), \quad (2.30)$$

Case 6: $\mu = 0$ and $\lambda = -\sigma$

$$Q_{26}(\xi) = -\tanh_A(\lambda\xi), \quad (2.31)$$

$$Q_{27}(\xi) = -\coth_A(\lambda\xi), \quad (2.32)$$

$$Q_{28}(\xi) = -\tanh_A(2\lambda\xi) \pm i\sqrt{pq}\operatorname{sech}_A(2\lambda\xi), \quad (2.33)$$

$$Q_{29}(\xi) = -\coth_A(2\lambda\xi) \pm \sqrt{pq}\operatorname{csch}_A(2\lambda\xi), \quad (2.34)$$

$$Q_{30}(\xi) = -\frac{1}{2} \left(\tanh_A\left(\frac{\lambda}{2}\xi\right) + \coth_A\left(\frac{\lambda}{2}\xi\right) \right), \quad (2.35)$$

Case 7: $\mu^2 = 4\lambda\sigma$

$$Q_{31}(\xi) = -\frac{2\lambda(\mu\xi \operatorname{Ln}(A) + 2)}{\mu^2\xi \operatorname{Ln}(A)}, \quad (2.36)$$

Case 8: $\mu = k, \lambda = mk(m \neq 0), \text{ and } \sigma = 0,$

$$Q_{32}(\xi) = A^{\xi k} - m, \quad (2.37)$$

Case 9: $\mu = \sigma = 0$

$$Q_{33}(\xi) = \lambda\xi \operatorname{Ln}A, \quad (2.38)$$

Case 10: $\mu = \lambda = 0$

$$Q_{34}(\xi) = \frac{-1}{\sigma\xi \operatorname{Ln}A}, \quad (2.39)$$

Case 11: $\mu \neq 0$ and $\lambda = 0.$

$$Q_{35}(\xi) = \frac{p\mu}{\sigma(\cosh_A(\mu\xi) - \sinh_A(\mu\xi) - p)}, \quad (2.40)$$

$$Q_{36}(\xi) = -\frac{\mu(\sinh_A(\mu\xi) + \cosh_A(\mu\xi))}{\sigma(\cosh_A(\mu\xi) - \sinh_A(\mu\xi) + q)}, \quad (2.41)$$

Case 12: $\mu = k$ and $\sigma = mk(m \neq 0)$ and $\lambda = 0.$

$$Q_{37}(\xi) = -\frac{pA^{k\xi}}{q - mpA^{k\xi}}, \quad (2.42)$$

Step 3: By using the homogeneous balance principle the value of N can be obtained between the highest order derivative and high-order terms in Eq.(2.3).

Step 4: Substituting Eq.(2.4) and Eq.(2.5) into Eq.(2.3), then collecting all the term of $Q^j(\xi)$ to set to zero yields a system of algebraic equation.

Step 5: With aid of MAPLE, the results of the system of algebraic equation can be obtained and then use the results of Eq.(2.5) to construct the exact solutions of Eq.(2.3).

However, the details of the generalized hyperbolic and trigonometric functions are given by [160].

2.2.2 The new sub-ODE method

Suppose that the solution of Eq.(2.3) is given by [166–168]

$$U(\xi) = \mu F^s(\xi), \quad \mu > 0. \quad (2.43)$$

Here μ is an arbitrary positive constant to be determined, while $F(\xi)$ satisfies the following ODE

$$F'^2(\xi) = AF^{2-2p}(\xi) + BF^{2-p}(\xi) + CF^2(\xi) + DF^{2+p}(\xi) + EF^{2+2p}(\xi), \quad p > 0. \quad (2.44)$$

- Step 1: It consists to determine the parameter s by using the balance principle as follows:

$$D(U) = s, \quad D(U^2) = 2s \dots, \quad D(U') = s + p, \quad D(U'') = s + 2p \dots, \quad (2.45)$$

- Step 2: Now, Eq.(2.2) and Eq.(2.3) can be plugged together into set of Eq.(2.1), thereafter collect all the coefficients of $F^{si}(\xi) [F(\xi)']^s$ ($i = 0, 1, 2, 3, \dots$) and equal them to zero, yields to a set of algebraic system of equation which will lead to determine the different coefficients A, B, C, D, E and μ . In the same time the s values should be $(0, 1)$.
- Step 3: The final procedure focusses to insert the obtained parameters in the following set of solutions of Eq.(2.1), which are listed in ref. [160].

Case 1: If $A = 0, B = 0, D = 0$, it is recovered bright soliton of Eq.(2.3):

$$F(\xi) = \left[\varepsilon \sqrt{-\frac{C}{E}} \operatorname{sech}(p\sqrt{C}\xi) \right]^{\frac{1}{p}}, \quad C > 0, \quad E < 0, \quad \varepsilon \pm 1, \quad (2.46)$$

a periodic solution

$$F(\xi) = \left[\varepsilon \sqrt{-\frac{C}{E}} \sec(p\sqrt{-C}\xi) \right]^{\frac{1}{p}}, \quad C < 0, \quad E > 0, \quad \varepsilon \pm 1, \quad (2.47)$$

and a rational solution

$$F(\xi) = \left[\frac{\varepsilon}{p\sqrt{E}\xi} \right]^{\frac{1}{p}}, \quad C = 0, \quad E > 0, \quad \varepsilon \pm 1. \quad (2.48)$$

Case 2: By setting the conditions $B = 0$, $D = 0$, $A = \frac{C^2}{4E}$, it is gained dark soliton-like solution of Eq.(2.3):

$$F(\xi) = \left[\varepsilon \sqrt{-\frac{C}{2E}} \tanh \left(p \sqrt{\frac{-C}{2}} \xi \right) \right]^{\frac{1}{p}}, \quad C < 0, \quad E > 0, \quad \varepsilon \pm 1, \quad (2.49)$$

and a periodic solution

$$F(\xi) = \left[\varepsilon \sqrt{\frac{C}{2E}} \tan \left(p \sqrt{\frac{C}{2}} \xi \right) \right]^{\frac{1}{p}}, \quad C > 0, \quad E > 0, \quad \varepsilon \pm 1. \quad (2.50)$$

Case 3: By setting the conditions $B = 0$, $D = 0$, we deduce three forms of Jacobian elliptic functions solutions of Eq.(2.3):

$$F(\xi) = \left[\varepsilon \sqrt{\frac{-Cm^2}{E(2m^2-1)}} \operatorname{cn} \left(p \sqrt{\frac{C}{2m^2-1}} \xi \right) \right]^{\frac{1}{p}}, \quad C > 0,$$

$$A = \frac{C^2 m^2 (m^2 - 1)}{E(2m^2 - 1)^2}, \quad \varepsilon \pm 1, \quad (2.51)$$

$$F(\xi) = \left[\varepsilon \sqrt{\frac{-C}{E(2-m^2)}} \operatorname{dn} \left(p \sqrt{\frac{C}{2-m^2}} \xi \right) \right]^{\frac{1}{p}}, \quad C > 0,$$

$$A = \frac{C^2 (1 - m^2)}{E(2 - m^2)^2}, \quad \varepsilon \pm 1, \quad (2.52)$$

and

$$F(\xi) = \left[\varepsilon \sqrt{\frac{-Cm^2}{E(1+m^2)}} \operatorname{sn} \left(p \sqrt{\frac{-C}{1+m^2}} \xi \right) \right]^{\frac{1}{p}},$$

$$C < 0, \quad A = \frac{C^2 m^2}{E(1 + m^2)^2}, \quad \varepsilon \pm 1. \quad (2.53)$$

Case 4: By setting the conditions $A = B = E = 0$, bright soliton-like solution of Eq.(2.3) is gained:

$$F(\xi) = \left[\frac{-C}{D} \operatorname{sech}^2 \left(\frac{p}{2} \sqrt{C} \xi \right) \right]^{\frac{1}{p}}, \quad C > 0, \quad D < 0, \quad (2.54)$$

a periodic solution

$$F(\xi) = \left[\frac{-C}{D} \sec^2 \left(\frac{p}{2} \sqrt{-C} \xi \right) \right]^{\frac{1}{p}}, \quad C < 0, \quad D > 0, \quad (2.55)$$

and a rational solution

$$F(\xi) = \left[\frac{4}{D(p\xi)^2} \right]^{\frac{1}{p}}, \quad C = 0, \quad D < 0. \quad (2.56)$$

Case 5: By setting the conditions $C = E = 0$, $D > 0$, the Weierstrass elliptic function solutions of Eq.(2.3) are recovered

$$F(\xi) = \left[\wp \left(\frac{p\sqrt{D}}{2}\xi, g_2, g_3 \right) \right]^{\frac{1}{p}}, \quad (2.57)$$

where $g_2 = \frac{-4B}{D}$, $g_3 = \frac{-4A}{D}$.

Case 6: Assuming $B = D = 0$, it is revealed Weierstrass elliptic function solutions to set of Eq.(2.3),

$$F(\xi) = \left[\frac{\wp(p\xi, g_2, g_3)}{E} - \frac{C}{3E} \right]^{\frac{1}{2p}}, \quad (2.58)$$

where $g_2 = \frac{4C^2-12AE}{3}$, $g_3 = \frac{4C(-2C^2+9AE)}{27}$.

$$F(\xi) = \left[\frac{3A}{3\wp(p\xi, g_2, g_3) - C} \right]^{\frac{1}{2p}}, \quad (2.59)$$

where $g_2 = \frac{4C^2-12AE}{3}$, $g_3 = \frac{4C(-2C^2+9AE)}{27}$.

$$F(\xi) = \left[\frac{6\sqrt{A}\wp(p\xi, g_2, g_3) + C\sqrt{A}}{3\wp'(p\xi, g_2, g_3)} \right]^{\frac{1}{p}}, \quad (2.60)$$

where $\wp'(p\xi, g_2, g_3) = \frac{d\wp(p\xi, g_2, g_3)}{d\xi}$, $g_2 = \frac{C^2}{12} + AE$, $g_3 = \frac{C(36AE-C^2)}{216}$.

$$F(\xi) = \left[\frac{3\sqrt{E^{-1}}\wp'(p\xi, g_2, g_3)}{6\wp(p\xi, g_2, g_3) + C} \right]^{\frac{1}{p}}, \quad (2.61)$$

where $A = \frac{5C^2}{26E}$, $g_2 = \frac{2C^2}{9}$, $g_3 = \frac{C^3}{54}$,

$$F(\xi) = \left[\sqrt{\frac{5C^2}{36E}} \frac{6\wp(p\xi, g_2, g_3) + C}{3\wp'(p\xi, g_2, g_3)} \right]^{\frac{1}{p}}, \quad (2.62)$$

while g_2 and g_3 are the invariants of the Weierstrass elliptic function.

Case 7: By setting the conditions $A = 0$, $B = 0$, we deduce three forms of solutions of Eq(2.3):

$$F(\xi) = \left[\frac{1}{\cosh(p\sqrt{C}\xi) - \frac{D}{2C}} \right]^{\frac{1}{p}}, \quad C > 0, \quad D < 2C, \quad E = \frac{D^2}{4C} - C, \quad (2.63)$$

$$F(\xi) = \left[\frac{1}{2} \sqrt{\frac{C}{E}} \left(1 + \varepsilon \tanh\left(\frac{p}{2}\sqrt{C}\xi\right) \right) \right]^{\frac{1}{p}}, \quad C > 0, \quad E > 0, \quad D = -2\sqrt{CE}, \quad \varepsilon = \pm 1 \quad (2.64)$$

and

$$F(\xi) = \left[\frac{4D}{(pD\xi)^2 - 4E} \right]^{\frac{1}{p}}, \quad C = 0, \quad E < 0. \quad (2.65)$$

Case 8: Considering $A = B = 0$, $C > 0$, we have gained combined bright soliton and hyperbolic functions solutions of Eq(2.3):

$$F(\xi) = \left[\frac{2C \operatorname{sech}^2\left(\frac{p}{2}\sqrt{C}\xi\right)}{2\sqrt{D^2 - 4CE} - (\sqrt{D^2 - 4CE} + D) \operatorname{sech}^2\left(\frac{p}{2}\sqrt{C}\xi\right)} \right]^{\frac{1}{p}}, \quad D^2 - 4CE > 0 \quad (2.66)$$

$$F(\xi) = \left[\frac{2C \operatorname{csch}^2\left(\frac{p}{2}\sqrt{C}\xi\right)}{2\sqrt{D^2 - 4CE} + (\sqrt{D^2 - 4CE} - D) \operatorname{csch}^2\left(\frac{p}{2}\sqrt{C}\xi\right)} \right]^{\frac{1}{p}}, \quad D^2 - 4CE > 0 \quad (2.67)$$

$$F(\xi) = \left[\frac{2C}{\varepsilon \sqrt{D^2 - 4CE} \cosh(p\sqrt{C}\xi) - D} \right]^{\frac{1}{p}}, \quad D^2 - 4CE > 0, \quad \varepsilon = \pm 1 \quad (2.68)$$

$$F(\xi) = \left[\frac{2C}{\varepsilon \sqrt{-(D^2 - 4CE)} \sinh(p\sqrt{C}\xi) - D} \right]^{\frac{1}{p}}, \quad D^2 - 4CE < 0, \quad \varepsilon = \pm 1 \quad (2.69)$$

$$F(\xi) = \left[-\frac{C}{D} \left(1 + \varepsilon \tanh\left(\frac{p}{2}\sqrt{C}\xi\right) \right) \right]^{\frac{1}{p}}, \quad D^2 - 4CE = 0, \quad \varepsilon = \pm 1 \quad (2.70)$$

$$F(\xi) = \left[-\frac{C}{D} \left(1 + \varepsilon \coth\left(\frac{p}{2}\sqrt{C}\xi\right) \right) \right]^{\frac{1}{p}}, \quad D^2 - 4CE = 0, \quad \varepsilon = \pm 1 \quad (2.71)$$

$$F(\xi) = \left[-\frac{C \operatorname{sech}^2\left(\frac{p}{2}\sqrt{C}\xi\right)}{D + 2\varepsilon\sqrt{CE} \tanh\left(\frac{p}{2}\sqrt{C}\xi\right)} \right]^{\frac{1}{p}}, \quad E > 0, \quad \varepsilon = \pm 1 \quad (2.72)$$

$$F(\xi) = \left[\frac{C \operatorname{csch}^2\left(\frac{p}{2}\sqrt{C}\xi\right)}{D + 2\varepsilon\sqrt{CE} \coth\left(\frac{p}{2}\sqrt{C}\xi\right)} \right]^{\frac{1}{2}}, \quad E > 0, \quad \varepsilon = \pm 1 \quad (2.73)$$

$$F(\xi) = \left[\frac{-CD \operatorname{sech}^2\left(\frac{p}{2}\sqrt{C}\xi\right)}{D^2 - CE \left(1 + \varepsilon \tanh\left(\frac{p}{2}\sqrt{C}\xi\right)\right)^2} \right]^{\frac{1}{2}}, \quad (2.74)$$

$$F(\xi) = \left[\frac{CD \operatorname{csch}^2\left(\frac{p}{2}\sqrt{C}\xi\right)}{D^2 - CE \left(1 + \varepsilon \coth\left(\frac{p}{2}\sqrt{C}\xi\right)\right)^2} \right]^{\frac{1}{2}}. \quad (2.75)$$

Case 9: Considering $A = B = 0$, $C < 0$, we gained combined bright soliton and hyperbolic functions as solutions

$$F(\xi) = \left[\frac{-2C \sec^2\left(\frac{p}{2}\sqrt{-C}\xi\right)}{2\sqrt{D^2 - 4CE} - (\sqrt{D^2 - 4CE} - D) \sec^2\left(\frac{p}{2}\sqrt{-C}\xi\right)} \right]^{\frac{1}{p}}, \quad D^2 - 4CE > 0 \quad (2.76)$$

$$F(\xi) = \left[\frac{2C \csc^2\left(\frac{p}{2}\sqrt{-C}\xi\right)}{2\sqrt{D^2 - 4CE} - (\sqrt{D^2 - 4CE} + D) \csc^2\left(\frac{p}{2}\sqrt{-C}\xi\right)} \right]^{\frac{1}{p}}, \quad D^2 - 4CE > 0 \quad (2.77)$$

$$F(\xi) = \left[\frac{2C \sec(p\sqrt{-C}\xi)}{\varepsilon\sqrt{D^2 - 4CE} - D \sec(p\sqrt{-C}\xi)} \right]^{\frac{1}{p}}, \quad D^2 - 4CE > 0, \quad \varepsilon = \pm 1, \quad (2.78)$$

$$F(\xi) = \left[\frac{2C \csc(p\sqrt{-C}\xi)}{\varepsilon\sqrt{D^2 - 4CE} - D \csc(p\sqrt{-C}\xi)} \right]^{\frac{1}{p}}, \quad D^2 - 4CE > 0, \quad \varepsilon = \pm 1, \quad (2.79)$$

$$F(\xi) = \left[-\frac{C \sec^2\left(\frac{p}{2}\sqrt{-C}\xi\right)}{D + 2\varepsilon\sqrt{-CE} \tan\left(\frac{p}{2}\sqrt{-C}\xi\right)} \right]^{\frac{1}{p}}, \quad E > 0, \quad \varepsilon = \pm 1, \quad (2.80)$$

$$F(\xi) = \left[-\frac{C \csc^2\left(\frac{p}{2}\sqrt{-C}\xi\right)}{D + 2\varepsilon\sqrt{-CE} \cot\left(\frac{p}{2}\sqrt{-C}\xi\right)} \right]^{\frac{1}{p}}, \quad D^2 - 4CE > 0, E > 0, \quad \varepsilon = \pm 1. \quad (2.81)$$

Case 10: For $A = 0$, $B = \frac{8C^2}{27D}$, $E = \frac{D^2}{4C}$, it is gained hyperbolic function solutions of Eq(5)

$$F(\xi) = \left[-\frac{8C \tanh^2\left(\frac{p}{2}\sqrt{\frac{-C}{3}}\xi\right)}{3D(3 + \tanh^2\left(\frac{p}{2}\sqrt{\frac{-C}{3}}\xi\right))} \right]^{\frac{1}{p}}, \quad C < 0, \quad (2.82)$$

$$F(\xi) = \left[-\frac{8C \coth^2\left(\frac{p}{2}\sqrt{\frac{-C}{3}}\xi\right)}{3D(3 + \coth^2\left(\frac{p}{2}\sqrt{\frac{-C}{3}}\xi\right))} \right]^{\frac{1}{p}}, \quad C < 0, \quad (2.83)$$

it is gained trigonometric function solutions

$$F(\xi) = \left[\frac{8C \tan^2\left(\frac{p}{2}\sqrt{\frac{C}{3}}\xi\right)}{3D(3 - \tan^2\left(\frac{p}{2}\sqrt{\frac{C}{3}}\xi\right))} \right]^{\frac{1}{p}}, \quad C > 0. \quad (2.84)$$

$$F(\xi) = \left[\frac{8C \cot^2\left(\frac{p}{2}\sqrt{\frac{C}{3}}\xi\right)}{3D(3 - \cot^2\left(\frac{p}{2}\sqrt{\frac{C}{3}}\xi\right))} \right]^{\frac{1}{p}}, \quad C > 0, \quad (2.85)$$

Case 11: For $A = B = 0$,

$$F(\xi) = \left[\frac{4Cp^2 e^{(p\varepsilon\sqrt{C}\xi)}}{(e^{\varepsilon p\sqrt{C}\xi} - Dp^2)^2 - 4CEp^4} \right]^{\frac{1}{p}}, \quad C > 0, \quad \varepsilon = \pm 1, \quad (2.86)$$

$$F(\xi) = \left[\frac{4Cp^2 e^{(p\varepsilon\sqrt{C}\xi)}}{-1 + 4CEp^4 e^{2\varepsilon p\sqrt{C}\xi}} \right]^{\frac{1}{p}}, \quad C > 0, D = 0, \quad \varepsilon = \pm 1, \quad (2.87)$$

$$F(\xi) = \left[\frac{\varepsilon}{p\sqrt{E}\xi} \right]^{\frac{1}{p}}, \quad E > 0, C = D = 0, \quad \varepsilon = \pm 1. \quad (2.88)$$

Case 12: For $A = 0$ the Jacobian elliptic function solutions it is revealed

For $E > 0$, $B = \frac{D^3(m^2-1)}{32m^2E^2}$, $C = \frac{D^2(5m^2-1)}{16m^2E}$,

$$F(\xi) = \left[-\frac{D}{4E} \left(1 + \varepsilon sn \left(\frac{pD}{4m} \sqrt{\frac{1}{E}} \xi \right) \right) \right]^{\frac{1}{p}}, \quad \varepsilon = \pm 1, \quad (2.89)$$

$$F(\xi) = \left[-\frac{D}{4E} \left(1 + \varepsilon \frac{1}{msn \left(\left(\frac{pD}{4m} \sqrt{\frac{1}{E}} \xi \right) \right)} \right) \right]^{\frac{1}{p}}, \quad \varepsilon = \pm 1, \quad (2.90)$$

For $E > 0$, $B = \frac{D^3(1-m^2)}{32E^2}$, $C = \frac{D^2(5-m^2)}{16E}$, it is stated

$$F(\xi) = \left[-\frac{D}{4E} \left(1 + \varepsilon msn \left(\frac{pD}{4} \sqrt{\frac{1}{E}} \xi \right) \right) \right]^{\frac{1}{p}}, \quad \varepsilon = \pm 1, \quad (2.91)$$

$$F(\xi) = \left[-\frac{D}{4E} \left(1 + \frac{\varepsilon}{sn \left(\left(\frac{pD}{4} \sqrt{\frac{1}{E}} \xi \right) \right)} \right) \right]^{\frac{1}{p}}, \quad \varepsilon = \pm 1, \quad (2.92)$$

For $E < 0$, $B = \frac{D^3}{32m^2E^2}$, $C = \frac{D^2(4m^2+1)}{16m^2E}$, it is revealed

$$F(\xi) = \left[-\frac{D}{4E} \left(1 + \varepsilon cn \left(\frac{pD}{4m} \sqrt{-\frac{1}{E}} \xi \right) \right) \right]^{\frac{1}{p}}, \quad \varepsilon = \pm 1, \quad (2.93)$$

$$F(\xi) = \left[-\frac{D}{4E} \left(1 + \frac{\varepsilon \sqrt{1-m^2} sn \left(\frac{pD}{4m} \sqrt{-\frac{1}{E}} \xi \right)}{dn \left(\frac{pD}{4m} \sqrt{-\frac{1}{E}} \xi \right)} \right) \right]^{\frac{1}{p}}, \quad \varepsilon = \pm 1. \quad (2.94)$$

For $E < 0$, $B = \frac{m^2D^3}{32(m^2-1)E^2}$, $C = \frac{D^2(5m^2-4)}{16(m^2-1)E}$, it is revealed

$$F(\xi) = \left[-\frac{D}{4E} \left(1 + \frac{\varepsilon}{\sqrt{1-m^2}} dn \left(\frac{pD}{4} \sqrt{-\frac{1}{(1-m^2)E}} \xi \right) \right) \right]^{\frac{1}{p}}, \quad \varepsilon = \pm 1, \quad (2.95)$$

$$F(\xi) = \left[-\frac{D}{4E} \left(1 + \frac{\varepsilon}{dn \left(\left(\frac{pD}{4} \sqrt{-\frac{1}{(1-m^2)E}} \xi \right) \right)} \right) \right]^{\frac{1}{p}}, \quad \varepsilon = \pm 1. \quad (2.96)$$

For $E < 0$, $B = \frac{m^2 D^3}{32E^2}$, $C = \frac{D^2(m^2+4)}{16E}$, hence

$$F(\xi) = \left[-\frac{D}{4E} \left(1 + \varepsilon dn \left(\frac{pD}{4} \sqrt{-\frac{1}{E}\xi} \right) \right) \right]^{\frac{1}{p}}, \quad \varepsilon = \pm 1, \quad (2.97)$$

$$F(\xi) = \left[-\frac{D}{4E} \left(1 + \frac{\varepsilon \sqrt{1-m^2}}{dn \left(\left(\frac{pD}{4} \sqrt{-\frac{1}{E}\xi} \right) \right)} \right) \right]^{\frac{1}{p}}, \quad \varepsilon = \pm 1, \quad (2.98)$$

For $E > 0$, $B = \frac{D^3}{32(1-m^2)E^2}$, $C = \frac{D^2(4m^2-5)}{16(m^2-1)E}$, it is revealed

$$F(\xi) = \left[-\frac{D}{4E} \left(1 + \frac{\varepsilon}{cn \left(\left(\frac{pD}{4} \sqrt{\frac{1}{(1-m^2)E}\xi} \right) \right)} \right) \right]^{\frac{1}{p}}, \quad \varepsilon = \pm 1. \quad (2.99)$$

$$F(\xi) = \left[-\frac{D}{4E} \left(1 + \frac{\varepsilon dn \left(\frac{pD}{4} \sqrt{\frac{1}{(1-m^2)E}\xi} \right)}{\sqrt{1-m^2} sn \left(\frac{pD}{4} \sqrt{\frac{1}{(1-m^2)E}\xi} \right)} \right) \right]^{\frac{1}{p}}, \quad \varepsilon = \pm 1. \quad (2.100)$$

Case 13: For $A = E = 0$, it is recovered Jacobian elliptic function

For $D < 0$, $C > 0$, $B = \frac{m^2 C^2 (m^2-1)}{D(2m^2-1)^2}$, we get

$$F(\xi) = \left[-\frac{m^2 C}{D(2m^2-1)} cn^2 \left(\frac{p}{2} \sqrt{\frac{C}{2m^2-1}\xi} \right) \right]^{\frac{1}{p}}, \quad (2.101)$$

For $D > 0$, $C < 0$, $B = \frac{m^2 C^2}{D(m^2+1)^2}$, then

$$F(\xi) = \left[-\frac{m^2 C}{D(m^2+1)} sn^2 \left(\frac{p}{2} \sqrt{-\frac{C}{m^2+1}\xi} \right) \right]^{\frac{1}{p}}, \quad (2.102)$$

$$F(\xi) = \left[-\frac{m^2 C}{D(m^2+1)} cd^2 \left(\frac{p}{2} \sqrt{-\frac{C}{m^2+1}\xi} \right) \right]^{\frac{1}{p}}, \quad (2.103)$$

For $D < 0$, $C > 0$, $B = \frac{(1-m^2)C^2}{D(2-m^2)^2}$, consequently the last one

$$F(\xi) = \left[-\frac{C}{D(2-m^2)} dn^2 \left(\frac{p}{2} \sqrt{\frac{C}{2-m^2}\xi} \right) \right]^{\frac{1}{p}}. \quad (2.104)$$

2.3 Description of model

2.3.1 Description of physical model and justification

- **Justification of physical model**

Our starting point is the finding from the literature review that:

- An isolated SQUID consisting of a loop with JJ is less stable to noise and has reduced sensitivity ;
- Identical JJ arrays have a great advantage over an individual JJ, in terms of amplitude and sensitivity, in terms of dynamics and also in terms of magnetic noise reduction;
- Series arrays are very sensitive to dispersion phenomena and present difficulties in polarizing such a JJ array;
- For parallel networks, calculations predict improved sensitivity, but this is difficult to model;
- The models recently proposed by Abdoukary .al (2016) and Houwe .al (2017) incorporate JJs but are applied to meta-materials, and the frequencies obtained are below the infrared fibration frequencies of the array. This shows that the proposed model does not take into account all the phenomena involved, in particular the parasitic effect.

In this work, we have chosen to integrate the JJ in a right hand line. For this, we integrated the JJ next to the nonlinear C_2 capacitor for the substituted one, thus bringing the capacitor rather linear. Moreover, at very high frequency, the JJ will create capacitive effects on the line in the horizontal direction, and these effects are modeled by the capacitor C_1 . This is justified by the fact that, the right hand line which is a conventional line models a normal conductor, while the left hand line models an artificial conductor. This will allow to test not only the very high frequency conduction capability of current conductive materials, but also to synthesize and control these materials to build coherent arrays of junctions for several technical applications.

- Identical JJ arrays have a great advantage over an individual JJ, in terms of amplitude and sensitivity, in terms of dynamics and also in terms of magnetic noise reduction;
- Series arrays are very sensitive to dispersion phenomena and present difficulties in polarizing such a JJ array;
- For parallel networks, calculations predict improved sensitivity, but this is difficult to model;

- The models recently proposed by Abdoukary and al. (2016), Houwe and al. (2017) incorporate JJs but are applied to meta-materials, and the frequencies obtained are below the infrared fibration frequencies of the array. This shows that the proposed model does not take into account all the phenomena involved, in particular the parasitic effect.

In this work, we have chosen to integrate the JJ in a right hand line. For this, we integrated the JJ next to the nonlinear C_2 capacitor for the substituted one, thus bringing the capacitor rather linear. Moreover, at very high frequency, the JJ will create capacitive effects on the line in the horizontal direction, and these effects are modeled by the capacitor C_1 . This is justified by the fact that, the right hand line which is a conventional line models a normal conductor, while the left hand line models an artificial conductor. This will allow to test not only the very high frequency conduction capability of current conductive materials, but also to synthesize and control these materials to build coherent arrays of junctions for several technical applications.

- **Physical model**

Figure 16 shows the n^{th} elementary cell of the nonlinear electrical transmission line with Josephson junction. It is modeled by a linear inductor L_1 in parallel with a linear C_1 in the series branch and a linear capacitor C_2 in parallel with a nonlinear Josephson junction current J_n . The junction is considered here as the one that brings nonlinearity to the cell, in its response to the current so the expression of the junction of rank n is :

$$J_n = J_0 \sin\left(2\pi \frac{\phi_n}{\phi_0}\right) \quad (2.105)$$

where the dimensionless parameter μ_0 is given by $\mu_0 = \frac{C_2}{C_1}$, $\phi_j = 2\pi \frac{\phi_n}{\phi_0}$ is the quantum phase at node j, and $\phi_0 = 2,064.10^{-15} Tm^2$, $J_0 = 200nA$ [69]. The whole line is thus an assembly of n elementary and identical cells. Let's consider the cell of rank n: V_n is the voltage which crosses the capacitor C_1 , the choke L_1 , the condenser C_2 , and the junction J_n of rank n while I_n is the current which crosses this same assembly of cell n^{th} .

2.3.2 Analytical treatment

By using the famous Kirchhoff Laws in current and voltage on the lattice of Figure 16 reveals the following nonlinear discrete equations which describes the modulated waves in the lattice :

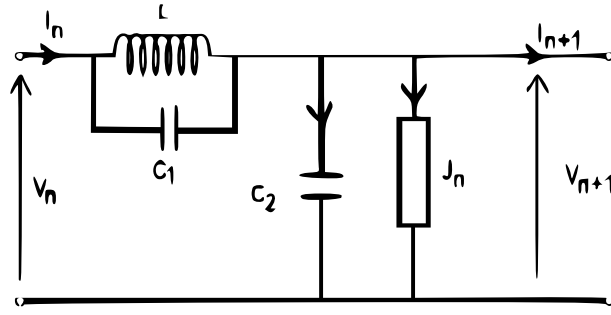


Figure 16: Schematic representation of the nonlinear electrical transmission line with Josephson junction

The law of the nodes leads to the following relation:

$$i_n = i_L + i_{C_1}, \quad (2.106)$$

$$i_{n+1} = i_{L_1} + i_{C_1} - i_{C_2} - J_n, \quad (2.107)$$

The law of meshes gives us the following relation:

$$V_{n-1} - V_n = V_{C_1}, \quad (2.108)$$

$$V_{n-1} - V_n = V_L, \quad (2.109)$$

$$V_n = V_{C_1} + V_{C_2}, \quad (2.110)$$

with,

$$V_n = \frac{d\phi_n}{dt}. \quad (2.111)$$

By combining the three equations, then replacing Josephson's current J_n by $J_0 \sin\left(2\frac{\pi\phi_n}{\phi_0}\right)$ we deduce the following equation:

$$\frac{\phi_{n-1} - 2\phi_n + \phi_{n+1}}{L} + C_1 \frac{d^2}{dt^2} (\phi_{n-1} - 2\phi_n + \phi_{n+1}) + C_2 \frac{d^2\phi_n}{dt^2} + J_0 \sin\left(2\frac{\pi\phi_n}{\phi_0}\right) = 0, \quad (2.112)$$

By setting $\omega_0^2 = \frac{1}{L_1 C_1}$, $\mu_0^2 = \frac{C_2}{C_1}$, and the plasma frequency $\omega_j = \sqrt{2\pi J_0 / C_1 \phi_0}$, $\phi_0 = 2.064 \times 10^{-15} T m^2$.

The characteristic frequency of the oscillations, then by changing the variable we get:

$$\frac{d^2}{dt^2} (\phi_{n+1} - 2\phi_n + \phi_{n-1}) + \omega_0^2 (\phi_{n+1} - 2\phi_n + \phi_{n-1}) + \mu_0 \frac{d^2 \phi_n}{dt^2} + \omega_j^2 \sin(\phi_n) = 0 \quad (2.113)$$

Whose physical parameters of the isolated Josephson junction are given : $C_1 = 1 pF$; $L_1 = 470 \mu H$; $J_0 = 100 nA$; $\phi_0 = 2.064 \times 10^{-15} T m^2$.

For a chain of N identical cells, we obtain a set of n coupled non-linear differential equations, assuming the distances between the meshes very small and making the Taylor expansion in the neighborhood of ϕ_n led to the fully integrable sine-Gordon equation. The equation obtained from sine-Gordon being fully integrable, which justifies that the energy obtained is conserved during propagation. As indicated in the Hamiltonian below:

$$H = \sum_n \left[\frac{1}{2} \mu_0 \left(\frac{d\phi_n}{dt} \right)^2 + \frac{1}{2} \left(\frac{d}{dt} (\phi_n + \phi_{n+1}) \right)^2 + \frac{1}{4} \omega_0^2 (\phi_n - \phi_{n+1})^2 \times (\phi_{n-1} - \phi_n)^2 \right] - \sum_n [\omega_j \cos(\phi_n)]. \quad (2.114)$$

Thus, the energy to be propagated in this line is also localized, it is the result of the balance between the effects of the dispersion brought by the first term of the equation and the strong nonlinearity introduced by the Josephson Junction current represented in the equation by the term of degree three which comes from the third order approximation of sine. This aspect is also revealed in the dispersion relation, which we now derive. To obtain an analytical treatment of the nonlinear wave that the model of (2.113) can possess, the reductive (quasi-discrete) perturbation method will be applied as follows [47].

To do so, it is considered (2.113) in case of low-amplitude waves ($\phi_n \ll 1$). Mathematically, that is to say that we are going to develop the sine function with the order two $\sin(\phi_n) = \phi_n - \frac{1}{6} \phi_n^3$, which allows us to obtain the following equation :

$$\frac{d^2}{dt^2} (\phi_{n+1} - 2\phi_n + \phi_{n-1}) + \omega_0^2 (\phi_{n+1} - 2\phi_n + \phi_{n-1}) + \mu_0 \frac{d^2 \phi_n}{dt^2} + \omega_j^2 \phi_n - \frac{\omega_j^2}{6} \phi_n^3 = 0. \quad (2.115)$$

We know that this equation (2.11) admit a planar wave solution of small amplitude ($\phi_0 \ll 1$) in the following form $\exp(i\theta_n)$, with $\theta_n = kn - \omega t$, where n , ω , k respectively the position, the angular frequency and the wave number. We place ourselves in the case where the amplitude of the previous plane wave is nonlinear and associated with a quasi-discrete envelope, then we use the method of reduction by the perturbation in the quasi-discrete limit in equation (2.115). According to the authors [47], the solution of (2.115) is assumed to have the following general form :

$$\phi_n = \epsilon \phi_1(x, \tau) \exp(i\theta_n) + \epsilon^2 \phi_{02}(x, \tau) + \epsilon^2 \phi_2(x, \tau) \exp(2i\theta_n) + \dots + c.c., \quad (2.116)$$

cc the conjugate complex of the preceding term, ϵ a positive parameter related to the amplitude of the soliton such as: $\epsilon \ll 1$. ϕ_1 ; ϕ_{02} ; ϕ_2 and their respective conjugate complex are unknown functions, representing the small variations of the envelope which, respectively depend on :

$$x = \epsilon (n - v_g t), \quad \tau = \epsilon^2 t \quad (2.117)$$

By introducing this form of solution Eq. (2.116) in Eq. (2.115) and adopting ($\frac{\partial}{\partial t} = \frac{\partial}{\partial \tau} \cdot \frac{\partial \tau}{\partial t} + \frac{\partial}{\partial x} \cdot \frac{\partial x}{\partial t} = \epsilon^2 \frac{\partial}{\partial \tau} - \epsilon v_g \frac{\partial}{\partial x}$), we obtain the algebraic equations around the terms: $\epsilon^p \phi_1^s(x, \tau) e^{q i(kn - \omega t)}$ with p and q integer. From the factors $\epsilon^1 \phi_1(x, \tau) e^{i(kn - \omega t)}$, $\frac{\partial}{\partial x} \phi_1(x, \tau) e^{i(kn - \omega t)}$ and $\frac{\partial^2}{\partial x^2} \phi_1(x, \tau) e^{i(kn - \omega t)}$ we deduce respectively the dispersion relation, the speed of the group and the envelope propagation equation in the conventional transmission line with Josephson junction, from the multiscale expansion after collecting all the terms in the form below set to zero.

2.3.3 Linear analysis: Linear dispersion and group velocity

Given that a planar wave solution of small amplitude ($\phi_0 \ll 1$) in the following form $\phi_n = \phi_0 e^{i(kx - \omega t)}$, with x ; ω ; k respectively the position, the angular frequency and the wave number. By using the perturbation of Eq.(2.116), in the order ϵ^1 , we derive the following algebraic equation :

$$\begin{aligned} \epsilon^1 \phi_1(x, \tau) e^{i(kn - \omega t)} & : 4\omega_0^2 (\sin(k/2))^2 \phi_1(x, \tau) - \mu_0^2 \phi_1(x, \tau) \omega^2 + \omega_j^2 \phi_1(x, \tau) \\ & - 4\phi_1(x, \tau) (\cos(k/2))^2 \omega^2 + 4\phi_1(x, \tau) \omega^2 \end{aligned} \quad (2.118)$$

To the above algebraic equation, we derive the following dispersion relation below :

$$\omega^2 = -\frac{4 \sin^2 \left(\frac{k}{2}\right) \omega_0^2 - \omega_j^2}{\mu_0 - 4 \sin^2 \left(\frac{k}{2}\right)}. \quad (2.119)$$

From the linear dispersion relation Figure 17 (a), the wave number is taken in the first Brillouin zone ($0 \leq k \leq \pi$). Therefore, it is revealed two cut off frequencies given by $\omega_{min} = \sqrt{\frac{\omega_j^2 - 4\omega_0^2}{\mu_0 - 4}}$ and $\omega_{max} = \sqrt{\frac{\omega_j^2}{\mu_0}}$ respectively. Which leads to the following respective frequencies:

$$f_{min} = \frac{1}{2\pi} \sqrt{\frac{\omega_j^2 - 4\omega_0^2}{\mu_0 - 4}} \quad (2.120)$$

;

$$f_{max} = \frac{1}{2\pi} \sqrt{\frac{\omega_j^2}{\mu_0}} \quad (2.121)$$

.

It follows from this result that, the width of the permitted band depends on the value of the inductance, for a very large inductance value compared to the capacity of the dielectric, the permitted band is zero and we have an insulator.

By using the following perturbation of Eq.(2.116), in the order ϵ^2 , we derive the following algebraic equation :

$$\begin{aligned} \epsilon^2 \frac{\partial}{\partial x} \phi_1(x, \tau) e^{i(kn - \omega t)} &: -2\omega_0^2 \sin(k) \frac{\partial}{\partial x} \phi_1(x, \tau) + 2\mu_0^2 \omega \left(\frac{\partial}{\partial x} \phi_1(x, \tau) \right) v_g \\ &- 2 \sin(k) \left(\frac{\partial}{\partial x} \phi_1(x, \tau) \right) \omega^2 + 8 \left(\frac{\partial}{\partial x} \phi_1(x, \tau) \right) (\cos(k/2))^2 i\omega v_g \\ &- 8\omega \left(\frac{\partial}{\partial x} \phi_1(x, \tau) \right) v_g \end{aligned} \quad (2.122)$$

To the above algebraic equation, we derive the following group velocity :

$$v_g = \frac{(\omega^2 - \omega_0^2) \sin(k)}{\omega \left(4 \cos^2 \left(\frac{k}{2}\right) + \mu_0 - 4 \right)}. \quad (2.123)$$

We note that in the figure 17b, the speed of the group is zero at the two extremes of frequency f_{min} and f_{max} , however this speed reaches its maximum value for $k = \frac{\pi}{2}$. We also note that, the speed of the group is positive in all the allowed frequency band, which is also completely in phase with the theoretical predictions.

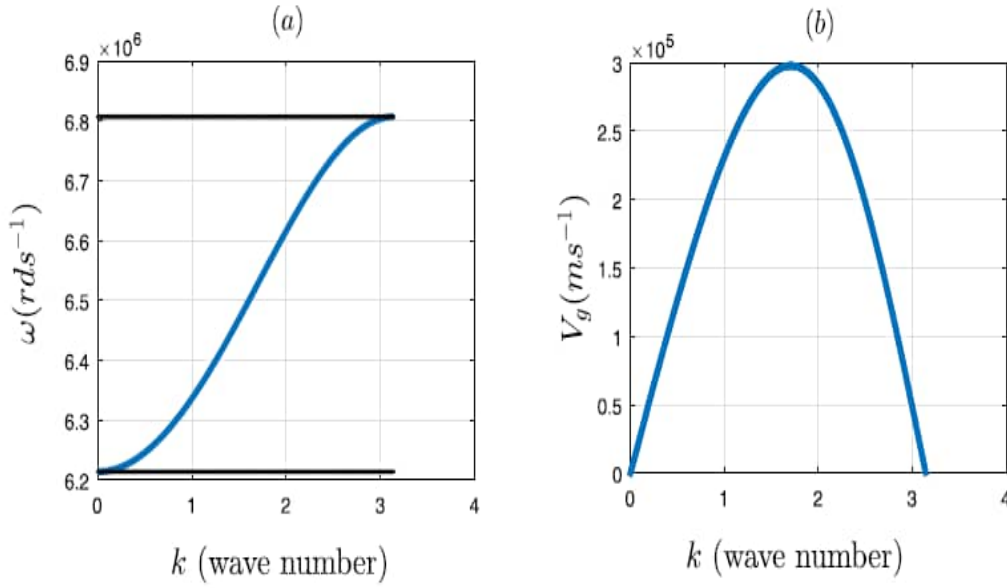


Figure 17: (a) is the plot of the dispersion relation versus wave number and (b) the group velocity versus wave number at $J = 200nA$, $L_1 = 480\mu H$, $C_1 = 1pF$, $C_2 = 2pF$.

2.3.4 2.2.2.3 Nonlinear analysis: NLS equation and soliton solution

By using the perturbation of Eq.(2.116), in the order ϵ^3 we derive the following algebraic equation :

$$\begin{aligned}
\epsilon^3 \frac{\partial^2}{\partial x^2} \phi_1(x, \tau) e^{i(kn - \omega t)} & : -\omega_0^2 \cos(k) \frac{\partial^2}{\partial x^2} \phi_1(x, \tau) + \mu_0^2 \left(-2i\omega \frac{\partial}{\partial \tau} \phi_1(x, \tau) \right) \\
& + \mu_0^2 \left(\left(\frac{\partial^2}{\partial x^2} \phi_1(x, \tau) \right) v_g^2 \right) - \omega_j^2 \phi_{11}(x, \tau) (\phi_1(x, \tau))^2 \\
& + 4 \left(\frac{\partial^2}{\partial x^2} \phi_1(x, \tau) \right) (\cos(k/2))^2 v_g^2 - 8 \left(\frac{\partial}{\partial \tau} \phi_1(x, \tau) \right) \\
& \times (\cos(k/2))^2 i\omega - \cos(k) \left(\frac{\partial^2}{\partial x^2} \phi_1(x, \tau) \right) \omega^2 \\
& - 4 \left(\frac{\partial^2}{\partial x^2} \phi_1(x, \tau) \right) \sin(k) \omega v_g - 4 \left(\frac{\partial^2}{\partial x^2} \phi_1(x, \tau) \right) v_g^2 \\
& + 8i\omega \frac{\partial}{\partial \tau} \phi_1(x, \tau), \tag{2.124}
\end{aligned}$$

To the above algebraic equation, we derive the following nonlinear Schrödinger equation :

$$i\partial_\tau \phi_1 + P\partial_{xx} \phi_1 + Q|\phi_1|^2 \phi_1 = 0, \tag{2.125}$$

with P and Q the dispersion and nonlinearity coefficient respectively and depend of the frequency or the wave number through the dispersion relation, given by the following expressions

$$P = \frac{\left((4 \cos^4 \left(\frac{k}{2}\right) - 4 - 2\mu_0 \cos^2 \left(\frac{k}{2}\right) + \mu_0) \omega^2 + \omega_0^2 (-4 \cos^2 \left(\frac{k}{2}\right) + 4 \cos^4 \left(\frac{k}{2}\right)) \right) (\omega^2 - \omega_0^2)}{(4 \cos^2 \left(\frac{k}{2}\right) + \mu_0 - 4)^2 \omega^3}. \quad (2.126)$$

it is also known that the dispersion coefficient P can be found straightforward using the formula

$$P = \frac{1}{2} \frac{\partial^2 \omega}{\partial k^2} :$$

$$Q = \frac{1}{4 \omega} \frac{\omega_j^2}{(4 \cos^2 \left(\frac{k}{2}\right) + \mu_0 - 4)}, \quad (2.127)$$

The most significant parameters related to the plane wave propagation in NETLs are: the dispersion Eq.(2.119), the group velocity $v_g = d\omega/dk$ Eq.(2.123), the phase velocity $v_g = d\omega/dk$, the dispersion coefficient Eq.(2.126), the nonlinearity coefficient Eq.(2.23). Thus, in order to understand the evolution of these different parameters as a function of time, we will first make a linear analysis, then a non-linear analysis of these parameters and finally we will present the solution of the solitons derived from the NLS obtained.

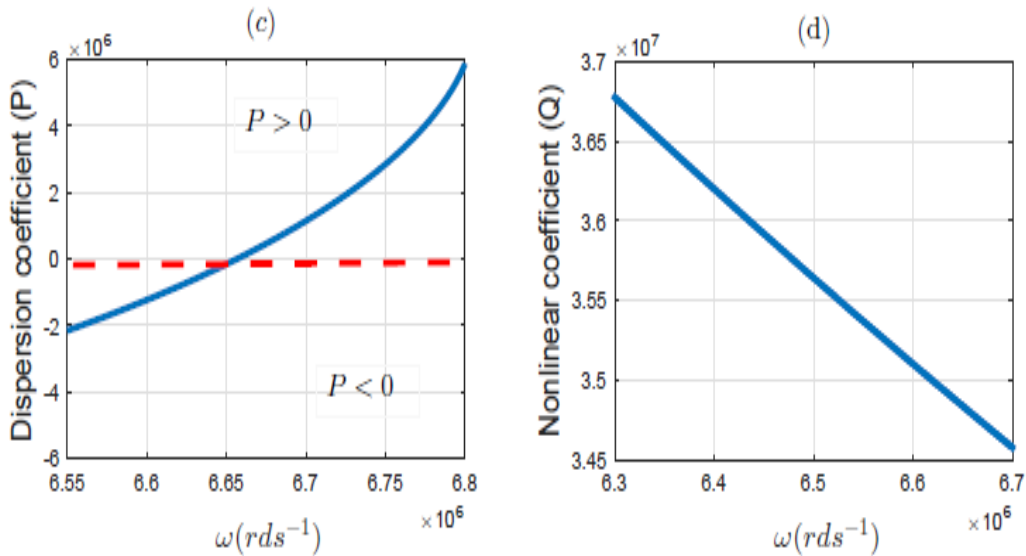


Figure 18: (a) is the plot of the dispersion coefficient and (b) nonlinearity coefficient at $J = 200nA$, $L_1 = 480\mu H$, $C_1 = 1pF$, $C_2 = 2pF$.

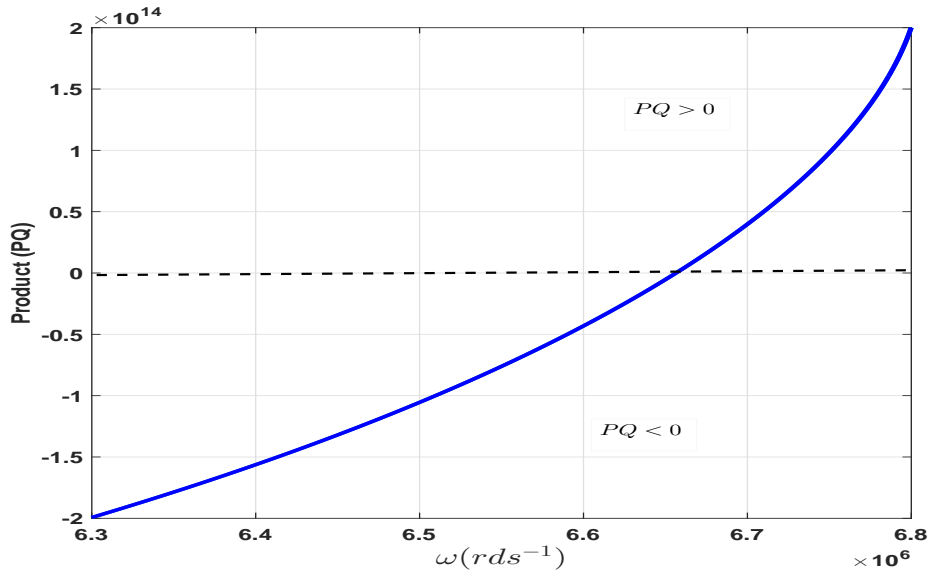


Figure 19: Illustration of the bright ($6.3 \times 10^8 \text{kHz} < f < 6.655 \times 10^8 \text{kHz}$) and dark ($6.656 \times 10^8 \text{kHz} < f < 6.8 \times 10^8 \text{kHz}$) formation areas depending on the sign of the product (PQ) versus angular frequency at $J_0 = 200 \text{nA}$, $L_1 = 480 \mu\text{H}$, $C_1 = 1 \text{pF}$, $C_2 = 2 \text{pF}$.

We know that Eq.(2.125) is a NLSE which is fully integrable and therefore admits known soliton solutions. Several works have shown that depending on the sign of the product PQ , the NLSE equation admits either a bright soliton (which corresponds to a stable modulation) or a dark soliton (for an instability of the modulation). However, the type of soliton obtained depends on the sign of the product PQ , such that if $PQ > 0$ it admits a bright soliton solution, whereas if $PQ < 0$ one has a dark soliton solution. Thus, figure 18 (b) shows that Q is positive over the entire admitted band, so the sign of the product depends only on P . The observation of figure 18 (a), highlights two regimes of cutoff frequencies that correspond to a bright and dark formation. Thus, for ($6.3 \times 10^8 \text{kHz} < f < 6.655 \times 10^8 \text{kHz}$) the bright soliton is set up, while the dark soliton is formed at ($6.656 \times 10^8 \text{kHz} < f < 6.8 \times 10^8 \text{kHz}$). From the above curves (fig.19), $PQ > 0$ for frequency belonging to $6.3 \times 10^8 \text{kHz} < f < 6.655 \times 10^8 \text{kHz}$ and we have the following soliton Bright solution:

$$\phi_1(x, \tau) = \phi_0 \operatorname{sech}(\lambda(-v_g \tau + x)) e^{kx - \omega \tau} \quad (2.128)$$

Similarly, $PQ < 0$ for frequency belonging to $6.656 \times 10^8 \text{kHz} < f < 6.8 \times 10^8 \text{kHz}$ and we have the following soliton dark solution :

$$\phi_1(x, \tau) = \phi_0 \tanh(\lambda(-v_g \tau + x)) e^{kx - \omega \tau} \quad (2.129)$$

With $\lambda = \phi_0 \sqrt{|\frac{Q}{2P}|}$ the inverse of the width of the wave packet; $k = \frac{v_g}{2P}$ is the wave number of the soliton; $\omega = \frac{v_g v_p}{2P}$ the angular frequency; $\phi_0 = \sqrt{\frac{v_g^2 - v_g v_p}{2PQ}}$ wave amplitude [63]. Our model of NLSE being obtained and admitting several known solution for some condition in particular : the bright and dark soliton, the peregrine and the super rogue waves. It is a question for us to give the analytical representation of these different soliton and to verify the characteristics of their propagation in our line model. In the following paragraph, we will analyze the stability of our line in order to identify the areas of stability and instability, then the key parameters of control and to generate various models localized waves.

2.4 Modulation instability

The modulation instability is a fundamental phenomenon discovered independently by Lighthill [169] in 1965, by Benjamin and Feir in 1967 [170], by Zakharov (1968) and by Whitham (1974). Zakharov and Ostrovsky [171] have assembled and synthesized the beginnings of this instability which appears in various fields of physics such as hydrodynamics (it is in this context that we study it) but also nonlinear optics, plasma theory, laser beams and electromagnetic transmission lines for example. The modulation instability is a non-linear phenomenon which consists in the growth of a modulation (periodic structure at the start of a perturbation) superimposed on a continuous (or quasi-continuous) signal. The amplification of this modulation is due to the conjunction of a Kerr-type nonlinearity and the dispersion of the medium. When the evolution of the field is described by Schrödinger's nonlinear propagation equation. The modulation instability within an optical fiber can occur in the anomalous dispersion regime, but also in a normal dispersion regime with pumping close to the dispersion zero associated with conditions on the higher order dispersion coefficients. Indeed, in the normal dispersion regime, the combined effects of nonlinearity and dispersion tend to stabilize the continuous wave. However, there is a case where it is possible to obtain the MI process, when the pumping takes place close to the zero dispersion of the fiber (with conditions of dispersion

of the fiber (with conditions on higher dispersion orders). Modulation instability or modulation instability is an effect of reinforcement, by non-linearity, of a deformation of a periodic wave, leading to the generation of gain bands in the frequency spectrum. It can cause the wave to break into a train of pulses. It depends strongly on the frequency of the disturbance. At some frequencies, a disturbance will have little effect, while at others, the disturbance will grow exponentially. The expression of the gain spectrum can be obtained as detailed below. Random disturbances generally have a broad spectrum that will cause the generation of spectral bands that reflect the gain spectrum. Since modulation instability causes a signal to grow, it can be considered as a form of amplification: by injecting an input signal at the maximum frequency of the gain spectrum, it is possible to create an optical amplifier.

2.4.1 Definition

The modulation instability is an phenomena which arises from the interplay between dispersive and nonlinear effects and manifests itself in the exponential growth of weak perturbations [172, 173]. The gain leads to amplification of sidebands, which break up the otherwise uniform wave and generate fine localized structures. Thus, it may act as a precursor for the formation of solitons [169].

2.4.2 Some examples of modulation instability

The modulation stability phenomenon has been identified and studied in various physical systems, such as fluids, plasmas, nonlinear optics, metamaterials, discrete nonlinear systems, and BECs, to name a few [172–176]. However, the investigation criteria evolve according to the type of medium modeled and the phenomenon to be observed. It is a question here for us to present some existing approaches in the literature.

2.3.2.1 Modulation instability in the anharmonic Peyrard-Bishop model of DNA

Tabi et al. [174] studied the modulation instability in the PBD model. To do so, they considered the Salerno equation of the following DNA model:

$$i \frac{d\psi_n}{dt} + (P_1 + Q_1 |\psi_n|^2)(\psi_{n+1} + \psi_{n-1}) + Q_2 |\psi_n|^2 \psi_n = 0 \quad (2.130)$$

Where $P_1 = \frac{K}{2\omega_b}$, $Q_1 = \frac{\eta}{3\beta\omega_g^2 + 6\eta}$, $Q_2 = \frac{\eta + \beta\omega_g^2}{3\beta\omega_g^2 + 6\eta}$, $\omega_g = \frac{2a^2 D}{m}$, $\eta = \frac{b^2 S \rho}{m}$ and $K = \frac{k_1}{m}$.

Equation (2.26) has an exact plane-wave solution as

$$\psi_n(t) = \psi_0 \exp^{i(qn - \Lambda t)} \quad (2.131)$$

The wavenumber q , the angular frequency Λ and the amplitude ψ_0 satisfy the following dispersion relation:

$$\Lambda = 4P_1 \sin^2\left(\frac{q}{2}\right) - [2P_1 + (2Q_1 \cos(q) + Q_2)\psi_0^2] \quad (2.132)$$

To examine the linear stability of the initial plane waves, we look for a solution of the form:

$$\psi_n(t) = \psi_0[1 + B_n(t)] \exp^{i(qn - \Lambda t)} \quad (2.133)$$

where the perturbation amplitude $B_n(t)$ is assumed to be small in comparison with the carrier wave amplitude ψ_0 . Then, one obtains an algebraic equation describing the evolution of the perturbation $B_n(t)$. Furthermore, we assume a general solution of the above-mentioned system of the form :

$$B_n(t) = B_1 \exp^{i(Qn - \Omega t)} + B_2 \exp^{-i(Qn - \Omega^* t)} \quad (2.134)$$

where the asterisk denotes complex conjugation, Q and Ω represent, respectively, the wavenumber and the angular frequency of the perturbation amplitude and B_1 and B_2 are complex constant amplitudes.

Inserting this modulated solution into the equation describing the evolution of the perturbation and linearizing around the unperturbed plane wave, we obtain the linear homogeneous system for B_1 and B_2 :

$$\begin{pmatrix} a_{11} - \Omega & a_{12} \\ a_{21} & a_{22} + \Omega \end{pmatrix} \begin{pmatrix} B_1 \\ B_2 \end{pmatrix} = \begin{pmatrix} 0 \\ 0 \end{pmatrix} \quad (2.135)$$

The condition for the existence of non-trivial solutions of this linear homogenous system is given by a second order equation for the frequency Ω , that is :

$$(a_{11} - \Omega)(a_{22} - \Omega) - a_{12}a_{21} = 0 \quad (2.136)$$

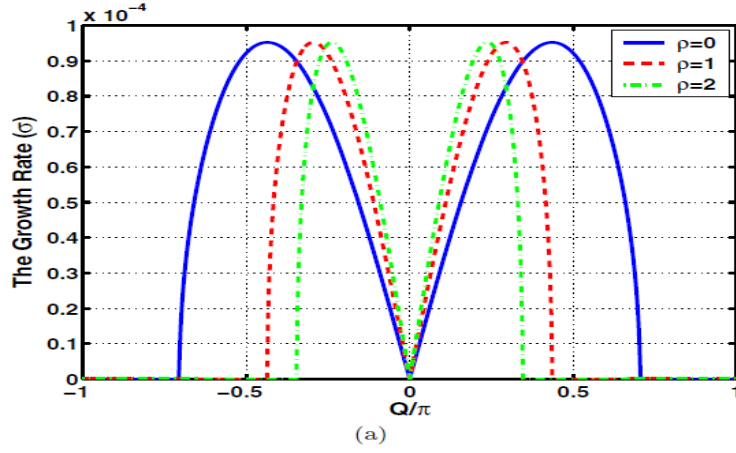


Figure 20: (Color online) Growth rate versus the wavenumber of the perturbation Q for $q = \frac{\pi}{8}$, $\omega_b = 1$, $S = 2.5 \times 10^{-12} eV$, $D = 0.05 eV$ and $b = 0.35 \times 10^{10}$. This has been plotted for three values of the anharmonic stacking coupling constant ρ . Note also that the carrier wave with $q = \frac{\pi}{8}$ and $\rho = 0$ is unstable to perturbation of any wavenumber.

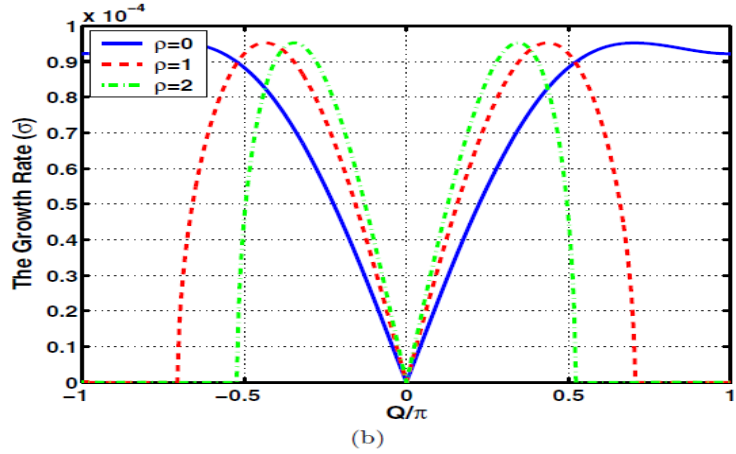


Figure 21: (Color online) Growth rate versus the wavenumber of the perturbation Q for $q = 0$, $\omega_b = 1$, $S = 2.5 \times 10^{-12}$, $D = 0.05 eV$ and $b = 0.35 \times 10^{10}$. This has been plotted for three values of the anharmonic stacking coupling constant ρ . Note also that the carrier wave with $q = \frac{\pi}{8}$ and $\rho = 0$ is unstable to perturbation of any wavenumber (blue line).

with

$$\begin{aligned}
a_{11} &= -2P_1[\sin(Q)\sin(q) - (\cos(Q) - 1)\cos(q)] \\
&\quad - 2Q_1|\psi_0^2|[\sin(Q)\sin(q) - \cos(Q)\cos(q)] + Q_2|\psi_0|^2 \\
a_{12} &= a_{21} = (2Q_1\cos(q) + Q_2)|\psi_0|^2 \\
a_{22} &= 2P_1[\sin(Q)\sin(q) + (\cos(Q) - 1)\sin(q)] \\
&\quad + 2Q_1|\psi_0^2|[\sin(Q)\sin(q) - \cos(Q)\cos(q)] + Q_2|\psi_0|^2
\end{aligned} \tag{2.137}$$

Equation (2.136) can be rewritten as:

$$\begin{aligned}
(\Omega^2) &= [\Omega + 2P_1\sin(Q)\sin(q) + 2Q_1|\psi_0|^2\sin(Q)\sin(q)]^2 \\
&= 16(P_1 + Q_1\psi_0^2)\sin^2\left(\frac{Q}{2}\cos(q)\right) \\
&\quad \times [(P_1 + Q_1\psi_0^2)\sin^2\left(\frac{Q}{2}\cos(q)\right) - (2Q_1\cos(q) + Q_2)|\psi_0|^2]
\end{aligned} \tag{2.138}$$

- If $(\Omega_1)^2$ is negative, two complex numbers are solutions of the above equation and the exponential growth takes place with rate :

$$\sigma(Q) = 4\sin\left(\frac{Q}{2}\right)\sqrt{(P_1 + Q_1\psi_0^2)[(2Q_1\cos(q) + Q_2)|\psi_0|^2]\sin^2\left(\frac{Q}{2}\cos(q)\right)\cos(q)} \tag{2.139}$$

This is possible if the initial amplitude $|\psi_0|$ exceeds the threshold amplitude $|\psi_{0cr}|$ defined as follows :

$$|\psi_0|^2 \geq |\psi_{0cr}|^2 = \frac{2P_1\sin^2\left(\frac{Q}{2}\right)\cos(q)}{2Q_1\cos^2\left(\frac{Q}{2}\right)\cos(q) + Q_2} \tag{2.140}$$

The obtained results show that, the stacking potential has an impact on the stability/instability region (the white regions represent the stability areas, while the hatched region indicates the instability area). Similarly, the modulation wave amplitude growth rates for carrier waves with three values of ρ are plotted in figure 20 and figure 21. It is shown that the instability growth rate can be dramatically affected by the stacking potential of PBDs. It is again clear that for the PB model ($\rho = 0$), the dynamics of the system has a large instability region (see blue lines

in figures 20 and 21), whereas in the case of the PBD model ($\rho = 1$ or $\rho = 2$), the instability growth rate is dramatically reduced by the anharmonicity of the stacking energy (see red and green lines in figures 20 and 21). For all these cases, the growth rate is maximum in general. On the other hand, the carrier wave with $q = \frac{\pi}{8}$ and $\rho = 0$ is unstable to perturbation of any wavenumber (see the blue line in figure 20).

2.3.2.2 Modulation Instability Analysis of an integrable model of (2+1)-Dimensional Heisenberg Ferromagnetic Spin Chain Equation

Inc and al. [175] studied the modulation instability in the following Heisenberg Ferromagnetic Spin Chain Equation describes the magnetic ordering in ferromagnetic materials :

$$iq_t + \alpha q_{xx} + \nu q_{yy} + \delta q_{xy} - \gamma \psi |q|^2 = 0, \quad i = \sqrt{-1}, \quad (2.141)$$

with $\alpha = \sigma^4(J + J_2)$, $\nu = \sigma^4(J_1 + J_2)$, $\delta = 2\sigma^4 J_2$, $\gamma = 2\sigma^4 A$.

Where x , t and y are the independent variables and $q(x; t; y)$ is the dependent variable. The term σ is the lattice parameter, J and J_1 are the coefficients of bilinear exchange interactions along the X and Y axis. J_2 refers to the neighboring interaction on the diagonal, while A denote the uniaxial crystal field anisotropy parameter. The HFSC describes the magnetic ordering in ferromagnetic materials.

We discuss the MI. In order to study the MI, we use the standard linear- stability analysis. Equation (2.141) has the perturbed steady-state solution of the form :

$$q(x, t, y) = \left(\sqrt{P_0} + a(x, y, t) \right) e^{i\phi_{NL}}, \quad \phi_{NL} = \gamma P x \quad (2.142)$$

where P_0 represent the incident power.

We investigate the evolution of the perturbation $a(x, t, y)$ using the concept of linear stability analysis. Substituting Eq.(2.142) into Eq.(2.141) and linearizing the result in $a(x, t, y)$, we acquire:

$$iq_t + \alpha q_{xx} + \nu q_{yy} + \delta q_{xy} - \gamma P_0(a + a^*) = 0 \quad (2.143)$$

The linear equation equation (2.143) can be solved in the frequency domain easily. But because of the a^* component, the Fourier terms at frequencies Ω and $-\Omega$ are coupled. So, we seek for

$$a(x, t, y) = a_1 e^{i(Kx + K_1 y - \Omega t)} + a_2 e^{-i(Kx + K_1 y - \Omega t)} \quad (2.144)$$

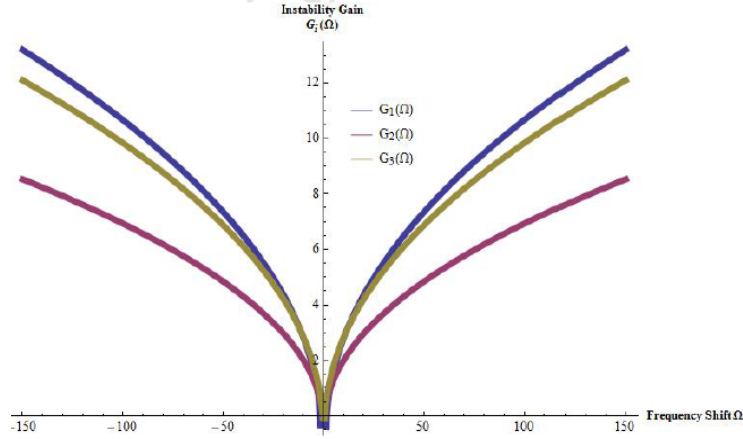


Figure 22: Gain spectra of modulation instability (growth rate) Eq.(2.44) for three values of the nonlinear length with $\gamma = 3$; $P_0 = (0,2; 0,4; 0,5)$; $k_1 = (0,85; 0,5; 0,2)$; $\delta = (0,8; 0,8; 0,9)$; $\mu = (1,7; 0,2; 2)$; $\alpha = (0,8; 2; 1)$:

where K is the wave number, Ω is the frequency and k_1 is transverse wave number of the perturbation respectively. Equations (2.144) and (2.143) give a set of two homogeneous equations in a_1 and a_2 . Substituting Eq.(2.144) into Eq.(2.143), separation the coefficients of $e^{i(Kx+K_1y-\Omega t)}$ and $e^{-i(Kx+K_1y-\Omega t)}$ and solving the result, we obtain the following dispersion relation as :

$$K = \frac{-\delta k_1 \pm \sqrt{\delta^2 k_1^2 - 4\alpha\gamma P_0 \pm 4\alpha\sqrt{\Omega^2 + \gamma^2 P_0^2}}}{2\alpha} \quad (2.145)$$

The dispersion relation equation (2.145) shows that steady-state stability depends on whether light experiences anomalous or normal group velocity dispersion inside the fiber.

- If $(\sqrt{\delta^2 k_1^2 - 4\alpha\gamma P_0 \pm 4\alpha\sqrt{\Omega^2 + \gamma^2 P_0^2}}) > 0$, the wave number K is real and the steady state is stable against small perturbations.
- If $(\sqrt{\delta^2 k_1^2 - 4\alpha\gamma P_0 \pm 4\alpha\sqrt{\Omega^2 + \gamma^2 P_0^2}}) < 0$ the wave number K is imaginary since the perturbation grows exponentially, the occurrence of modulation instability.

Thus, the growth rate of the modulation stability gain spectrum $g(\Omega)$ can be expressed as :

$$g(\Omega) = 2Im(K) = \frac{1}{\alpha} \sqrt{\delta^2 k_1^2 - 4\alpha\gamma P_0 \pm 4\alpha\sqrt{\Omega^2 + \gamma^2 P_0^2}} \quad (2.146)$$

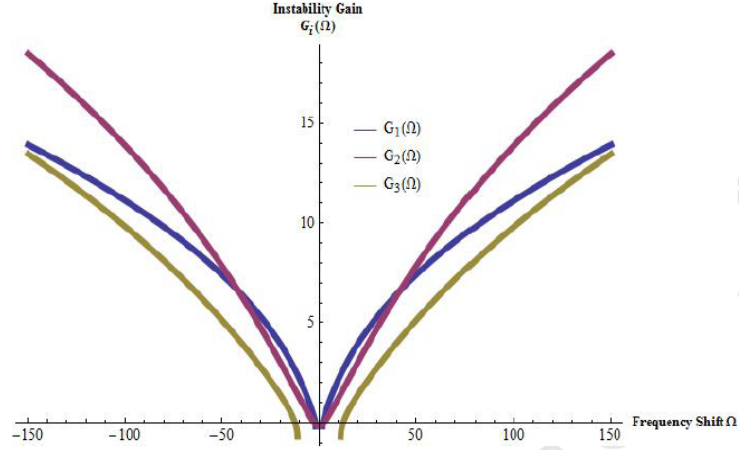


Figure 23: Gain spectra of modulation instability (growth rate) Eq.(2.44) for three values of the nonlinear length with $\gamma = 3$; $P_0 = (10; 15; 20)$; $k_1 = (0,85; 0,5; 0,2)$; $\delta = (0,8; 0,8; 0,9)$; $\mu = (1,7; 0,2; 2)$; $\alpha = (0,8; 2; 1)$:

The modulation-instability gain is significantly affected by the incident power P_0 . From figure 22 and figure 23, it can be seen that the MI growth rates will appear to disperse with increase in P_0 values. The main reason is due to increase in the gain along the fiber length because of the increase in incident power P_0 as shown in figure 23.

2.3.2.3 Modulation Instability Analysis in Dispersive Metamaterial

Inc and al. [141] studied the instability to the NLSE describing the propagation in dispersive metamaterial is given by :

$$\psi_x = -\frac{i \operatorname{sgn}(\beta_2)}{2} \psi_{tt} + \delta_3 \psi_{ttt} + i v N^2 \{ |\psi|^2 \psi + i s_1 (|\psi|^2 \psi)_t - \tau_r \psi (|\psi|^2)_t \} \quad (2.147)$$

We suppose that Equation (2.147) has the perturbed steady-state solution of the form :

$$\psi(x, t) = \left(\sqrt{P_0} + a(x, y, t) \right) e^{i\phi_{NL}}, \quad \phi_{NL} = \gamma P_0 x \quad (2.148)$$

where P_0 represent the incident power.

We investigate the evolution of the perturbation $a(x; t)$ using the concept of linear stability analysis. Substituting Equation (2.148) into equation (2.147) and linearizing the result in $a(x; t)$, we acquire :

$$a_x = -i\mu a_{tt} + i\{\gamma P_0(a + a^*) + i s_1 \gamma P_0(2a_t + a_t^*) + \tau \gamma P_0(a_t + a_t^*)\} = 0 \quad (2.149)$$

Because of the ρ^* component, the Fourier terms at frequencies Ω and $-\Omega$ are coupled. So, we seek for :

$$\rho(t, x, z) = a_1 e^{i(Kx - \Omega t)} + a_2 e^{-i(Kx - \Omega t)} \quad (2.150)$$

where K is the wave number, is the frequency of the perturbation respectively. We give a set of two homogeneous equations in a_1 and a_2 .

Substitution Eq.(2.150) into Eq.(2.149), we get the following system of equations for a_1 and a_2 upon separating the coefficients of $e^{i(Kx - \Omega t)}$ and $e^{-i(Kx - \Omega t)}$

$$\begin{aligned} K a_2 + \mu \Omega^2 a_2 + \gamma a_1 P_0 + \gamma a_2 P_0 - i \gamma \tau \Omega a_1 P_0^2 - i \gamma \tau \Omega a_2 P_0^2 - \gamma \Omega a_1 P_0^2 s_1 - 2 \gamma \Omega a_2 P_0^2 s_1 &= 0 \\ - K a_1 + \mu \Omega^2 a_1 + \gamma a_1 P_0 + \gamma a_2 P_0 - i \gamma \tau \Omega a_1 P_0^2 - i \gamma \tau \Omega a_2 P_0^2 + \gamma \Omega a_1 P_0^2 s_1 + 2 \gamma \Omega a_2 P_0^2 s_1 &= 0 \end{aligned} \quad (2.151)$$

From Eq.(2.151), one can easily obtain the following coefficient matrix of a_1 and a_2 :

$$\begin{pmatrix} \Gamma_{11} & \Gamma_{12} \\ \Gamma_{21} & \Gamma_{22} \end{pmatrix} \begin{pmatrix} a_1 \\ a_2 \end{pmatrix} = \begin{pmatrix} 0 \\ 0 \end{pmatrix} \quad (2.152)$$

$$\Gamma_{11} = \gamma P_0 (1 + P_0 (-i \tau \Omega - \Omega s_1)), \quad (2.153)$$

$$\Gamma_{12} = (K + \mu \Omega^2 + \gamma P_0 + \gamma \Omega P_0 (-i \tau - 2 s_1)),$$

$$\Gamma_{21} = (-K + \mu \Omega^2 + \gamma P_0 + \gamma \Omega P_0 (i \tau + 2 s_1)),$$

$$\Gamma_{22} = \gamma P_0 (1 + \Omega P_0 (i \tau + s_1))$$

The coefficient matrix Eq.(2.152) has a nontrivial solution if the determinant vanishes. By expanding the determinant, we obtain the following dispersion relation

$$\begin{aligned} K^2 - \mu^2 \Omega^4 - 2 \gamma \mu \Omega^2 P_0 - 2 i \gamma \tau K \Omega P_0^2 - 4 K \gamma \Omega P_0^2 s_1 + 2 i \gamma^2 \tau \Omega^2 P_0^2 s_1 \\ + 3 \gamma^2 \Omega^2 P_0^4 s_1^2 = 0 \end{aligned} \quad (2.154)$$

The dispersion relation Equation (2.154) has the following solutions

$$\begin{aligned} K &= i \gamma \tau \Omega P_0^2 + 2 \gamma \Omega P_0^2 s_1 \\ &\pm \sqrt{\mu^2 \Omega^4 + 2 \gamma \mu \Omega^2 P_0 - \gamma^2 \tau^2 \Omega^2 P_0^4 + 2 i \gamma^2 \tau \Omega^2 P_0^4 s_1 + \gamma^2 \Omega^2 P_0^4 s_1^2} \end{aligned} \quad (2.155)$$

The stability of the steady state is determined by equation (2.154).

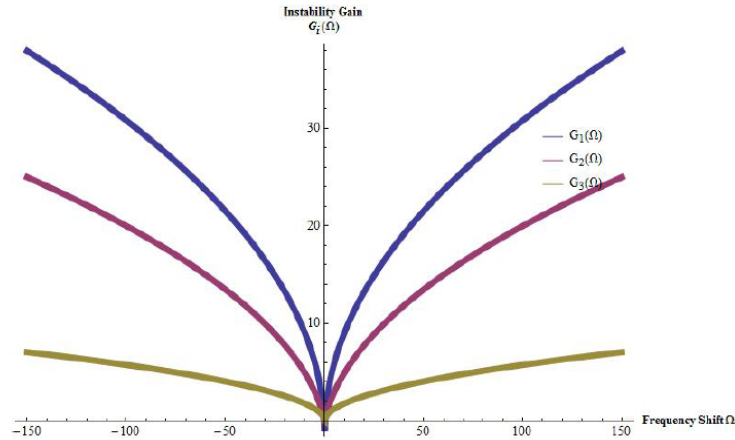


Figure 24: Gain spectra of modulation instability (growth rate) Eq.(55) for three values of the nonlinear length with $\gamma = 3$; $P_0 = (0,2; 0,4; 0,5)$; $k_1 = (0,85; 0,5; 0,2)$; $\delta = (0,8; 0,8; 0,9)$; $\mu = (1,7; 0,2; 2)$; $\alpha = (0,8; 2; 1)$

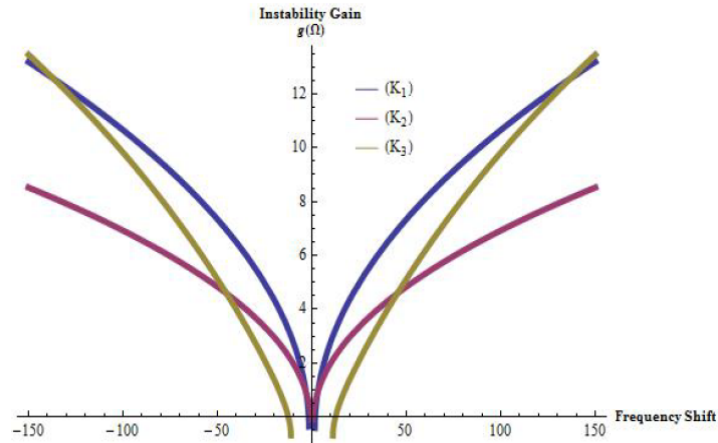


Figure 25: Gain spectra of modulation instability (growth rate) Eq.(55) for three values of the nonlinear length with $\gamma = 3$; $P_0 = (10; 15; 20)$; $k_1 = (0,85; 0,5; 0,2)$; $\delta = (0,8; 0,8; 0,9)$; $\mu = (1,7; 0,2; 2)$; $\alpha = (0,8; 2; 1)$:

- If K has an imaginary part, the steady-state solution is unstable since the perturbation grows exponentially.
- If the wave number K is real, the steady state is stable against small perturbations. It can be seen from equation (2.53) that the modulation always exists because the imaginary part $Im(K) \neq 0$: Finally, we obtain the MI gain spectrum as

$$g(\Omega) = 2Im(K) = 2\{i\gamma\tau\Omega P_0^2 + 2\gamma\Omega P_0^2 s_1 \pm \sqrt{\mu^2\Omega^4 + 2\gamma\mu\Omega^2 P_0 - \gamma^2\tau^2\Omega^2 P_0^4 + 2i\gamma^2\tau\Omega^2 P_0^4 s_1 + \gamma^2\Omega^2 P_0^4 s_1^2}\} \quad (2.156)$$

The modulation instability gain is significantly affected by the incident power P_0 . From figure 24 and figure 25, it can be seen that the MI growth rates will appear to disperse with increase in P_0 values. The main reason is due to increase in the gain along the fiber length as a result of the increase in incident power P_0 .

2.4.3 Modulation instability of our system

In this part of our work, we wish to test the modulation instability of our system based on the NLS equation (2.125). For this purpose, we consider the plane wave solution of this equation in the form :

$$\phi_1 = \phi_{10} e^{i\phi_{20}\tau}. \quad (2.157)$$

With $\phi_{20} = Q|\phi_{10}|^2$.

Where ϕ_{10} and ϕ_{20} is respectively the amplitude and the frequency of the carrier waves.

Thus we perturb the amplitude of the plane wave solution in the following form :

$$\phi_1 = (\phi_{10} + \epsilon\phi_{11}) e^{i\phi_{20}\tau} \quad (2.158)$$

with $\phi_{11} = \phi_{12} e^{i(Kx + \Omega\tau)} + cc$, where the wave number and the angular frequency perturbation are given respectively by K and Ω . While ϕ_{12} is a constant representing the amplitude of the disturbance.

When we introduce this perturbation into Equation (2.125) and separate the real and imaginary

parts, then after collecting in the terms in power of ϵ and solving the system, we obtain the following dispersion relation:

$$\Omega^2 = P^2 K^2 (K^2 - 2\frac{Q}{P}|\phi_{10}|^2) \quad (2.159)$$

The obtained dispersion relation Eq.(2.159) depends on the ratio Q/P .

- If $Q/P < 0$, $(K^2 - 2\frac{Q}{P}|\phi_{10}|^2)$ will always be positive, which means that the angular frequency of perturbation will be real. Thus the perturbation will not generate an instability of the plane wave. The plane wave is said to be modulationally stable.
- If $Q/P > 0$, $(K^2 - 2\frac{Q}{P}|\phi_{10}|^2)$ will be negative and for these values of K , the angular frequency of the perturbation Ω will be complex. Thus for certain values of the wavenumber K , the frequency of the perturbation will increase exponentially leading to the instability of the plane wave. The plane wave is said to be modulationally unstable.

Let's continue with the case where $Q/P > 0$, that is to say $(K^2 - 2\frac{Q}{P}|\phi_{10}|^2) < 0$ and let's look for the value of K corresponding to this zone of instability of the wave modulation:

$$K < \sqrt{\frac{2Q}{P}|\phi_{10}|^2} \quad (2.160)$$

The maximum value reached in this zone of instability is by K is $K_c = \sqrt{\frac{2Q}{P}|\phi_{10}|^2}$ and this value is called the critical value of the modulation wave number and ϕ_{10} is the amplitude of plane initial wave.

In this condition the growth rate is reading as [22] :

$$\Gamma_{gr} = |P|K^2 \sqrt{\frac{K_c^2}{K^2} - 1}, \quad (2.161)$$

2.5 Conclusion

In short, we have presented the methodology that will guide our research. To do so, we first presented the modeling process that led to the nonlinear transmission line model that will support our study. Using Kirchhoff's laws for the n^{th} rank mesh, the line leads to a discrete second order equation. This discrete equation after using the reductive perturbation method in the semi-discrete approximation will lead to different order of perturbation one, two and

three, to the dispersion, group velocity and simple 1-NLSE respectively. The dispersion and nonlinearity curves show that this equation admits two types of solitons, namely dark and bright solitons. These solitons can present a modulation instability. For this, a method of investigation of the modulation instability of the model has been presented, after having presented some existing methods of investigation. It is also established that this equation admits for certain values of the system parameters, solutions of well known modulated waves of type rogue and peregrine waves and other localized wave profiles. It appears from this presentation that the use of the Josephson junction parameters, in particular the plasma frequency, is a key parameter for the stability of the line and the increase of the bandwidth at very high frequencies. This observation comes from the contribution of this parameter on the coefficient of nonlinearity of the equation, which allows the increase of the nonlinearity of the line and also gives the possibility of obtaining a multitude of localized waves depending on the choice of model. We will use the numerical method, in particular with the MATLAB ODE solver software, to verify the analytical results of the propagated profiles. In the next chapter, we will discuss the different models of localized waves propagated in a nonlinear electrical transmission line with Josephson junction and the instability of the system.

Chapter 3

Results and Discussions

3.1 Introduction

The study of the propagation of localized waves in nonlinear power lines continues to arouse interest since the work of the pioneers Hirota and Suzuki [5]. Indeed, a succession of numerical and analytical works followed with great satisfaction, in particular on the dynamics of localized waves in NETLs [142, 177, 178]. The analysis of various excitations in highly nonlinear media such as the resolution of quantum mechanical problems, plasma waves, the control of medical systems, signal transport and communication means find their salvation through NETLs [22–25, 179]. Indeed, a NETL is a circuit in which we can incorporate various components such as: capacitors, inductors and JJs that provide a non-linear response to current and voltage. It is therefore a favorable environment for the synthesis of soliton propagation, PS, SRW, and others. Several works have allowed the propagation of bright and dark solitary waves with the NLS equation as propagation support in the presence of weak nonlinearity and dispersion in NETLs [36, 67, 176, 180–183].

Thus, nowadays, in order to overcome the problem of data transfer, which are more and more important, a recourse is made to superconducting components. However, almost all electronic superconductors are based on JJs. Because of its high nonlinearity, the nonlinear electrical transmission line with JJs has been the subject of various works especially in the field of superatransmission. The use of high nonlinearity components has allowed the propagation of new localized wave profiles at very high frequencies, such as PSs, SRWs and other exotic

wave patterns in the presence of a modulation instability. RWs and PSs, responsible for a large number of maritime disasters, have been highlighted in various studies over the decades [88,184–189]. Indeed, as for all nonlinear and dispersive systems, NETLs have a modulation instability. Thus, for transverse line perturbations, the exact cutoff frequencies of the growth rate have been revealed and the modulation instability gain spectrum of solitary wave instabilities has been obtained for left-handed lines [47,48,173]. However, no work has been done to propagate rational solitons at very high frequency in straight handlines, while these have multiple applications. In this chapter, we first use the linearization technique and small perturbations to study the unstable or stable region of the modulated wave propagation in the structure. For this, we use the effect of the plasma frequency as well as other system parameters. Next, we will perform the analytical study of solitary waves such as the bright soliton and the dark soliton. As we mentioned in chapter 2, we propagate soliton solutions, such as Peregrine soliton and super rogue wave, and we describe their analytical behavior. Then we will verify the analytical results by a numerical method.

3.2 Application of the methods

This section apply the methods described above to construct exact traveling-wave solutions of the conformable derivative nonlinear differential equation governing wave propagation in electrical transmission line. To obtain the NODE, we used the conformable derivative properties. Assuming $u(x, t) = U(\xi)$ and (1) becomes

$$[(1 + b_1U + b_2U^2)k_2^2 - u_0^2k_1^2] U'' + (b_1 + 2b_2U)k_2^2U'^2 - \frac{1}{12}u_0^2\delta^2k_1^4U^{(4)} = 0. \quad (3.1)$$

Where $U = U(\xi)$.

3.2.1 On solving the nonlinear differential governing low-pass electrical transmission lines by using the new extended direct algebraic method

Employing the homogeneous balance principle to Eq.(3.1), gives $N = 1$. Thus, Eq.(2.4) can be expressed

$$U(\xi) = g_0 + g_1 Q(\xi), \quad (3.2)$$

Substituting Eq.(3.2) and Eq.(2.5) into Eq.(3.1), we obtained a set of algebraic equation in terms of $Q^j(\xi)$. After setting all the terms obtained to zero, and then with the aid of Maple, we recovered the following results.

S1: for $\mu^2 - 4\lambda\sigma < 0$ and $\sigma \neq 0$, it is obtained

$$g_0 = g_0, \quad g_1 = g_1, \quad b_1 = -\frac{1}{12} \frac{g_1^2 (\mu^2 - 4\lambda\sigma)^2 (g_1 \mu - 2g_0 \sigma) \delta^2 (Ln(A))^2}{u_0^2 (8g_1^2 \lambda \sigma - 12g_1 g_0 \mu \sigma + g_1^2 \mu^2 + 12g_0^2 \sigma^2) (-g_1^2 \lambda + g_1 g_0 \mu - g_0^2 \sigma)},$$

$$b_2 = -\frac{1}{12} \frac{g_1^2 (\mu^2 - 4\lambda\sigma)^2 \delta^2 (Ln(A))^2 \sigma}{u_0^2 (8g_1^2 \lambda \sigma - 12g_1 g_0 \mu \sigma + g_1^2 \mu^2 + 12g_0^2 \sigma^2) (-g_1^2 \lambda + g_1 g_0 \mu - g_0^2 \sigma)}, \quad k_1 = \frac{\sqrt{-\frac{\mu^2 - 4\lambda\sigma}{8g_1^2 \lambda \sigma - 12g_1 g_0 \mu \sigma + g_1^2 \mu^2 + 12g_0^2 \sigma^2}} g_1}{u_0},$$

$$k_2 = -\sqrt{-\frac{\mu^2 - 4\lambda\sigma}{8g_1^2 \lambda \sigma - 12g_1 g_0 \mu \sigma + g_1^2 \mu^2 + 12g_0^2 \sigma^2}} g_1$$

$$u_{11}(x, t) = g_0 + g_1 \left[\frac{-\mu}{2\sigma} + \frac{\sqrt{-(\mu^2 - 4\lambda\sigma)}}{2\sigma} \tan_A \left(\frac{\sqrt{-(\mu^2 - 4\lambda\sigma)}}{2} \xi \right) \right], \quad (3.3)$$

$$u_{12}(x, t) = g_0 + g_1 \left[-\frac{\mu}{2\sigma} + \frac{\sqrt{-(\mu^2 - 4\lambda\sigma)}}{2\sigma} \cot_A \left(\frac{\sqrt{-(\mu^2 - 4\lambda\sigma)}}{2} \xi \right) \right], \quad (3.4)$$

$$u_{13}(x, t) = g_0 + g_1 \left[-\frac{\mu}{2\sigma} + \frac{\sqrt{-(\mu^2 - 4\lambda\sigma)}}{2\sigma} \tan_A \left(\sqrt{-(\mu^2 - 4\lambda\sigma)} \xi \right) \right]$$

$$\pm g_1 \left[\frac{\sqrt{-pq(\mu^2 - 4\lambda\sigma)}}{2\sigma} \sec_A \left(\sqrt{-(\mu^2 - 4\lambda\sigma)} \xi \right) \right], \quad (3.5)$$

$$u_{14}(x, t) = g_0 + g_1 \left[-\frac{\mu}{2\sigma} - \frac{\sqrt{-(\mu^2 - 4\lambda\sigma)}}{2\sigma} \cot_A \left(\sqrt{-(\mu^2 - 4\lambda\sigma)} \xi \right) \right]$$

$$\pm g_1 \left[\frac{\sqrt{-pq(\mu^2 - 4\lambda\sigma)}}{2\sigma} \csc_A \left(\sqrt{-(\mu^2 - 4\lambda\sigma)} \xi \right) \right], \quad (3.6)$$

$$\begin{aligned}
u_{15}(x, t) = & g_0 + g_1 \left[-\frac{\mu}{2\sigma} - \frac{\sqrt{-(\mu^2 - 4\lambda\sigma)}}{2\sigma} \tan_A \left(\frac{\sqrt{-(\mu^2 - 4\lambda\sigma)}}{4} \xi \right) \right] \\
- & g_1 \left[\frac{\sqrt{-(\mu^2 - 4\lambda\sigma)}}{2\sigma} \cot_A \left(\frac{\sqrt{-(\mu^2 - 4\lambda\sigma)}}{4} \xi \right) \right], \tag{3.7}
\end{aligned}$$

S2: for $\mu^2 - 4\lambda\sigma > 0$ and $\sigma \neq 0$, it is obtained

$$g_0 = g_0, g_1 = g_1, b_1 = -\frac{1}{12} \frac{g_1^2 (\mu^2 - 4\lambda\sigma)^2 (g_1 \mu - 2g_0 \sigma) \delta^2 (Ln(A))^2}{u_0^2 (8g_1^2 \lambda \sigma - 12g_1 g_0 \mu \sigma + g_1^2 \mu^2 + 12g_0^2 \sigma^2) (-g_1^2 \lambda + g_1 g_0 \mu - g_0^2 \sigma)},$$

$$\begin{aligned}
b_2 = & -\frac{1}{12} \frac{g_1^2 (\mu^2 - 4\lambda\sigma)^2 \delta^2 (Ln(A))^2 \sigma}{u_0^2 (8g_1^2 \lambda \sigma - 12g_1 g_0 \mu \sigma + g_1^2 \mu^2 + 12g_0^2 \sigma^2) (-g_1^2 \lambda + g_1 g_0 \mu - g_0^2 \sigma)}, k_1 = \frac{\sqrt{-\frac{\mu^2 - 4\lambda\sigma}{8g_1^2 \lambda \sigma - 12g_1 g_0 \mu \sigma + g_1^2 \mu^2 + 12g_0^2 \sigma^2}} g_1}{u_0}, \\
k_2 = & -\sqrt{-\frac{\mu^2 - 4\lambda\sigma}{8g_1^2 \lambda \sigma - 12g_1 g_0 \mu \sigma + g_1^2 \mu^2 + 12g_0^2 \sigma^2}} g_1
\end{aligned}$$

$$u_{21}(x, t) = g_0 + g_1 \left[-\frac{\mu}{2\sigma} + \frac{\sqrt{(\mu^2 - 4\lambda\sigma)}}{2\sigma} \tanh_A \left(\frac{\sqrt{(\mu^2 - 4\lambda\sigma)}}{2} \xi \right) \right], \tag{3.8}$$

$$u_{22}(\xi) = g_0 + g_1 \left[-\frac{\mu}{2\sigma} + \frac{\sqrt{(\mu^2 - 4\lambda\sigma)}}{2\sigma} \coth_A \left(\frac{\sqrt{(\mu^2 - 4\lambda\sigma)}}{2} \xi \right) \right], \tag{3.9}$$

$$\begin{aligned}
u_{23}(x, t) = & g_0 + g_1 \left[-\frac{\mu}{2\sigma} + \frac{\sqrt{(\mu^2 - 4\lambda\sigma)}}{2\sigma} \tanh_A \left(\sqrt{(\mu^2 - 4\lambda\sigma)} \xi \right) \right] \\
\pm & g_1 \left[i \frac{\sqrt{pq(\mu^2 - 4\lambda\sigma)}}{2\sigma} \operatorname{sech}_A \left(\sqrt{(\mu^2 - 4\lambda\sigma)} \xi \right) \right], \tag{3.10}
\end{aligned}$$

$$\begin{aligned}
u_{24}(x, t) = & g_0 + g_1 \left[-\frac{\mu}{2\sigma} - \frac{\sqrt{(\mu^2 - 4\lambda\sigma)}}{2\sigma} \coth_A \left(\sqrt{(\mu^2 - 4\lambda\sigma)} \xi \right) \right] \\
\pm & g_1 \left[\frac{\sqrt{pq(\mu^2 - 4\lambda\sigma)}}{2\sigma} \operatorname{csch}_A \left(\sqrt{(\mu^2 - 4\lambda\sigma)} \xi \right) \right], \tag{3.11}
\end{aligned}$$

$$\begin{aligned}
u_{25}(x, t) = & g_0 + g_1 \left[-\frac{\mu}{2\sigma} - \frac{\sqrt{-(\mu^2 - 4\lambda\sigma)}}{4\sigma} \tanh_A \left(\frac{\sqrt{(\mu^2 - 4\lambda\sigma)}}{4} \xi \right) \right] \\
- & g_1 \left[\frac{\sqrt{(\mu^2 - 4\lambda\sigma)}}{4\sigma} \coth_A \left(\frac{\sqrt{(\mu^2 - 4\lambda\sigma)}}{4} \xi \right) \right], \tag{3.12}
\end{aligned}$$

S3: for $\lambda\sigma > 0$ and $\mu = 0$, it is obtained

$$g_0 = g_0, g_1 = g_1, b_1 = 6 \frac{\sigma (u_0 k_1 - k_2) (u_0 k_1 + k_2) g_0}{3 k_2^2 \sigma g_0^2 - g_1^2 \lambda + 2 k_2^2 g_1^2 \lambda}, b_2 = -3 \frac{(u_0 k_1 + k_2) (u_0 k_1 - k_2) \sigma}{3 k_2^2 \sigma g_0^2 - g_1^2 \lambda + 2 k_2^2 g_1^2 \lambda},$$

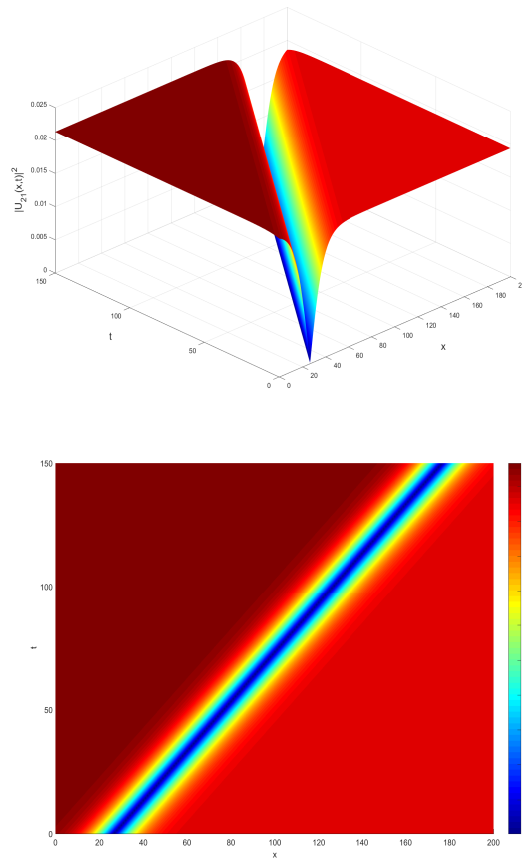


Figure 26: Spatiotemporal plot evolution and contour plot of dark solitons $|u_{21}(x, t)|^2$ at $\alpha = 1$, $A_1 = e$, $k_1 = -k_2 = 3.840$, $g_0 = 0.001, g_1 = 0.018$, $\lambda = -0.312$, $\sigma = -0.0185$.

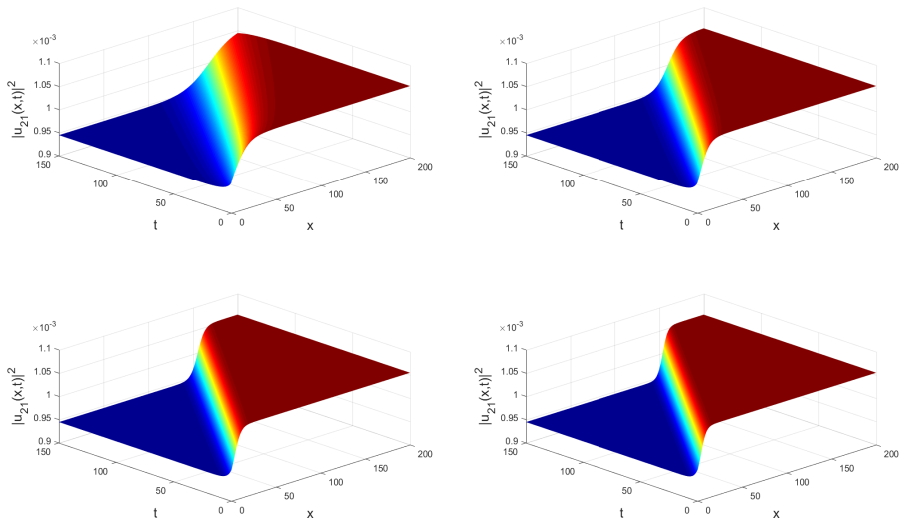


Figure 27: Spatiotemporal plot evolution of kink-like solitons $|u_{21}(x, t)|^2$ at $\alpha = 0.75, \alpha = 0.85, \alpha = 0.95$ and $\alpha = 1$, $A = e, k_1 = -k_2 = 25.840, g_0 = 0.001, g_1 = -0.18, \mu = -0.015, \lambda = -0.0312, \sigma = -2.000185$ respectively

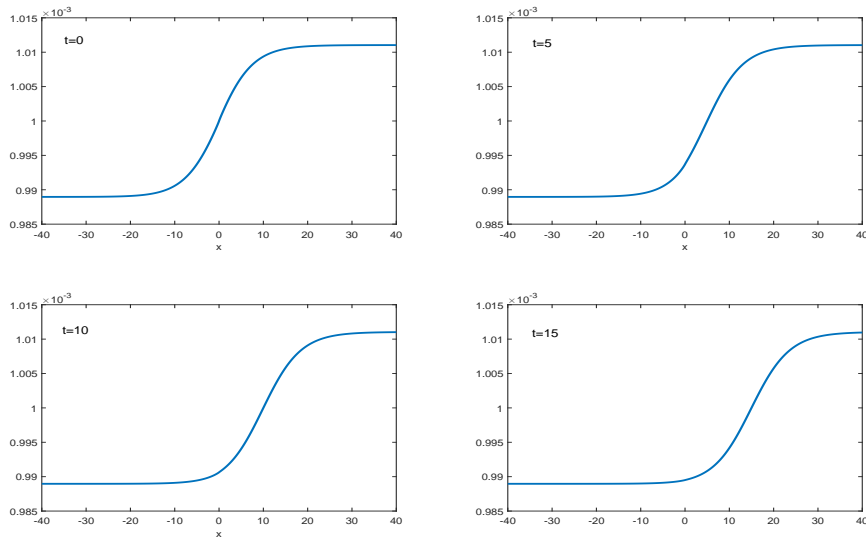


Figure 28: Spatiotemporal plot evolution of 2D of kink-like solitons $|u_{23}(x, t)|^2$ at $\alpha = 0.95, A = e, k_1 = -k_2 = 20.840, g_0 = -0.001, g_1 = 0.18, \mu = -0.015, \lambda = -0.0312, \sigma = -10.000185$.

$$k_1 = k_1, k_2 = k_2, \delta = \frac{\sqrt{-\frac{(3+3k_2^2)(u_0k_1-k_2)(u_0k_1+k_2)}{\sigma(3k_2^2\sigma g_0^2-g_1^2\lambda+2k_2^2g_1^2\lambda)}g_1}}{\text{Ln}(A)u_0k_1^2}.$$

$$u_{31}(x, t) = g_0 + g_1 \sqrt{\frac{\lambda}{\sigma}} \tan_A \left(\sqrt{\lambda\sigma\xi} \right), \quad (3.13)$$

$$u_{32}(x, t) = g_0 - g_1 \sqrt{\frac{\lambda}{\sigma}} \cot_A \left(\sqrt{\lambda\sigma\xi} \right), \quad (3.14)$$

$$u_{33}(x, t) = g_0 + g_1 \left[\sqrt{\frac{\lambda}{\sigma}} \tan_A \left(\sqrt{2\lambda\sigma\xi} \right) \pm \sqrt{pq\frac{\lambda}{\sigma}} \sec_A \left(\sqrt{2\lambda\sigma\xi} \right) \right], \quad (3.15)$$

$$u_{34}(x, t) = g_0 + g_1 \left[-\sqrt{\frac{\lambda}{\sigma}} \cot_A \left(\sqrt{2\lambda\sigma\xi} \right) \pm \sqrt{pq\frac{\lambda}{\sigma}} \csc_A \left(\sqrt{2\lambda\sigma\xi} \right) \right], \quad (3.16)$$

$$u_{35}(x, t) = g_0 + g_1 \left[\frac{1}{2} \sqrt{\frac{\lambda}{\sigma}} \left(\tan_A \left(\frac{\sqrt{\lambda\sigma}}{2} \xi \right) - \sqrt{\frac{\lambda}{\sigma}} \cot_A \left(\frac{\sqrt{\lambda\sigma}}{2} \xi \right) \right) \right], \quad (3.17)$$

S4: for $\lambda\sigma < 0$ and $\mu = 0$, yields to

$$g_0 = \frac{1}{3} \sqrt{\frac{3\lambda(-1+2u_0^2k_1^2)}{\sigma}} g_1, \quad g_1 = g_1, \quad b_1 = -\frac{2}{3} \frac{u_0\delta^2k_1^3(\text{Ln}(A))^2\sigma^2\sqrt{-3\frac{\lambda(-1+2u_0^2k_1^2)}{\sigma}}}{g_1(1+u_0^2k_1^2)},$$

$$b_2 = \frac{u_0^2\delta^2k_1^4(\text{Ln}(A))^2\sigma^2}{g_1^2(1+u_0^2k_1^2)}, \quad k_1 = k_1, \quad k_2 = \pm u_0k_1$$

$$u_{41}(x, t) = \frac{1}{3} \sqrt{\frac{3\lambda(-1+2u_0^2k_1^2)}{\sigma}} g_1 - g_1 \sqrt{\frac{-\lambda}{\sigma}} \tanh_A \left(\sqrt{-\lambda\sigma\xi} \right), \quad (3.18)$$

$$u_{42}(x, t) = \frac{1}{3} \sqrt{\frac{3\lambda(-1+2u_0^2k_1^2)}{\sigma}} g_1 - g_1 \sqrt{\frac{-\lambda}{\sigma}} \coth_A \left(\sqrt{-\lambda\sigma\xi} \right), \quad (3.19)$$

$$u_{43}(x, t) = \frac{1}{3} \sqrt{\frac{3\lambda(-1+2u_0^2k_1^2)}{\sigma}} g_1 - g_1 \left[\sqrt{\frac{-\lambda}{\sigma}} \tanh_A \left(\sqrt{2\lambda\sigma\xi} \right) \pm i \sqrt{pq\frac{-pq\lambda}{\sigma}} \text{sech}_A \left(2\sqrt{-\lambda\sigma\xi} \right) \right], \quad (3.20)$$

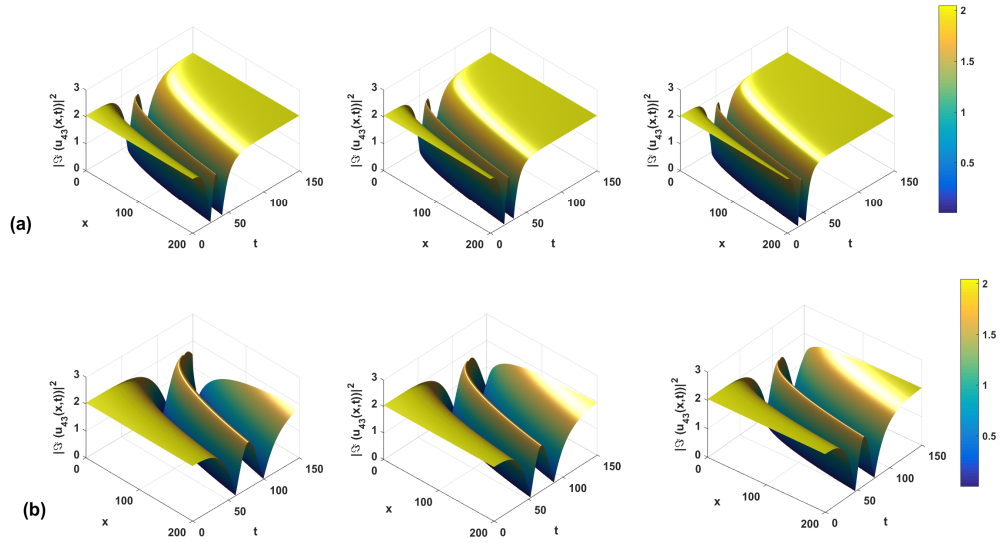


Figure 29: Spatiotemporal plot evolution of the W-shape bright soliton of $|\mathfrak{S}u_{43}(x, t)|^2$ for (a) $[\alpha = 0.52, \alpha = 0.54, \alpha = 0.56]$ (b) $[\alpha = 0.45, \alpha = 0.46, \alpha = 0.47]$ at $A = e$, $k_1 = 10.75$, $k_2 = 2.15$, $u_0 = 0.2$, $g_0 = 3.33$, $g_0 = 0.75$, $p = q = 1$, $\mu = 0$, $\lambda = -0.5$, $\sigma = 0.02$, $p = 0.8$, $q = 0.5$.

$$u_{44}(x, t) = \frac{1}{3} \frac{\sqrt{-\frac{3\lambda(-1+2u_0^2k_1^2)}{\sigma}} g_1}{u_0 k_1} - g_1 \left[\sqrt{\frac{-\lambda}{\sigma}} \coth_A \left(2\sqrt{-\lambda\sigma}\xi \right) \pm \sqrt{-pq\frac{\lambda}{\sigma}} \operatorname{csch}_A \left(2\sqrt{-\lambda\sigma}\xi \right) \right], \quad (3.21)$$

$$u_{45}(x, t) = \frac{1}{3} \frac{\sqrt{-\frac{3\lambda(-1+2u_0^2k_1^2)}{\sigma}} g_1}{u_0 k_1} - g_1 \left[\frac{1}{2} \left(\sqrt{\frac{-\lambda}{\sigma}} \tanh_A \left(\frac{\sqrt{-\lambda\sigma}}{2}\xi \right) + \sqrt{\frac{-\lambda}{\sigma}} \coth_A \left(\frac{\sqrt{-\lambda\sigma}}{2}\xi \right) \right) \right], \quad (3.22)$$

S5: for $\lambda = \sigma$ and $\mu = 0$, it is obtained

$$g_0 = g_0, g_1 = g_1, b_1 = \frac{6(u_0 k_1 - k_2)(u_0 k_1 + k_2) g_0}{-g_1^2 + 3k_2^2 g_0^2 + 2k_2^2 g_1^2}, b_2 = -\frac{3(u_0 k_1 - k_2)(u_0 k_1 + k_2)}{-g_1^2 + 3k_2^2 g_0^2 + 2k_2^2 g_1^2}, k_1 = k_1, k_2 = k_2$$

$$\delta = \frac{\sqrt{-\frac{(3+3k_2^2)(u_0 k_1 - k_2)(u_0 k_1 + k_2)}{-g_1^2 + 3k_2^2 g_0^2 + 2k_2^2 g_1^2}} g_1}{\operatorname{Ln}(A)\sigma u_0 k_1^2},$$

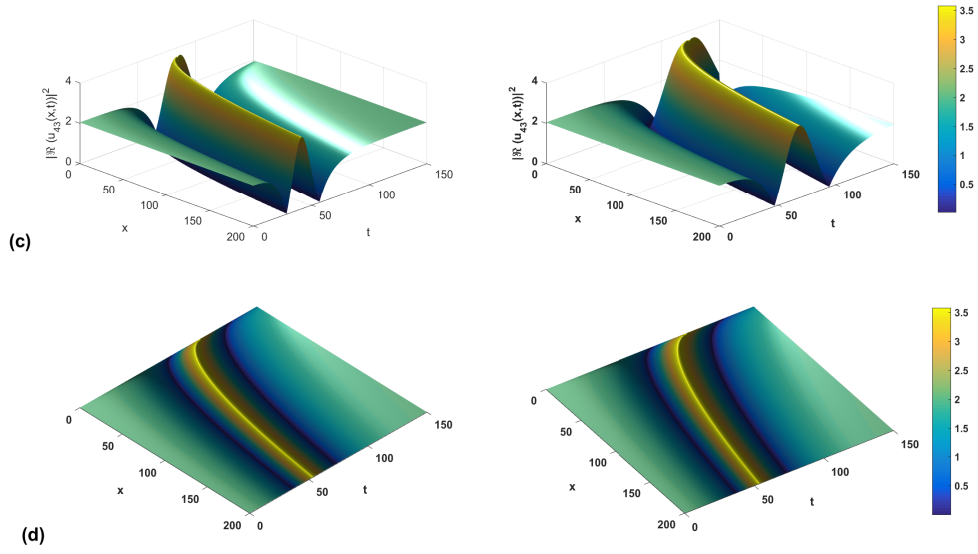


Figure 30: Contour plot evolution of the W-shape bright soliton of $|\Im u_{43}(x,t)|^2$ for (c) $[\alpha = 0.5, \alpha = 0.47]$ (d) $[\alpha = 0.48, \alpha = 0.49]$ at $A = e, k_1 = 10.75, k_2 = 2.15, u_0 = 0.2, g_0 = 3.33, g_0 = 0.75, p = q = 1, \mu = 0, \lambda = -0.5, \sigma = 0.02, p = 0.8, q = 0.75$.

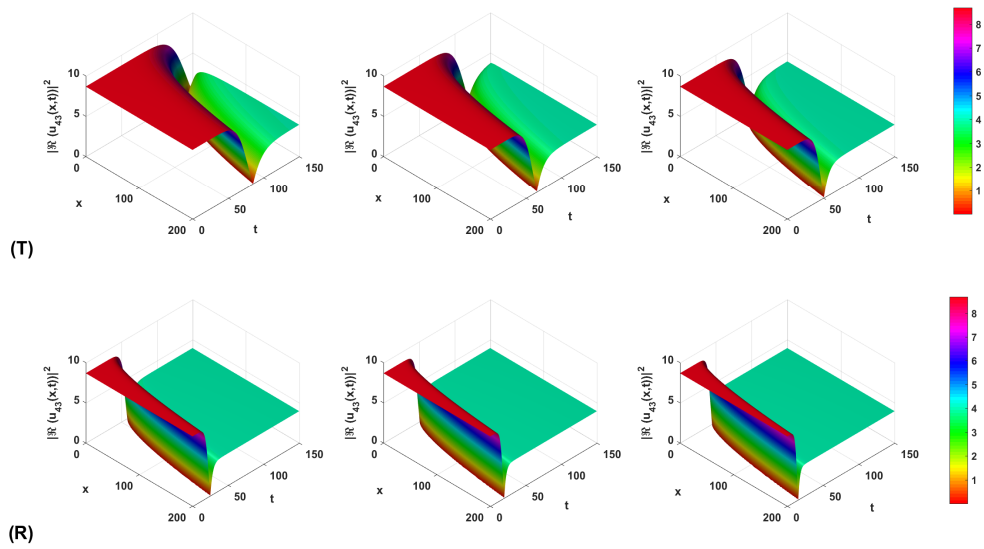


Figure 31: Spatiotemporal plot evolution of the dark soliton of $|\Re u_{43}(x,t)|^2$ for (T) $[\alpha = 0.45, \alpha = 0.47, \alpha = 0.49]$ (R) $[\alpha = 0.55, \alpha = 0.57, \alpha = 0.59]$ at $A = e, k_1 = 10.75, k_2 = 2.15, u_0 = 0.2, g_0 = 3.33, g_0 = 0.75, p = 0.71, q = 0.95, \mu = 0, \lambda = -0.5, \sigma = 0.02$.

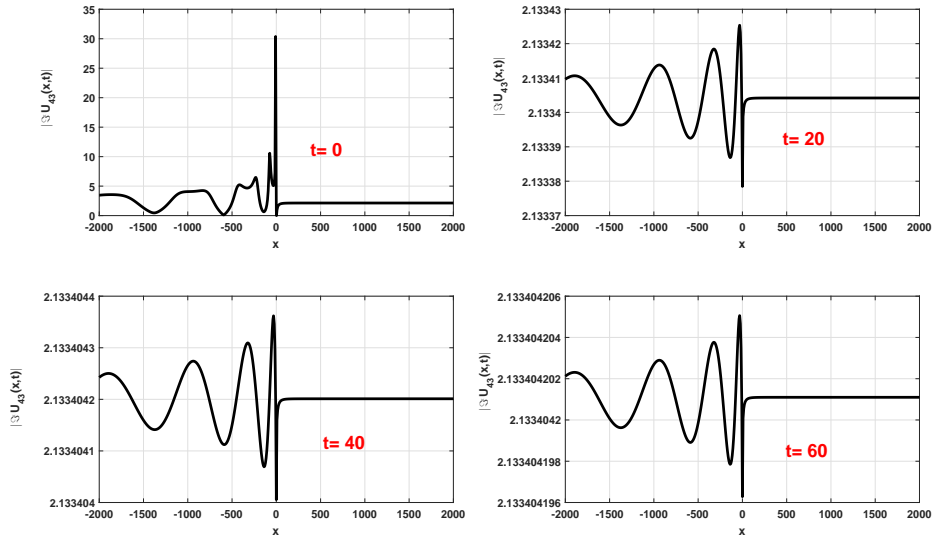


Figure 32: Plot evolution of $|\mathfrak{S}u_{43}(x,t)|^2$ for $\alpha = 0.48, A = e, k_1 = 20.75, k_2 = 2.15, u_0 = 0.2, g_0 = 3.33, g_0 = 0.75, p = 0.71, q = 0.95, \mu = 0, \lambda = -0.5, \sigma = 0.02$.

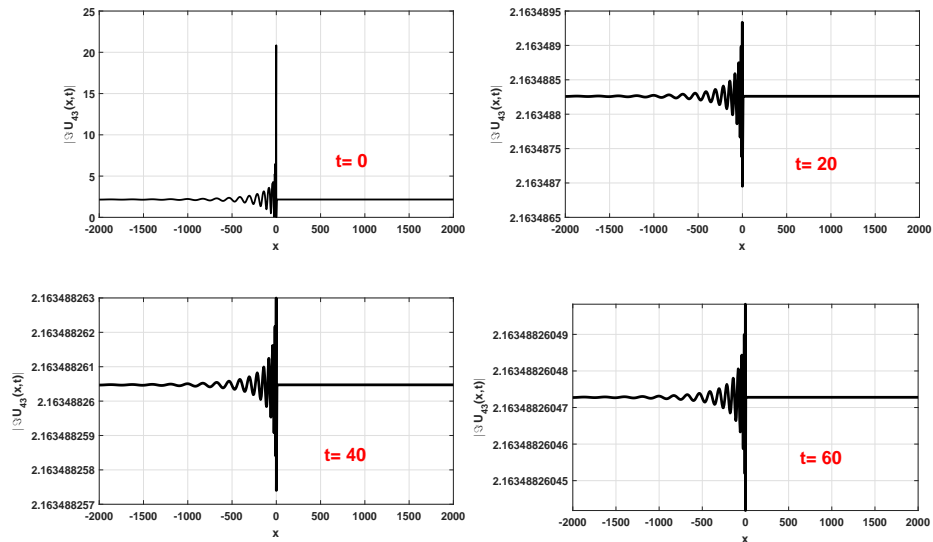


Figure 33: Plot evolution of breather corresponding to $|\mathfrak{S}u_{43}(x,t)|^2$ for $\alpha = 0.48, A = e, k_1 = 25.75, k_2 = 18.54, u_0 = 0.72, g_0 = 3.33, g_0 = 0.75, p = 0.8, q = 0.4, \mu = 0, \lambda = -0.5, \sigma = 0.02$.

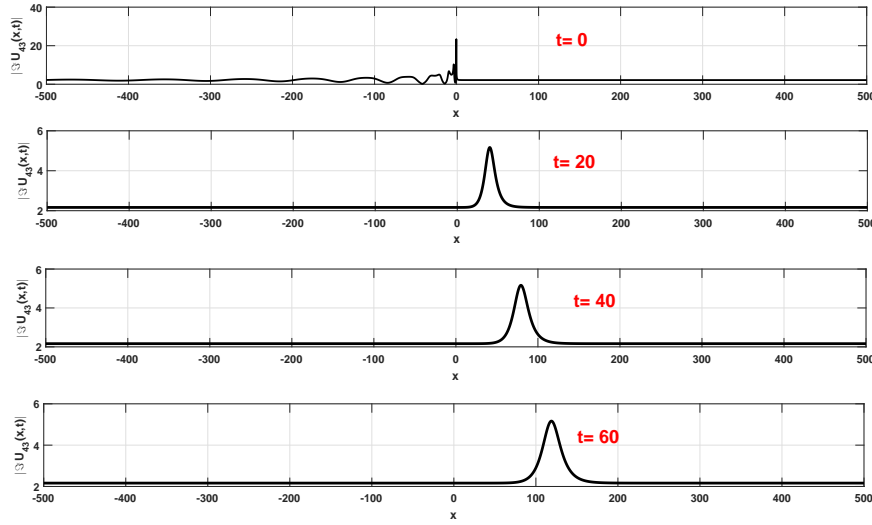


Figure 34: Plot evolution of of the bright soliton $|\mathfrak{S}u_{43}(x, t)|^2$ for $\alpha = 0.48$, $A = e$, $k_1 = 25.75$, $k_2 = -18.54$, $u_0 = -0.72$, $g_0 = 3.33$, $g_0 = 0.75$, $p = 0.8$, $q = 0.4$, $\mu = 0$, $\lambda = -0.5$, $\sigma = 0.02$.

$$u_{51}(x, t) = g_0 + g_1 \tan_A(\lambda\xi), \quad (3.23)$$

$$u_{52}(x, t) = g_0 - g_1 \cot_A(\lambda\xi), \quad (3.24)$$

$$u_{53}(x, t) = g_0 + g_1 [\tan_A(2\lambda\xi) \pm \sqrt{pq} \sec_A(2\lambda\xi)], \quad (3.25)$$

$$u_{54}(x, t) = g_0 - g_1 [\cot_A(2\lambda\xi) \pm \sqrt{pq} \csc_A(2\lambda\xi)], \quad (3.26)$$

$$u_{55}(x, t) = g_0 + g_1 \left[\frac{1}{2} \left(\tan_A\left(\frac{\lambda}{2}\xi\right) - \cot_A\left(\frac{\lambda}{2}\xi\right) \right) \right], \quad (3.27)$$

S6: for $\lambda = -\sigma$ and $\mu = 0$, it is obtained the set of result

$$g_0 = \frac{1}{3} \frac{\sqrt{3-6u_0^2k_1^2}g_1}{u_0k_1}, \quad g_1 = g_1, \quad b_1 = -\frac{2}{3} \frac{u_0\delta^2k_1^3(\ln(A))^2\sigma^2\sqrt{3-6u_0^2k_1^2}}{g_1(1+u_0^2k_1^2)}, \quad b_2 = \frac{u_0^2\delta^2k_1^4(\ln(A))^2\sigma^2}{g_1^2(1+u_0^2k_1^2)},$$

$$k_1 = k_1, \quad k_2 = \pm u_0k_1, \quad \delta = \frac{\sqrt{-\frac{(3+3k_2^2)(u_0k_1-k_2)(u_0k_1+k_2)}{-g_1^2+3k_2^2g_0^2+2k_2^2g_1^2}g_1}}{\ln(A)\sigma u_0k_1^2}$$

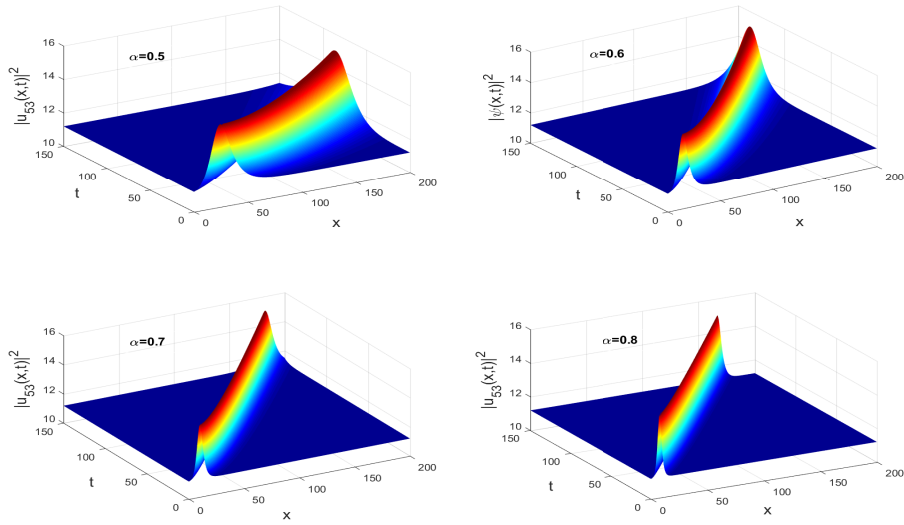


Figure 35: Spatiotemporal Plot evolution of bright $|u_{53}(x,t)|^2$ at $A = e$, $k_1 = -k_2 = 20.40$, $g_0 = -5.001, g_1 = -10.18$, $\lambda = -0.002$.

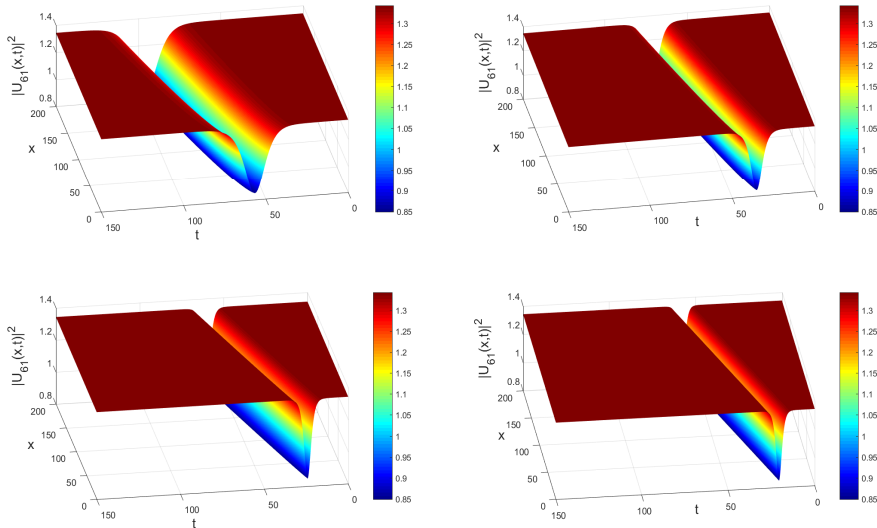


Figure 36: Spatiotemporal plot of dark solitons $|u_{61}(x,t)|^2$ at $\alpha = 0.85$, $\alpha = 0.90$, $\alpha = 0.95$, $\alpha = 1$, respectively and $g_1 = -1.04$, $A = e$, $k_1 = -4.84$, $k_2 = -0.90$, $u_0 = 5.125$, $\sigma = -1.185$.

$$u_{61}(x, t) = \frac{1}{3} \frac{\sqrt{3 - 6 u_0^2 k_1^2} g_1}{u_0 k_1} - g_1 \tanh_A(\lambda \xi), \quad (3.28)$$

$$u_{62}(x, t) = \frac{1}{3} \frac{\sqrt{3 - 6 u_0^2 k_1^2} g_1}{u_0 k_1} - g_1 \coth_A(\lambda \xi), \quad (3.29)$$

$$u_{63}(x, t) = \frac{1}{3} \frac{\sqrt{3 - 6 u_0^2 k_1^2} g_1}{u_0 k_1} - g_1 [\tanh_A(2\lambda \xi) \pm i \sqrt{pq} \operatorname{sech}_A(2\lambda \xi)], \quad (3.30)$$

$$u_{64}(x, t) = \frac{1}{3} \frac{\sqrt{3 - 6 u_0^2 k_1^2} g_1}{u_0 k_1} - g_1 [\coth_A(2\lambda \xi) \pm \sqrt{pq} \operatorname{csch}_A(2\lambda \xi)], \quad (3.31)$$

$$u_{65}(x, t) = \frac{1}{3} \frac{\sqrt{3 - 6 u_0^2 k_1^2} g_1}{u_0 k_1} - g_1 \left[\frac{1}{2} \left(\tanh_A\left(\frac{\lambda}{2} \xi\right) + \coth_A\left(\frac{\lambda}{2} \xi\right) \right) \right], \quad (3.32)$$

S7: for $\mu^2 = 4\lambda\sigma$, it is obtained the following result

$$g_0 = g_0, g_1 = g_1, b_1 = -\frac{2(u_0 k_1 - k_2)(u_0 k_1 + k_2)(-3g_0\sigma g_1^2\lambda + 3g_0^2\sigma g_1\sqrt{\lambda\sigma} - g_0^3\sigma^2 + \sqrt{\lambda\sigma}g_1^3\lambda)}{k_2^2(-g_1^2\lambda + 2g_1g_0\sqrt{\lambda\sigma} - g_0^2\sigma)^2}, b_2 = \frac{(u_0 k_1 - k_2)(u_0 k_1 + k_2)\sigma}{k_2^2(-g_1^2\lambda + 2g_1g_0\sqrt{\lambda\sigma} - g_0^2\sigma)},$$

$$k_1 = k_1, k_2 = k_2, \delta = \frac{\sqrt{\frac{(k_2^2 + 1)(u_0 k_1 - k_2)(u_0 k_1 + k_2)}{\sigma(-g_1^2\lambda + 2g_1g_0\sqrt{\lambda\sigma} - g_0^2\sigma)}} g_1}{Ln(A)u_0 k_1^2 k_2},$$

$$u_{71}(x, t) = g_0 - g_1 \frac{2\lambda(\mu\xi Ln(A) + 2)}{\mu^2\xi Ln(A)}, \quad (3.33)$$

S10: for $\mu = \lambda = 0$, it is obtained the following results

$$g_0 = g_0, g_1 = g_1, b_1 = 2 \frac{(u_0 k_1 - k_2)(u_0 k_1 + k_2)}{k_2^2 g_0}, b_2 = -b_1, k_1 = k_1, k_2 = k_2, \delta = \frac{\sqrt{-(1+k_2^2)(u_0 k_1 - k_2)(u_0 k_1 + k_2)} g_1}{Ln(A)\sigma u_0 k_2 k_1^2 g_0}$$

$$u_{101}(x, t) = g_0 + g_1 \frac{-1}{\sigma\xi Ln A}, \quad (3.34)$$

S11: for $\mu \neq 0$, and $\lambda = 0$, it is obtained the following results

$$\mathbf{R1:} \quad g_0 = g_0, \quad g_1 = g_1, \quad b_1 = \frac{6\sigma(u_0k_1-k_2)(u_0k_1+k_2)g_0}{3k_2^2\sigma g_0^2 - g_1^2\lambda + 2k_2^2g_1^2\lambda}, \quad b_2 = -\frac{3\sigma(u_0k_1-k_2)(u_0k_1+k_2)}{3k_2^2\sigma g_0^2 - g_1^2\lambda + 2k_2^2g_1^2\lambda}, \quad k_1 = k_1, \quad k_2 = k_2,$$

$$\delta = \frac{\sqrt{-\frac{3(1+k_2^2)(u_0k_1-k_2)(u_0k_1+k_2)}{\sigma(3k_2^2\sigma g_0^2 - g_1^2\lambda + 2k_2^2g_1^2\lambda)}g_1}}{\text{Ln}(A)u_0k_1^2},$$

$$u_{111}(x, t) = g_0 + g_1 \left[\frac{p\mu}{\sigma(\cosh_A(\mu\xi) - \sinh_A(\mu\xi) - p)} \right], \quad (3.35)$$

$$\mathbf{R2:} \quad g_0 = \frac{1}{3} \frac{\sqrt{-\frac{3\lambda(-1+2u_0^2k_1^2)}{\sigma}g_1}}{u_0k_1}, \quad g_1 = g_1, \quad b_1 = -\frac{2}{3} \frac{u_0\delta^2k_1^3(\text{Ln}(A))^2\sigma^2\sqrt{-3\frac{\lambda(-1+2u_0^2k_1^2)}{\sigma}}}{g_1(1+u_0^2k_1^2)}, \quad b_2 = \frac{u_0^2\delta^2k_1^4(\text{Ln}(A))^2\sigma^2}{g_1^2(1+u_0^2k_1^2)},$$

$$k_1 = k_1, \quad k_2 = \pm u_0k_1$$

$$u_{112}(x, t) = \frac{1}{3} \frac{\sqrt{-\frac{3\lambda(-1+2u_0^2k_1^2)}{\sigma}g_1}}{u_0k_1} + g_1 \left[\frac{p\mu}{\sigma(\cosh_A(\mu\xi) - \sinh_A(\mu\xi) - p)} \right], \quad (3.36)$$

S12: for $\mu = k, \sigma = mk(m \neq 0)$, and $\lambda = 0$, it is obtained the following result

$$g_0 = g_0, \quad g_1 = g_1, \quad b_1 = \frac{12(u_0k_1-k_2)(u_0k_1+k_2)(-g_1+2g_0m)m}{12k_2^2g_0^2m^2+k_2^2g_1^2+g_1^2-12k_2^2g_1g_0m}, \quad b_2 = -\frac{12m^2(u_0k_1-k_2)(u_0k_1+k_2)}{12k_2^2g_0^2m^2+k_2^2g_1^2+g_1^2-12k_2^2g_1g_0m}, \quad k_1 = k_1,$$

$$k_2 = k_2, \quad \delta = \frac{2\sqrt{-\frac{(3k_2^2+1)(u_0k_1-k_2)(u_0k_1+k_2)}{12k_2^2g_0^2m^2+k_2^2g_1^2+g_1^2-12k_2^2g_1g_0m}g_1}}{\text{Ln}(A)u_0k_1^2k}$$

$$u_{121}(x, t) = g_0 - g_1 \frac{pA^{k\xi}}{q - mpA^{k\xi}}, \quad (3.37)$$

where $u(x, t) = U(\xi)$, $\xi = \frac{k_1}{\Gamma(1+\alpha)}t^\alpha + \frac{k_2}{\Gamma(1+\alpha)}x^\alpha$, and $p, q > 0$. Therefore, in this paper ξ_0 is considered as zero value. The details of the generalized hyperbolic and triangular functions are given in [17]. It is observed that, for cases (8), (9) et (10) none solutions have been obtained.

3.2.2 On solving the nonlinear differential governing low-pass electrical transmission lines by using the new sub-ODE equation

The initial step is to use the balance principle which between the higher order derivative and the higher order nonlinear term. So, it is obtained $3s + 2p = 4s \Rightarrow s = 2p$. Consequently, Eq.(3.1) read

$$U(\xi) = \mu F^{2p}(\xi), \quad (3.38)$$

Inserting Eq.(2.44) and Eq.(2.43) into Eq.(3.1) gives the set of system of equation in terms of $F^{jp}(\xi)$. Setting the obtained system of algebraic equation to zero and making used MAPLE it is revealed the following set of results:

Result 1: $A = 0$, $B = 0$, $C = \frac{63}{4} \frac{b_1^2}{(-192b_2+7b_1^2)p^2\delta^2}$, $D = 0$, $E = E$, $\mu = \frac{1}{18} \frac{(-192b_2+7b_1^2)p^2\delta^2 E}{b_1 b_2}$, $k_1 = \frac{2}{3}i\sqrt{3}$, $k_2 = 8\sqrt{-\frac{3b_2}{-192b_2+7b_1^2}}u_0$.

Hence, it is recovered three types of solutions to Eq.(2.2)

Case 1: If $A = 0$, $B = 0$, $D = 0$, bright type is obtained

$$u_{2,1,1}(x, t) = \mu \left[\varepsilon \sqrt{-\frac{C}{E}} \operatorname{sech} \left(p\sqrt{C}\xi \right) \right]^{\frac{1}{2p}}, \quad C > 0, \quad E < 0, \quad \varepsilon \pm 1, \quad (3.39)$$

a periodic solution

$$u_{2,1,2}(x, t) = \mu \left[\varepsilon \sqrt{-\frac{C}{E}} \sec \left(p\sqrt{-C}\xi \right) \right]^{\frac{1}{2p}}, \quad C < 0, \quad E > 0, \quad \varepsilon \pm 1, \quad (3.40)$$

and a rational solution

$$u_{2,1,3} = \mu \left[\frac{\varepsilon}{p\sqrt{E}\xi} \right]^{\frac{1}{2p}}, \quad C = 0, \quad E > 0, \quad \varepsilon \pm 1. \quad (3.41)$$

Result 2: $A = \frac{3969}{64} \frac{b_1^4}{(54b_2+7b_1^2)^2 E \delta^4 p^4}$, $B = 0$, $C = \frac{63}{4} \frac{b_1^2}{(54b_2+7b_1^2)p^2\delta^2}$, $D = 0$, $E = E$, $\mu = \frac{4}{27} \frac{(54b_2+7b_1^2)p^2\delta^2 E}{b_1 b_2}$, $k_1 = \frac{2}{3}i\sqrt{3}$, $k_2 = 8\sqrt{-\frac{3b_2}{-192b_2+7b_1^2}}u_0$.

The corresponding solutions give:

Case 2: By setting the conditions $B = 0$, $D = 0$, $A = \frac{C^2}{4E}$, it is gained dark soliton-like solution of Eq.(2.3):

$$u_{2,2,1} = \mu \left[\varepsilon \sqrt{-\frac{C}{2E}} \tanh \left(p\sqrt{\frac{-C}{2}}\xi \right) \right]^{\frac{1}{2p}}, \quad C < 0, \quad E > 0, \quad \varepsilon \pm 1, \quad (3.42)$$

and a periodic solution

$$u_{2,2,2} = \left[\varepsilon \sqrt{\frac{C}{2E}} \tan \left(p\sqrt{\frac{C}{2}}\xi \right) \right]^{\frac{1}{2p}}, \quad C > 0, \quad E > 0, \quad \varepsilon \pm 1. \quad (3.43)$$

Case 3: By setting the conditions $B = 0$, $D = 0$, we deduce three forms of Jacobian elliptic functions solutions of Eq.(2.3):

$$u_{2,3,1} = \mu \left[\varepsilon \sqrt{\frac{-Cm^2}{E(2m^2-1)}} \operatorname{cn} \left(p \sqrt{\frac{C}{2m^2-1}} \xi \right) \right]^{\frac{1}{2p}}, \quad C > 0, \quad A = \frac{C^2 m^2 (m^2 - 1)}{E(2m^2 - 1)^2}, \quad \varepsilon \in \{\pm 1\} \quad (3.44)$$

$$u_{2,3,2} = \mu \left[\varepsilon \sqrt{\frac{-C}{E(2-m^2)}} \operatorname{dn} \left(p \sqrt{\frac{C}{2-m^2}} \xi \right) \right]^{\frac{1}{2p}}, \quad C > 0, \quad A = \frac{C^2(1-m^2)}{E(2-m^2)^2}, \quad \varepsilon \in \{\pm 1\} \quad (3.45)$$

and

$$u_{2,3,3} = \mu \left[\varepsilon \sqrt{\frac{-Cm^2}{E(1+m^2)}} \operatorname{sn} \left(p \sqrt{\frac{-C}{1+m^2}} \xi \right) \right]^{\frac{1}{2p}}, \quad C < 0, \quad A = \frac{C^2 m^2}{E(1+m^2)^2}, \quad \varepsilon \in \{\pm 1\} \quad (3.46)$$

Case 4: Assuming $B = D = 0$ and $E \neq 0$, it is revealed Weierstrass elliptic function solutions to set of Eq.(2.3),

$$u_{2,4,1} = \mu \left[\frac{\wp(p\xi, g_2, g_3)}{E} - \frac{C}{3E} \right]^{\frac{1}{4p}}, \quad (3.47)$$

where $g_2 = \frac{4C^2 - 12AE}{3}$, $g_3 = \frac{4C(-2C^2 + 9AE)}{27}$.

$$u_{2,4,2} = \mu \left[\frac{3A}{3\wp(p\xi, g_2, g_3) - C} \right]^{\frac{1}{2p}}, \quad (3.48)$$

where $g_2 = \frac{4C^2 - 12AE}{3}$, $g_3 = \frac{4C(-2C^2 + 9AE)}{27}$.

$$u_{2,4,3} = \mu \left[\frac{6\sqrt{A}\wp(p\xi, g_2, g_3) + C\sqrt{A}}{3\wp'(p\xi, g_2, g_3)} \right]^{\frac{1}{2p}}, \quad (3.49)$$

where $\wp'(p\xi, g_2, g_3) = \frac{d\wp(p\xi, g_2, g_3)}{d\xi}$, $g_2 = \frac{C^2}{12} + AE$, $g_3 = \frac{C(36AE - C^2)}{216}$.

$$u_{2,4,4} = \mu \left[\frac{3\sqrt{E^{-1}}\wp'(p\xi, g_2, g_3)}{6\wp(p\xi, g_2, g_3) + C} \right]^{\frac{1}{2p}}, \quad (3.50)$$

where $A = \frac{5C^2}{26E}$, $g_2 = \frac{2C^2}{9}$, $g_3 = \frac{C^3}{54}$,

$$u_{2,4,5} = \mu \left[\sqrt{\frac{5C^2}{36E}} \frac{6\wp(p\xi, g_2, g_3) + C}{3\wp'(p\xi, g_2, g_3)} \right]^{\frac{1}{2p}}, \quad (3.51)$$

while g_2 and g_3 are the invariants of the Weierstrass elliptic function and $\xi = \frac{k_1}{\Gamma(1+\alpha)} t^\alpha + \frac{k_2}{\Gamma(1+\alpha)} x^\alpha$.

3.3 Physical interpretation

Figure 26 is the spatiotemporal plot evolution of the dark soliton of $|u_{21}(x, t)|^2$ and Figures 27-28 are the plot evolution of anti-kink like solution $|u_{23}(x, t)|^2$. Furthermore, Figure 29-30 are the spatiotemporal plot evolution of the W-shape bright solutions of $|\Im u_{43}(x, t)|^2$. Moreover, by varying the fractional order parameter, figure 31 gives the profile of dark soliton with the effect of the latter. Besides, by considering the parameters of the line $k_1 = 25.75$, $k_2 = 18.54$ and $\alpha = 0.48$, we obtain the breather (see figure 32) which propagates at different times. This behavior appears to be new in the electrical transmission line. In Figures 32 and 33, we obtain the same behavior. However, in figure 34 we manage to reverse the behavior of the breather type over time by taking $k_2 = -18.54$. The soliton obtained is bright as a solution which propagates along the line, this exhibits the behavior of modulated waves in a nonlinear electrical transmission line. In addition, Figure 35 depicts the 3D bright solitons under the effect of the fractional derivative order. It is pointed out the deformation of the shape during the propagation of the latter. Figure 11 gives the normal shape of the dark soliton at $\alpha = 0.1$. The results obtained are more general than those reported by [16]. It is observed that, fractional order α has the effects on the width and on the amplitude of the obtained bright and dark soliton solutions (see figures 26, 27, 28, 29, 30, 31, 32, 33, 34, 35). Furthermore, dark and bright solitons obtained will be helpful to explain natural phenomena and the other solutions could be probably used in diverse applications in science and engineering.

Without doubt, it could be predicted that the derivative order affects the shape of the traveling-wave in the electrical transmission line. Otherwise, the obtained results of the nonlinear fractional differential equation governing wave propagating in the low-pass electrical transmission lines are essential to explain the phenomenon of the data transmission in telecommunication, as the latter depicts the natural event such as propagation with a finite speed and vibration. On the other hand, these obtained results can help to explain internal waves in the ocean, as it is well known that soliton are virtually hazardous for offshore engineering building such as gas and oil pipelines and shipping decks. The best important effect of solitons generation is the tidal energy conversion from barotropic to baroclinic component over large-scale oceanic bottom obstructions (shelf breaks, sea mounts, canyons and ridges). Otherwise, dark and bright solitary

waves are omnipresent everywhere strong tides happen in the quarter of irregular topography. Solitons are frequently important lineaments discovered in optical and radar satellite imagery of costal water. In this case, solitary waves can travel over several thousand kilometers and carry both load and impulse. However, during their propagation, a considerable velocity shear causes turbulence and mixing. The obtained mixing, frequently offer background nutritious into the water column, thus enrich the local region and changing the biology inside.

Finally, it emerges that using the extended direct algebraic method, we obtain a diversity of solutions such as dark (Eq.(3.8)), trigonometric function solutions Eqs.(3.3-3.7), singular solitons and combined solutions (Eqs.(3.10-3.12)). The virtue of this method lies in obtaining the W-shape bright soliton which is well known in nonlinear optical fibers. Otherwise, it is gained jacobian elliptic function solutions and Weierstrass elliptic function solutions by applying the Sub-equation method (see Eqs.(3.46-3.50)). On the other hand, by setting $C = \mu^2 - 4\lambda\sigma$ and $E = \sigma$ and assuming $g_0 = 0$ and $g_1 = 0$, Eq.(3.8) and Eq.(3.40) are the same.

3.4 Linear stability analysis and rogue waves

3.4.1 Modulation instability in the NETL with the Josephson junction

We observe that the dispersion relation obtained in equation (2.159) depends on the ratio $\frac{Q}{P}$. Moreover, the non linearity coefficient Q , depends proportionally on the plasma frequency ω_j of the grating. By plotting the variation of the quotient $\frac{Q}{P}$ versus ω for different values of ω_j as shown in figure 37(m). We can see that when the plasma frequency decreases, the nonlinearity decreases and the instability region decreases too (see figure 37(m)). Therefore, in $0 \leq \omega \leq 2,09$ ($rad.s^{-1}$), the gain spectrum is stable despite the small perturbation. At the same time, the ratio $\frac{Q}{P}$ is still positive for $2.09 < \omega \leq 3.5$ ($rad.s^{-1}$) (see Figure 37(m)) and the dispersion relation of the perturbation becomes complex. As a result, the modulation instability gain spectrum is unstable and the wavenumber K is below the critical value $K_c = \sqrt{\frac{2Q}{P}|\phi_{10}|^2}$. In general, we say that when the plasma frequency increases, the ratio $\frac{Q}{P}$ increases and consequently the instability zone of the line increases too. Moreover, we also investigate the influence of the capacitance C_2 on the variation of $\frac{Q}{P}$ as a function of (ω). It appears that, when C_2 increases

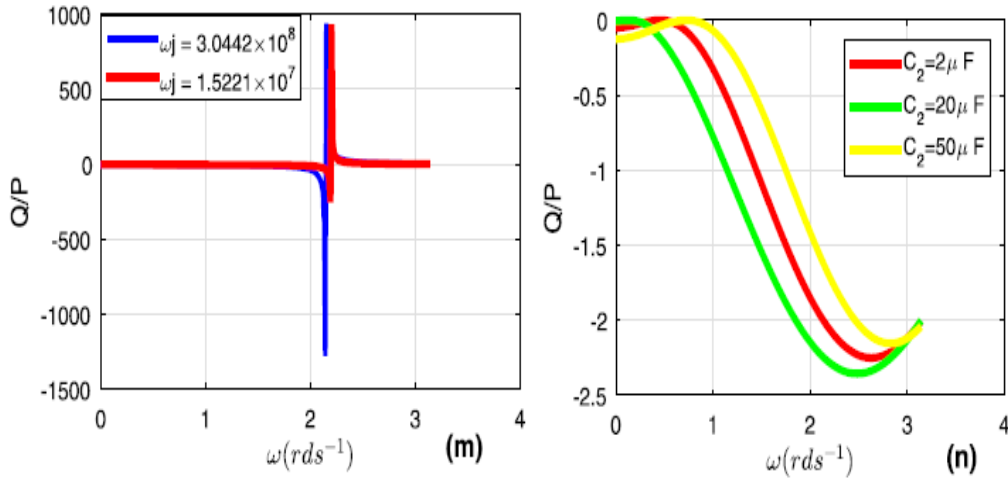


Figure 37: Illustration of the ratio bright (Q/P) versus angular frequency with the effect of plasma frequency (m) $\omega_j = 3.044 \times 10^{16} \text{rad.s}^{-1}$, $\omega_j = 3.0442 \times 10^{16} \text{rad.s}^{-1}$, $C_1 = 1 \text{pF}$, $C_1 = 2 \text{pF}$ and (n) the effect of the capacitor at $C_1 = 20 \text{pF}$ $J_0 = 200 \text{nA}$, $L_1 = 480 \mu\text{H}$.

slightly, the curve keeps its initial shape and remains almost stable on $0 \leq \omega \leq 3,5 (\text{rad.s}^{-1})$ (see figure 37(n)) by keeping its negative value. We can say that the capacitor C_2 has an opposite effect than the plasma frequency ω_j and therefore plays the role of control parameter for the stability of the line.

We now look for the variation of the growth rate of the modulation instability equation (2.161) as a function of the line parameters. Thus, to highlight the behavior of the growth rate (Γ_{gr}) of the modulation instability, we will plot the growth rate in terms of wavenumber with the effect of the plasma frequency. Figure 38 show that, as the plasma frequency increases, the critical value increases and consequently the instability gain also increases. Thus, when the plasma frequency reaches the critical value, the modulation instability gain spectrum is unstable for any value of the chosen angular frequency. It is observed instability zones for $0 < K < 6$ and $2 < K_c < 6$. However, in figure 39 we observed two slip lobes which highlight the identical instability zones opposite to the symmetry axis $K_c = 0$. The identical scenario is exposed in figure 40 a slip lobe for $-5 < K < 5$. We can summarize for this part that the line presents a stability zone for values of K_c lying in the interval $-2 < K_c < 2$. However, when we go out of this interval all the values of K_c lead to an instability of the line. Moreover, we can also

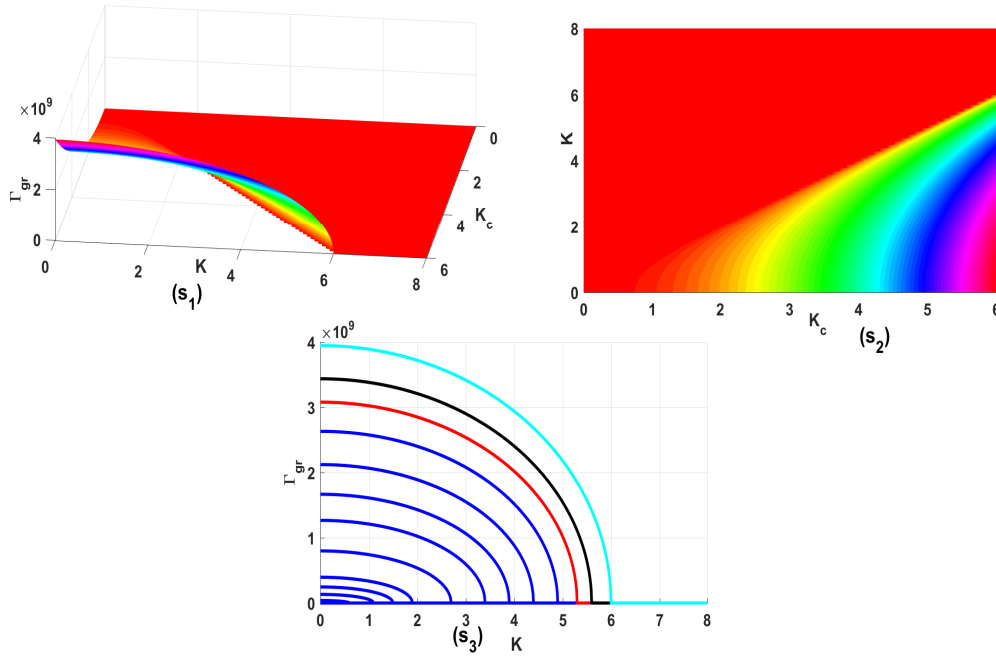


Figure 38: Illustration of the growth rate of MI in terms of wave number and critical wave number with the effect of plasma frequency (s_1) 3D, (s_2) contour plot and (s_3) 2D plot at $\omega_j = 3.044 \times 10^9 \text{rad.s}^{-1}$, $C_1 = 1 \text{pF}$, $C_2 = 400 \text{pF}$ at $J_0 = 200 \text{nA}$, $L_1 = 780 \mu\text{H}$.

see that the gain of instability increases as we move away from 2. The plasma frequency is the only one responsible for this instability of the line. This situation reflects the fact that there is a large gap between the non-linearity provided by the Q coefficient and the dispersion provided by the P coefficient. This increases the instability rate in the line and increases the generation of different localized wave patterns in the line.

Figure 41 shows the influence of the variation of the critical wavenumber, in particular the effect of the plasma frequency on the instability gain modulation instability. However, this time we take the value of the critical wavenumber close to zero which is the resonance. Thus, we fix the plasma frequency, i.e. the critical value of the wavenumber K_c , and we plot the gain as a function of the wavenumber. We see that for small values of K_c , i.e. for values of ω_j around $\omega_j = 6.7618 \times 10^3 \text{rad.s}^{-1}$ we see that the width of the modulation band narrows and the amplitude of the gain drops from 4.3×10^7 to 1.0×10^7 for the first curve. Then again for smaller values than the previous ones, the amplitude of the gain drop from 2.75×10^6 to 0.4×10^6 . This clearly shows that for small values of the plasma frequency or its order of magnitude, there is

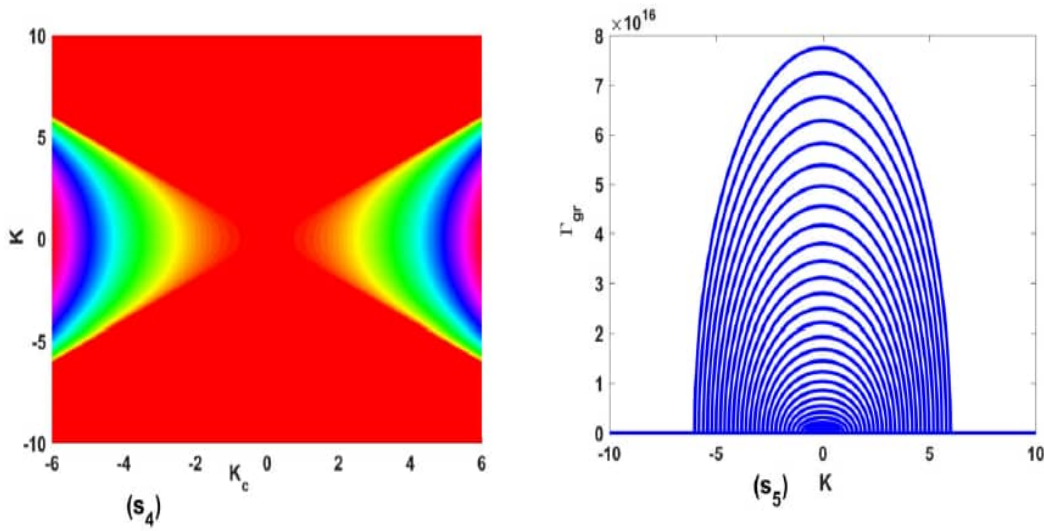


Figure 39: Illustration of the growth rate of MI in terms of wave number and critical wave number with the effect of plasma frequency (s_4) contour plot and (s_5) 2D plot at $\omega_j = 3.044 \times 10^8 \text{rad.s}^{-1}$, $C_1 = 0.1 \text{pF}$, $C_2 = 20 \text{pF}$ at $J_0 = 200 \text{nA}$, $L_1 = 780 \mu\text{H}$.

a significant loss of energy in the line. Moreover, we also note that the instability zone shrinks as the critical value K_c tends towards zero. This also reflects this loss of energy in the line.

Figure 42 shows the influence of the capacitors C_1 and C_2 on the modulation instability gain, for fixed values of ω_j . It appears from the different curves that, in addition to the fact that if ω_j decreases, the amplitude of the gain also decreases, this for constant values of C_1 and C_2 capacitors: When $C_1 = 400.2 \text{pF}$ and $C_2 = 720 \text{pF}$ or $\omega_j = 6.06 \times 10^3 \text{rad.s}^{-1}$. We then observe two sidebands whose maximum amplitude is 2.5×10^9 . However, when for $C_1 = 400.2 \text{pF}$ and $C_2 = 720 \text{pF}$ or $\omega_j = 6.06 \times 10^3 \text{rad.s}^{-1}$ we pass to $C_1 = 750 \text{pF}$ and $C_2 = 920 \text{pF}$ or $\omega_j = 3.20 \times 10^3 \text{rad.s}^{-1}$, this variation of the capacitors has no effect on the gain. The main effect remains the same as the one caused by the decrease of the plasma frequency on the instability gain. On the other hand, when for $C_1 = 400.2 \text{pF}$ and $C_2 = 720 \text{pF}$ or $\omega_j = 6.06 \times 10^3$ we go to $C_1 = 950 \text{pF}$ and $C_2 = 420 \text{pF}$ or $\omega_j = 6.761 \times 10^3 \text{rad.s}^{-1}$, this variation in capacitors has an effect on gain. Indeed, we would have expected that as the plasma frequency has increased, that the amplitude of the gain also increases. But no, because the fact that the capacitor C_1 is twice as large as the capacitor C_2 has had an antagonistic effect on the plasma frequency of the system. This shows that as the C_1 capacitor becomes larger and larger than the C_2 capacitor,

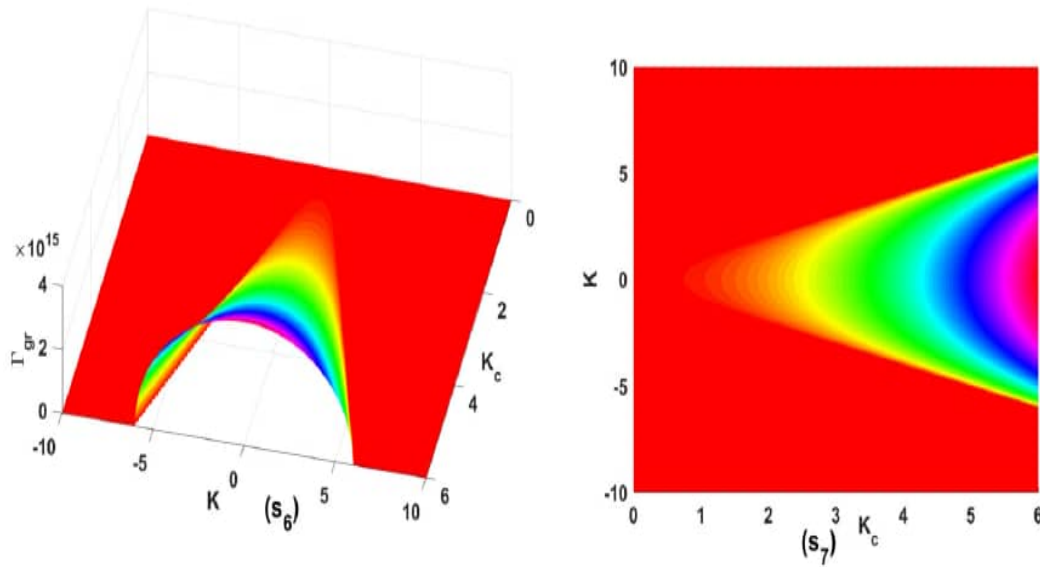


Figure 40: Illustration of the growth rate of MI in terms of wave number and critical wave number with the effect of plasma frequency (s_6) 3D and (s_7) contour plot at $\omega_j = 7.6104 \times 10^{15} \text{rad.s}^{-1}$, $C_1 = 40 \text{pF}$, $C_2 = 200 \text{pF}$ at $J_0 = 200 \text{nA}$, $L_1 = 780 \mu\text{H}$.

there is an increase in the energy dissipation in the line. Generally speaking, we can say that the capacitors C_1 and C_2 play a very important role in the stabilization of the line, as well as the plasma frequency ω_j .

We can conclude that the influence of different physical parameters of the line on the growth rate of modulation instability is shown in figures (37, 38, 39, 40, 41, 42). It appears from these different figures that the plasma frequency is the key parameter of the line, when this frequency increases, the instability zone increases and the instability rate also increases. The enlargement of the allowed range of K for modulation instability involving the possibility of generating non linear structures. These instability zones are described by an instability lobe, which represents the region where $\frac{Q}{P} > 0$ (unstable region), while the whole red region is equivalent to the region $\frac{Q}{P} < 0$ (stable region). Note that all these results are in agreement with our prediction. In the region $\frac{Q}{P} > 0$ which is the instability zone, a small perturbation of the plane wave can generate a wave of larger amplitude. Under this condition, the energy is assumed to localize in a small area in space and time, which then leads to the formation of localized wave patterns.

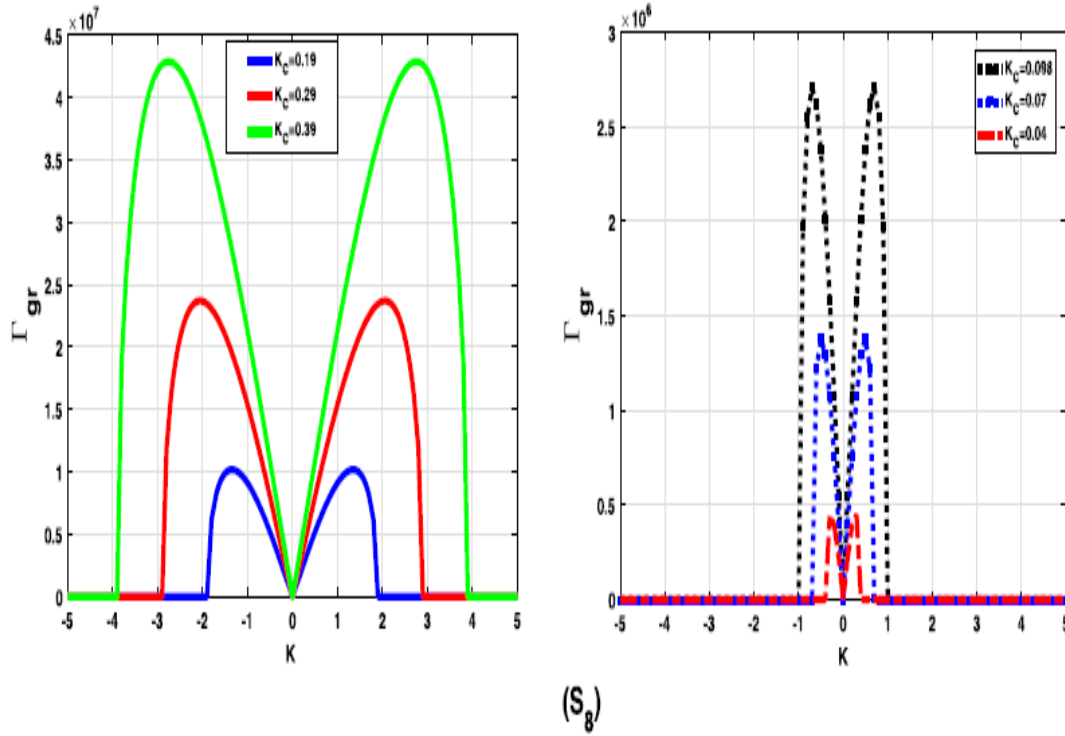


Figure 41: Illustration of the growth rate of MI in terms of wave number and critical wave number with the effect of plasma frequency (s6) 3D and (s7) contour plot at $\omega_j = 6.7618 \times 10^3 \text{rad.s}^{-1}$, $C_2 = 2C_1$ (blue line) and $C_1 = 2C_2$ (red line) at $J_0 = 200 \text{ nA}$, $L_1 = 480 \mu\text{H}$

3.4.2 Peregrine soliton

Recently, it has been investigated rogue waves to equation (2.125) [22,23]. The rogue waves solution takes the form of PSs or SRWs. In which follows, it will be pointed out PS and SRWs.

Starting from the fact that all the information and properties of the scattering wave are contained in the coefficients P and Q of the nonlinear Schrödinger equation (2.125), which are functions of the relevant parameters of the nonlinear electric transmission line with Josephson junction. In what follows, we study the effects of these system parameters on the characteristics of the Peregrine solitons.

For Peregrine soliton, it is used [6].

$$\phi_1(x, \tau) = \sqrt{\frac{2P}{Q}} \left(1 - \frac{4 + 16iP\tau}{16P^2\tau^2 + 4x^2 + 1} \right) e^{2iP\tau}. \quad (3.52)$$

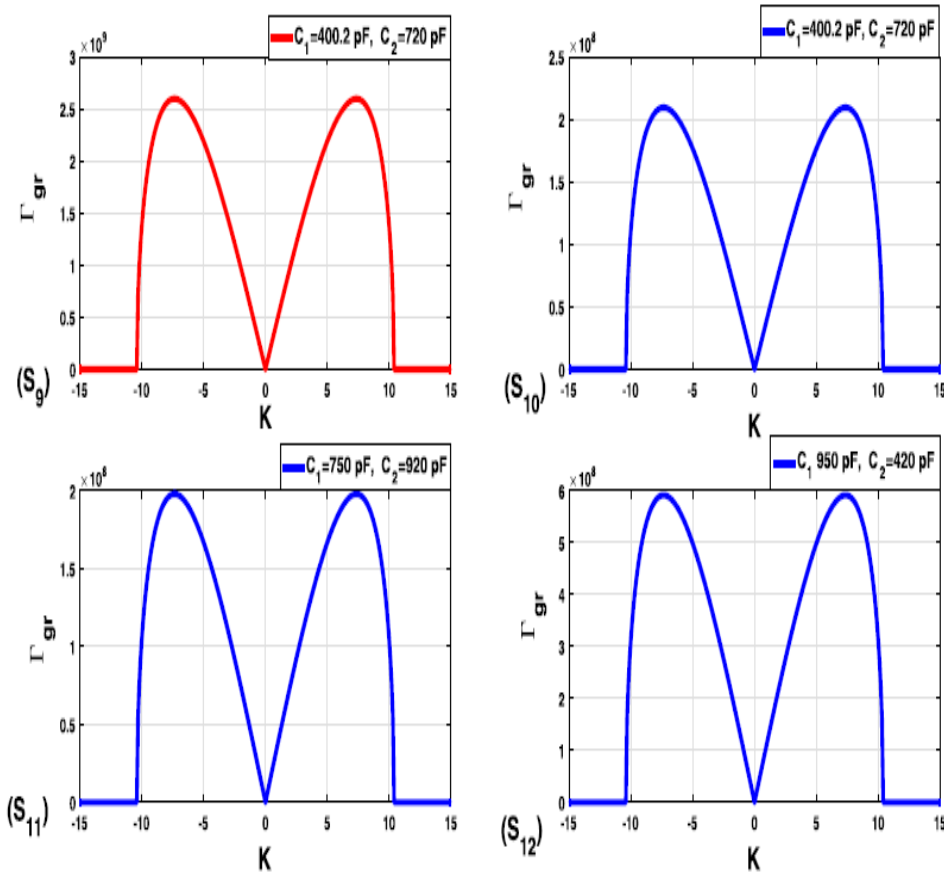


Figure 42: The comparison of the growth rate of MI under the influence of the capacitors C_1 and C_2 and fixed value of the critical wave number $(s_9)[\omega_j = 6.06 \times 10^3 \text{rd.s}^{-1} \text{rad.s}^{-1}]$, $(s_{10})[\omega_j = 4 \times 10^3 \text{rd.s}^{-1} \text{rad.s}^{-1}]$, $(s_{11})[\omega_j = 3.20 \times 10^3 \text{rd.s}^{-1} \text{rad.s}^{-1}]$, $(s_{12})[\omega_j = 6.761 \times 10^3 \text{rad.s}^{-1}]$ at $J_0=200\text{nA}$, $L_1 = 780\mu\text{H}$.

We can see that figure 43 has the shape of a peregrine structure, notably a large amplitude (the peak has a height at least three times that of the bottom) with a hole on each side. The evolution of the peregrine at different times (i.e. $\tau = 0 \text{ ms}$, $\tau = 5 \text{ ms}$, $\tau = 10 \text{ ms}$, $\tau = 15 \text{ ms}$, $\tau = 20 \text{ ms}$), shows that the peregrine keeps its shape and characteristics during the course. These observations confirm the theoretical assumptions that the wave energy is concentrated in a small region due to the nonlinear properties of the electric transmission line. Such a solution is able to concentrate a significant amount of wave energy in a relatively small area in space. Figure 33 shows the PS in 2D view, and one can clearly see the two pointed forks of the soliton.

The figure 45 presents the speed of disappearance and appearance of the PS $\tau = 0 \text{ ms}$,

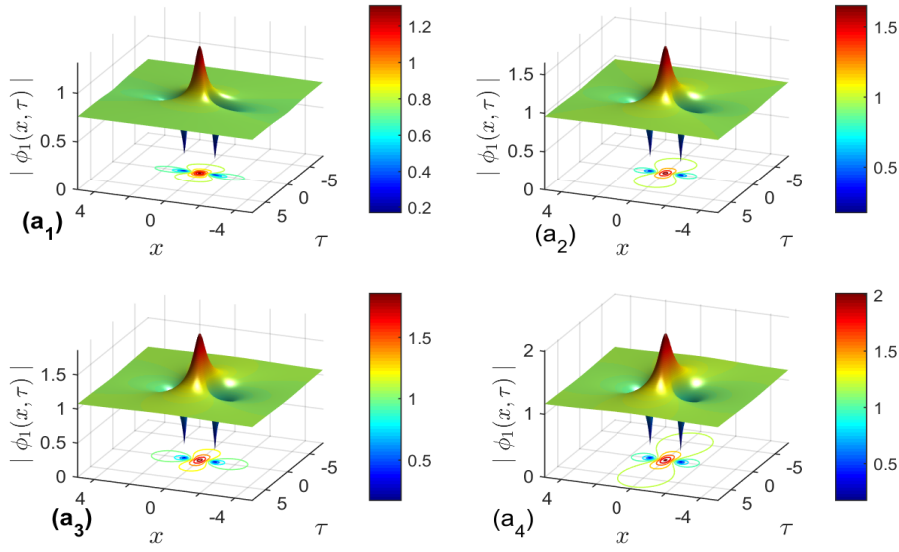


Figure 43: (S_8) is the 2D plot of the Peregrine rogue wave and (S_9) the 3D spatiotemporal evolution of the Peregrine rogue wave at $C_1 = 2pF$, $C_2 = 470pF$ at $J_0 = 200nA$, $L_1 = 480\mu H$.

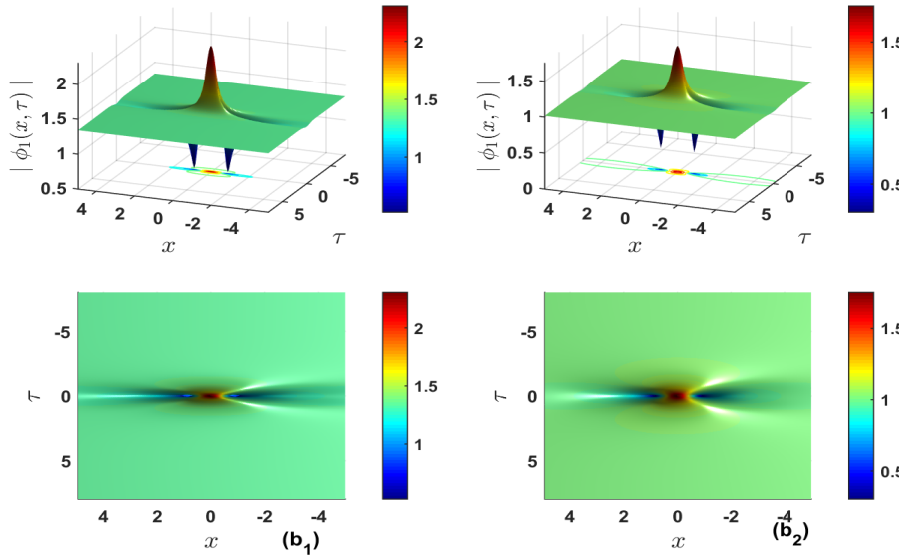


Figure 44: (s_{10}) is the contour plot of the Peregrine solitons and (s_{11}) the 2D spatiotemporal evolution of the Peregrine rogue wave at $C_1 = 20pF$, $C_2 = 470pF$ at $J_0 = 200nA$, $L_1 = 480\mu H$.

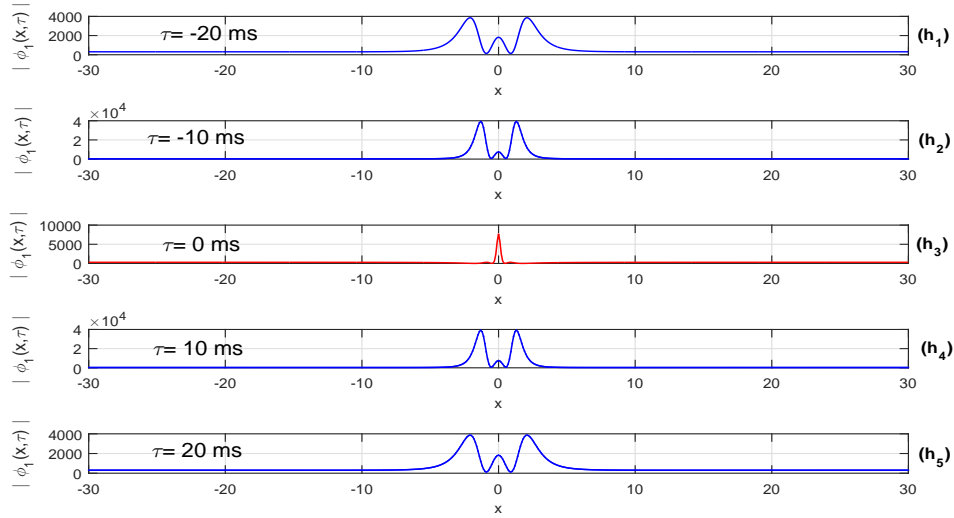


Figure 45: Spatiotemporal plot evolution of the Peregrine solitons at $\tau = 0 \text{ ms}$, $\tau = 5 \text{ ms}$, $\tau = 10 \text{ ms}$, $\tau = 15 \text{ ms}$, $\tau = 20 \text{ ms}$ for $C_1 = 420 \text{ pF}$, $C_2 = 480 \text{ pF}$ at $J_0 = 200 \text{ nA}$, $L_1 = 480 \text{ }\mu\text{H}$.

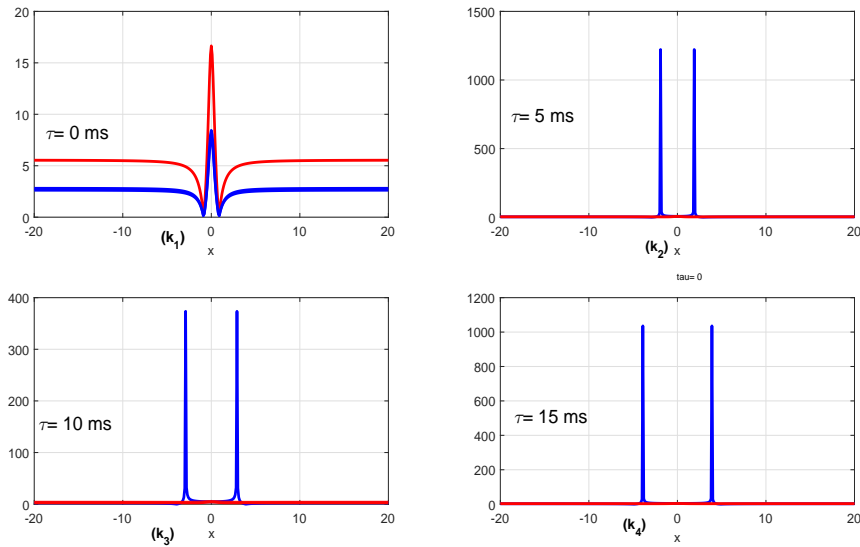


Figure 46: Spatiotemporal plot evolution of the Peregrine solitons $\tau = 0 \text{ ms}$, $\tau = 5 \text{ ms}$, $\tau = 10 \text{ ms}$, $\tau = 15 \text{ ms}$, $\tau = 20 \text{ ms}$ for $C_2 = 2C_1$ (blue line) and $C_1 = 2C_2$ (red line) at $J_0 = 200 \text{ nA}$, $L_1 = 480 \text{ }\mu\text{H}$.

$\tau = 5 \text{ ms}$, $\tau = 10 \text{ ms}$, $\tau = 15 \text{ ms}$, $\tau = 20 \text{ ms}$, the Peregrine has a high frequency of appearance and disappearance very high and with equal and equidistant time intervals. However, figure 46 represents the spatio-temporal evolution of the Peregrine wave with the effect of the capacitors (C_1 and C_2). It is highlighted by the (red line) when the capacitor C_1 is larger than C_2 . The (blue line) gives the major effect of the capacitor C_2 on the shape of the PS (the two peaks below in Fig.35, are exposed here by the blue line). When the capacitor C_1 becomes larger than the capacitor C_2 , the Peregrine shape disappears (red line) in figure 35. We can conclude by saying that, as previously indicated in the modulation instability, the capacitor C_1 when it becomes larger than C_2 limits the amplification of the gain, which is reflected here by the decrease in the amplitude of the peregrine or even its extinction. This situation translates into a loss of energy in the line, due to the increase of C_1 , i.e. the decrease of the plasma frequency.

3.4.3 Super rogues waves soliton

For SRWs, it is considered $\psi = \sqrt{\frac{Q}{2P}}\phi_1$ and $T = \tau P$, then equation (2.125) gives [22].

$$i\frac{\partial\psi}{\partial T} + \frac{\partial^2\psi}{\partial x^2} + 2|\psi|^2\psi = 0. \quad (3.53)$$

Now we can assume the solution of equation (3.53) as follows [22, 23].

$$\psi(x, T) = \left(1 - \frac{G + iH}{D}\right) e^{2iP\tau}, \quad (3.54)$$

where

$$\begin{aligned} G &= \left(x^2 + 4\tau^2 + \frac{3}{4}\right) \left(x^2 + 20\tau^2 + \frac{3}{4}\right) - \frac{3}{4}, \\ H &= 2T(4\tau^2 - 3x^2) + 2\tau \left[(2x^2 + 4\tau^2)^2 - \frac{15}{8}\right], \\ D &= \frac{1}{3}(x^2 + 4\tau^2)^3 + \frac{1}{4}(x^2 - 12\tau^2)^2 + \frac{3}{64}(12x^2 + 176\tau^2 + 1). \end{aligned} \quad (3.55)$$

It should be noted that this solution has a remarkable property when $x = 0$ et $\tau = 0$, there is an increase in the amplitude of the carrier wave. Figures 47-50 shows the effects of the nonlinear electrical transmission line parameters (C_1 , C_2 and L_1) and the wave number. From figure 47 and 48, it can be observe that when C_1 is more important than C_2 , the SRW emerges which is higher than the PS. From figure 49, it is given at different times $\tau = 0 \text{ ms}$, $\tau = 5 \text{ ms}$,

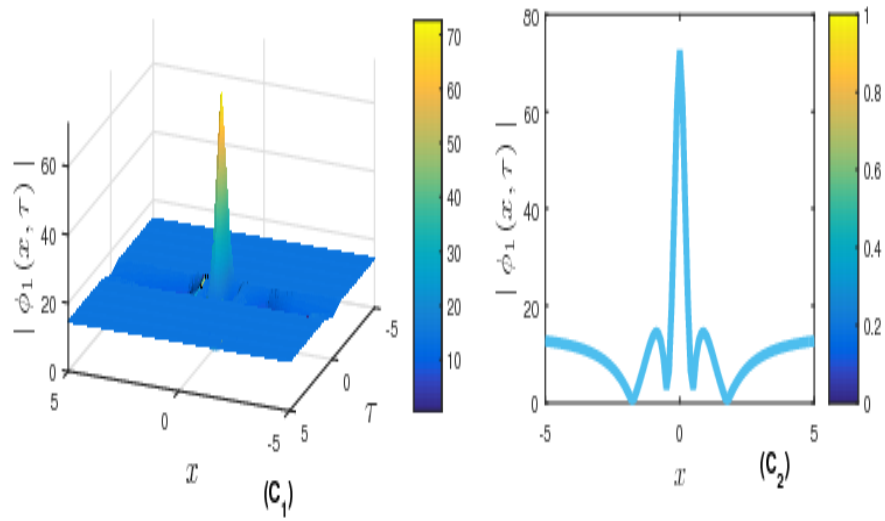


Figure 47: (C_1) Spatiotemporal plot evolution and (C_2) plot 2D of the SRWs at $C_2 = 210C_1$ at $J_0 = 200 \text{ nA}$, $L_1 = 480 \mu\text{H}$.

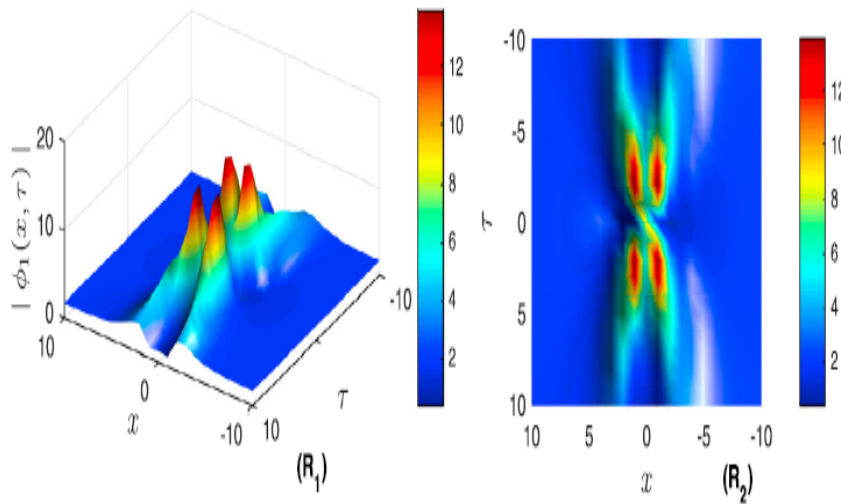


Figure 48: (R_1) Spatiotemporal plot evolution and (R_2) contour plot of the SRWs at $C_1 < C_2$ and $J_0 = 200 \text{ nA}$, $L_1 = 480 \mu\text{H}$.

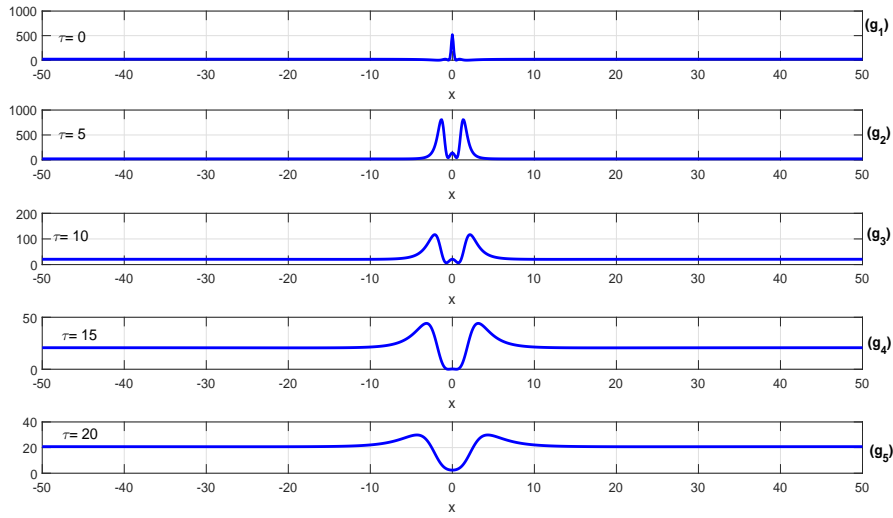


Figure 49: Spatiotemporal plot evolution of the SRWs at (g_1) $\tau = 0$ ms, (g_2) $\tau = 5$ ms, (g_3) $\tau = 10$ ms, (g_4) $\tau = 15$ ms, (g_5) $\tau = 20$ ms for $C_1 < C_2$ and $J_0 = 200$ nA, $L_1 = 480$ μ H.

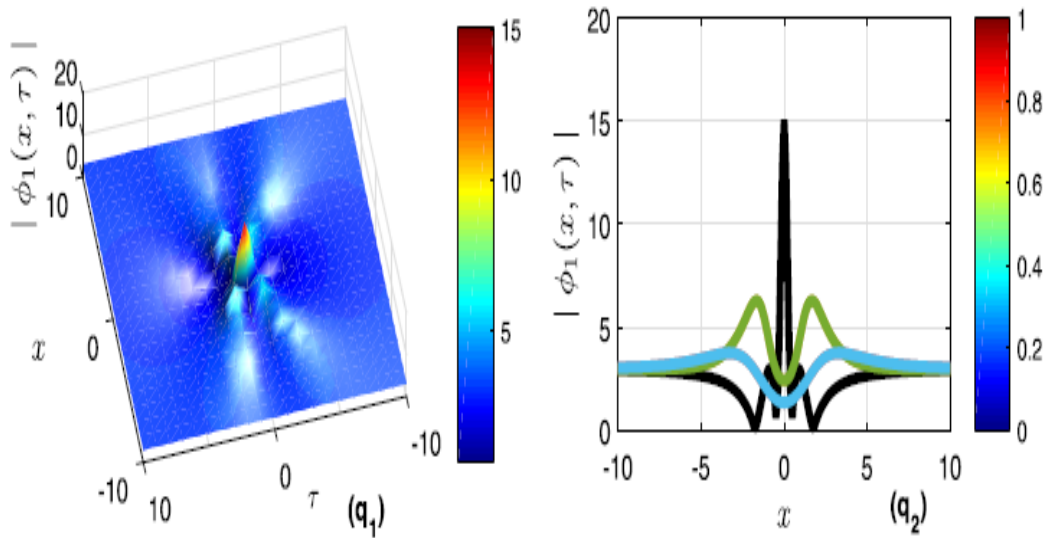


Figure 50: (q_1) Spatiotemporal plot evolution of the SRWs (q_2) and contour plot evolution at $C_2 = 18.75C_1$ and $J_0 = 200$ nA, $L_1 = 480$ μ H, $\phi_0 = 2.064 \times 10^{-10}$.

$\tau = 10 \text{ ms}$, $\tau = 15 \text{ ms}$, $\tau = 20 \text{ ms}$ the shape of the SRWs. At $\tau = 0 \text{ ms}$, the SRW is forming with a good shape, and progressively the SRW shape seem to be a PS, and we can affirm that when the capacitors value decrease, the amplifying SRW is stopping. However, figure 37 gives the most specific form of the SRW with decreasing amplitude. Furthermore, it is pointed out that the wave energy is located in a small area due to the nonlinear and dispersion terms of NLS equation. These obtained results highlight the dynamic progresses of the SRWs. In summary, the amplitude and width of the peregrine decreases with increasing $C_1 = 2C_2$, until it disappears figure 48. The opposite behavior is observed in the same figure 37 where the amplitude and width of the peregrine increases with the increase of $C_2 = 2C_1$. The PS predicts the energy concentration in a small region due to the highly nonlinear value contributed by JJ. Physically, increasing the C_2 parameters reduces the nonlinearity and disperses the energy, making the pulses shorter. On the other hand, an increase in ω_j would lead to an increase in nonlinearity and would then concentrate a significant amount of energy, making the pulses larger. We can see that the characteristics of the SRW are similar to those obtained for the PS. The amplitude and width of the SRW decrease with the increase of the C_2 parameter. On the other hand, the amplitude and width of the SRW increase with the increase of the non-thermal parameter ω_j . The absolute values of the Peregrine solution and the SRW solution are shown in figures 43 and 47, which shows the localization of the energy in a small area of space and time. One of the most interesting features of these solutions is that the SRWs excitations have higher amplitudes and are more concentrated compared to the PS. Such waves appear in regions where modulated waves are expected as a result of the interaction between nonlinear and dispersive effects. It is interesting to note that the RW originates from the modulation instability with resonance perturbations for which the dominant frequency and propagation constant are equal to those of the continuous wave background [107]. This feature will help us realize the dynamics of RWs in many different physical systems, such as nonlinear fibers, Bose Einstein condensates, wave water tanks, and plasmas. Also, note that RWs exist in unstable systems, but not all unstable systems allow for the existence of RWs. The results provide some useful tools for analyzing whether an RW can exist in a nonlinear system. Note that modulation instability analysis can only be used to understand the process of weak perturbation amplification for nonlinear localized waves; it cannot explain their entire dynamical processes. It is still necessary to develop new methods,

especially numerical simulation, to understand the whole dynamical processes of fundamental waves and even of higher order waves.

3.5 Enveloppe soliton : Bright and dark

This equation admits the following bright and dark solitons solutions respectively [140]. From the above curves, $PQ > 0$ for frequency belonging to $6.3 \times 10^8 kHz < f < 6.655 \times 10^8 kHz$ and we have the following soliton Bright solution:

$$\phi_1(x, \tau) = A \operatorname{sech} \left(A \sqrt{\left| \frac{Q}{2P} \right|} (x - v\tau) \right) e^{i(kx - \omega\tau)}, \quad (3.56)$$

Similarly, $PQ < 0$ for frequency belonging to $6.656 \times 10^8 kHz < f < 6.8 \times 10^8 kHz$ and we have the following soliton dark solution :

$$\phi_1(x, \tau) = A \tanh \left(A \sqrt{\left| \frac{Q}{2P} \right|} (x - v\tau) \right) e^{i(kx - \omega\tau)}. \quad (3.57)$$

With $k = \frac{v_g}{2P}$ is the wave number of the soliton; $\omega = \frac{v_g v_p}{2P}$ the angular frequency; $A = \sqrt{\frac{v_g^2 - v_g v_p}{2PQ}}$ wave amplitude [140].

The objective here is to show analytically the propagation of the above bright and dark solitons of nonlinear Schrödinger equation (2.125), which governs the propagation of the modulated waves in NETL with JJ. Thus, to illustrate the properties of the solitons in great details. Figure 52 plots the spatiotemporal profile of the dark soliton at different times, $t = 0$, $t = 0.01s$, $t = 0.02s$, and $t = 0.03s$, and the analytical evolution of the bright soliton in figure 40 at different times, $t = 0$, $t = 0.04s$, $t = 0.08s$ and $t = 0.12s$. It has been shown that the propagation of the robustness of dark soliton and bright soliton with stable shape and width. As a result, the soliton moves from left to right direction which corroborate a positive signs of group and phase velocities in the line. This behavior confirms the theoretical hypotheses on the conventional NETL. It emerges from this analysis that the plasma the variation of capacitance behaves as energy source in the structure. In the next section, it is used the some algebraic transformation to seek the behavior of the SRWs and PS in the NETL with JJ.

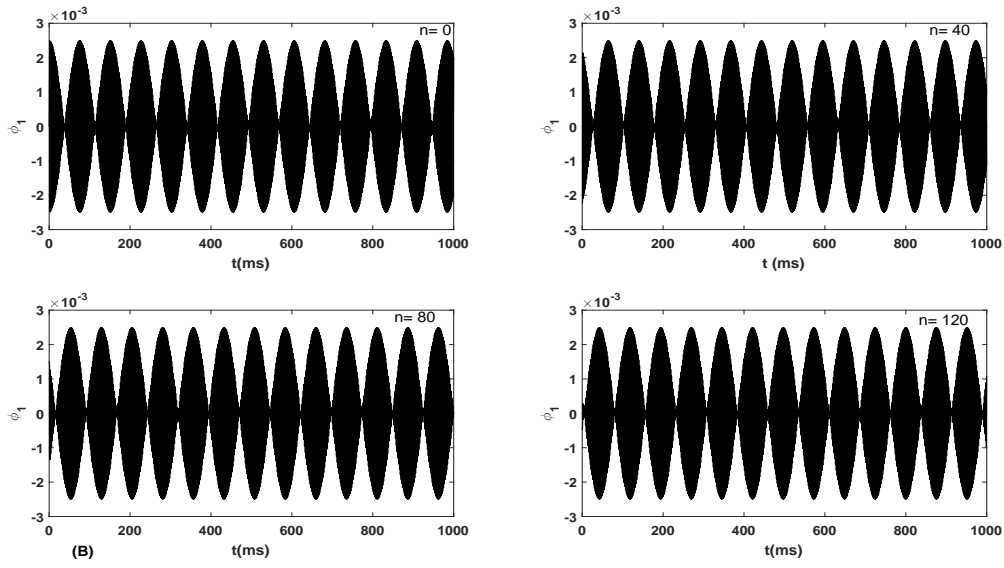


Figure 51: Spatiotemporal plot evolution of the bright soliton with ($t=0$) as initial condition at $C_1 = 50pF$, $C_2 = 750pF$, $\omega_j = 0.034$, $\omega = 0.0026$, and $J_0 = 200nA$, $L_1 = 240 \mu H$, $\phi_0 = 2.064 \times 10^{-10}$.

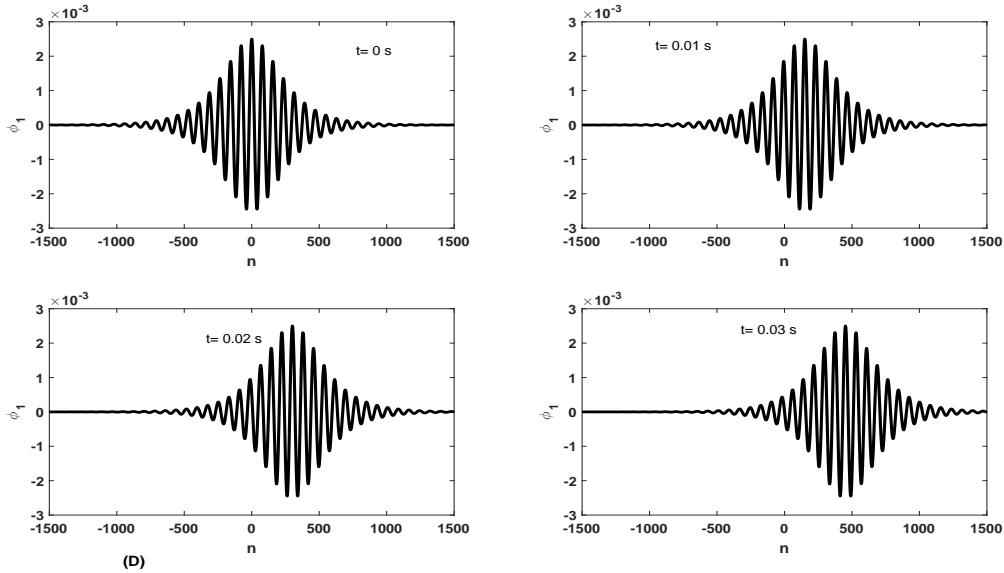


Figure 52: Spatiotemporal plot evolution of the dark soliton at $C_1 = 50pF$, $C_2 = 750pF$, $\omega_j = 0.034$, $\omega = 0.0026$, and $J_0 = 200nA$, $L_1 = 240 \mu H$, $\phi_0 = 2.064 \times 10^{-10}$.

3.6 Numerical simulation

The main objective of the previous section was to determine the parameter areas where the nonlinearities brought by the JJ balance with the dispersion to give rise to modulated waves and nonlinear patterns such as bright, dark, RWs solitons and other exotic patterns. In view of these results, we can consider a numerical analysis to better observe the phenomena predicted by the results obtained analytically. Given that, the linear stability analysis says nothing about the long time evolution of the disturbance, which requires direct numerical simulation to be validated. For this purpose, we use a direct numerical integration of the discrete equation (2.115), to point out the behavior of the perturbed plane wave and exhibit the propagation of the modulated waves bright and dark solitons in the structure. It is worth to indicate that we have predicted in the analytical section that the variation of the plasma frequency can induce unstable/stable modes in the system. So, to corroborate this prediction we have to consider the same parameters used above and seek the behavior of the solitonic waves.

3.6.1 Localized waves in NETL with JJ

In this section, we consider the following periodic solution as initial condition :

$$\phi_n = \phi_0 (1 + 0.01 \times \cos(Kn)) \cos(kn), \quad (3.58)$$

with ϕ_0 the initial amplitude, K the perturbed wave vector, k wave vector of the initial plane wave. For numerical simulation we assume:

$$\begin{aligned} \frac{d\phi_n}{dt} &= V_n, \\ \frac{d}{dt} (V_{n+1} - 2V_n + V_{n-1}) + \omega_0^2 (\phi_{n+1} - 2\phi_n + \phi_{n-1}) + \mu_0 \frac{dV_n}{dt} \\ &+ \omega_j^2 \phi_n - \frac{\omega_j^2}{6} \phi_n^3 = 0. \end{aligned} \quad (3.59)$$

After some mathematical manipulation, we use MATLAB ODE45 solver. We fix the cell index $N = 250$ and the propagation time $t = 1500s$ while the parameters of the of the JJ are keep fix as ion analytical investigation.

For $C_1 = 400.2pF$ and $C_1 = 750pF$ respectively with the corresponding plasma frequencies $\omega_j = 6.06 \times 10^3$ and $\omega_j = 3.20 \times 10^3$, in Figure 53a-b, it is shown the propagation of the trains

of pulse while the bottom panel (figure 53c-d) shows the evolution of the SRWs. We have equally exhibited that the amplitude of the SRW increases to 2 in figure 53d. It emerges that the plasma frequency is being as source of energy in the system.

Beside in figure 54a-b, we have fixed the value of the capacitor as well as the plasma frequency. From figure 54a we have set the wave vector $k = 0.1$ and at specific time of propagation $t = 10s$, it is emerged the SRWs where the higher peak amplitude is 3.5. For strong specific time of propagation $t = 20s$ and the wave vector is considered to $k = 0.5$, it is observed three peaks. One can observe that the variation of the wave vector at specific time of propagation generate the SRWs in the structure as it was predicted in our analytical investigation.

However, it is also shown that increasing the values of the structure parameters reduce the amplitude of the train of wave. Looking closely at the individual objects, we notice their similarity to RWs, where a train of pulse displayed against space presents an Akhmediev sniffer. This is a confirmation is given analytics, in which lower values of the capacitor C_1 support the appearance of RWs, showing their direct relationship with the appearance of modulation instability. In addition, increasing the value of modulation instability delays and reduces the amplitude of the wave train with the increase of the propagation time. This is therefore not a surprise but rather reinforces the fact that the exact solutions of the NLS equation that describes the nonlinear mode of modulation instability are the Akhmediev breathers. The advantage of the proposed model, which in the context of other nonlinearity, can support more exotic behaviors and give more insights for experimental investigations. This particular scenario is summarized in figure 53, shows a cross section of the molecular structures forming the trains. At the constant propagation distance, the same structures vary with the value of the plasma frequency, as shown in the figure 53-54. The instability is characterized by a train of extended bell-shaped solitons. The scenario changes when C_1 takes the respective values 2 and 3 times larger than C_2 , where we notice the emergence of trains of solitons with two bumps, with a lower band between the two. On a long distance propagation, we obtain the results presented analytically in figure 31. Remarkably, we observe persistence in the formation of RW trains, which confirms their robustness in the studied model. To go further, we should also point out that such Akhmediev blowers were classified as type B in ref. [153], where their appearance was also related to the development of modulation instability. The study of tools to control the

shape and characteristics of such structures has been the subject of a recent discussion, where it has been shown that the frequency of modulation may play an important role under conditions where the coefficients vary periodically [154]. This could lead to wave compression in some contexts, requiring additional bifurcation theory tools to be predicted and controlled. However, in the present case, the combination of the Josephson nonlinearity and the effects of the C_1 and C_2 capacitors also offers the possibility to the formation of soliton trains that include several modes, the only requirement being a judicious choice of the wave and system parameters. For example, by fixing the plasma frequency, Fig. 36, we show the wave modulation adopts different behaviors when the wave vector increases.

The interest of the JJ lies in their specific properties, significantly different from those of the variable capacitor. Their peculiarity is due to their high nonlinear indices which come from high refractive indices, leading to higher nonlinear coefficients than the variable capacitor. Thus, models including a JJ nonlinearity provide a good description of the characteristics of the modeled media, especially metals. In the context of high pumping powers, leading to large nonlinear absorption with complicated practical applications, relatively moderate nonlinear absorption can be provided by a saturation of the cubic nonlinearity provided by the JJ. These enhanced properties of suitable nonlinear saturable materials require improved models that illustrate their tunability, conditioned by a tunable absorption capacity when pumped by electron peers that are in resonance with no core material energy level. Intrinsically, the nonlinear response of the materials is a more complex function of the light flux intensity. In our case, the JJ and the metal can then constitute a composite material with specific properties. One example is the incorporation of Au nanoparticles which can significantly improve the nonlinear properties of graphene oxide [154].

3.6.2 Modulated waves patterns in NETL with JJ

As we have predicted in analytical results that both bright and dark can propagate in the line with JJ. Now we use the numerical simulation to seek the robustness of the obtained analytical investigation. For this fact, we consider equations (2.128 and 2.129) as initial conditions. The width of the modulated solitonic waves is $x_0 = 10$ and the initial position is $x(0)$.

For modulated wave bright soliton we use equation (2.24) and we set $k = 0,25$ with $C_2 = 20 pF$. From figure 44a-d, it is shown the propagation of the bright soliton at different time for the cell index $n = 150$. One can observe that obtained bright soliton spread from left to right with stable shape. This result is given for $C_1 = 400,2 pF$ witch correspond to $\omega_j = 6,06 \times 10^3 rad/s$. In figure 56a-d, we have fined the value of the $\omega_j = 3,20 \times 10^3 rad/s$ and varying the wave vector k . For $k = 0,1$, it is pointed out in figure 56a a modulated wave pattern has fulfilled with breather behavior. It is equally observing that the amplitude of the solitonic wave increases. Increasing strong enough the wave vector to $k = 0,5$ and $k = 0,75$ respectively in figure 56d, we exhibit the modulated waves bright soliton where the amplitude increases.

One result from this analysis the JJ can increase the amplitude of the bright soliton in nonlinear transmission line with JJ. This result, can open new features to the solitonic waves in nonlinear structures.

Following the same procedure as we did for bright soliton, we use the equation (2.129) as initial condition. In figure 57a-b, we have displayed the propagation of dark soliton for $C_1 = 960 pF$, $C_2 = 420 pF$ and $k = 0,75$. One emerges that the modulated wave dark soliton spreads with stable shape in the structure. Beside, in bottom panel figure 46c-d, we have increase the wave vector to $k = 1,25$ and it is shown that the dark soliton tends to expand preserves its shape.

One results that despite the fact that the dark soliton is a stable wave, it is propagated with stable shape in the system where the JJ is used. Figure 53a-b train of waves figures 53c-d localized waves like rogue waves at specific time of propagation. Figures 42a-b denotes the values of the plasma frequencies (a) $\omega_j = 6,06 \times 10^3 rad/s$; (b) $\omega_j = 3,20 \times 10^3 rad/s$. The other parameter are $J_0 = 200 nA$, $L_1 = 780 \mu H$. Figure 43 localized modes close to rogue wave (a-b) are respectively the variation of the excitation wave vector k . (a) $k = 0,5$ and $k = 1,4$. The other parameter are $C_1 = 400 pF$, $C_2 = 700 pF$ and $J_0 = 200 nA$

3.7 Conclusion

The purpose of this chapter is to establish to unearth the envelope solitons, the SRW and the PS to the NLS equation obtained by using the reductive perturbation method in the semi-discrete approximation. Through the coefficients of dispersion and non linearity the areas of

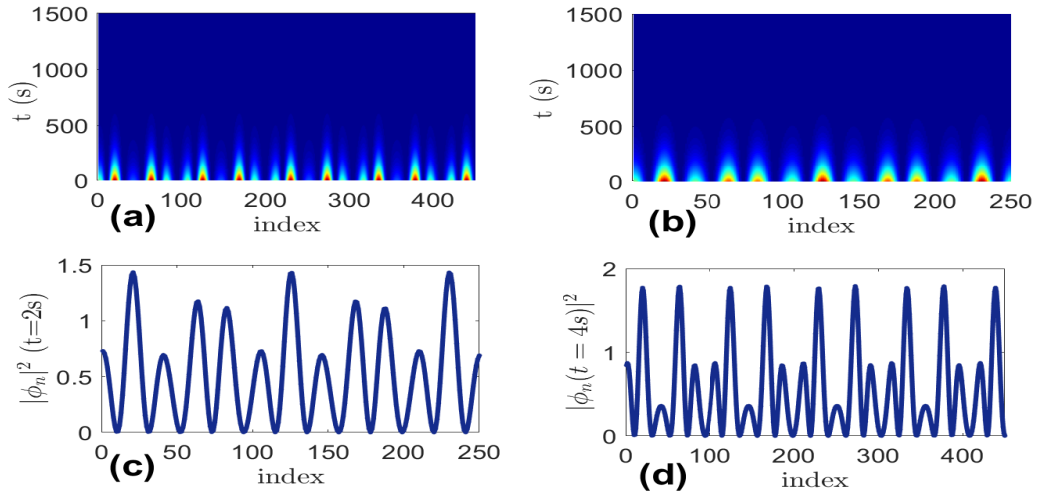


Figure 53: Localized waves like rogue waves at specific time of propagation with the values of the plasma frequencies (a) $\omega_j = 6,06 \times 10^3 \text{rad/s}$; (b) $\omega_j = 3,20 \times 10^3 \text{rad/s}$. The other parameter is $J_0 = 200 \text{nA}$, $L_1 = 780 \mu\text{H}$.

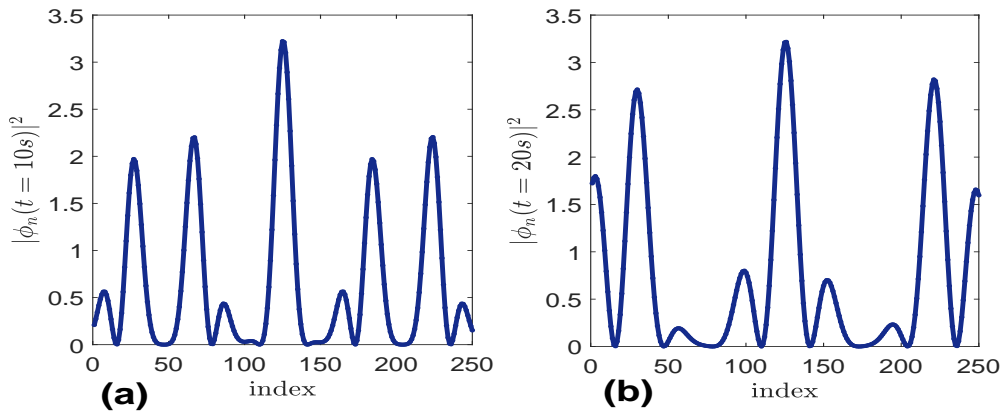


Figure 54: Localized modes close to rogue wave (a-b) are respectively the variation of the excitation wave vector k . (a) $k = 0,5$ and $k = 1,4$. The other parameter are $C_1 = 400 \text{pF}$, $C_2 = 700 \text{pF}$ and $J_0 = 200 \text{nA}$

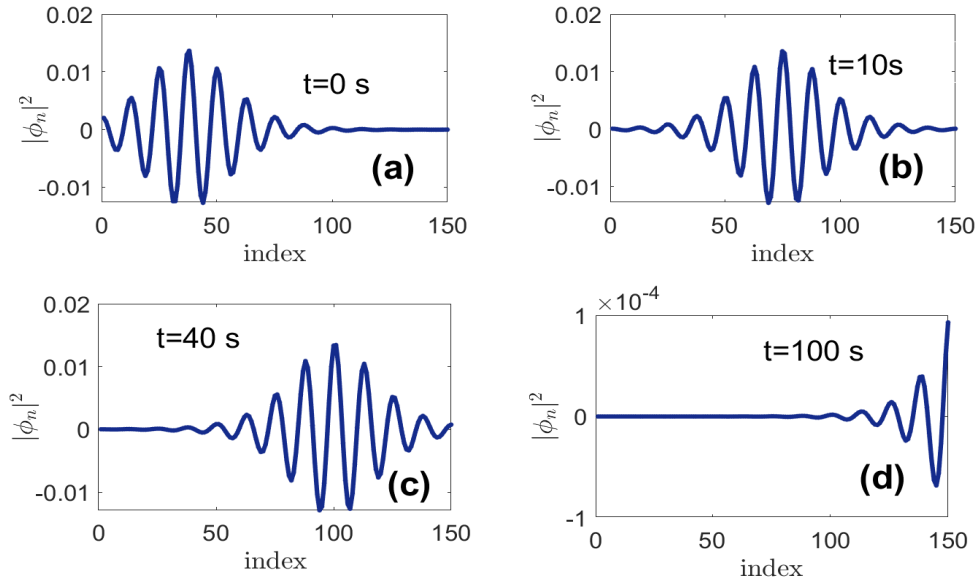


Figure 55: The propagation of the bright soliton at different time for the cell index $n = 150$, given for $C_1 = 400, 2pF$ witch correspond to $\omega_j = 6,06 \times 10^3 rad/s$. and $J_0 = 200nA$, $L_1 = 240 \mu H$, $\phi_0 = 2.064 \times 10^{-10}$.

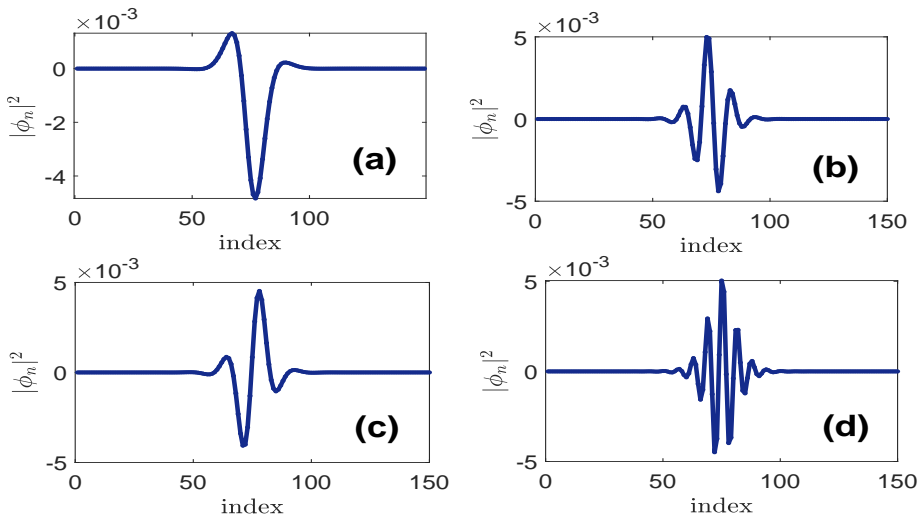


Figure 56: The propagation of the modulated wave pattern has fulfilled with breather behavior, with the value of the $\omega_j = 3,20 \times 10^3 rad/s$ and varying the wave vector k . For $k = 0, 1$, Increasing strong enough the wave vector to $k = 0,5$ and $k = 0,75$ and other parameters $J_0 = 200nA$, $L_1 = 240\mu H$ $\phi_0 = 2.064 \times 10^{-10}$.

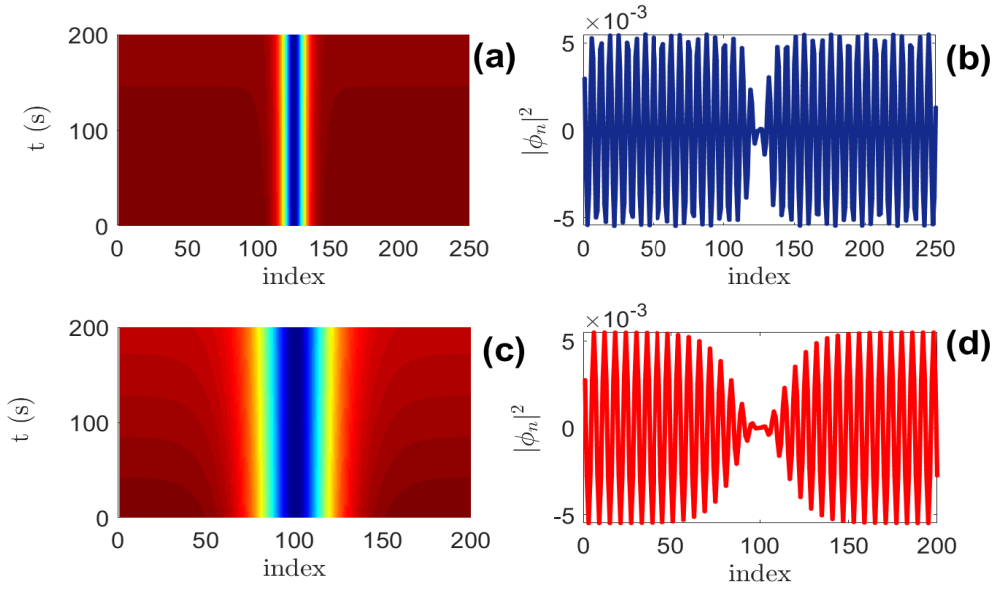


Figure 57: The propagation of dark soliton with $C_1 = 960 \text{ pF}$, $C_2 = 420 \text{ pF}$ and $k = 0,75$. When we have increase the wave vector to $k = 1,25$ and it is shown that the dark soliton tends to expand preserves its shape.

propagation of the bright and black solitons have been identified, thus the areas of instability. The most relevant observation is that the obtained RW show regions of energy concentration which are influenced by the parameters of the NETL with JJ. On the other hand, we realize that the frequency of the plasma related to the flow of the JJ, have an effect to the obtained results. It has been also study the modulation instability analysis to highlight the process of magnifying small perturbation for the solitary waves. Numerical investigation have been done to more understand the dynamic process of the RWs.

General Conclusion

At the start of this thesis, we hypothesized that an electrical transmission line model consisting of a parallel Josephson junction network, taking into account parasitic capacitive effects in the line, would facilitate the propagation of various localized wave profiles at infrared frequencies.

The answer to this hypothesis will lead us to formulate the following research objectives:

Using the fractional derivative, demonstrate the possibility of propagation in nonlinear transmission lines of rational solitons such as brilliant W-form solitons;

Construct a nonlinear transmission line model based on a compact parallel Josephson junction network capable of taking into account all the effects involved in the detection of a very high-frequency signal;

Use the reductive perturbation method in the semi-discrete approximation to construct the nonlinear Schrödinger equation (1-NLSE) representing the mathematical model of the line;

Demonstrate analytically the possibility of dark and bright soliton propagation, and other localized waveforms, using the modulation instability study;

Confirm the propagation of the various localized wave profiles above using numerical simulation.

The first objective was to demonstrate, using the fractional derivative, the possibility of propagation in nonlinear transmission lines of rational solitons such as bright W-form solitons. The new extended direct algebraic method makes it possible to demonstrate bright and dark W-form solitary waves, kink-type soliton solutions, periodic solutions and rational solutions. In addition, the use of the sub-ODE method has made it possible to add new types of solutions called elliptic Weierstrass functions. This article proposes a plethora of traveling waves that include the results obtained previously. By choosing appropriate values of the order of the

conformal derivative, the behaviors of the results obtained have been illustrated graphically in 3D and 2D, and these soliton solutions are identical to the results obtained in the nonlinear differential equations that describe the propagation of long waves in shallow water. This result shows that rational solitons propagate in non-linear transmission lines.

The second objective was to build a nonlinear transmission line model based on a compact parallel Josephson junction network capable of taking into account all the effects involved in the detection of a very high-frequency signal. After a literature review, on the one hand on the generalities of nonlinear power lines, including the basic concepts, the modeling process, the types of nonlinear components and the mathematical equations to which they lead. Secondly, on localized waves propagating in NETLs. It appears that the weakness of the nonlinear components used to date limits the possibility of obtaining certain localized wave profiles at very high frequencies. Whereas several recent works also show that the Josephson junction can overcome this problem thanks to its strong nonlinearity. But most of them have been applied to left-hand lines made of metamaterials with different structures. In this work, we chose to integrate the JJ into a straight line. To do so, we integrated the JJ next to the non-linear capacitor C_2 to substitute it, thus making the capacitor rather linear. In addition, at very high frequencies, the JJ creates capacitive effects on the line in the horizontal direction, and these effects are modeled by the C_1 capacitor. This is justified by the fact that the line on the right, which is a conventional line, models a normal conductor, while the line on the left models an artificial conductor. This will enable us not only to test the very high-frequency conduction capability of current conductive materials, but also to synthesize and control these materials in order to build coherent arrays of junctions for a number of technical applications. This confirms the relevance of this model for this investigation.

The third objective was to use the reductive perturbation method in the semi-discrete approximation to construct the nonlinear Schrödinger equation (1-NLSE) representing the mathematical model of the line from the previous model. We applied Kirchoff's laws to this cell and deduced the discrete Sine-Gordon equation that serves as the mathematical model for our line. In addition, given the sufficiently small amplitudes of the wave, we perform a limited sinusoidal

development and a semi-discrete approximation of the initial wave, which we subject to a slight transverse perturbation. By calculating the algebraic equations and cancelling the third-order coefficients, we obtain the NLSE that governs the envelope dynamics. This operation will enable us to highlight the essential parameters of the line, such as the dispersion relation, group velocity, dispersion coefficients and non-linearity. At the end of this operation, we'll present a few methods for analyzing modulation instability used in different fields of physics, and we'll introduce the method we've chosen for our study. This mathematical tool will enable us to establish the zone of wave propagation stability, identify the key parameters of our line stability and generate other localized wave models.

The fourth objective was to demonstrate analytically the possibility of dark and bright soliton propagation, and other localized waveforms, using the modulation instability study. In the first section, after analyzing the stability of our model, we see that there is indeed a zone of stable wave propagation and a zone of unstable wave propagation. This stability is strongly dependent on the plasma frequency, as determined by the non-linearity coefficient Q of the NLS equation. We deduced from this result that bright and dark solitons propagate in two regimes of cut-off frequencies. As the analytical solutions are known, we have represented the solitons at different times and appreciated the evolution and profile of the solitons during their evolution. Section 3 also introduces analytical solitons, in particular peregrine solitons and super-scare waves. In the second section, we study the propagation of peregrine solitons and super rogue waves. We already know that for certain parameter values, the instability energy is assumed to be localized in a small area in space and time, leading to the formation of rogue waves. For the Peregrine soliton, we have defined the expression obtained by [22], to which we have integrated our parameters, in particular the dispersion and nonlinearity coefficients. We have given illustrations of the analytical results of its 3D evolution. In addition, we have also provided illustrations of Peregrine in 3D for different values of the capacitor C_1 . The spatio-temporal evolution of the Peregrine soliton in the line at different instants has also been given ($t = 0ms, t = 5ms, t = 10ms, t = 15ms, t = 20ms$). In addition, the influence of capacitors C_1 and C_2 on the spatio-temporal evolution of the Peregrine soliton was also given. This shows that when the capacitor C_1 is larger than C_2 , the peregrine form disappears for SRWs. To verify the

propagation of SRWs, we defined the expression obtained by [22], to which we incorporated our parameters, in particular the dispersion and nonlinearity coefficients. We note that this solution has a remarkable property when $x = 0$ and $t = 0$, there is a significant increase in the amplitude of the carrier wave. The different waveforms also show the effects of line parameters (C_1 , C_2 and L_1) and wavenumber. We can also observe that when C_1 is greater than C_2 , the carrier wave emerges and is higher than the Peregrine soliton. The graphs show the evolution of the carrier wave profile in the line at various times ($t = 0ms, t = 5ms, t = 10ms, t = 15ms, t = 20ms$). At $t = 0ms$, the SRW forms with a good shape, and gradually the shape of the SRW seems to become peregrine again, and we can say that when the value of the capacitors decreases, the amplification of the SRW stops. The numerical analysis carried out confirmed the propagation of the various modulated wave profiles obtained analytically. In addition, this numerical analysis enabled us to assess the wave profile after a time t , which cannot be done by the analytical method.

In view of the different localized wave profiles obtained, we can say that the hypothesis formulated at the outset has been validated. As a result, our model is relevant to the design of a SQUID network capable of detecting very high-frequency waves in the infrared range, leading to a plethora of applications in different areas of life.

Appendix

3.8 Deduction of the discrete transmission line equation

By using the famous Kirchhoff Laws in current and voltage on the lattice of Figure 16 reveals the following nonlinear discrete equations which describes the modulated waves in the lattice :

The law of the nodes leads to the following relation:

the first nodes in front of i_n give the relation :

$$i_n = i_L + i_{C_1}, \quad (3.60)$$

the last nodes before i_{n+1} give the relation :

$$i_{n+1} = i_{L_1} + i_{C_1} - i_{C_2} - J_n, \quad (3.61)$$

The law of meshes gives us the following relation:

In the mesh bounded by V_{n-1} , V_{C_1} and V_n we have the following relation :

$$V_{n-1} - V_n = V_{C_1}, \quad (3.62)$$

In the mesh bounded by V_{n-1} , V_{L_1} and V_n we have the following relation :

$$V_{n-1} - V_n = V_L, \quad (3.63)$$

In the mesh bounded by V_{n-1} , V_{L_1} and V_{C_2} we have the following relation :

$$V_n = V_{C_1} + V_{C_2}, \quad (3.64)$$

Substituting relation Eq.(2.165), Eq.(2.164) in Eq.(2.163), we obtain the relation :

$$i_{n+1} = \frac{1}{L_1} \int (V_{n-1} - V_n)dt + C_1 \frac{d}{dt}(V_{n-1} - V_n) + C_2 \frac{d}{dt}V_n + J_n, \quad (3.65)$$

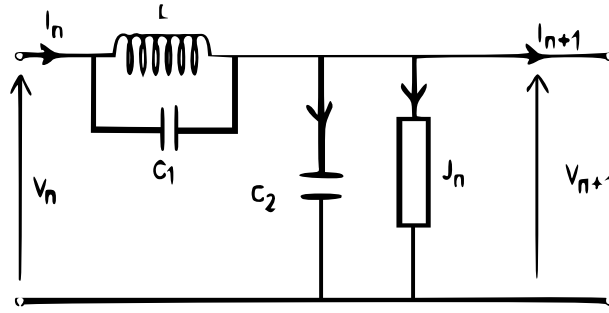


Figure 58: Schematic representation of the nonlinear electrical transmission line with Josephson junction

Substituting relation Eq.(2.165), Eq.(2.164) in Eq.(2.162), we obtain the relation :

$$i_{n+1} = \frac{1}{L_1} \int (V_{n-1} - V_n) dt + C_1 \frac{d}{dt} (V_{n-1} - V_n) \quad (3.66)$$

with,

$$V_n = \frac{d\phi_n}{dt}. \quad (3.67)$$

Equating Eq.(2.167) with Eq.(2.168) and substituting Eq.(2.169) we obtain the following relation :

$$\frac{\phi_{n-1} - 2\phi_n + \phi_{n+1}}{L} + C_1 \frac{d^2}{dt^2} (\phi_{n-1} - 2\phi_n + \phi_{n+1}) + C_2 \frac{d}{dt} V_n + J_n = 0, \quad (3.68)$$

Then replacing Josephson's current J_n by $J_0 \sin\left(2 \frac{\pi \phi_n}{\phi_0}\right)$ we deduce the following equation:

$$\frac{\phi_{n-1} - 2\phi_n + \phi_{n+1}}{L} + C_1 \frac{d^2}{dt^2} (\phi_{n-1} - 2\phi_n + \phi_{n+1}) + C_2 \frac{d^2 \phi_n}{dt^2} + J_0 \sin\left(2 \frac{\pi \phi_n}{\phi_0}\right) = 0, \quad (3.69)$$

3.9 How the junction works as a SQUID magnetic field sensor

In 1962, twenty-two-year-old British physicist Brian D. Josephson came up with the idea that Cooper pairs could cross an insulating barrier without breaking. This prediction was verified

experimentally with junctions between two superconducting materials (niobium) separated by an insulator, in this case Nb-oxide-Nb, structures henceforth known as Josephson junctions. The Cooper pairs retain their phase coherence if the insulator is thin enough. Josephson treats the device as two weakly coupled quantum objects (interacting weakly with each other), with respective energy and wave functions U_2 and U_1 , Ψ_1 and Ψ_2 . When a potential difference V is applied between the two electrodes, the energy difference is :

$$\Delta E = U_2 - U_1 = 2eV. \quad (3.70)$$

The Josephson equations have three notable consequences: - The continuous Josephson effect is verified when $V = 0$: a supercurrent J of Cooper pairs is observed up to a maximum current density J_0 depending on the energy height and thickness da barrier. - The alternating Josephson effect is observed when a continuous potential difference V_0 is applied between the two electrodes, the Cooper pair current becomes oscillatory and there is emission of an electromagnetic wave of frequency f , given by Planck's relation, $E = \hbar f$. In this case, we obtain:

$$f = \frac{2eV}{\hbar} = \frac{V}{\Phi_0}, \quad (3.71)$$

where Φ_0 is the flux quantum, that is : $f = 0.810^{11} Hz.mV^{-1}$. So, for an applied voltage of $1mV$, we're in the microwave range, with wavelengths on the order of millimeters. - The mixing effect is observed if, in addition to an applied DC voltage V_0 , a microwave of frequency f is sent to the NIS device. The latter emits a wave at a frequency $f_0 = V_0/\Phi_0$, which mixes with the external frequency f . A continuous step is obtained in the characteristic of current J as a function of $V = 0$ whenever $f_0 = n.f$, with n an integer. These steps are called "Shapiro steps", after the experimenter who first observed them. These three effects have been demonstrated experimentally by numerous teams and are very well established. They have led to numerous applications, described below.

- The effect of a magnetic field on a Josephson junction: the case of SQUIDS.

Some important applications are based on the influence of a magnetic field on the Josephson effect. For the magnetic field has an important effect on superconductivity; it controls the phase

of the Cooper pair wave function. When we measure the current through a Josephson junction by varying the magnetic field, we observe that the maximum pair current I_{max} is controlled by the magnetic flux Φ . There's a perfect analogy with the diffraction of light by a slit. In this case, it's the magnetic flux that controls the phase of the superconducting wave function, whereas for the light wave, it's the distance traveled.

Bibliography

- [1] Josephson, B. D. " Possible new effects in superconductive tunneling, " Phys. Lett, vol. **1**, n° 17, p. 251-253, 1962.
- [2] Recoba Pawlowski, E. : Réseaux de SQUIDS à haute température critique pour applications dans le domaine des récepteurs hyperfréquences. Thèse de doctorat de l'Université Paris-Saclay.(2019).
- [3] Cormier, G. Cours genie électrique (GELE5222), chapitre 1 : Propagation d'ondes, (2010).
- [4] Muroya, K., Saitoh, N., and Watanabe, S. Physical Society of Japan, **51** (1982), <https://doi.org/10.1143/JPSJ.51.1024>.
- [5] Hirota, R., Suzuki, K. Theoretical and experimental studies of lattice solitons in nonlinear lumped networks, Proc IEEE **61** (1973) 1483.
- [6] Kenmogne, F., Ndombou, G. B., Yemélé, D., and Fomethe, A., Chaos, Solitons and Fractals, **75**(2015) 263.
- [7] Tse Ve Koon, K., Leon, L., Marquié, P., and Tchofo-Dinda, P., Phys. Rev. E-Stat. Nonlinear, Soft Matter Phys., **75** (2007).
- [8] French, D.M., Hoff, B.W., Heidger, S., Shiffler, D. Dielectric nonlinear transmission line, Proc. of 18th IEEE Int. Pulsed Power Conf. (Chicago, IL,2011), pp. 341-345.
- [9] Ikezi, H., DeGrassie, J.S., Drake, J. Soliton generation at 10 MW level in the very high frequency band, Appl. Phys. Lett. **58** (1991) 986-987.
- [10] Kuek, N.S., Liew, A.C., Schamiloglu, E., and Rossi, J.O. "Oscillating pulse generator based on a nonlinear inductive line," IEEE Trans. Plasma Sci. no. 10, **41** (2013) 2619-2624.

-
- [11] Fatoorehchi, H., Abolghasemi, H., and Zarghami, R., "Analytical approximate solutions for a general nonlinear resistor-nonlinear capacitor circuit model," *Appl. Math. Model.*, no. 19, **39** (2015) 6021-6031.
- [12] Ikezi, H., Wojtowicz, S.S., Waltz, R.E., de Grassie, J.S., and Baker, D.R., "High power soliton generation at microwave frequencies," *J. Appl. Phys.*, **64** (1988) 3277-3281.
- [13] Brown, M.P., and Smith, P.W. "High power, pulsed soliton generation at radio and microwave frequencies," in *Proc. 11th IEEE Int. Pulsed Power Conf.*, **1** (1997) 346-354.
- [14] Darling, J.D.C., and Smith, P.W. "High power pulse burst generation by soliton-type oscillation on nonlinear lumped element transmission lines," in *Proc. 17th IEEE Int. Pulsed Power Conf.*, (2009) 119-123.
- [15] Sanders, J.M., Lin, J.H., Ness, R., Kuthi, A., and Gundersen, M. "Pulse sharpening and soliton generation with nonlinear transmission lines for producing RF bursts," in *Proc. IEEE Int. Power Modulator High Voltage Conf.*, (2010) 632-635.
- [16] French, D.M., Lau, Y.Y., and Gilgenbach, R.M. "High power nonlinear transmission lines with nonlinear inductance," in *Proc. IEEE Int. Power Modulator High Voltage Conf.*, (2010) 598-599.
- [17] Belyantsev, A.M., Dubnev, A.I., Klimin, S.L., Kobelev, Y.A., and Ostrovskii, L.A. "Generation of radio pulses by an electromagnetic shock wave in a ferrite loaded transmission line," *Tech. Phys.*, **40** (1995) 820-826.
- [18] Seddon, N., Spikings, C.R. and Dolan, J.E. "RF pulse formation in nonlinear transmission lines," in *Proc. 16th IEEE Int. Pulsed Power Conf.*, (2007) 678-681.
- [19] Rossi, J.O., Rizzo, P.N., and Yamasaki, F.S. "Prospects for applications of hybrid lines in RF generation," in *Proc. IEEE Int. Power Modulator High Voltage Conf.*, (2010) 632-635.
- [20] Kuek, N.S., Liew, A.C., Schamiloglu, E., and Rossi, J.O. "Circuit modeling of nonlinear lumped element transmission lines," in *Proc. 18th IEEE Int. Pulsed Power Conf.*, (2011) 185-192.

- [21] Houwe, A., Abbagari, S., Inc, M., Gambo, B., Doka, Y.S., Kofane, T.C., Nisar, K.S. Chirped solitons in discrete electrical transmission line, *Results Phys.* **18** (2020) 103188.
- [22] Duan, J.K., Bai, Y.L. Rogue wave in coupled electric transmission line, *Indian J. Phys.* **92** (2018) 369-375.
- [23] Duan, J.K., Bai, Y.L., Wei, Q., Fan, M.H. Super rogue waves in coupled electric transmission lines, *Indian J. Phys.* **94**(2020) 879.
- [24] Peterson, G.E. Electrical transmission lines as models for soliton propagation in materials: elementary aspects of video solitons, *AT and T Bell Lab. Tech. J.* **63** (1984) 901.
- [25] Nejoh, Y. Envelope soliton of the electron plasma wave in a nonlinear transmission line, *Phys. Scr.* **31** (1985) 415.
- [26] Asma M., Othman W.A.M., Wong B.R. and Biswas A. Optical soliton perturbation with quadratic-cubic nonlinearity by semi-inverse variational principle *Proc.Romanian Acad. Ser. A*, **4** (2017) 331.
- [27] Vladimir P. M., Whether There is the Intrinsic Hall Effect in a Multi-Band Superconductor, *J. Phys. Soc. Jpn.*, **81** (2012) 1247.
- [28] Marcello D., The threshold of effective damping for semilinear wave equations, *Math. Methods Appl. Sci.*, **6** (2015) 1106.
- [29] Lennels J. and Fokas A. S., Chirp free bright optical soliton perturbation with Fokas Lenells equation by traveling wave hypothesis and semi-inverse variational principle, *Optik*, **170** (2018)431.
- [30] Ling L., Feng B.F. and Zhu Z., Multi-soliton, multi-breather and higher order rogue wave solutions to the complex short pulse equation, *Physica D: Nonlinear Phenomena*, **327** (2016)13.
- [31] Zhang Y., Yang J. W., Chow K. W. and Wu C.F., Solitons, breathers and rogue waves for the coupled Fokas-Lenells system via Darboux transformation 2017 *Nonlinear Anal. Real World Appl.* **33** 237.

- [32] Jawad A. J. M., Biswas A., Zhou Q., Moshokoa S. P. and Belic M., Optical soliton perturbation of Fokas-Lenells equation with two integration Schemes, *Optik*. **165** (2018)111.
- [33] Hirota R. and Satsuma J., Soliton solutions of a coupled Korteweg-de Vries equation, *Phys. Lett. A.*, **85** (1981) 407.
- [34] Yildirim A., Mohyud-Din S. T. and Zhang D. H., Analytical solutions to the pulsed Klein-Gordon equation using modified variational iteration method (MVIM) and Boubaker polynomials expansion scheme (BPES), *Comput. Math. Appl.*, **59** (2010) 2473.
- [35] Hourria T., Crutcher S., Yildirim A., Hayat T., Omar. M. A. and Biswas A., Bright and Dark solitons of the modified complex Ginzburg Landau equation with parabolic and dual-power law nonlinearity, *Romanian Reports in Physics*, **64** (2012) 367.
- [36] Remoissenet, M. Waves Called Solitons, 3rd edn., Springer, Berlin, 1999.
- [37] Orkun, T., Senol, M., Kurt, A., Özkanc, O.: New solutions of fractional Drinfeld-Sokolov-Wilson system in shallow water waves. *Ocean Engineering*. **161**, 62-68 (2018)
- [38] Rezazadeh, H., Khodadad, F.S., Manafian, J.: New structure for exact solutions nonlinear time fractional Sharma-Tasso-Olver equation via conformable fraction derivative. *Appl. Appl. Math. Int. J.* **12**, 405-414 (2017)
- [39] Rezazadeh, H., Korkmaz, A., Eslami, M., Vahidi, J., Asghari, R.: Traveling wave solution of conformable fractional generalized reaction Dufing model by generalized projective Riccati equation method. *Opt. Quantum Electronics*. **50**, 1-13 (2018).
- [40] Aminikhah, H., Sheikhan, A.R., Rezazadeh, H.: Sub-equation method for the fractional regularized long-wave equations with conformable fractional derivatives. *Scientia Iranica*. **3**, 1048-1054 (2016)
- [41] Alphonse, H., Sabi'u, J., Hammouch, Z., Doka, S.Y.: Solitary pulses of the conformable derivative nonlinear differential equation governing wave propagation in low-pass electrical transmission line. *Physica Scripta*. **95**, 1-15 (2020)

- [42] Hammouch, Z., Mekkaoui, T.: Travelling-wave solutions for some fractional partial differential equation by means of generalized trigonometry functions. *International Journal of Applied Mathematical Research*. **1**, 206-212 (2012).
- [43] Kumar, D., Singh, J., Baleanu, D.: Modified Kawahara equation within a fractional derivative with non-singular Kernel. *Thermal sci.* **22**, 789-796 (2018).
- [44] Sousa, J.V.D.C., Oliviera, E.: A New Truncated M-Fractional Derivative Type Unifying Some Fractional Derivative Types with Classical Properties. *International Journal of Analysis and Application*. **16**, 83-96 (2018).
- [45] Chen, W., Rylyakov, A.V., Patel, V., Lukens, J.E., and Likharev, K.K., "Rapid single flux quantum T-flip flop operating up to 770 GHz," *IEEE Trans. Appl. Supercond*, **9** (1999) 3212-3215.
- [46] Kadin, A. M., Mancini, C. A., Fieldman, M. J. et Brock, D. K. : "Can RSFQ logic circuits be scaled to deep submicron junctions ?," *IEEE Trans. Appl. Supercond*, **11** (2001) 1050-1055.
- [47] Abdoukary, S., English, L.Q., and Mohamadou, A. "Envelope solitons in a left-handed nonlinear transmission line with Josephson junction," *Chaos, Solitons Fractals* **85**(2016) 44.
- [48] Alphonse, H., Klofai, Y., Malwe, B.H., and Doka, Y.S., "Exact Travelling Envelope Solitons and Kink-soliton Solutions for the Josephson Nonlinear Left-handed Transmission Line" *Applied Mathematics and Physics*, **5** (2017) 77-84.
- [49] Menzri, D., : Etude des structures planaires blindées en tenant compte de l'épaisseur métallique des rubans. Magister, univ constantine, compte de juin (2007).
- [50] Steattett, R., English, L. Q. : *Phys. D. Appl. Phys.*, **40** 5394 (2007).
- [51] Koon, K. T. V., Marquié, P. and Dinda, P. T. *Phys. Rev. E-Stat. Nonlinear, Soft Matter Phys*, **90**, 2014.
- [52] Al-daloo, M.; Soltan, A.; Yakovlev, A. Overview study of on-chip interconnect modeling approaches and its trend. In *Proceedings of the 2018 7th International Conference on Modern Circuits and Systems Technologies (MOCASST)*, Thessaloniki, Greece, (2018) 1-5.

- [53] Al-Daloo, M., Soltan, A., Yakovlev, A. Advance Interconnect Circuit Modeling Design Using Fractional-Order Elements. IEEE Trans. Comput. Aided Des. Integr. Circuits Syst. **39** (2020) 2722-2734.
- [54] Mohamed, B. : Course on the theory of transmission lines.
- [55] Essimbi, Z.B., and Arashenkov. I.B.V.: Phys. Rev. E, **71** (2006) 448.
- [56] Veselago, V.G. : "The electrodynamics of substances with simulataneously negative values of ϵ and m " Sov Phys.USPEKHI, **10** (1968)509.
- [57] Nikoo, M.S., and Hashemi, S.M.A., : " New soliton solution of varactor-loaded nonlinear transmission lines," IEEE Trans. Microw. Theory Techn.,**65** (2017) 4084-4092.
- [58] Vicario, G.B., and Kiritani, Y. : "Slow-Motion Tunnel Effect : an Enquiry into Vertical Organization of Perceptual Events, " Gestal Theory, **21**(1999).
- [59] Setzu, R. : Etude et réalisation de jonctions Josephson en nitrure de niobium à barrière semimétallique en TaN ; application aux circuits logiques micro-ondes à impulsions quantiques RSFQ, Grenoble I: Université Joseph-Fourier, (2007).
- [60] Setzu, R. : Etude et réalisation des jonctions Josephson en NBN, à barrière sémi-métallique en TaN (2007).
- [61] Likharev K. K. : "supraconducting weak links",Rev.Mod.Phys.(1979)51-1 .
- [62] Démoulin, B. Éléments sur la théorie des lignes de transmission : d1322, Techniques de l'ingénieur, (2014).
- [63] Peyrard, M., and Dauxois, T. : Wave called soliton. (1994).
- [64] Scott, A. C. : Active and Nonlinear Wave Propagation in Electronics. Wiley-Interscience, New York (1970)
- [65] Nejoh, Y. : Cusp solitons, shock waves and envelope solitons in a new non-linear transmission line. J. Phys. A **20** (1987) 1733

- [66] Kengne, E., Liu, W., M.: Exact solutions of the derivative nonlinear Schrödinger equation for a nonlinear transmission line. *Phys. Rev. E* **73** (2006) 026603.
- [67] Kengne, E., Vaillancourt, R., Malomed, B.A. : Coupled nonlinear Schrödinger equations for solitary-wave and kink signals propagating in discrete nonlinear dispersive transmission lines. *Int. J. Mod. Phys. B* **23** (2009) 133.
- [68] Marquié, R., Bilbault, J., M., Remoissenet, M.: Nonlinear Schrödinger models and modulational instability in real electrical lattices. *Phys. D* **87** (1995)371.
- [69] Marquié, P., Bilbault, J.M., Remoissenet, M. : Observation of nonlinear localized modes in an electrical lattice. *Phys. Rev. E* **51** (1995)6127.
- [70] Abdourahman, Kengne, E. : Generation of nonlinear modulated waves in a modified Noguchi electrical transmission network. *Chaos, Solitons Fractals* **92**(2016)8.
- [71] Kengne, E., Vaillancourt, R. : propagation of solitary waves on lossy nonlinear transmission lines, *International Journal of Modern Physics B*, **23**(2009) 118.
- [72] Dugowson, S. : Les differentielles metaphysiques histoire et philosophie de la generalisation de l'ordre de derivation, Universite Paris 13, Villetaneuse, France, 1994.
- [73] Ross B. : The Development of Fractional Calculus 1695-1900. *Historia Math*, **4** 75-89 (1977).
- [74] Miller, K.S., and Ross, B. : An Introduction to the Fractional Calculus and Fractional Differential Equations, John Wiley and Sons, New York, NY, USA, 1993.
- [75] Machado, J., T., Kiryakova, V., and Mainardi, F. : " Recent history of fractional calculus," *Communications in Nonlinear Science and Numerical Simulation*, **16** (2011) 1140-1153.
- [76] Riemann, B. : Versuch Einer Allgemeinen Auffassung der Integration und Differentiation. *Gesammelte Mathematische Werke und Wissenschaftlicher Nachlass*, Teubner, Leipzig, 1876, Dover, New York, NY, USA, 1953.
- [77] Grünwald, A. K. : " Uber "begrenzte" derivationen und deren anwendung," *Zeitschrift für Mathematik und Physik*, **12** (1867) 441-480.

- [78] Letnikov, A. V. : "Theory of differentiation with an arbitrary index," Sbornik: Mathematics, **3** (1868) 1-66.
- [79] Weyl, H. "Bemerkungen zum begriff des differential quotient en gebrochener ordnung vierteljahresschr," Naturforschende Gesellschaft in Zürich, **62**(1917)296-302.
- [80] Riesz, M. : "L'intégrale de Riemann-Liouville et le probleme de Cauchy," Acta Mathematica, **81** (1949) 1-222.
- [81] Riesz, M. : "L'intégrale de Riemann-Liouville et le problème de Cauchy pour l'équation des ondes," Bulletin de la Société Mathématique, France, **7** (1939) 153-170.
- [82] Caputo, M. : "Linear models of dissipation whose q is almost frequency independent-ii," Geophysical Journal of the Royal Astronomical Society, **13** (1967) 529-539.
- [83] Monje, C., A., Chen, Y., Vinagre, B.M., Xue, D., and Feliu, V. : Fractional-Order Systems and Controls: Fundamentals and applications, Springer, London, UK, (2010).
- [84] Figueiredo C., R., Chiacchio, A.O., and Capelas de Oliveira, E. : "Differentiation to fractional orders and the fractional telegraph equation," Journal of Mathematical Physics, **49** (2008) 033505.
- [85] Podlubny, I. : Fractional Differential Equations: An Introduction to Fractional Derivatives, Fractional Differential Equations, to Methods of Their Solution, **198** Mathematics in Science and Engineering, Academic Press, San Diego, Calif, USA, (1999).
- [86] Fellah, Z. E. A., Depollier, C. : Application of fractional calculus to the sound waves propagation in rigid porous materials: Validation via ultrasonic measurement, Acta Acustica, **88** (2002) 34.39.
- [87] Sebaa, N., Fellah, Z.E.A., Lauriks, W., Depollier, C. : Application of fractional calculus to ultrasonic wave propagation in human cancellous bone, Signal Processing archive, **86** (2006) 2668-2677.
- [88] Khalil, R., Al Horani, M., Yousef, A., Sababheh, M. : A new definition of fractional derivative, J. Comput. Appl. Math. **264** (2014) 65-70.

- [89] Soczkiewicz : Application of fractional calculus in the theory of viscoelasticity Molecular and Quantum Acoustics, **23** (2002)397-404.
- [90] Abdeljawad, T. : On conformable fractional calculus, J. Comput. Appl. Math., **279** (2015) 57-66.
- [91] Ryszard S. : Fractional derivatives in electrical circuit theory critical remarks. Archives of electrical engennering **66** (2017) 155-163. DOI 10.1515/ae-2017-0011.
- [92] Aydin, O.; Samanci, B.; Ozoguz, I.S. : Characterization of Microstrip Transmission Lines Using Fractional-order Circuit Model. Balk. J. Electr. Comput. Eng. **6** (2018) 266-270.
- [93] Yang, C.; Yu, H., Shang, Y.; Fei,W. : Characterization of CMOS Metamaterial Transmission Line by Compact Fractional-Order Equivalent Circuit Model. IEEE Trans. Electron Devices **62** (2015) 3012-3018.
- [94] Jiang, Y., Zhang, B. : Comparative Study of Riemann-Liouville and Caputo Derivative Definitions in Time-Domain Analysis of Fractional-order Capacitor. IEEE Trans. : Circuits Syst. II Express Briefs **67** (2019) 2184-2188.
- [95] Rysard, S. : "The Use of Fractional Order Derivatives for Eddy Current Non-Destructive Testing" 44th Annual Review of Progress in Quantitative Nondestructive Evaluation, Volume 37 AIP Conf. Proc. (1949) 230016-1-230016-10, <https://doi.org/10.1063/1.5031663>.
- [96] Pu, Y., F., Yuan, X., and Yu, B. : "Analog Circuit Implementation of Fractional-Order Memristor: Arbitrary-Order Lattice Scaling Fractional Memristor", IEEE Transactions on Circuits and Systems I: Regular Papers, **65** (2018) 2903-2916.
- [97] Fendzi-Donfack, E., Nguenang, J.P., and Nana, L. : Fractional analysis for nonlinear electrical transmission line and nonlinear Schroedinger equations with incomplete sub-equation. Eur. Phys. J. Plus **32** (2018) 133.
- [98] Russell, J., S. Report on waves. : In 14th meeting of the British Association for the Advancement of Science, **311** (1844) 390.

- [99] Boussinesq, J. : Théorie de l'intumescence liquide appelée onde solitaire ou de translation se propageant dans un canal rectangulaire. *Comptes Rendus Acad. Sci (Paris)*, **72** (1871) 755-759.
- [100] Korteweg, D., J., and de Vries, G. : On the change of form of long waves advancing in a rectangular channel, and a new type of long stationary wave. *Phil. Mag*, **39** (1895) 422-443.
- [101] Zabusky, N., J. and Kruskal, M. D. : Interaction of Solitons in a Collisionless Plasma and the Recurrence of Initial States, *Rev. Lett.*, **15**(1965)240.
- [102] Lonngren, K. : In *Solitons in Action*, edited by K. Lonngren and A. Scott Academic, New York, (1978) 127.
- [103] Zakharov, V., E., and Shabat, A.B., : *Zh. Eksp. Teor. Fiz.* **61** (1971)118.
- [104] Lake, B., M., Yuen, H.C., Rungaldier, H., and Ferguson, W.E. : Nonlinear deep-water waves: Theory and experiment. Part 2. Evolution of a continuous wave train, *J. Fluid Mech.*,**83** (1977) 49 - 74, doi:10.1017/S0022112077001037.
- [105] Yagi, T., and Noguchi, A. : *Electron. Lett.* **13** (1977) 683.
- [106] Kumara, H and Saravanan, P. : Topological and non-topological soliton solutions to the 1 + 3-dimensional Gross-Pitaevskii equation with quadratic potential term.*Scientia Iranica B* **24** (2017) 2429.
- [107] Akhmediev, N., Ankiewicz, A., Taki, M. : *Phys. Lett. A* **373** (2009) 675.
- [108] Dysthe, K., B., Trulsen, K. : *Phys. Scr. T* **82** (1999) 48.
- [109] Kharif, C., Pelinovsky, E. : *Eur. J. Mech. B (Fluids)* **22** (2003) 603.
- [110] Müller, C. Garrett, A. Osborne, Rogue waves: in: The fourteenth Aha Hulikoa Hawaiian Winter Workshop, *Oceanography* **18** (2005) 66.
- [111] Peregrine, D., H. : Water waves, nonlinear Schrödinger equations and their solutions, *J. Aust. Math. Soc. Ser. B*,**25** (1983) 16-43.

- [112] Akhmediev, N., Soto-Crespo, J. M., Ankiewicz, A. and Devine, N. : Early detection of rogue waves in a chaotic wave field, *Phys. Lett. A*, **375** (2011b) 2999-3001.
- [113] Chabchoub, A., Hoffmann, N.P., and Akhmediev, N. : Rogue wave observation in a water wave tank, *Phys. Rev. Lett.*, **106**, (2011) 204502.
- [114] Kibler, B., Fatome, J., Finot, C., Millot, G., Dias, F., Genty, G., Akhmediev, N., and Dudley, J.M. : The Peregrine soliton in nonlinear fibre optics, *Nat. Phys.*, **6** (2010) 790-795.
- [115] Li, Z., Li, L., Tian, H. and Zhou, G. : New types of solitary wave solutions for the higher order nonlinear Schrödinger equation *Phys. Rev. Lett.* **84** (2000) 4096-9.
- [116] Li-Chen Zhao, Sheng-Chang Li, and Liming Ling : Rational W-shaped solitons on a continuous-wave background in the Sasa-Satsuma equation. *Physical Review E* **89** (2014) 023210.
- [117] Chowdury, A., Ankiewicz, A. and Akhmediev, A. : *Proc. R. Soc. A*, **471** (2015) 20150130.
- [118] Liu, C., Yang, Z.Y., Zhao, L.C. and Yang, W.L. : *Phys. Rev. E*, **91** (2015) 022904.
- [119] Liu, C., Yang, Z.Y., Zhao, L.C. and Yang, W.L., *Ann. Phys.*, **362** (2015) 130.
- [120] Hasegawa, A., Tappert, F. : Transmission of stationary nonlinear optical pulses in dispersive dielectric fibers. II. Normal dispersion, *Appl. Phys. Lett.* **23** (1973) 171-175.
- [121] Emplit, P., Hamaide, J.P., Reynaud, F., Froehly, C., Barthélémy, A. : Picosecond steps and dark pulses through nonlinear single mode fibers, *Opt. Commun* **40** (1987) 374-379.
- [122] Keiichi M., Noriko S., Shinsuke W., : Experiment on Lattice Soliton by Nonlinear LC Circuit - Observation of a Dark Soliton. *Journal of the Physical Societ.* **51** (1982) 3.
- [123] Tala-Tebue, E., Tsoigni-Fozap, D.C., Kenfack-Jiotsa, A., Kofane, T.C. : Envelope periodic solutions for a discrete network with the Jacobi elliptic functions and the alternative $(\frac{G'}{G})$ -expansion method including the generalized Riccati equation. *Eur Phys J Plus* **129** (2014). <https://doi.org/10.1140/epjp/i2014-14136-9>.

- [124] Nagashima, H., Amagishi, Y. : Experiment on the Toda lattice using nonlinear transmission lines. *J. Phys. Soc. Jpn.* **45** (1978) 680-688.
- [125] Toda, M.: Vibration of a chain with nonlinear interaction. *J.Phys. Soc. Jpn.* **22** (1967) 431- 436.
- [126] Freeman, R.H., Karbowiak, A.E. : An investigation of nonlinear transmission lines and shock waves. *J Phys D: Appl Phys* **10** (1977) 633.
- [127] Marquié, P., Bilbault, J.M., Remoissenet, M. : Generation of envelope and hole solitons in an experimental transmission line. *Phys. Rev. E* **49** (1994) 828-835.
- [128] Yemele,D., Marquié, P.,Bilbault, J.M. : Long time dynamics of modulated waves in a nonlinear discrete LC transmission line. *Phys. Rev. E* **68** (2003) 016605-016615.
- [129] Stearret, R., English, L.Q. : Experimental generation of intrinsic localized modes in a discrete electrical transmission line. *J. Phys. D: Appl. Phys.* **40** (2007) 5394-5398.
- [130] Essimbi, Z. B., Barashenkov, I. V. : Spatially localized voltage oscillations in an electrical lattice. *J. Phys. D : Appl. Phys.* **35** (2002) 1438-1441.
- [131] Abdou, M. A., Soliman, A. A. : New exact travelling wave solutions for space-time fractional nonlinear equations describing nonlinear transmission lines. *Results Phys* **9** (2018) 1497-501.
- [132] Watanabe, S. : Soliton and generation of tail in nonlinear dispersive media with weak dissipation. *J Phys Soc Jap.*, **45** (1978) 276.
- [133] Yoshinaga, T. : Second order KDV soliton on a nonlinear transmission line. *J Phys Soc Japan*, **49** (1980) 2072.
- [134] Toda, M. : Wave propagation in anharmonic lattices. *J. Phys. Soc. Jpn.* **23** (1967) 501-506.
- [135] Donfack, E., F., Nguenang, J., P., Nana, L. : On the traveling waves in nonlinear electrical transmission lines with intrinsic fractional-order using discrete tanh method. *Chaos, Solitons Fractals* **131** (2020) 109486.

- [136] Tala-Tebue, E. and Zayed, E.M.E. : New Jacobi elliptic function solutions, solitons and other solutions for the $(2 + 1)$ -dimensional nonlinear electrical transmission line equation. *Eur Phys J Plus* **133** (2018). <https://doi.org/10.1140/epjp/i2018-12118-7>.
- [137] Kengne, E., Abdourahman, Lakhssassi, A. : Interacting signal packets in a lossless nonlinear transmission network with linear dispersion. *Chin J Phys* **63** (2020) 271-89.
- [138] Nogushi, A. : Solitons in a Nonlinear Inhomogeneous Transmission Line. *Elec Commun Jpn* **57** (1974) 9.
- [139] Jager, D. and Tegude, F.J. : Nonlinear wave propagation along periodic-loaded transmission line. *Appl Phys* **15** (1978) 393.
- [140] Fukushima, K., Wadati, M., Kotera, T., Sawada, K. and Narahara, Y. : Experimental and theoretical study of the recurrence phenomena in nonlinear transmission line. *J Phys Soc Jpn* **48** (1980) 1029-35.
- [141] Liu, J., Fang, X., Niu, X. and Zhang, X. : M-shaped dissipative solitons with polarization-dependent evolution dynamics. *Opt Commun* **48** (2019) 102-5.
- [142] Kofane, T., C., Michaux, B. and Remoissenet, M. : Theoretical and experimental studies of diatomic lattice solitons using an electrical transmission line. *J Phys C: Solid State Phys* **21** (1988) 1395.
- [143] Freeman, R., H., Karbowiak, A.E. : An investigation of nonlinear transmission lines and shock waves. *J Phys D: Appl Phys* **10** (1977) 633.
- [144] Liu, W-M, Kengne, E. : NLSE of single transmission lines, Theoretical. *Math Computat Phys* **45** (2019) 45-105.
- [145] Edwards, J., T., Ford, N.J. and Simpson, A.C. : *J. Comput. Appl. Math.* **148** (2002) 401 (2002).
- [146] Muslim, M. : *Math. Comput. Model.* **49** (2009) 1164.
- [147] El-Sayed, A., M. A. and Gaber, M. : *Phys. Lett. A* **359** (2006) 175.

- [148] El-Sayed, A., M., A., Behiry, S.H. and Raslan, W.E. : *Comput. Math. Appl.* **59** (2010) 1759.
- [149] He, J.H. : *Commun. Nonlinear Sci. Numer. Simul.* **2**, 230 (1997).
- [150] Wu, G., Lee, M.W.E. : *Phys. Lett. A* **374** (2010) 2506.
- [151] Guo, S., Mei, L. : *Phys. Lett. A* **375** (2011) 309.
- [152] He, H., : *J. Comput. Methods Appl. Mech. Eng.* **178** (1999) 257.
- [153] He, H. : *J. Int. J. Non-Linear Mech.* **35** (2000) 37.
- [154] Odibat, Z., Momani, S. : *Appl. Math. Lett.* **21** (2008) 194.
- [155] Cui, M. : *J. Comput. Phys.* **228** (2009) 7792.
- [156] Huang, Q., Huang, G. and Zhan, H. : *Adv. Water Resour.* **31** (2008) 1578.
- [157] Zhang, S., Zhang, H., Q. : *Phys. Lett. A* **375** (2011) 1069.
- [158] Guo, M., S., Mei, Q.L., Li, Y., Sun, F.Y. : *Phys. Lett. A* **376** (2012) 407.
- [159] Lu, B. : *Phys. Lett. A* **376** (2012) 2045.
- [160] Alphonse, H., Souleymanou, A., Lanre, A., Hadi, R., H., Serge Y. D. : Peculiar optical solitons and modulated waves patterns in anti.cubic nonlinear media with cubic.quintic non-linearity, *Optical and Quantum Electronics* **55** (2023) 719. <https://doi.org/10.1007/s11082-023-04950-2>
- [161] Alphonse, H., Souleymanou, A., Youssoufa S., Douvagaï, Yu-Ming Chu, Inc, M., Hadi, R., Serge Y. D. : Analytical survey of the predator-Prey model with fractional derivative order, *Photonic and Optics Collection*, **11** (2021) 035127 <https://doi.org/10.1063/5.0038826>
- [162] Huitzilin Y., M., Hadi, R., Souleymanou, A., Mukam, S., P., T., Mostafa, E., Kuetche, K., V., Bekir, A.: The extended modified method applied to optical solitons solutions in birefringent fibers with weak nonlocal nonlinearity and four wave mixing, *Chinese Journal of Physics*, (2019), doi: <https://doi.org/10.1016/j.cjph.2019.02.002>

- [163] Savaissou, N., Souleymanou, A., Alphonse, H., Inc, M., Gambo, B., Serge Y. D. : Diverse chirped optical solitons and new complex traveling waves in nonlinear optical fibers, *Commun. Theor. Phys.* **72** (2020) 065501, <https://doi.org/10.1088/1572-9494/ab7ecd>
- [164] Souleymanou, A., Alphonse, H., Mukam, S., P., Hadi, R., Inc, M., Serge Y. D., Bouetou, B., T. : Optical solitons to the nonlinear Schrödinger equation in metamaterials and modulation instability, *Eur. Phys. J. Plus* **136** (2021) 710 <https://doi.org/10.1140/epjp/s13360-021-01683-7>.
- [165] Hadi, R., Seyed, M., M., Mostafa, E., Mohammadreza, R., Mohammad, M., Souleymanou, A. : New optical solitons of nonlinear conformable fractional Schrödinger-Hirota equation, *Optik* (2018) <https://doi.org/10.1016/j.ijleo.2018.06.111>.
- [166] Elsayed, Zayed, M., E., Mohamed, Alngar, E., M. : Application of newly proposed sub-ODE method to locate chirped optical solitons to Triki-Biswas equation, *Optik - International Journal for Light and Electron Optics* **207** (2020) 164360.
- [167] Mingliang, Wang., Xiangzheng, L., Jinliang Zhang, A. : Sub-ODE method and solitary wave solutions for higher order nonlinear Schrodinger equation, *Physics Letters A* **363** (2007) 96-101.
- [168] Souleymanou, A., Alphonse, H., Serge, Y., D., Bouetou, B., T., Inc, M., Kofane, T., C. : W-shaped profile and multiple optical soliton structure of the coupled nonlinear Schrodinger equation with the four-wave mixing term and modulation instability spectrum, *Physics Letters A* **418** (2021)127710.
- [169] Lighthill, M.J. : "Contributions to the theory of waves in nonlinear dispersive systems", *J.nst. dispersifs non linéaires*", *J.nst. Math. Appl.* (1965) 269 - 306.
- [170] Benjamin, T., B., Feir, J. : The disintegration of wave trains on deep water Part 1, *Theory. J. Fluid Mech.* **27** (1967) 417-430.
- [171] Zakharov, V.E., and Ostrovsky, L.A. : "Modulation instability : the beginning". *Physica*, **238** (2009) 540 - 548.
- [172] Agrawal, G., P. : *Nonlinear Fiber Optics*, 4th ed. (Academic Press, San Diego, CA, 2006).

- [173] Zanga, D, Fewo, S., I., Tabi, C, B., and Kofané. T. C. : Phys. Rev. A **105** (2022) 023502.
- [174] Tabi, C., B., Mohamadou. A., Kofane, T., C. Modulational instability in the anharmonic Peyrard-Bishop model of DNA. Eur. Phys. J. B **74** (2010) 151–158.
- [175] Inc, M., Aliyu, A., I., Yusuf, A., Baleanu D. : Optical solitons and modulation instability analysis of an integrable model of (2+1)-dimensional Heisenberg ferromagnetic spin chain equation. Superlattices Microstruct. **112** (2017) 628-638.
- [176] Inc, M, Aliyu, A., I., Yusuf, A., Baleanu D. : Dark and combined optical solitons, and modulation instability analysis in dispersive metamaterial, Optik, **157** (217) 484–491.
- [177] Kengne, E., Chui, S.,T., Liu, W., M. : Modulational instability criteria for coupled nonlinear transmission lines with dispersive elements. Phys. Rev. E **74** (2006) 036614.
- [178] Kengne, E., Lakhssassi, A., Liu, W. M. : Modeling of matter-wave solitons in a nonlinear inductor-capacitor network through a Gross-Pitaevskii equation with time-dependent linear potential. Phys. Rev. E **96** (2017) 022221.
- [179] Alphonse, H., Souleymanou, A., Inc, M., Gambo, B., Serge Y. D., Kofane, T., C., Nisar, K., S. : Chirped solitons in discrete electrical transmission line. Results in Physics **18** (2020) 103188.
- [180] Noguchi, A. : Solitons in a nonlinear transmission line. Electron. Commun. Jpn. A **57** (1974) 9.
- [181] Nai, A., Ankiewicz, A., Taki, M. : Waves that appear from nowhere and disappear without a trace, Phys. Lett. A **373** (2009) 675.
- [182] Yemele, D. and Kenmogne, F. : Compact envelope dark solitary wave in a discrete nonlinear electrical transmission line. Phys. Lett. A **373** (2009) 3801.
- [183] Malomed, B., A. : A variety of dynamical settings in dual-core nonlinear fibers, In: Handbook of Optical Fibers, Vol. 1 (G.-D. Peng, Editor: Springer, Singapore, 2019) 421-474.
- [184] Soto-Crespo, J. M., Nail, A., Grelu, Ph., Belhache, F. : Quantized separations of phase-locked soliton pairs in fiber lasers, Optics Letters **28** (2003) 1757.

-
- [185] Soto-Crespo, J., Devine, N., Nai, A. : Integrable turbulence and rogue waves: Breathers or solitons?. *Phys. Rev. Lett.* **116** (2016) 103901.
- [186] Frisquet, B., Chabchoub A., Fatome, J., Finot, C., Kibler, B., Millot, G. : Two-stage linear- nonlinear shaping of an optical frequency comb as rogue nonlinear Schrödinger-equation-solution generator. *Phys. Rev. A* **89** (2014) 023821.
- [187] Ankiewicz, A., Clarkson, P. A., Nai, A. : Rogue waves, rational solutions, the patterns of their zeros and integral relations. *Journal of Physics A: Mathematical and Theoretical* **43** (2010) 122002.
- [188] Erkintalo, M., Genty, G., Wetzell, B., Dudley, J.M. : Akhmediev breather evolution in optical fiber for realistic initial conditions. *Phys. Lett. A* **375** (2011) 2029.
- [189] Shrira, V.I., Geogjaev. V. V. : What makes the Peregrine soliton so special as a prototype of freak waves? *J Eng Math* **67** (2010)11Ü22 DOI 10.1007/s10665-009-9347-2

List of Publications

- **Optical and W-shaped bright solitons of the conformable derivative nonlinear differential equation**

Hamadou Halidou, Alphonse Houwe, Souleymanou Abbagari, Mustafa Inc, Serge Y. Doka, Thomas Bouetou Bouetou,

Journal of Computational Electronics (2021) **20** 1739-1759.

- **Rational W-shape solitons on a nonlinear electrical transmission line with Josephson junction**

Hamadou Halidou, Souleymanou Abbagari, Alphonse Houwe, Mustafa Inc, Thomas Bouetou Bouetou,

Physics Letters A (2022) **430** 127951.



Rational W-shape solitons on a nonlinear electrical transmission line with Josephson junction



Hamadou Halidou^a, Souleymanou Abbagari^{a,b}, Alphonse Houwe^c, Mustafa Inc^{d,e,f,*}, Bouetou B. Thomas^g

^a Laboratory of Mechanics, Materials and Structures, Department of Physics, University of Yaounde I, P.O. Box 812, Yaounde, Cameroon

^b Department of Basic Science, Faculty of Mines and Petroleum Industries, University of Maroua, P.O. Box 08, Kaele, Cameroon

^c Department of Physics, The University of Maroua, P.O. Box 814, Maroua, Cameroon

^d Biruni University, Department of Computer Engineering, Istanbul, Turkey

^e Firat University, Science Faculty, Department of Mathematics, 23119 Elazig, Turkey

^f Department of Medical Research, China Medical University Hospital, China Medical University, Taichung, Taiwan

^g National Advanced School of Engineering, University of Yaounde I, Cameroon

ARTICLE INFO

Article history:

Received 30 May 2021

Accepted 16 January 2022

Available online 31 January 2022

Communicated by B. Malomed

Keywords:

Envelope solitons

Rational W-shape solitons

Nonlinear Schrödinger equation

ABSTRACT

This paper examines envelope solitons, rational W-shape solitons to a Nonlinear Electrical Transmission Line (NETL) with Josephson junction (JJ) that consist of the N^{th} cells of circuits. By employing the reductive perturbation approach in the semi-discrete approximation, we obtain the nonlinear Schrödinger equation (NLSE). From this equation, the frequency ranges of propagation of bright and dark solitons were obtained. As in most of the works, the NLSE obtained is well known as the seat of rogue waves and Peregrine solitons. The nonlinearity provided by the JJ, combined with the dispersion, made it possible to study the Modulation Instability (MI) gain spectrum. The 3D and 2D graphical representations illustrated the instability zones and the W-rational solutions have followed by using numerical simulation. The results obtained in this paper are of a very capital contribution for the study of rogue waves in nonlinear transmission lines or other physical problems.

© 2022 Elsevier B.V. All rights reserved.

1. Introduction

Work on the study of nonlinear power lines has been the focus of interest since the work of pioneers Hirota and Suzuki was born [1]. Indeed, a succession of numerical and analytical works followed with great satisfaction, especially on the dynamics of waves modulated in NETL [2–4]. The analysis of the miscellaneous of the nonlinear excitations in mediums with strong nonlinearity and the resolution of the problems of quantum mechanical type, the plasma waves, the control of the medical systems, the transport of the signal and the communication support have their salvation thanks to NETL [5–9]. A NETL is a circuit which consists for the most part of capacitors, inductors and JJ which are nonlinear in their response to current and voltage respectively. It therefore constitutes a favorable environment for the propagation of solitons, Peregrine solitons, rogue waves and so on. The nonlinear electrical transmission line with JJ has been at the center of various works in the field of supra transmission. Almost the majority of superconductors electronics are held on JJ.

However, several works on the investigation of bright or dark solitary waves obeying the NLSE in the presence of weak nonlinearity and dispersion in NETL, have been full of basket in recent years [10–16]. The NLSE has been widely studied, and has exhibited nonlinear event, such as rogue waves, Peregrine solitons and modulation instability. Regarding the rogue waves (RWs) which are in charge of great number of maritime catastrophe have been pointed out in diverse studies for decades [17,18].

A succession of theoretical works has been developed to explain the virtues of these waves, which probably comes from nowhere and disappears without a trace [19–23]. One of its waves, is the single rogue wave which is a solution of NLSE. It is also known as the Peregrine soliton [20].

* Corresponding author at: Firat University, Science Faculty, Department of Mathematics, 23119 Elazig, Turkey.

E-mail addresses: hamadouhalidou@gmail.com (H. Halidou), abbagaris@yahoo.fr (S. Abbagari), ahouw220@yahoo.fr (A. Houwe), minc@firat.edu.tr (M. Inc), tbouetou@yahoo.fr (B.B. Thomas).

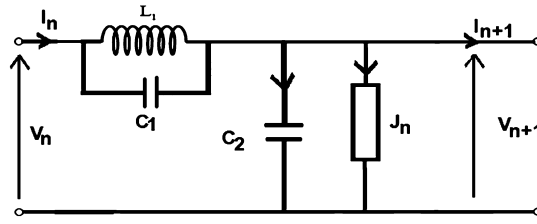


Fig. 1. Schematic representation of the nonlinear electrical transmission line with Josephson junction.

These obtained results in NETL, present an instability like any other nonlinear system which progresses with a MI of the plane wave and a posterior production of localized pulses. In this way, for transverse disturbances, the exact cut-off frequencies of the growth rate have been highlighted and the MI gain spectrum of solitary waves instabilities has been obtained [24].

In this paper, to investigate envelope solitons, RWs and Peregrine solitons, we used the quasi-discrete method to build the one-dimensional nonlinear Schrödinger equation (1-NLSE) to the nonlinear electrical transmission line with JJ. The paper is organized as follows: Section 1 is devoted to model description and analytical treatment. In section, the linear analysis technique is used to point out the MI gain spectrum, follows by the investigation of the RWs. The last section concludes the works.

2. Model description and analytical treatment

Fig. 1 shows the n^{th} elementary cell of the NETL with JJ. It is modeled by a linear inductor L_1 in parallel with a linear C_1 in the series branch and a linear capacitor C_2 in parallel with a nonlinear JJ current J_n . By using the famous Kirchhoff Laws in current and voltage on the lattice of Fig. 1 it reveals the following nonlinear discrete equations which describes the modulated waves in the lattice

$$\frac{d^2}{dt^2} (\phi_{n+1} - 2\phi_n + \phi_{n-1}) + \omega_0^2 (\phi_{n+1} - 2\phi_n + \phi_{n-1}) + \mu_0 \frac{d^2 \phi_n}{dt^2} + \omega_j^2 \sin(\phi_n) = 0, \tag{1}$$

while the voltage V_n and the JJ current J_n are given respectively by

$$V_n = \frac{d\phi_n}{dt}, \quad J_n = J_0 \sin\left(2\pi \frac{\phi_n}{\phi_0}\right), \tag{2}$$

in the same time $\omega_0^2 = \frac{1}{L_1 C_1}$, $\mu_0^2 = \frac{C_2}{C_1}$, and the plasma frequency $\omega_j = \sqrt{2\pi J_0 / C_1 \phi_0}$, $\phi_0 = 2.064 \times 10^{-15} Tm^2$. Now, integrating this equation gives the Hamiltonian of the system as

$$H = \sum_n \left[\frac{1}{2} \mu_0 \left(\frac{d\phi_n}{dt}\right)^2 + \frac{1}{2} \left(\frac{d}{dt} (\phi_n + \phi_{n+1})\right)^2 + \frac{1}{4} \omega_0^2 (\phi_n - \phi_{n+1})^2 \times (\phi_{n-1} - \phi_n)^2 - \omega_j \cos(\phi_n) \right]. \tag{3}$$

From Eq. (3) it is highlighted the conservation of the energy in the lattice. To establish the NLSE which admits solitary waves like (bright and dark solitons), it will be adopted quasi discrete approximation which will assume the inherent discreteness of the system. This oncoming permits to describe the quasi-discrete envelope solitons, typified by the discrete carrier and slowly varying continuum envelope. A solution of Eq. (1) is given as

$$\phi_n = \epsilon \phi_1(x, \tau) \exp(i\theta_n) + \epsilon^2 \phi_{02}(x, \tau) + \epsilon^2 \phi_2(x, \tau) \exp(2i\theta_n) + \dots + c.c., \tag{4}$$

where c.c. is the complex conjugate and the slow scales $x = \epsilon(n - v_g t)$ and $\tau = \epsilon^2 t$, while $\exp(i\theta_n)$, with $\theta_n = kn - \omega t$. Where ω is the carrier frequency, k is the wave number and ϵ is the small parameter. Also v_g is the group velocity. To do so, it is considered Eq. (1) in case of low-amplitude waves i.e. $(\phi_n \ll 1)$. Then Eq. (1) becomes

$$\frac{d^2}{dt^2} (\phi_{n+1} - 2\phi_n + \phi_{n-1}) + \omega_0^2 (\phi_{n+1} - 2\phi_n + \phi_{n-1}) + \mu_0 \frac{d^2 \phi_n}{dt^2} + \omega_j^2 \phi_n - \frac{\omega_j^2}{6} \phi_n^3 = 0. \tag{5}$$

Plugging Eq. (4) into Eq. (5) gives:

To order $O(\epsilon)$ proportional $\exp(i\theta_n)$ points out the linear dispersion relation,

$$\omega^2 = -\frac{4 \sin^2\left(\frac{k}{2}\right) \omega_0^2 - \omega_j^2}{\mu_0 - 4 \sin^2\left(\frac{k}{2}\right)}. \tag{6}$$

To order $O(\epsilon^2)$ proportional $\exp(i\theta_n)$ gives the group velocity dispersion

$$v_g = \frac{(\omega^2 - \omega_0^2) \sin(k)}{\omega \left(4 \cos^2\left(\frac{k}{2}\right) + \mu_0 - 4\right)}. \tag{7}$$

Then order $O(\epsilon^3)$ proportional $\exp(i\theta_n)$, the following nonlinear Schrödinger equation is obtained

$$i \partial_\tau \phi_1 + P \partial_{xx} \phi_1 + Q |\phi_1|^2 \phi_1 = 0, \tag{8}$$

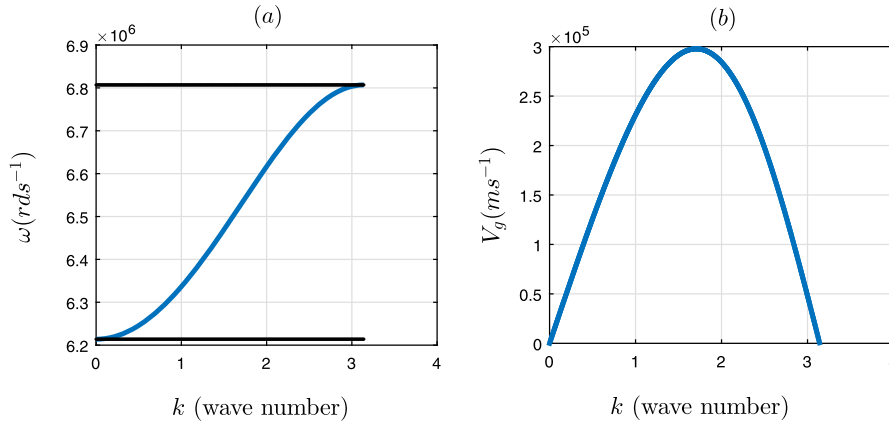


Fig. 2. (a) is the plot of the dispersion relation versus wave number and (b) the group velocity versus wave number at $J = 200nA$, $L_1 = 480\mu H$, $C_1 = 1pF$, $C_2 = 2pF$.

the nonlinear coefficient gives

$$Q = \frac{1}{4} \frac{\omega_j^2}{\omega \left(4 \cos^2 \left(\frac{k}{2} \right) + \mu_0 - 4 \right)}, \quad (9)$$

and the dispersion coefficient is

$$P = \frac{\left(\left(4 \cos^4 \left(\frac{k}{2} \right) - 4 - 2\mu_0 \cos^2 \left(\frac{k}{2} \right) + \mu_0 \right) \omega^2 + \omega_0^2 \left(-4 \cos^2 \left(\frac{k}{2} \right) + 4 \cos^4 \left(\frac{k}{2} \right) \right) \right) (\omega^2 - \omega_0^2)}{\left(4 \cos^2 \left(\frac{k}{2} \right) + \mu_0 - 4 \right)^2 \omega^3}. \quad (10)$$

From the linear dispersion relation Fig. 2(a), the wave number is taken in the first Brillouin zone ($0 \leq k \leq \pi$). Therefore, it is revealed two cut off frequencies given by $\omega_{min} = \sqrt{\frac{\omega_j^2 - 4\omega_0^2}{\mu_0 - 4}}$ and $\omega_{max} = \sqrt{\frac{\omega_j^2}{\mu_0}}$ respectively. Besides, it is stressed the behavior of the group velocity versus the wave number in Fig. 2(b). Furthermore, in Fig. 3, it is shown the dispersion relation and nonlinear coefficient curves. We observe two regions of the propagation of the soliton solution in the lattice from the dispersion curve (see Fig. 3(a)). Otherwise, the nonlinear coefficient is permanently positive, so the product will give a good pipe of the solitary waves propagation in the lattice. Several works have been shown that depending on the sign of the product PQ the NLSE Eq. (8) admits either bright soliton (which correspond to modulation stable), or dark soliton (for modulation instability). Observing Fig. 4, it is pointed out two regimes of cut off frequencies which correspond to bright and dark formation. So, for $(6.3 \times 10^8 kHz < f < 6.655 \times 10^8 kHz)$ the bright soliton is set out, meanwhile the dark soliton is formed at $(6.656 \times 10^8 kHz < f < 6.8 \times 10^8 kHz)$. In addition, Figs. 5(m) and 5(n) point out the behavior of the ration (Q/P) versus the angular frequency. It is observed the effect of the plasma frequency ω_j and the capacitor C_2 . Despite the presence of the JJ, the capacitor has contributed hardly to the formation of solitons. The given Figs. 3(c) and 3(b) correspond to the dispersion term and nonlinear coefficient. Moreover the NLSE Eq. (8) with different kind of nonlinear excitation, enclosing Peregrine rogue wave (RW), Akhmediev breather (AB), Kuznetsov-Ma breather (K-M) have been established recently [20–22]. One of the concerns, is to find the different regimes of MI of these obtained results. It is imperative to make known that the small disturbances in the MI regimes refer to unstable zones and therefore are amplified exponentially, while for small perturbation in the modulation stable regime, they are stable and do not grow. In the next section, the MI and the super rogue will be studied.

3. Modulation instability and rogue waves

3.1. Modulation instability

It is derived the MI based on the NLSE Eq. (8) in this part of the paper. To this, it is considered the plane wave solution of the NLSE Eq. (8) in the form of $\phi_1 = \phi_{10} e^{iQ|\phi_{10}|^2 \tau}$. Introducing the perturbation term into the plane wave as $\phi_1 = \phi_{10} + \epsilon \phi_{20} e^{i(Kx + \Omega \tau)} + c.c.$, where the wave number and the frequency perturbation are given respectively by K and Ω . While ϕ_{20} is the amplitude of the carrier frequency. Inserting this hypothesis into Eq. (8), gives the following dispersion relation:

$$\Omega^2 = P^2 K^2 (K^2 - 3 \frac{Q}{P} |\phi_{10}|^2). \quad (11)$$

The obtained dispersion relation Eq. (11) depends on the ratio Q/P . So, it is also pointed out that the ratio depends on the plasma frequency (ω_j) of the lattice.

Inspecting Eq. (11), if the ratio $(Q/P < 0)$ i.e. $0 \leq \omega \leq 2.09 (rds^{-1})$ (Fig. 5(m)) and $0 \leq \omega \leq 3.5 (rds^{-1})$ (see Fig. 5(n)), the MI gain spectrum is stable despite the small perturbation. In the same time, the ratio (Q/P) is always positive for $2.09 < \omega \leq 3.5 (rds^{-1})$ (see Fig. 5(m)) and the perturbation relation becomes complex. Consequently the MI gain spectrum is unstable and the wave number is small compared to critical wave number value i.e. $K < K_c = \sqrt{\frac{3Q}{P} |\phi_{10}|^2}$. In this condition the growth rate is reading as [22]

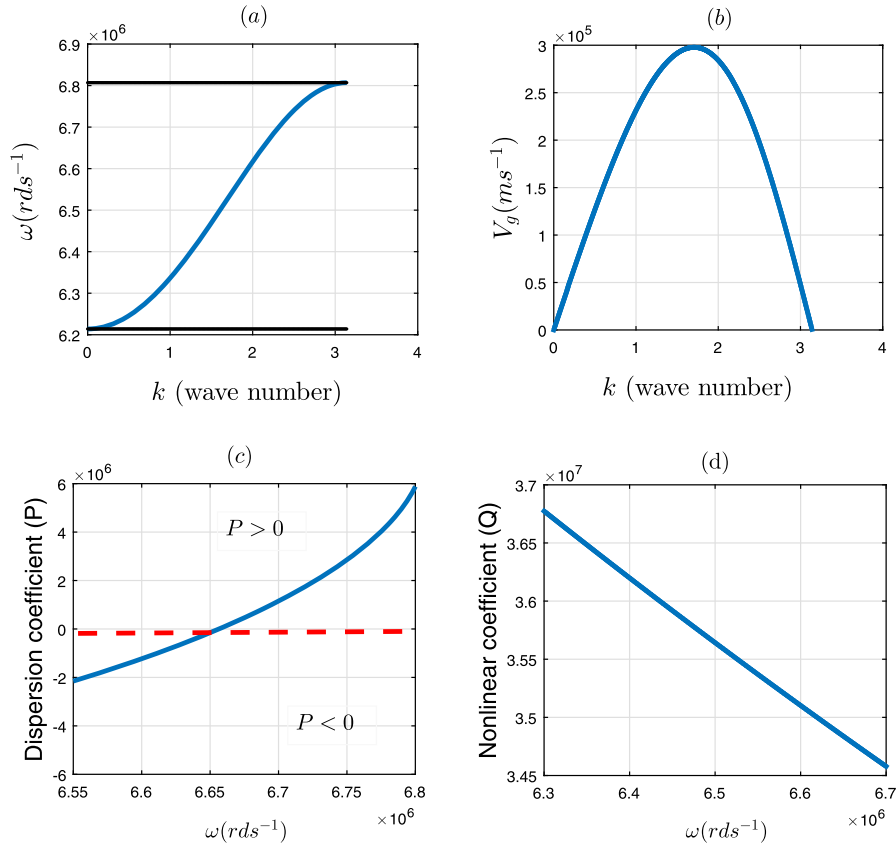


Fig. 3. (a) is the plot of the dispersion relation versus wave number and (b) the group velocity versus wave number at $J = 200nA$, $L_1 = 480\mu H$, $C_1 = 1pF$, $C_2 = 2pF$.

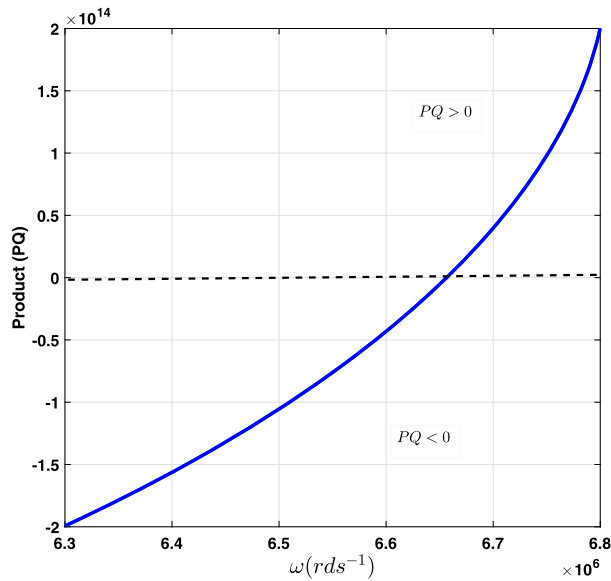


Fig. 4. Illustration of the bright ($6.3 \times 10^8 kHz < f < 6.655 \times 10^8 kHz$) and dark ($6.656 \times 10^8 kHz < f < 6.8 \times 10^8 kHz$) formation areas depending on the sign of the product (PQ) versus angular frequency at $J_0 = 200nA$, $L_1 = 480\mu H$, $C_1 = 1pF$, $C_2 = 2pF$.

$$\Gamma_{gr} = |P|K^2 \sqrt{\frac{K_c^2}{K^2} - 1}, \tag{12}$$

where K_c is the critical wave number. In addition, the ratio (Q/P) value increases when the plasma frequency increases (see Fig. 5(m) and 5(n)). Thus, when the plasma frequency reach the critique value, the MI gain spectrum is unstable for any value of the angular frequency chosen in the range of $0 \leq \omega \leq 3.5(rd s^{-1})$ (see figure (n)). However, to highlight the behavior of the growth rate (Γ_{gr}) of the modulation instability it will be plotted the growth rate in terms of the wave number with the effect of plasma frequency.

Fig. 6 shows the growth rate of MI versus the wave number. It is observed instability zones for $0 \leq K < 6$ and $2 < K < 5$. However, in Fig. 7 is observed two slides lobes which emphasize the instability zones. The identical scenario is set out in Fig. 8 one slide lobe for

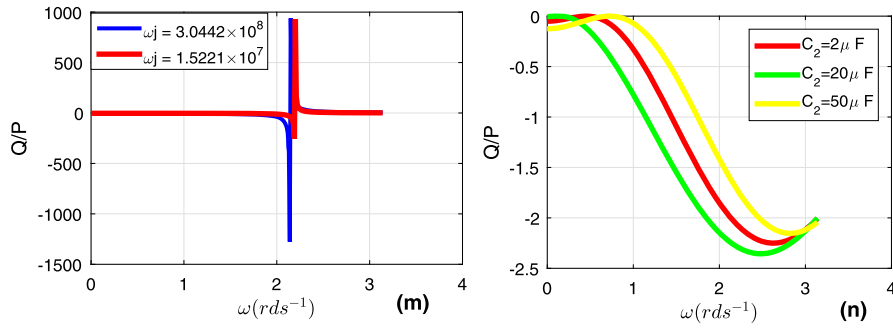


Fig. 5. Illustration of the ratio bright (Q/P) versus angular frequency with the effect of plasma frequency (m) $\omega_j = 3.044 \times 10^{16}$, $\omega_j = 3.0442 \times 10^{16}$, $C_1 = 1pF$, $C_1 = 2pF$ and (n) the effect of the capacitor at $C_2 = 20pF$ $J_0 = 200nA$, $L_1 = 480\mu H$.

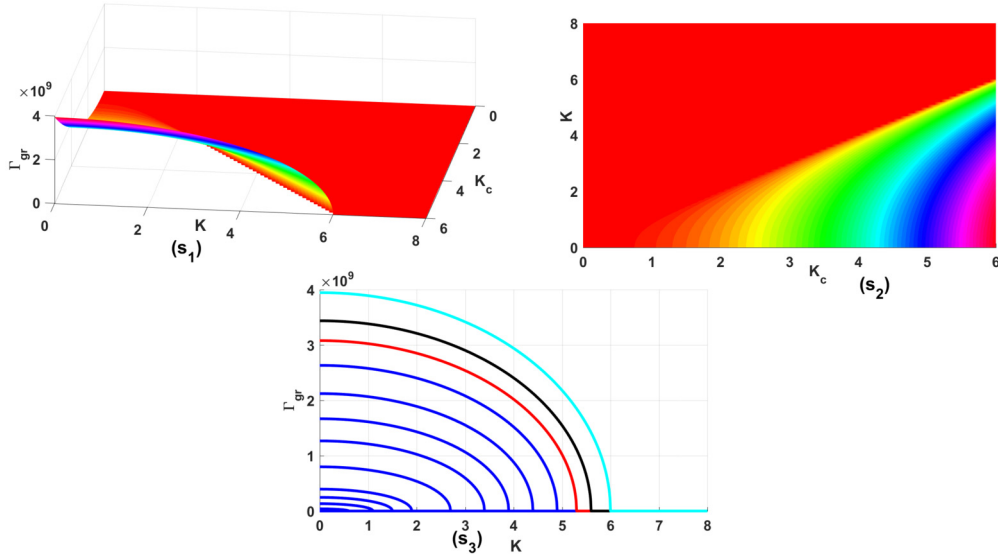


Fig. 6. Illustration of the growth rate of MI in terms of wave number and critical wave number with the effect of plasma frequency (s_1) 3D, (s_2) contour plot and (s_3) 2D plot at $\omega_j = 3.044 \times 10^9$, $C_1 = 1pF$, $C_2 = 400pF$ at $J_0 = 200nA$, $L_1 = 780\mu H$. (For interpretation of the colors in the figure(s), the reader is referred to the web version of this article.)

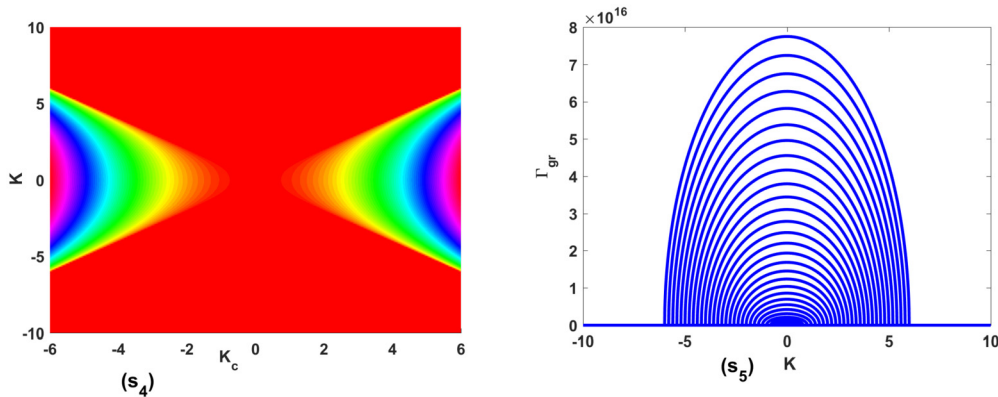


Fig. 7. Illustration of the growth rate of MI in terms of wave number and critical wave number with the effect of plasma frequency (s_4) contour plot and (s_5) 2D plot at $\omega_j = 3.044 \times 10^8$, $C_1 = 0.1pF$, $C_2 = 20pF$ at $J_0 = 200nA$, $L_1 = 780\mu H$.

$-5 \leq K < 5$. Furthermore, in Fig. 9, it is formed the growth rate of the MI with the variation of the critical wave number. It is pointed out that when the critical wave number increases the MI band increases and its became different when the critical wave number decreases the MI band decreases. On the other hand, Fig. 10 is obtained by varying the values of the capacitors. This situation shows the variation of the plasma frequency of the Josephson junction.

3.2. Rogue waves solutions

Recently, it has been investigated rogue waves to Eq. (8) [6,7]. The rogue waves solution takes the form of Peregrine solitons or super rogue wave. In which follows, it will be pointed out Peregrine and super rogue wave to Eq. (8). For Peregrine soliton, we set [6]

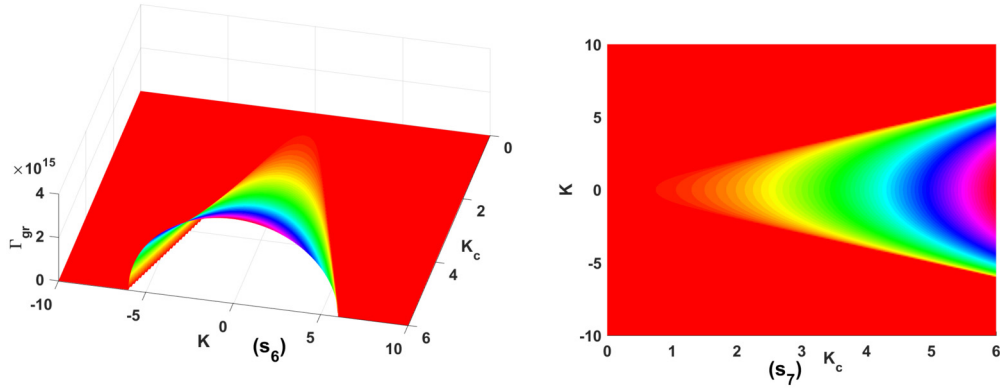


Fig. 8. Illustration of the growth rate of MI in terms of wave number and critical wave number with the effect of plasma frequency (s_6) 3D and (s_7) contour plot at $\omega_j = 7.6104 \times 10^{15}$, $C_1 = 40\text{pF}$, $C_2 = 200\text{pF}$ at $J_0 = 200\text{nA}$, $L_1 = 780\mu\text{H}$.

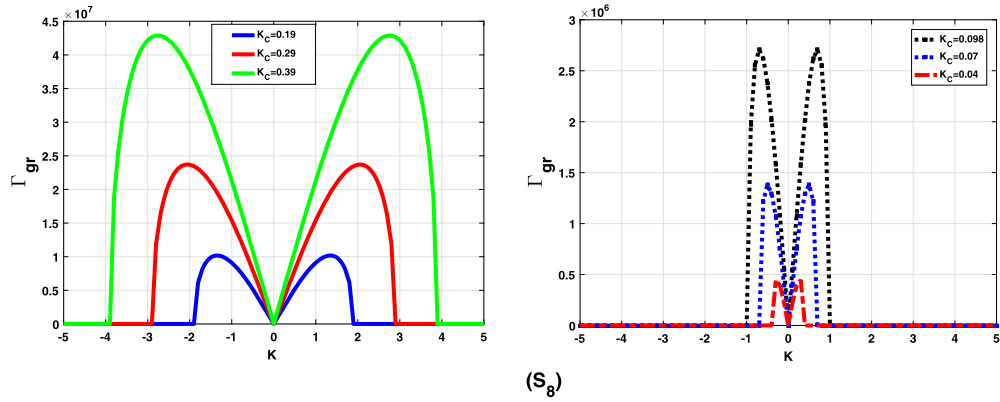


Fig. 9. The comparison of the growth rate of MI under the influence of the critical wave number (s_8) $\omega_j = 6.7618 \times 10^3$, $C_1 = 450\text{pF}$, $C_2 = 750\text{pF}$ at $J_0 = 200\text{nA}$, $L_1 = 780\mu\text{H}$.

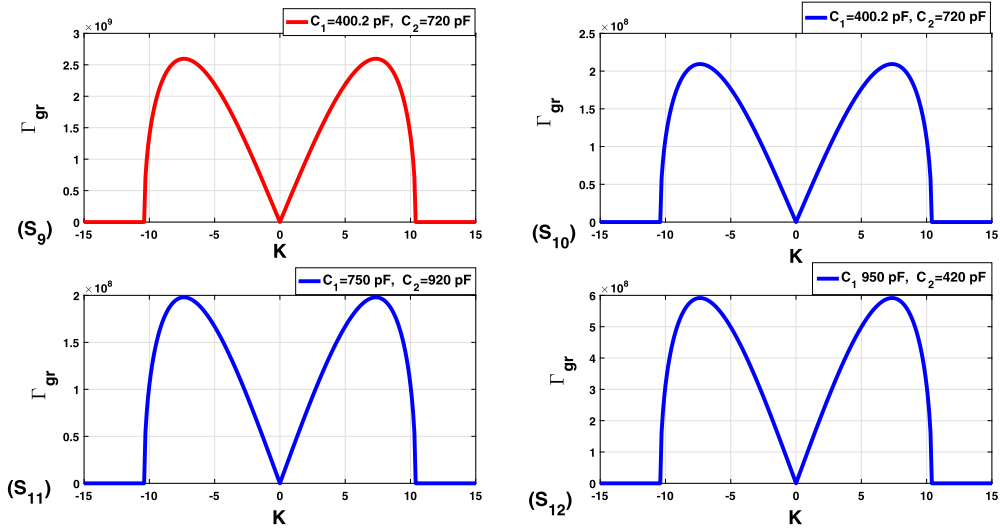


Fig. 10. The comparison of the growth rate of MI under the influence of the capacitors C_1 and C_2 and fixed value of the critical wave number (s_9) $\omega_j = 6.06 \times 10^3$, (s_{10}) $\omega_j = 4 \times 10^3$, (s_{11}) $\omega_j = 3.20 \times 10^3$, (s_{12}) $\omega_j = 6.761 \times 10^3$ at $J_0 = 200\text{nA}$, $L_1 = 780\mu\text{H}$.

$$\phi_1(x, \tau) = \sqrt{\frac{2P}{Q}} \left(1 - \frac{4 + 16iP\tau}{16P^2\tau^2 + 4x^2 + 1} \right) e^{2iP\tau}. \tag{13}$$

Figs. 11 depict the analytical results Eq. (13) which are the 3D evolution of the Peregrine soliton. Furthermore, Figs. 12 are illustration of the contour plot and 3D Peregrine solitons respectively under the effect of the capacitor (C_1). At the time, Fig. 11 is the spatiotemporal evolution of the Peregrine at different time (i.e. $\tau = 0\text{ms}$, $\tau = 5\text{ms}$, $\tau = 10\text{ms}$, $\tau = 15\text{ms}$, $\tau = 20\text{ms}$). However, Fig. 12 is the spatiotemporal evolution of the Peregrine rogue wave with the effect of capacitors (C_1 and C_2). It is pointed out by the (red line) when the capacitor C_1 is bigger than C_2 . The (blue line) gives the major effect of the capacitor C_2 on the Peregrine soliton shape (the two pikes below in

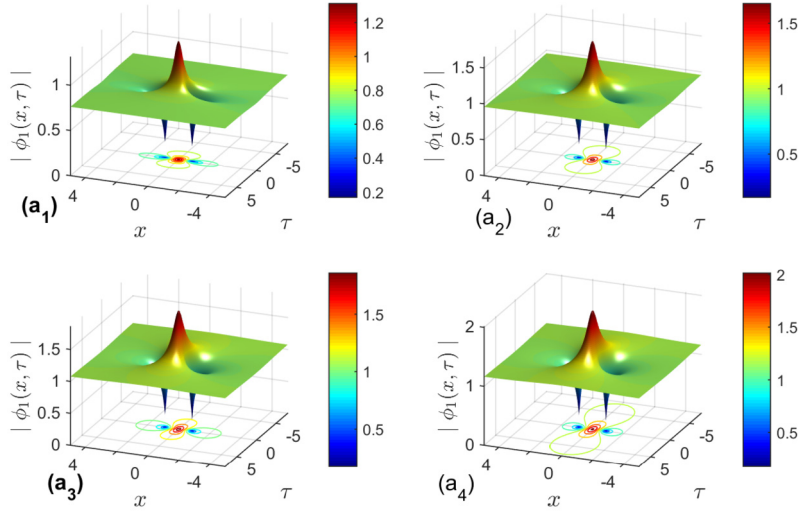


Fig. 11. (S_8) is the 2D plot of the Peregrine rogue wave and (S_9) the 3D spatiotemporal evolution of the Peregrine rogue wave at $C_1 = 2pF$, $C_2 = 470pF$ at $J_0 = 200nA$, $L_1 = 480\mu H$.

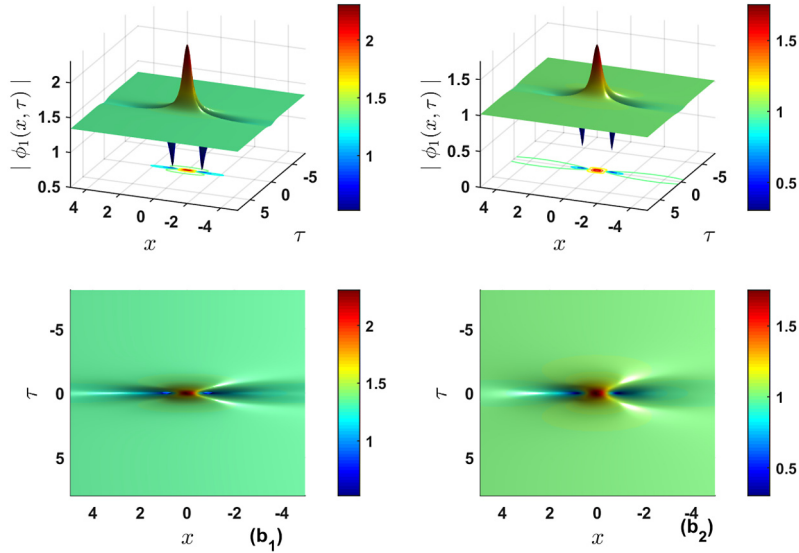


Fig. 12. (s_{10}) is the contour plot of the Peregrine solitons and (s_{11}) the 2D spatiotemporal evolution of the Peregrine rogue wave at $C_1 = 20pF$, $C_2 = 470pF$ at $J_0 = 200nA$, $L_1 = 480\mu H$.

Fig. 10, are exhibited here by the blue line). While capacitor C_1 becomes more important than capacitor C_2 , the Peregrine shape vanishes (red line) (Fig. 13, Fig. 14). To turns to the super rogue waves (SRWs), we set $\psi = \sqrt{\frac{Q}{2p}} \phi_1$ and $T = \tau P$, then Eq. (8) gives [4].

$$i \frac{\partial \psi}{\partial T} + \frac{\partial^2 \psi}{\partial x^2} + 2|\psi|^2 \psi = 0. \tag{14}$$

Now we can assume the solution of Eq. (14) as follows [4,6].

$$\psi(x, T) = \left(1 - \frac{G + iH}{D}\right) e^{2iP\tau}, \tag{15}$$

where

$$\begin{aligned} G &= \left(x^2 + 4\tau^2 + \frac{3}{4}\right) \left(x^2 + 20\tau^2 + \frac{3}{4}\right) - \frac{3}{4}, \\ H &= 2T \left(4\tau^2 - 3x^2\right) + 2\tau \left[\left(2x^2 + 4\tau^2\right)^2 - \frac{15}{8}\right], \\ D &= \frac{1}{3} \left(x^2 + 4\tau^2\right)^3 + \frac{1}{4} \left(x^2 - 12\tau^2\right)^2 + \frac{3}{64} \left(12x^2 + 176\tau^2 + 1\right). \end{aligned} \tag{16}$$

It should be noted that this solution has a remarkable property when $x = 0$ et $\tau = 0$, there is an increase in the amplitude of the carrier wave. Figs. 15, 16, 17 and 18 show the effects of the NETL parameters (C_1 , C_2 and L_1) and the wave number. From Fig. 15 and 16, it can

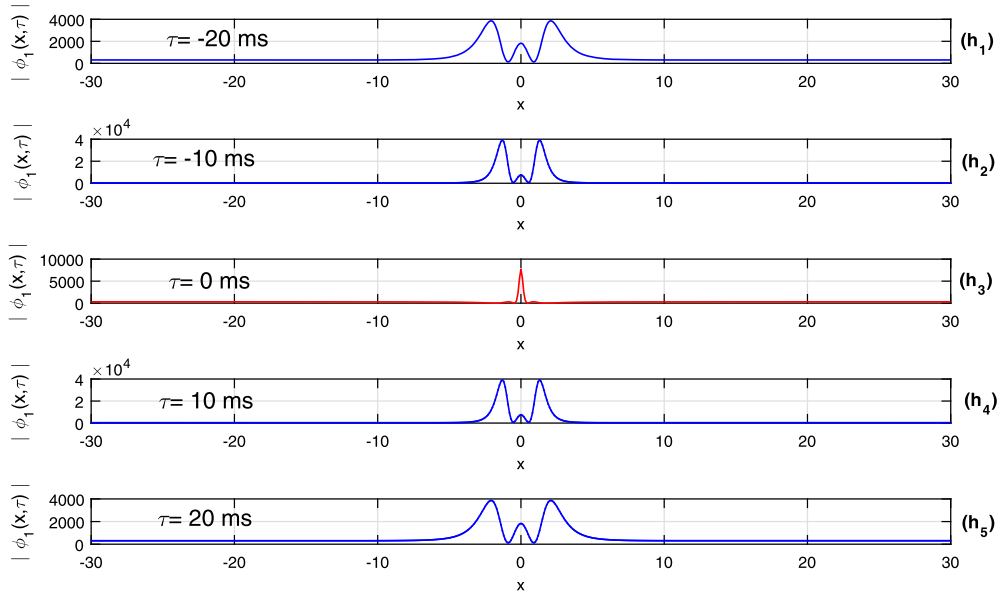


Fig. 13. Spatiotemporal plot evolution of the Peregrine solitons at $\tau = 0 \text{ ms}$, $\tau = 5 \text{ ms}$, $\tau = 10 \text{ ms}$, $\tau = 15 \text{ ms}$, $\tau = 20 \text{ ms}$ for $C_1 = 420 \text{ pF}$, $C_2 = 480 \text{ pF}$ at $J_0 = 200 \text{ nA}$, $L_1 = 480 \text{ }\mu\text{H}$.

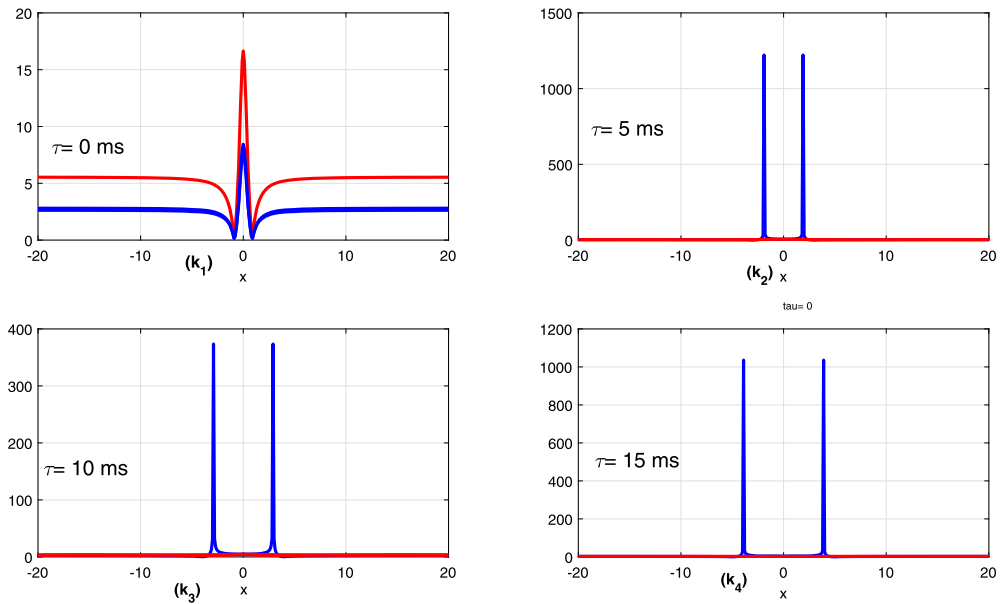


Fig. 14. Spatiotemporal plot evolution of the Peregrine solitons $\tau = 0 \text{ ms}$, $\tau = 5 \text{ ms}$, $\tau = 10 \text{ ms}$, $\tau = 15 \text{ ms}$, $\tau = 20 \text{ ms}$ for $C_2 = 2C_1$ (blue line) and $C_1 = 2C_2$ (red line) at $J_0 = 200 \text{ nA}$, $L_1 = 480 \text{ }\mu\text{H}$.

be observed that when C_1 is more important than C_2 , the SRW emerges which is higher than the Peregrine soliton. From Fig. 17, it is given at different times $\tau = 0 \text{ ms}$, $\tau = 5 \text{ ms}$, $\tau = 10 \text{ ms}$, $\tau = 15 \text{ ms}$, $\tau = 20 \text{ ms}$ the shape of the SRWs. At $\tau = 0 \text{ ms}$, the SRW is forming with a good shape, and progressively the SRW shape seems to be a Peregrine soliton, and we can affirm that when the capacitors value decrease, the amplifying rogue wave is stopping. However, Fig. 16 gives the most specific form of the SRW with decreasing amplitude. Furthermore, it is pointed out that the wave energy is located in a small area due to the nonlinear and dispersion terms of NLSE. These obtained results highlight the dynamic progresses of the SRWs.

4. Envelope solitons: bright and dark

The nonlinear Schrödinger equation in Eq. (8) admits the following bright and dark solitons solutions respectively [10]:

$$\begin{aligned} \phi_1(x, \tau) &= A \operatorname{sech} \left(A \sqrt{\left| \frac{Q}{2P} \right|} |x - v\tau| \right) e^{i(kx - \omega\tau)}, \\ \phi_1(x, \tau) &= A \tanh \left(A \sqrt{\left| \frac{Q}{2P} \right|} |x - v\tau| \right) e^{i(kx - \omega\tau)}. \end{aligned} \tag{17}$$

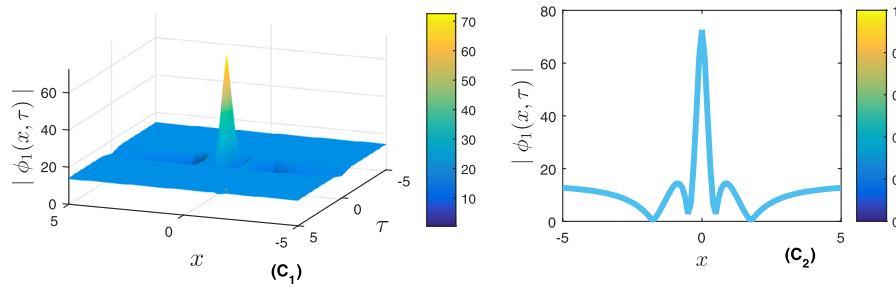


Fig. 15. (C₁) Spatiotemporal plot evolution and (C₂) plot 2D of the SRWs at $C_2 = 210C_1$ at $J_0 = 200 \text{ nA}$, $L_1 = 480 \mu\text{H}$.

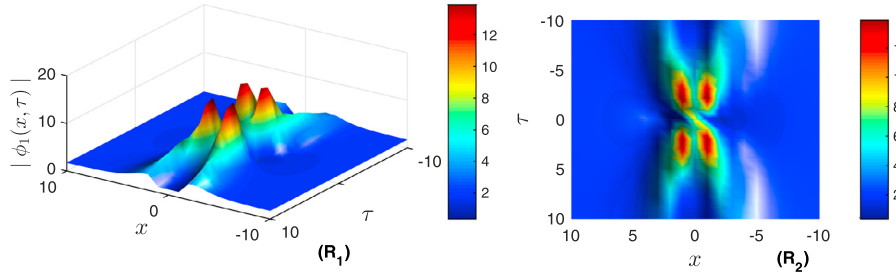


Fig. 16. (R₁) Spatiotemporal plot evolution and (R₂) contour plot of the SRWs at $C_1 < C_2$ and $J_0 = 200 \text{ nA}$, $L_1 = 480 \mu\text{H}$.

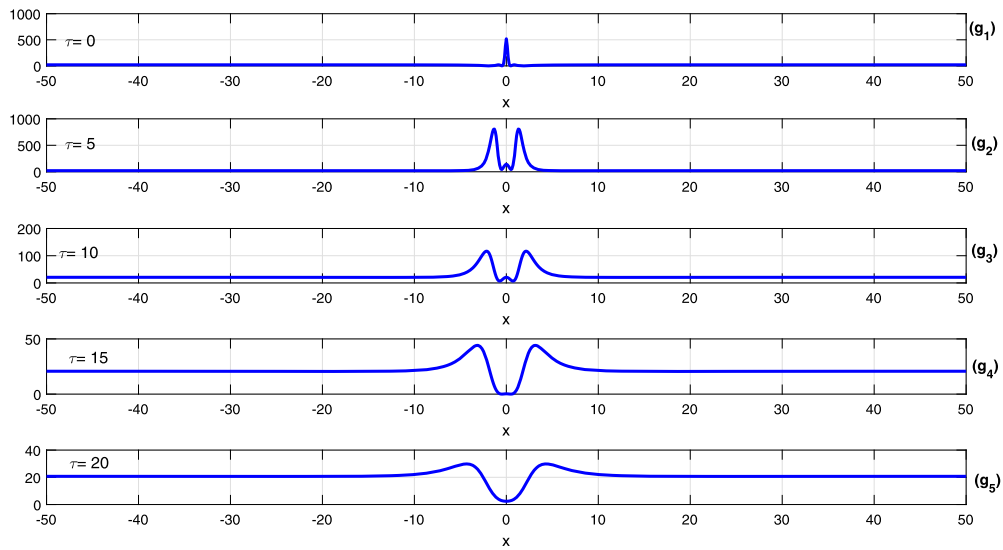


Fig. 17. Spatiotemporal plot evolution of the SRWs at (g_1) $\tau = 0 \text{ ms}$, (g_2) $\tau = 5 \text{ ms}$, (g_3) $\tau = 10 \text{ ms}$, (g_4) $\tau = 15 \text{ ms}$, (g_5) $\tau = 20 \text{ ms}$ for $C_1 < C_2$ and $J_0 = 200 \text{ nA}$, $L_1 = 480 \mu\text{H}$.

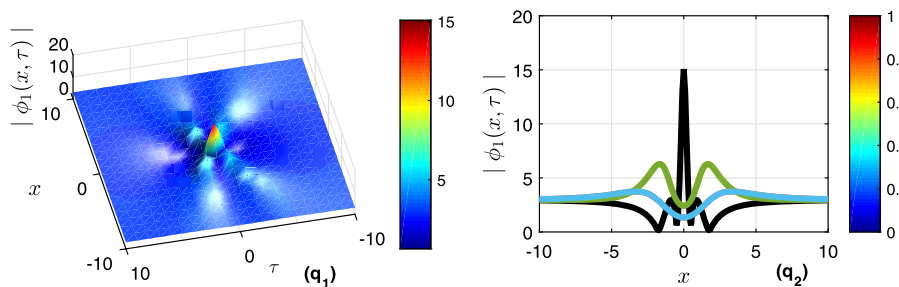


Fig. 18. (q_1) Spatiotemporal plot evolution of the SRWs (q_2) and contour plot evolution at $C_2 = 18.75C_1$ and $J_0 = 200 \text{ nA}$, $L_1 = 480 \mu\text{H}$, $\phi_0 = 2.064 \times 10^{-10}$.

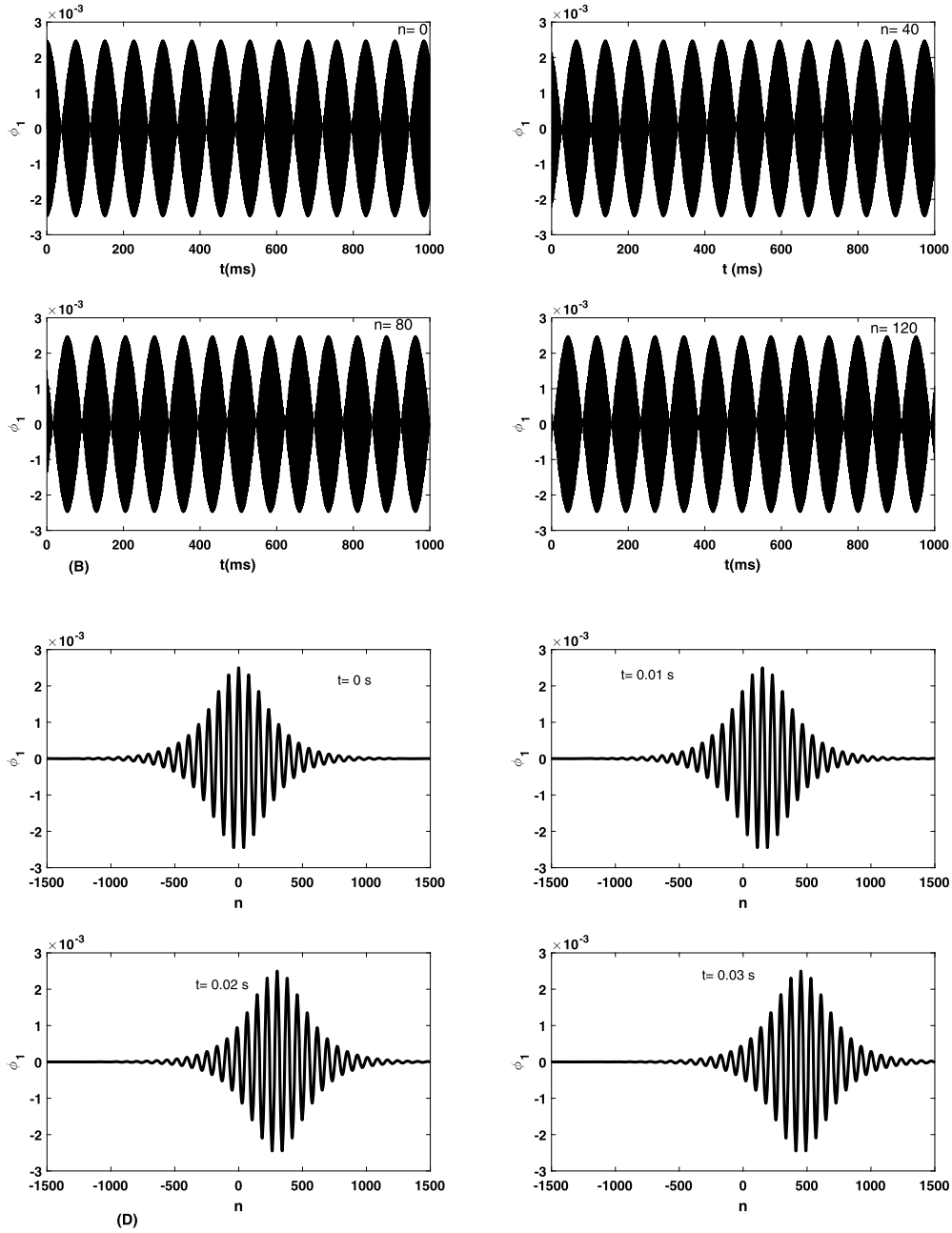


Fig. 19. (B) Spatiotemporal plot evolution of the bright soliton with ($t=0$) as initial condition and (D) the evolution of the dark soliton at $C_1 = 50pF$, $C_2 = 750pF$, $\omega_j = 0.034$, $\omega = 0.0026$, and $J_0 = 200nA$, $L_1 = 240 \mu H$, $\phi_0 = 2.064 \times 10^{-10}$.

To investigate envelope soliton to the discrete equation given in Eq. (5) it will be used numerical simulation by considering the given set of Eq. (15) with ($t=0$) as initial condition. The first step is to use the Runge-Kutta of order 4, to integrate Eq. (5), to observe the behavior of the wave which propagates in the lattice. It is assumed $N = 1001$.

Figs. 19 (B) and (D) are bright and dark evolution with ($t=0$) as initial condition of Eq. (15). However, Fig. 20(f_1) and 20(f_2) are analytical plot evolution and numerical simulation of the bright soliton respectively. We observe that the maximum amplitude of the plane wave which propagates is around $0.003V$. Moreover, the wave propagates in a sinusoidal and regular manner along the NETL with JJ. We also note the similarity between the curves obtained numerically and analytically. This result confirms the predictions made analytically on the signs of the dispersion and nonlinearity coefficients.

5. Conclusion

The purpose of this paper is to establish to unearth the envelope solitons, the super rogue waves and the Peregrine soliton to the NLSE obtained by using the reductive perturbation method in the semi-discrete approximation. Through the coefficients of dispersion and non-linearity the areas of propagation of the bright and black solitons have been identified, thus the areas of instability. The most relevant observation is that the obtained rogue waves show regions of energy concentration which are influenced by the parameters of the NETL with JJ. On the other hand, we realize that the frequency of the plasma related to the flow of the JJ, has an effect to the obtained results.

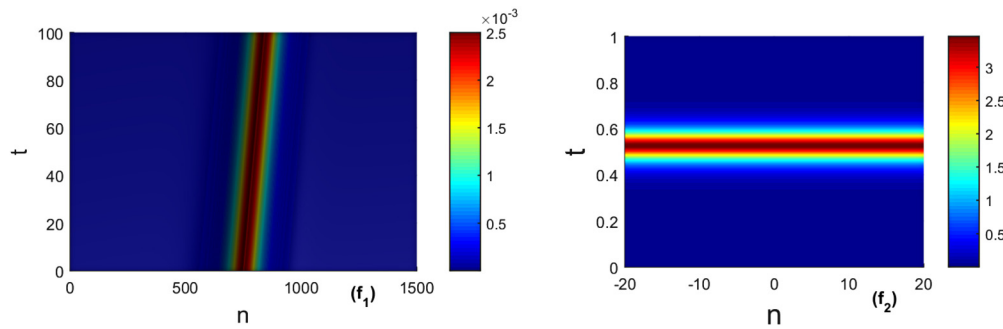


Fig. 20. (f_1) Analytical result contour plot evolution and numerical simulation (f_2) of the bright soliton with ($t = 0$) as initial condition at $C_1 = 50pF$, $C_2 = 750pF$, $\omega_j = 0.034$, $f = 1.5MHz$, and $J_0 = 200nA$, $L_1 = 240 \mu H$, $\phi_0 = 2.064 \times 10^{-10}$.

It has been also studied the MI analysis to highlight the process of magnifying small perturbation for the solitary waves. The next work, will be focused to numerical investigation to more understand the dynamic process of the rogue waves.

Declaration of competing interest

The authors declare that they have no known competing financial interests or personal relationships that could have appeared to influence the work reported in this paper.

References

- [1] R. Hirota, K. Suzuki, Studies on lattice solitons by using electrical networks, *J. Phys. Soc. Jpn.* 28 (1970) 1366.
- [2] E. Kengne, S.T. Chui, W.M. Liu, Modulational instability criteria for coupled nonlinear transmission lines with dispersive elements, *Phys. Rev. E* 74 (2006) 036614.
- [3] E. Kengne, A. Lakhssassi, W.M. Liu, Modeling of matter-wave solitons in a nonlinear inductor-capacitor network through a Gross-Pitaevskii equation with time-dependent linear potential, *Phys. Rev. E* 96 (2017) 022221.
- [4] T.C. Kofane, B. Michaux, M. Remoissenet, Theoretical and experimental studies of diatomic lattice solitons using an electrical transmission line, *J. Phys. C, Solid State Phys.* 21 (1988) 1395.
- [5] H. Alphonse, A. Souleymanou, M. Inc, B. Gambo, Y.D. Serge, T.C. Kofane, K.S. Nisar, Chirped solitons in discrete electrical transmission line, *Results Phys.* 18 (2020) 103188.
- [6] J.K. Duan, Y.L. Bai, Rogue wave in coupled electric transmission line, *Indian J. Phys.* 92 (2018) 369–375.
- [7] J.K. Duan, Y.L. Bai, Q. Wei, M.H. Fan, Super rogue waves in coupled electric transmission lines, *Indian J. Phys.* 94 (2020) 879.
- [8] G.E. Peterson, Electrical transmission lines as models for soliton propagation in materials: elementary aspects of video solitons, *AT&T Bell Lab. Tech. J.* 63 (1984) 901.
- [9] Y. Nejoh, Envelope soliton of the electron plasma wave in a nonlinear transmission line, *Phys. Scr.* 31 (1985) 415.
- [10] S. Abdoukary, T. Beda, S.Y. Doka, F.I. Ndzana, L. Kavitha, A. Mohamadou, Dissipative discrete system with nearest-neighbor interaction for the nonlinear electrical lattice, *J. Mod. Phys.* 3 (2012) 438.
- [11] M. Remoissenet, *Waves Called Solitons*, 3rd edn., Springer, Berlin, 1999.
- [12] A. Noguchi, Solitons in a nonlinear transmission line, *Electron. Commun. Jpn.*, A 57 (1974) 9.
- [13] E. Kengne, R. Vaillancourt, B.A. Malomed, Coupled nonlinear Schrödinger equations for solitary-wave and kink signals propagating in discrete nonlinear dispersive transmission lines, *Int. J. Mod. Phys. B* 23 (2009) 133.
- [14] A. Nai, A. Ankiewicz, M. Taki, Waves that appear from nowhere and disappear without a trace, *Phys. Lett. A* 373 (2009) 675.
- [15] D. Yemele, F. Kenmogne, Compact envelope dark solitary wave in a discrete nonlinear electrical transmission line, *Phys. Lett. A* 373 (2009) 3801.
- [16] B.A. Malomed, A Variety of Dynamical Settings in Dual-Core Nonlinear Fibers, *Handbook of Optical Fibers*, Springer, Singapore, 2018 12.
- [17] J.M. Soto-Crespo, A. Nail, Ph. Grellu, F. Belhache, Quantized separations of phase-locked soliton pairs in fiber lasers, *Opt. Lett.* 28 (2003) 1757.
- [18] J. Soto-Crespo, N. Devine, A. Nai, Integrable turbulence and rogue waves: breathers or solitons? *Phys. Rev. Lett.* 116 (2016) 103901.
- [19] B. Frisquet, A. Chabchoub, J. Fatome, C. Finot, B. Kibler, G. Millot, Two-stage linear-nonlinear shaping of an optical frequency comb as rogue nonlinear Schrödinger-equation-solution generator, *Phys. Rev. A* 89 (2014) 023821.
- [20] A. Ankiewicz, P.A. Clarkson, A. Nai, Rogue waves, rational solutions, the patterns of their zeros and integral relations, *J. Phys. A, Math. Theor.* 43 (2010) 122002.
- [21] M. Erkintalo, G. Genty, B. Wetzel, J.M. Dudley, Akhmediev breather evolution in optical fiber for realistic initial conditions, *Phys. Lett. A* 375 (2011) 2029.
- [22] I. Victor, V.G. Shrira Vladimir, What makes the Peregrine soliton so special as a prototype of freak waves? *J. Eng. Math.* 67 (2010) 11–22.
- [23] B. Kibler, J. Fatome, C. Finot, G. Millot, F. Dias, G. Genty, N. Akhmediev, J.M. Dudley, The Peregrine soliton in nonlinear fibre optics, *Nat. Phys.* 6 (2010) 790–795.
- [24] W.S. Duan, Nonlinear waves propagating in the electrical transmission line, *Europhys. Lett.* 66 (2004) 192.



Optical and W-shaped bright solitons of the conformable derivative nonlinear differential equation

Hamadou Halidou¹ · Alphonse Houwe² · Souleymanou Abbagari^{1,3} · Mustafa Inc^{4,5,6} · Serge Y. Doka⁷ · Thomas Bouetou Bouetou⁸

Received: 16 June 2021 / Accepted: 20 July 2021 / Published online: 13 August 2021
© The Author(s), under exclusive licence to Springer Science+Business Media, LLC, part of Springer Nature 2021

Abstract

In this paper, we construct diverse solitary wave solutions for the nonlinear differential equation governing wave propagation in the low-pass nonlinear electrical transmission lines with conformable derivatives. However, by employing the new extended direct algebraic method and the improved Sub-ODE equation, we recovered W-shape bright soliton, dark soliton, periodic solutions, rational solutions and Weierstrass elliptic function solutions. The obtained results are new in nonlinear electrical transmission lines field. In addition, the acquired solitons are depicted with the appropriate parameters values of the methods and the nonlinear electrical transmission lines. The shape of the W-bright and dark soliton solutions points out the effect of the derivative order. Finally, the results indicate that the two integrations methods are a most applicable and forceful integration tools for emphasizing the soliton solutions.

Keywords W-shape bright soliton · Conformable derivative order · Electrical transmission lines

1 Introduction

Recently, there has been significant attentiveness in fractional calculus used in the analysis of the traveling wave solutions of nonlinear differential equations [1–19]. Fractional calculus is an extension of ordinary calculus, where derivatives and integrals of an arbitrary real order are defined. Many types of fractional calculus definitions that

have been given in literature cannot be adopted for classical properties such as Rolle and mean value theorem, chain rules and so on. Furthermore, the conformable fractional is confused to the fractional derivative and integral with $\alpha \in (0,1)$ order. Beside of this, several types of operators have been also used like fractional derivatives during the past few years.

✉ Mustafa Inc
minc@firat.edu.tr; hamadouhalidou@yahoo.fr;
ahouw220@yahoo.fr; abbagaris@yahoo.fr

Hamadou Halidou
hamadouhalidou@yahoo.fr

Alphonse Houwe
ahouw220@yahoo.fr

Souleymanou Abbagari
abbagaris@yahoo.fr

Serge Y. Doka
numami@gmail.com

Thomas Bouetou Bouetou
tbouetou@gmail.com

¹ Laboratory of Mechanics, Materials and Structures, Department of Physics, Faculty of Science, University of Yaounde I, P.O. Box 812, Yaounde, Cameroon

² Department of Physics, Faculty of Science, University of Maroua, P.O. Box 814, Maroua, Cameroon

³ Department of Basic Science, Faculty of Mines and Petroleum Industries, University of Maroua, P.O. Box 08, Maroua, Cameroon

⁴ Department of Computer Engineering, Biruni University, Istanbul, Turkey

⁵ Department of Mathematics, Science Faculty, Firat University, 23119 Elazig, Turkey

⁶ Department of Medical Research, China Medical University Hospital, China Medical University, Taichung, Taiwan

⁷ Department of Physics, Faculty of Science, University of Ngaoundere, P.O. Box 454, Ngaoundere, Cameroon

⁸ National Advanced School of Engineering, University of Yaounde I, Yaounde, Cameroon

Moreover, fractional calculus has been extensively used nowadays to formulate exact problems in mathematics and other field of science. On this way, new class of analytical solutions of nonlinear conformable time-fractional coupled Drinfeld–Sokolov–Wilson equation was proposed by Orkun et al. [20]. This proposal arise in shallow water flow simulations, when particular forms are employed to plan the shallow water equations like Sine-Gordon expansion technique. Likewise, Rezazadeh et al. used the conformable fractional to generalized kuramoto sivashinsky equation to build solitary wave solutions [21], Rezazadeh et al.. adopted the first integral method with conformable time-fractional derivative [22]. Exact solutions of fractional partial differential equations (PDEs), have become very important to explain wave propagation phenomena in deep waters like fiber optic transport and in shallow ones.

The fractional derivatives which are well knowing in modern mathematics have been proposed by the popular mathematicians such as Riemann et al. [23]. However, several definitions of fractional derivatives were obtained such as Atangana–Baleanu derivative in Caputo direction, Atangana–Baleanu fractional derivative in Riemann–Liouville sense, the new truncated M-fractional derivative of Igor [24], Abdon [25] and Sousa and Oliveira [26], just to name a few.

Therefore, the conformable nonlinear ordinary differential equations have supplied interesting solitary waves solutions of many physical phenomena by using relevant mathematical methods. Beside of this, it have been obtained soliton turbulence to examine ocean wave data. That is why soliton turbulence becomes very interesting in study nowadays [27]. Furthermore, in the last decade, innumerable integration scheme has been proposed to construct exact analytical solutions and the approached numerical solutions to conformal nonlinear differential equations such as such as the sub-equation method, the Sinh–Gordon expansion method, the new extended direct algebraic method, $\exp(-\psi(\xi))$ -expansion method, the rational hyperbolic method, the generalized auxiliary equation technique, the generalized Kudryashov (GK), the fractional and variational iteration algorithm I, the improved algorithm to the variational iteration algorithm-II, the efficient local meshless method, the local meshless collocation method, a new generalized Jacobi elliptic function method, the extended tanh method, the rational hyperbolic functions method, the rational exponential functions method, the tanh–coth method just to name a few [1, 3, 4, 28–55]. It is also difficult to find a suitable method which can give a variety of analytical solutions known in the literature. Most often, several methods are used to collect a good quantity of physically explainable solutions. In this paper, it will be a question of using two methods known for their variety in analytical solutions, they are namely the new extended direct algebraic method and the improved new Sub-ODE method.

In this study, we explore new, accurate solitary wave solutions for the conformable derivative nonlinear differential equation that governs wave propagation in the nonlinear electrical transmission line (NELT) loaded by the diode vector BB112 [41].

$$\begin{aligned} & (1 + b_1 u(x, t) + b_2 u(x, t)^2) D_t^{2\alpha} u(x, t) \\ & + (b_1 + 2b_2 u(x, t)) (D_t^\alpha u(x, t))^2 \\ & - u_0^2 D_{xx}^{2\alpha} u(x, t) \\ & - \frac{u_0^2 \delta^2}{12} D_{xxxx}^{4\alpha} u(x, t) = 0, \quad 0 < \alpha \leq 1. \end{aligned} \quad (1)$$

The details of the derivation of (1) was proposed in [41]. However, $u(x, t)$ is the voltage in transmission line and δ and u_0 are constants, while the variable x is the propagation distance and t represents the slow time. However, b_1 and b_2 are constants.

To reach the goal, Sect. 2 summarizes the conformable derivative theorem. The glimpse of the methods applied are given in Sect. 3 and in Sect. 4 we apply the methods to the conformable nonlinear differential equation governing wave propagation in low-pass electrical transmission lines, follows by some graphical illustrations. The last section gives the summary of the work.

2 Sight of the conformable derivative order

Considering the following short definition of the conformable derivative of order $\alpha \in (0, 1)$:

$$\frac{d^\alpha g(t)}{dt^\alpha} = \lim_{\zeta \rightarrow +\infty} \frac{g(t + \zeta t^{1-\alpha}) - g(t)}{\zeta}, \quad g : (0, \infty) \rightarrow \mathbb{R}. \quad (2)$$

Theorem 1 *Let $\alpha \in (0, 1]$ and $g = g(t)$, $h = h(t)$ be α -conformable differentiable at $t < 0$. Hence,*

- $D_t^\alpha (ag + bh) = aD_t^\alpha g + bD_t^\alpha h$, and $a, b \in \mathbb{R}$.
- $D_t^\alpha (t^\beta) = \beta t^{\beta-\alpha}$ and $\beta \in \mathbb{R}$.
- $D_t^\alpha (gh) = hD_t^\alpha (g) + fD_t^\alpha (h)$.
- $D_t^\alpha \left(\frac{g}{h} \right) = \frac{hD_t^\alpha (g) - fD_t^\alpha (h)}{g^2}$.

3 Overview of the methods

3.1 The new extended direct algebraic method

The fundamental of the new extended direct algebraic method is given by the following steps [42].

Step 1: Adopting the partial differential equation (PDE) in the following form

$$H(u, D_t^\alpha u, D_x^\alpha u, D_y^\alpha u, D_t^{2\alpha} u, D_t^\alpha D_x^\beta u, \dots) = 0, \quad 0 < \alpha, \beta < 1, \tag{3}$$

where $u(x, t)$ is an unknown function and H is a polynomial of u .

Surmise the traveling-wave hypothesis as follows and then adopting $u(x, t) = U(\xi)$

$$\xi = \frac{k_1}{\alpha} t^\alpha + \frac{k_2}{\alpha} x^\alpha \tag{4}$$

while k_1, k_2 are constants to be determined, and $k_1, k_2 \neq 0$. Thus, the PDE can turn into ordinary differential equation

$$F(U, k_1 U', k_1 k_2 U'', k_1^3 U''', \dots) = 0, \tag{5}$$

and prime denotes the derivative with respect to ξ .

Step 2: Considering that (5) has the solution in the following expression

$$U(\xi) = \sum_{j=0}^N g_j Q^j(\xi), \quad g_n \neq 0, \tag{6}$$

where $g_j (0 \leq j \leq N)$ are constants to be determined later and $Q(\xi)$ satisfies the following ODE

$$Q'(\xi) = Ln(A)(\lambda + \mu Q(\xi) + \sigma Q^2(\xi)), \tag{7}$$

and $A \neq 0, 1$.

The solutions of ODE (7) are:

Case 1. $\mu^2 - 4\lambda\sigma < 0$ and $\sigma \neq 0$

$$Q_1(\xi) = -\frac{\mu}{2\sigma} + \frac{\sqrt{-(\mu^2 - 4\lambda\sigma)}}{2\sigma} \tan_A \left(\frac{\sqrt{-(\mu^2 - 4\lambda\sigma)}}{2} \xi \right), \tag{8}$$

$$Q_2(\xi) = -\frac{\mu}{2\sigma} + \frac{\sqrt{-(\mu^2 - 4\lambda\sigma)}}{2\sigma} \cot_A \left(\frac{\sqrt{-(\mu^2 - 4\lambda\sigma)}}{2} \xi \right), \tag{9}$$

$$Q_3(\xi) = -\frac{\mu}{2\sigma} + \frac{\sqrt{-(\mu^2 - 4\lambda\sigma)}}{2\sigma} \tan_A \left(\sqrt{-(\mu^2 - 4\lambda\sigma)} \xi \right) \pm \frac{\sqrt{-pq(\mu^2 - 4\lambda\sigma)}}{2\sigma} \sec_A \left(\sqrt{-(\mu^2 - 4\lambda\sigma)} \xi \right), \tag{10}$$

$$Q_4(\xi) = -\frac{\mu}{2\sigma} - \frac{\sqrt{-(\mu^2 - 4\lambda\sigma)}}{2\sigma} \cot_A \left(\sqrt{-(\mu^2 - 4\lambda\sigma)} \xi \right) \pm \frac{\sqrt{-pq(\mu^2 - 4\lambda\sigma)}}{2\sigma} \csc_A \left(\sqrt{-(\mu^2 - 4\lambda\sigma)} \xi \right), \tag{11}$$

$$Q_5(\xi) = -\frac{\mu}{2\sigma} - \frac{\sqrt{-(\mu^2 - 4\lambda\sigma)}}{2\sigma} \tan_A \left(\frac{\sqrt{-(\mu^2 - 4\lambda\sigma)}}{4} \xi \right) - \frac{\sqrt{-(\mu^2 - 4\lambda\sigma)}}{2\sigma} \cot_A \left(\frac{\sqrt{-(\mu^2 - 4\lambda\sigma)}}{4} \xi \right). \tag{12}$$

Case 2. $\mu^2 - 4\lambda\sigma > 0$ and $\sigma \neq 0$

$$Q_6(\xi) = -\frac{\mu}{2\sigma} + \frac{\sqrt{(\mu^2 - 4\lambda\sigma)}}{2\sigma} \tanh_A \left(\frac{\sqrt{(\mu^2 - 4\lambda\sigma)}}{2} \xi \right), \tag{13}$$

$$Q_7(\xi) = -\frac{\mu}{2\sigma} + \frac{\sqrt{(\mu^2 - 4\lambda\sigma)}}{2\sigma} \coth_A \left(\frac{\sqrt{(\mu^2 - 4\lambda\sigma)}}{2} \xi \right), \tag{14}$$

$$Q_8(\xi) = -\frac{\mu}{2\sigma} + \frac{\sqrt{(\mu^2 - 4\lambda\sigma)}}{2\sigma} \tanh_A \left(\sqrt{(\mu^2 - 4\lambda\sigma)} \xi \right) \pm i \frac{\sqrt{pq(\mu^2 - 4\lambda\sigma)}}{2\sigma} \operatorname{sech}_A \left(\sqrt{(\mu^2 - 4\lambda\sigma)} \xi \right), \tag{15}$$

$$Q_9(\xi) = -\frac{\mu}{2\sigma} - \frac{\sqrt{(\mu^2 - 4\lambda\sigma)}}{2\sigma} \coth_A \left(\sqrt{(\mu^2 - 4\lambda\sigma)} \xi \right) \pm \frac{\sqrt{pq(\mu^2 - 4\lambda\sigma)}}{2\sigma} \operatorname{csch}_A \left(\sqrt{(\mu^2 - 4\lambda\sigma)} \xi \right), \tag{16}$$

$$Q_{10}(\xi) = -\frac{\mu}{2\sigma} - \frac{\sqrt{-(\mu^2 - 4\lambda\sigma)}}{4\sigma} \tanh_A \left(\frac{\sqrt{(\mu^2 - 4\lambda\sigma)}}{4} \xi \right) - \frac{\sqrt{(\mu^2 - 4\lambda\sigma)}}{4\sigma} \coth_A \left(\frac{\sqrt{(\mu^2 - 4\lambda\sigma)}}{4} \xi \right). \tag{17}$$

Case 3. $\lambda\sigma > 0$ and $\mu = 0$

$$Q_{11}(\xi) = \sqrt{\frac{\lambda}{\sigma}} \tan_A \left(\sqrt{\lambda\sigma} \xi \right), \tag{18}$$

$$Q_{12}(\xi) = -\sqrt{\frac{\lambda}{\sigma}} \cot_A \left(\sqrt{\lambda\sigma} \xi \right), \tag{19}$$

$$Q_{13}(\xi) = \sqrt{\frac{\lambda}{\sigma}} \tan_A \left(\sqrt{2\lambda\sigma} \xi \right) \pm \sqrt{pq} \frac{\lambda}{\sigma} \sec_A \left(\sqrt{2\lambda\sigma} \xi \right), \tag{20}$$

$$Q_{14}(\xi) = -\sqrt{\frac{\lambda}{\sigma}} \cot_A \left(\sqrt{2\lambda\sigma} \xi \right) \pm \sqrt{pq} \frac{\lambda}{\sigma} \csc_A \left(\sqrt{2\lambda\sigma} \xi \right), \tag{21}$$

$$Q_{15}(\xi) = \frac{1}{2} \sqrt{\frac{\lambda}{\sigma}} \left(\tan_A \left(\frac{\sqrt{\lambda\sigma}}{2} \xi \right) - \sqrt{\frac{\lambda}{\sigma}} \cot_A \left(\frac{\sqrt{\lambda\sigma}}{2} \xi \right) \right). \quad (22)$$

Case 4. $\lambda\sigma < 0$ and $\mu = 0$

$$Q_{16}(\xi) = -\sqrt{\frac{-\lambda}{\sigma}} \tanh_A \left(\sqrt{-\lambda\sigma} \xi \right), \quad (23)$$

$$Q_{17}(\xi) = -\sqrt{\frac{-\lambda}{\sigma}} \coth_A \left(\sqrt{-\lambda\sigma} \xi \right), \quad (24)$$

$$Q_{18}(\xi) = -\sqrt{\frac{-\lambda}{\sigma}} \tanh_A \left(\sqrt{2\lambda\sigma} \xi \right) \pm i \sqrt{pq \frac{-pq\lambda}{\sigma}} \operatorname{sech}_A \left(2\sqrt{-\lambda\sigma} \xi \right), \quad (25)$$

$$Q_{19}(\xi) = -\sqrt{\frac{-\lambda}{\sigma}} \coth_A \left(2\sqrt{-\lambda\sigma} \xi \right) \pm \sqrt{-pq \frac{\lambda}{\sigma}} \operatorname{csch}_A \left(2\sqrt{-\lambda\sigma} \xi \right), \quad (26)$$

$$Q_{20}(\xi) = -\frac{1}{2} \left(\sqrt{\frac{-\lambda}{\sigma}} \tanh_A \left(\frac{\sqrt{-\lambda\sigma}}{2} \xi \right) + \sqrt{\frac{-\lambda}{\sigma}} \coth_A \left(\frac{\sqrt{-\lambda\sigma}}{2} \xi \right) \right). \quad (27)$$

Case 5. $\mu = 0$ and $\lambda = \sigma$

$$Q_{21}(\xi) = \tan_A(\lambda\xi), \quad (28)$$

$$Q_{22}(\xi) = -\cot_A(\lambda\xi), \quad (29)$$

$$Q_{23}(\xi) = \tan_A(2\lambda\xi) \pm \sqrt{pq} \sec_A(2\lambda\xi), \quad (30)$$

$$Q_{24}(\xi) = -\cot_A(2\lambda\xi) \pm \sqrt{pq} \csc_A(2\lambda\xi), \quad (31)$$

$$Q_{25}(\xi) = \frac{1}{2} \left(\tan_A \left(\frac{\lambda}{2} \xi \right) - \cot_A \left(\frac{\lambda}{2} \xi \right) \right). \quad (32)$$

Case 6. $\mu = 0$ and $\lambda = -\sigma$

$$Q_{26}(\xi) = -\tanh_A(\lambda\xi), \quad (33)$$

$$Q_{27}(\xi) = -\coth_A(\lambda\xi), \quad (34)$$

$$Q_{28}(\xi) = -\tanh_A(2\lambda\xi) \pm i \sqrt{pq} \operatorname{sech}_A(2\lambda\xi), \quad (35)$$

$$Q_{29}(\xi) = -\coth_A(2\lambda\xi) \pm \sqrt{pq} \operatorname{csch}_A(2\lambda\xi), \quad (36)$$

$$Q_{30}(\xi) = -\frac{1}{2} \left(\tanh_A \left(\frac{\lambda}{2} \xi \right) + \coth_A \left(\frac{\lambda}{2} \xi \right) \right). \quad (37)$$

Case 7. $\mu^2 = 4\lambda\sigma$

$$Q_{31}(\xi) = -\frac{2\lambda(\mu\xi \operatorname{Ln}(A) + 2)}{\mu^2 \xi \operatorname{Ln}(A)}. \quad (38)$$

Case 8. $\mu = k$, $\lambda = mk$ ($m \neq 0$), and $\sigma = 0$,

$$Q_{32}(\xi) = A^{\xi k} - m. \quad (39)$$

Case 9. $\mu = \sigma = 0$

$$Q_{33}(\xi) = \lambda \xi \operatorname{Ln} A. \quad (40)$$

Case 10. $\mu = \lambda = 0$

$$Q_{34}(\xi) = \frac{-1}{\sigma \xi \operatorname{Ln} A}. \quad (41)$$

Case 11. $\mu \neq 0$ and $\lambda = 0$.

$$Q_{35}(\xi) = \frac{p\mu}{\sigma(\cosh_A(\mu\xi) - \sinh_A(\mu\xi) - p)}, \quad (42)$$

$$Q_{36}(\xi) = -\frac{\mu(\sinh_A(\mu\xi) + \cosh_A(\mu\xi))}{\sigma(\cosh_A(\mu\xi) - \sinh_A(\mu\xi) + q)}. \quad (43)$$

Case 12. $\mu = k$ and $\sigma = mk$ ($m \neq 0$) and $\lambda = 0$.

$$Q_{37}(\xi) = -\frac{pA^{k\xi}}{q - mpA^{k\xi}}. \quad (44)$$

Step 3. By using the homogeneous balance principle the value of N can be obtained between the highest order derivative and high-order terms in (5).

Step 4. Substituting (6) and (7) into (5), then collecting all the term of $Q^i(\xi)$ to set to zero yields a system of algebraic equation.

Step 5. With aid of MAPLE, the results of the system of algebraic equation can be obtained and then use the results of (7) to construct the exact solutions of (5).

However, the details of the generalized hyperbolic and trigonometric functions are given by [42].

3.2 The new sub-ODE method

Suppose that the solution of Eq. (5) is given by

$$U(\xi) = \mu F^s(\xi), \quad \mu > 0. \quad (45)$$

Here μ is an arbitrary positive constant to be determined, while $F(\xi)$ satisfies the following ODE

$$F'^2(\xi) = AF^{2-2p}(\xi) + BF^{2-p}(\xi) + CF^2(\xi) + DF^{2+p}(\xi) + EF^{2+2p}(\xi), \quad p > 0. \tag{46}$$

- Step 1: it consists to determine the parameter s by using the balance principle as follows:

$$D(U) = s, \quad D(U^2) = 2s \dots, \quad D(U') = s + p, \tag{47}$$

$$D(U'') = s + 2p \dots,$$

- Step 2: now, Eqs. (4) and (5) can be plugged together into set of Eq. (3), thereafter collect all the coefficients of $F^{si}(\xi)[F(\xi)']^s$ ($i = 0, 1, 2, 3, \dots$) and equal them to zero, yields to a set of algebraic system of equation which will lead to determine the different coefficients A, B, C, D, E and μ . In the same time the s values should be (0, 1).
- Step 3: the final procedure focusses to insert the obtained parameters in the following set of solutions of Eq. (3), which are listed in Ref. [51, 52].

Case 1. If $A = 0, B = 0, D = 0$, it is recovered bright soliton of Eq. (5):

$$F(\xi) = \left[\epsilon \sqrt{-\frac{C}{E}} \operatorname{sech}(p\sqrt{C}\xi) \right]^{\frac{1}{p}}, \quad C > 0, \quad E < 0, \quad \epsilon \pm 1, \tag{48}$$

a periodic solution

$$F(\xi) = \left[\epsilon \sqrt{-\frac{C}{E}} \sec(p\sqrt{-C}\xi) \right]^{\frac{1}{p}}, \quad C < 0, \quad E > 0, \quad \epsilon \pm 1, \tag{49}$$

and a rational solution

$$F(\xi) = \left[\frac{\epsilon}{p\sqrt{E}\xi} \right]^{\frac{1}{p}}, \quad C = 0, \quad E > 0, \quad \epsilon \pm 1. \tag{50}$$

Case 2. By setting the conditions $B = 0, D = 0, A = \frac{C^2}{4E}$, it is gained dark soliton-like solution of Eq. (5):

$$F(\xi) = \left[\epsilon \sqrt{-\frac{C}{2E}} \tanh\left(p\sqrt{\frac{-C}{2}}\xi\right) \right]^{\frac{1}{p}}, \tag{51}$$

$$C < 0, \quad E > 0, \quad \epsilon \pm 1,$$

and a periodic solution

$$F(\xi) = \left[\epsilon \sqrt{\frac{C}{2E}} \tan\left(p\sqrt{\frac{C}{2}}\xi\right) \right]^{\frac{1}{p}}, \tag{52}$$

$$C > 0, \quad E > 0, \quad \epsilon \pm 1.$$

Case 3. By setting the conditions $B = 0, D = 0$, we deduce three forms of Jacobian elliptic functions solutions of Eq. (5):

$$F(\xi) = \left[\epsilon \sqrt{\frac{-Cm^2}{E(2m^2 - 1)}} \operatorname{cn}\left(p\sqrt{\frac{C}{2m^2 - 1}}\xi\right) \right]^{\frac{1}{p}}, \tag{53}$$

$$C > 0, \quad A = \frac{C^2m^2(m^2 - 1)}{E(2m^2 - 1)^2}, \quad \epsilon \pm 1,$$

$$F(\xi) = \left[\epsilon \sqrt{\frac{-C}{E(2 - m^2)}} \operatorname{dn}\left(p\sqrt{\frac{C}{2 - m^2}}\xi\right) \right]^{\frac{1}{p}}, \tag{54}$$

$$C > 0, \quad A = \frac{C^2(1 - m^2)}{E(2 - m^2)^2}, \quad \epsilon \pm 1,$$

and

$$F(\xi) = \left[\epsilon \sqrt{\frac{-Cm^2}{E(1 + m^2)}} \operatorname{sn}\left(p\sqrt{\frac{-C}{1 + m^2}}\xi\right) \right]^{\frac{1}{p}}, \tag{55}$$

$$C < 0, \quad A = \frac{C^2m^2}{E(1 + m^2)^2}, \quad \epsilon \pm 1.$$

Case 4. By setting the conditions $A = B = E = 0$, bright soliton-like solution of Eq. (5) is gained:

$$F(\xi) = \left[\frac{-C}{D} \operatorname{sech}^2\left(\frac{p}{2}\sqrt{C}\xi\right) \right]^{\frac{1}{p}}, \quad C > 0, \quad D < 0, \tag{56}$$

a periodic solution

$$F(\xi) = \left[\frac{-C}{D} \sec^2\left(\frac{p}{2}\sqrt{-C}\xi\right) \right]^{\frac{1}{p}}, \quad C < 0, \quad D > 0, \tag{57}$$

and a rational solution

$$F(\xi) = \left[\frac{4}{D(p\xi)^2} \right]^{\frac{1}{p}}, \quad C = 0, \quad D < 0. \tag{58}$$

Case 5. By setting the conditions $C = E = 0, D > 0$, the Weierstrass elliptic function solutions of Eq. (5) are recovered

$$F(\xi) = \left[\wp\left(\frac{p\sqrt{D}}{2}\xi, g_2, g_3\right) \right]^{\frac{1}{p}}, \tag{59}$$

where $g_2 = \frac{-4B}{D}, g_3 = \frac{-4A}{D}$.

Case 6. Assuming $B = D = 0$, it is revealed Weierstrass elliptic function solutions to set of Eq. (5),

$$F(\xi) = \left[\frac{\wp(p\xi, g_2, g_3)}{E} - \frac{C}{3E} \right]^{\frac{1}{2p}}, \tag{60}$$

where $g_2 = \frac{4C^2-12AE}{3}$, $g_3 = \frac{4C(-2C^2+9AE)}{27}$.

$$F(\xi) = \left[\frac{3A}{3\wp(p\xi, g_2, g_3) - C} \right]^{\frac{1}{2p}}, \tag{61}$$

where $g_2 = \frac{4C^2-12AE}{3}$, $g_3 = \frac{4C(-2C^2+9AE)}{27}$.

$$F(\xi) = \left[\frac{6\sqrt{A}\wp(p\xi, g_2, g_3) + C\sqrt{A}}{3\wp'(p\xi, g_2, g_3)} \right]^{\frac{1}{p}}, \tag{62}$$

where $\wp'(p\xi, g_2, g_3) = \frac{d\wp(p\xi, g_2, g_3)}{d\xi}$, $g_2 = \frac{C^2}{12} + AE$, $g_3 = \frac{C(36AE-C^2)}{216}$.

$$F(\xi) = \left[\frac{3\sqrt{E^{-1}}\wp'(p\xi, g_2, g_3)}{6\wp(p\xi, g_2, g_3) + C} \right]^{\frac{1}{p}}, \tag{63}$$

where $A = \frac{5C^2}{26E}$, $g_2 = \frac{2C^2}{9}$, $g_3 = \frac{C^3}{54}$,

$$F(\xi) = \left[\sqrt{\frac{5C^2}{36E}} \frac{6\wp(p\xi, g_2, g_3) + C}{3\wp'(p\xi, g_2, g_3)} \right]^{\frac{1}{p}}, \tag{64}$$

while g_2 and g_3 are the invariants of the Weierstrass elliptic function.

Case 7. By setting the conditions $A = 0, B = 0$, we deduce three forms of solutions of Eq. (5):

$$F(\xi) = \left[\frac{1}{\cosh(p\sqrt{C}\xi) - \frac{D}{2C}} \right]^{\frac{1}{p}}, \quad C > 0, D < 2C, \tag{65}$$

$$E = \frac{D^2}{4C} - C,$$

$$F(\xi) = \left[\frac{1}{2} \sqrt{\frac{C}{E}} \left(1 + \varepsilon \tanh\left(\frac{p}{2}\sqrt{C}\xi\right) \right) \right]^{\frac{1}{p}}, \quad C > 0, \tag{66}$$

$$E > 0, \quad D = -2\sqrt{CE}, \quad \varepsilon = \pm 1,$$

and

$$F(\xi) = \left[\frac{4D}{(pD\xi)^2 - 4E} \right]^{\frac{1}{p}}, \quad C = 0, E < 0. \tag{67}$$

Case 8. Considering $A = B = 0, C > 0$, we have gained combined bright soliton and hyperbolic functions solutions of Eq. (5):

$$F(\xi) = \left[\frac{2C\operatorname{sech}^2\left(\frac{p}{2}\sqrt{C}\xi\right)}{2\sqrt{D^2 - 4CE} - (\sqrt{D^2 - 4CE} + D)\operatorname{sech}^2\left(\frac{p}{2}\sqrt{C}\xi\right)} \right]^{\frac{1}{p}}, \quad D^2 - 4CE > 0, \tag{68}$$

$$F(\xi) = \left[\frac{2C\operatorname{csch}^2\left(\frac{p}{2}\sqrt{C}\xi\right)}{2\sqrt{D^2 - 4CE} + (\sqrt{D^2 - 4CE} - D)\operatorname{csch}^2\left(\frac{p}{2}\sqrt{C}\xi\right)} \right]^{\frac{1}{p}}, \quad D^2 - 4CE > 0, \tag{69}$$

$$F(\xi) = \left[\frac{2C}{\varepsilon\sqrt{D^2 - 4CE} \cosh(p\sqrt{C}\xi) - D} \right]^{\frac{1}{p}}, \quad D^2 - 4CE > 0, \quad \varepsilon = \pm 1, \tag{70}$$

$$F(\xi) = \left[\frac{2C}{\varepsilon\sqrt{-(D^2 - 4CE)} \sinh(p\sqrt{C}\xi) - D} \right]^{\frac{1}{p}}, \quad D^2 - 4CE < 0, \quad \varepsilon = \pm 1, \tag{71}$$

$$F(\xi) = \left[-\frac{C}{D} \left(1 + \varepsilon \tanh\left(\frac{p}{2}\sqrt{C}\xi\right) \right) \right]^{\frac{1}{p}}, \quad D^2 - 4CE = 0, \quad \varepsilon = \pm 1, \tag{72}$$

$$F(\xi) = \left[-\frac{C}{D} \left(1 + \varepsilon \coth\left(\frac{p}{2}\sqrt{C}\xi\right) \right) \right]^{\frac{1}{p}}, \quad D^2 - 4CE = 0, \quad \varepsilon = \pm 1, \tag{73}$$

$$F(\xi) = \left[-\frac{C\operatorname{sech}^2\left(\frac{p}{2}\sqrt{C}\xi\right)}{D + 2\varepsilon\sqrt{CE} \tanh\left(\frac{p}{2}\sqrt{C}\xi\right)} \right]^{\frac{1}{p}}, \quad E > 0, \quad \varepsilon = \pm 1, \tag{74}$$

$$F(\xi) = \left[\frac{C\operatorname{csch}^2\left(\frac{p}{2}\sqrt{C}\xi\right)}{D + 2\varepsilon\sqrt{CE} \coth\left(\frac{p}{2}\sqrt{C}\xi\right)} \right]^{\frac{1}{2}}, \quad E > 0, \quad \varepsilon = \pm 1, \tag{75}$$

$$F(\xi) = \left[\frac{-CD\operatorname{sech}^2\left(\frac{p}{2}\sqrt{C}\xi\right)}{D^2 - CE\left(1 + \varepsilon \tanh\left(\frac{p}{2}\sqrt{C}\xi\right)\right)^2} \right]^{\frac{1}{2}}, \tag{76}$$

$$F(\xi) = \left[\frac{CD\operatorname{csch}^2\left(\frac{p}{2}\sqrt{C}\xi\right)}{D^2 - CE\left(1 + \varepsilon \coth\left(\frac{p}{2}\sqrt{C}\xi\right)\right)^2} \right]^{\frac{1}{2}}. \tag{77}$$

Case 9. Considering $A = B = 0, C < 0$, we gained combined bright soliton and hyperbolic functions as solutions

$$F(\xi) = \left[\frac{-2C \sec^2(\frac{p}{2}\sqrt{-C\xi})}{2\sqrt{D^2 - 4CE} - (\sqrt{D^2 - 4CE} - D) \sec^2(\frac{p}{2}\sqrt{-C\xi})} \right]^{\frac{1}{p}}, \quad D^2 - 4CE > 0, \tag{78}$$

$$F(\xi) = \left[\frac{8C \cot^2(\frac{p}{2}\sqrt{\frac{C}{3}\xi})}{3D(3 - \cot^2(\frac{p}{2}\sqrt{\frac{C}{3}\xi}))} \right]^{\frac{1}{p}}, \quad C > 0. \tag{87}$$

Case 11. For $A = B = 0$,

$$F(\xi) = \left[\frac{2C \csc^2(\frac{p}{2}\sqrt{-C\xi})}{2\sqrt{D^2 - 4CE} - (\sqrt{D^2 - 4CE} + D) \csc^2(\frac{p}{2}\sqrt{-C\xi})} \right]^{\frac{1}{p}}, \quad D^2 - 4CE > 0, \tag{79}$$

$$F(\xi) = \left[\frac{2C \sec(p\sqrt{-C\xi})}{\epsilon\sqrt{D^2 - 4CE} - D \sec(p\sqrt{-C\xi})} \right]^{\frac{1}{p}}, \quad D^2 - 4CE > 0, \quad \epsilon = \pm 1, \tag{80}$$

$$F(\xi) = \left[\frac{2C \csc(p\sqrt{-C\xi})}{\epsilon\sqrt{D^2 - 4CE} - D \csc(p\sqrt{-C\xi})} \right]^{\frac{1}{p}}, \quad D^2 - 4CE > 0, \quad \epsilon = \pm 1, \tag{81}$$

$$F(\xi) = \left[-\frac{C \sec^2(\frac{p}{2}\sqrt{-C\xi})}{D + 2\epsilon\sqrt{-CE} \tan(\frac{p}{2}\sqrt{-C\xi})} \right]^{\frac{1}{p}}, \quad E > 0, \quad \epsilon = \pm 1, \tag{82}$$

$$F(\xi) = \left[\frac{4Cp^2 e^{(p\epsilon\sqrt{C}\xi)}}{(e^{\epsilon p\sqrt{C}\xi} - Dp^2)^2 - 4CEp^4} \right]^{\frac{1}{p}}, \quad C > 0, \quad \epsilon = \pm 1, \tag{88}$$

$$F(\xi) = \left[-\frac{C \csc^2(\frac{p}{2}\sqrt{-C\xi})}{D + 2\epsilon\sqrt{-CE} \cot(\frac{p}{2}\sqrt{-C\xi})} \right]^{\frac{1}{p}}, \quad D^2 - 4CE > 0, E > 0, \quad \epsilon = \pm 1. \tag{83}$$

Case 10. For $A = 0, B = \frac{8C^2}{27D}, E = \frac{D^2}{4C}$, it is gained hyperbolic function solutions of Eq. (5)

$$F(\xi) = \left[-\frac{8C \tanh^2(\frac{p}{2}\sqrt{\frac{-C}{3}\xi})}{3D(3 + \tanh^2(\frac{p}{2}\sqrt{\frac{-C}{3}\xi}))} \right]^{\frac{1}{p}}, \quad C < 0, \tag{84}$$

$$F(\xi) = \left[\frac{4Cp^2 e^{(p\epsilon\sqrt{C}\xi)}}{-1 + 4CEp^4 e^{2\epsilon p\sqrt{C}\xi}} \right]^{\frac{1}{p}}, \quad C > 0, D = 0, \quad \epsilon = \pm 1, \tag{89}$$

$$F(\xi) = \left[\frac{\epsilon}{p\sqrt{E}\xi} \right]^{\frac{1}{p}}, \quad E > 0, C = D = 0, \quad \epsilon = \pm 1. \tag{90}$$

$$F(\xi) = \left[-\frac{8C \coth^2(\frac{p}{2}\sqrt{\frac{-C}{3}\xi})}{3D(3 + \coth^2(\frac{p}{2}\sqrt{\frac{-C}{3}\xi}))} \right]^{\frac{1}{p}}, \quad C < 0, \tag{85}$$

Case 12. For $A = 0$ the Jacobian elliptic function solutions it is revealed

$$\text{For } E > 0, B = \frac{D^3(m^2-1)}{32m^2E^2}, C = \frac{D^2(5m^2-1)}{16m^2E},$$

it is gained trigonometric function solutions

$$F(\xi) = \left[\frac{8C \tan^2(\frac{p}{2}\sqrt{\frac{C}{3}\xi})}{3D(3 - \tan^2(\frac{p}{2}\sqrt{\frac{C}{3}\xi}))} \right]^{\frac{1}{p}}, \quad C > 0, \tag{86}$$

$$F(\xi) = \left[-\frac{D}{4E} \left(1 + \epsilon \operatorname{sn} \left(\frac{pD}{4m} \sqrt{\frac{1}{E}\xi} \right) \right) \right]^{\frac{1}{p}}, \quad \epsilon = \pm 1, \tag{91}$$

$$F(\xi) = \left[-\frac{D}{4E} \left(1 + \frac{1}{\operatorname{msn}\left(\left(\frac{pD}{4m} \sqrt{\frac{1}{E}} \xi\right)\right)} \right) \right]^{\frac{1}{p}}, \quad \varepsilon = \pm 1, \tag{92}$$

for $E > 0$, $B = \frac{D^3(1-m^2)}{32E^2}$, $C = \frac{D^2(5-m^2)}{16E}$, it is stated

$$F(\xi) = \left[-\frac{D}{4E} \left(1 + \varepsilon \operatorname{msn}\left(\frac{pD}{4} \sqrt{\frac{1}{E}} \xi\right) \right) \right]^{\frac{1}{p}}, \quad \varepsilon = \pm 1, \tag{93}$$

$$F(\xi) = \left[-\frac{D}{4E} \left(1 + \frac{\varepsilon}{\operatorname{sn}\left(\left(\frac{pD}{4} \sqrt{\frac{1}{E}} \xi\right)\right)} \right) \right]^{\frac{1}{p}}, \quad \varepsilon = \pm 1, \tag{94}$$

for $E < 0$, $B = \frac{D^3}{32m^2E^2}$, $C = \frac{D^2(4m^2+1)}{16m^2E}$, it is revealed

$$F(\xi) = \left[-\frac{D}{4E} \left(1 + \varepsilon \operatorname{cn}\left(\frac{pD}{4m} \sqrt{-\frac{1}{E}} \xi\right) \right) \right]^{\frac{1}{p}}, \quad \varepsilon = \pm 1, \tag{95}$$

$$F(\xi) = \left[-\frac{D}{4E} \left(1 + \frac{\varepsilon \sqrt{1-m^2} \operatorname{sn}\left(\frac{pD}{4m} \sqrt{-\frac{1}{E}} \xi\right)}{\operatorname{dn}\left(\frac{pD}{4m} \sqrt{-\frac{1}{E}} \xi\right)} \right) \right]^{\frac{1}{p}}, \quad \varepsilon = \pm 1. \tag{96}$$

for $E < 0$, $B = \frac{m^2D^3}{32(m^2-1)E^2}$, $C = \frac{D^2(5m^2-4)}{16(m^2-1)E}$, it is revealed

$$F(\xi) = \left[-\frac{D}{4E} \left(1 + \frac{\varepsilon}{\sqrt{1-m^2}} \operatorname{dn}\left(\frac{pD}{4} \sqrt{-\frac{1}{(1-m^2)E}} \xi\right) \right) \right]^{\frac{1}{p}}, \quad \varepsilon = \pm 1, \tag{97}$$

$$F(\xi) = \left[-\frac{D}{4E} \left(1 + \frac{\varepsilon}{\operatorname{dn}\left(\left(\frac{pD}{4} \sqrt{-\frac{1}{(1-m^2)E}} \xi\right)\right)} \right) \right]^{\frac{1}{p}}, \quad \varepsilon = \pm 1. \tag{98}$$

for $E < 0$, $B = \frac{m^2D^3}{32E^2}$, $C = \frac{D^2(m^2+4)}{16E}$, hence

$$F(\xi) = \left[-\frac{D}{4E} \left(1 + \varepsilon \operatorname{dn}\left(\frac{pD}{4} \sqrt{-\frac{1}{E}} \xi\right) \right) \right]^{\frac{1}{p}}, \quad \varepsilon = \pm 1, \tag{99}$$

$$F(\xi) = \left[-\frac{D}{4E} \left(1 + \frac{\varepsilon \sqrt{1-m^2}}{\operatorname{dn}\left(\left(\frac{pD}{4} \sqrt{-\frac{1}{E}} \xi\right)\right)} \right) \right]^{\frac{1}{p}}, \quad \varepsilon = \pm 1, \tag{100}$$

for $E > 0$, $B = \frac{D^3}{32(1-m^2)E^2}$, $C = \frac{D^2(4m^2-5)}{16(m^2-1)E}$, it is revealed

$$F(\xi) = \left[-\frac{D}{4E} \left(1 + \frac{\varepsilon}{\operatorname{cn}\left(\left(\frac{pD}{4} \sqrt{\frac{1}{(1-m^2)E}} \xi\right)\right)} \right) \right]^{\frac{1}{p}}, \quad \varepsilon = \pm 1. \tag{101}$$

$$F(\xi) = \left[-\frac{D}{4E} \left(1 + \frac{\varepsilon \operatorname{dn}\left(\frac{pD}{4} \sqrt{\frac{1}{(1-m^2)E}} \xi\right)}{\sqrt{1-m^2} \operatorname{sn}\left(\frac{pD}{4} \sqrt{\frac{1}{(1-m^2)E}} \xi\right)} \right) \right]^{\frac{1}{p}}, \quad \varepsilon = \pm 1. \tag{102}$$

Case 13. For $A = E = 0$, it is recovered Jacobian elliptic function.

For $D < 0$, $C > 0$, $B = \frac{m^2C^2(m^2-1)}{D(2m^2-1)^2}$, we get

$$F(\xi) = \left[-\frac{m^2C}{D(2m^2-1)} \operatorname{cn}^2\left(\frac{p}{2} \sqrt{\frac{C}{2m^2-1}} \xi\right) \right]^{\frac{1}{p}}, \tag{103}$$

for $D > 0$, $C < 0$, $B = \frac{m^2C^2}{D(m^2+1)^2}$, then

$$F(\xi) = \left[-\frac{m^2C}{D(m^2+1)} \operatorname{sn}^2\left(\frac{p}{2} \sqrt{-\frac{C}{m^2+1}} \xi\right) \right]^{\frac{1}{p}}, \tag{104}$$

$$F(\xi) = \left[-\frac{m^2C}{D(m^2+1)} \operatorname{cd}^2\left(\frac{p}{2} \sqrt{-\frac{C}{m^2+1}} \xi\right) \right]^{\frac{1}{p}}, \tag{105}$$

for $D < 0$, $C > 0$, $B = \frac{(1-m^2)C^2}{D(2-m^2)^2}$, consequently the last one

$$F(\xi) = \left[-\frac{C}{D(2-m^2)} \operatorname{dn}^2\left(\frac{p}{2} \sqrt{\frac{C}{2-m^2}} \xi\right) \right]^{\frac{1}{p}}. \tag{106}$$

4 Application of the methods

This section apply the methods described above to construct exact traveling-wave solutions of the conformable derivative nonlinear differential equation governing wave propagation

in electrical transmission line [4]. To obtain the NODE, we used the conformable derivative properties. Assuming $u(x, t) = U(\xi)$ and (1) becomes

$$[(1 + b_1 U + b_2 U^2)k_2^2 - u_0^2 k_1^2] U''' + (b_1 + 2b_2 U)k_2^2 U'^2 - \frac{1}{12} u_0^2 \delta^2 k_1^4 U^{(4)} = 0. \tag{107}$$

where $U = U(\xi)$.

4.1 On solving the nonlinear differential governing low-pass electrical transmission lines by using the New Extended Direct Algebraic Method

Employing the homogeneous balance principle to (107), gives $N = 1$. Thus, (6) can be expressed

$$U(\xi) = g_0 + g_1 Q(\xi), \tag{108}$$

Substituting (108) and (7) into (107), we obtained a set of algebraic equation in terms of $Q^j(\xi)$. After setting all the terms obtained to zero, and then with the aid of Maple, we recovered the following results.

SI: for $\mu^2 - 4\lambda\sigma < 0$ and $\sigma \neq 0$, it is obtained

$$g_0 = g_0, \quad g_1 = g_1,$$

$$b_1 = -\frac{1}{12} \frac{g_1^2 (\mu^2 - 4\lambda\sigma)^2 (g_1 \mu - 2g_0 \sigma) \delta^2 (\ln(A))^2}{u_0^2 (8g_1^2 \lambda \sigma - 12g_1 g_0 \mu \sigma + g_1^2 \mu^2 + 12g_0^2 \sigma^2) (-g_1^2 \lambda + g_1 g_0 \mu - g_0^2 \sigma)},$$

$$b_2 = -\frac{1}{12} \frac{g_1^2 (\mu^2 - 4\lambda\sigma)^2 \delta^2 (\ln(A))^2 \sigma}{u_0^2 (8g_1^2 \lambda \sigma - 12g_1 g_0 \mu \sigma + g_1^2 \mu^2 + 12g_0^2 \sigma^2) (-g_1^2 \lambda + g_1 g_0 \mu - g_0^2 \sigma)},$$

$$k_1 = \frac{\sqrt{-\frac{\mu^2 - 4\lambda\sigma}{8g_1^2 \lambda \sigma - 12g_1 g_0 \mu \sigma + g_1^2 \mu^2 + 12g_0^2 \sigma^2}} g_1}{u_0},$$

$$k_2 = -\sqrt{-\frac{\mu^2 - 4\lambda\sigma}{8g_1^2 \lambda \sigma - 12g_1 g_0 \mu \sigma + g_1^2 \mu^2 + 12g_0^2 \sigma^2}} g_1$$

$$u_{12}(x, t) = g_0 + g_1 \left[-\frac{\mu}{2\sigma} + \frac{\sqrt{-(\mu^2 - 4\lambda\sigma)}}{2\sigma} \cot_A \left(\frac{\sqrt{-(\mu^2 - 4\lambda\sigma)}}{2} \xi \right) \right], \tag{110}$$

$$u_{13}(x, t) = g_0 + g_1 \left[-\frac{\mu}{2\sigma} + \frac{\sqrt{-(\mu^2 - 4\lambda\sigma)}}{2\sigma} \tan_A \left(\sqrt{-(\mu^2 - 4\lambda\sigma)} \xi \right) \pm \frac{\sqrt{-pq(\mu^2 - 4\lambda\sigma)}}{2\sigma} \sec_A \left(\sqrt{-(\mu^2 - 4\lambda\sigma)} \xi \right) \right], \tag{111}$$

$$u_{14}(x, t) = g_0 + g_1 \left[-\frac{\mu}{2\sigma} - \frac{\sqrt{-(\mu^2 - 4\lambda\sigma)}}{2\sigma} \cot_A \left(\sqrt{-(\mu^2 - 4\lambda\sigma)} \xi \right) \pm \frac{\sqrt{-pq(\mu^2 - 4\lambda\sigma)}}{2\sigma} \csc_A \left(\sqrt{-(\mu^2 - 4\lambda\sigma)} \xi \right) \right], \tag{112}$$

$$u_{11}(x, t) = g_0 + g_1 \left[\frac{-\mu}{2\sigma} + \frac{\sqrt{-(\mu^2 - 4\lambda\sigma)}}{2\sigma} \tan_A \left(\frac{\sqrt{-(\mu^2 - 4\lambda\sigma)}}{2} \xi \right) \right], \tag{109}$$

$$u_{15}(x, t) = g_0 + g_1 \left[-\frac{\mu}{2\sigma} - \frac{\sqrt{-(\mu^2 - 4\lambda\sigma)}}{2\sigma} \tan_A \left(\frac{\sqrt{-(\mu^2 - 4\lambda\sigma)}}{4} \xi \right) - \frac{\sqrt{-(\mu^2 - 4\lambda\sigma)}}{2\sigma} \cot_A \left(\frac{\sqrt{-(\mu^2 - 4\lambda\sigma)}}{4} \xi \right) \right], \tag{113}$$

$$u_{25}(x, t) = g_0 + g_1 \left[-\frac{\mu}{2\sigma} - \frac{\sqrt{-(\mu^2 - 4\lambda\sigma)}}{4\sigma} \tanh_A \left(\frac{\sqrt{(\mu^2 - 4\lambda\sigma)}}{4} \xi \right) - \frac{\sqrt{(\mu^2 - 4\lambda\sigma)}}{4\sigma} \coth_A \left(\frac{\sqrt{(\mu^2 - 4\lambda\sigma)}}{4} \xi \right) \right], \tag{118}$$

S2: for $\mu^2 - 4\lambda\sigma > 0$ and $\sigma \neq 0$, it is obtained

$$g_0 = g_0, \quad g_1 = g_1,$$

$$b_1 = -\frac{1}{12} \frac{g_1^2 (\mu^2 - 4\lambda\sigma)^2 (g_1\mu - 2g_0\sigma) \delta^2 (\text{Ln}(A))^2}{u_0^2 (8g_1^2\lambda\sigma - 12g_1g_0\mu\sigma + g_1^2\mu^2 + 12g_0^2\sigma^2) (-g_1^2\lambda + g_1g_0\mu - g_0^2\sigma)},$$

$$b_2 = -\frac{1}{12} \frac{g_1^2 (\mu^2 - 4\lambda\sigma)^2 \delta^2 (\text{Ln}(A))^2 \sigma}{u_0^2 (8g_1^2\lambda\sigma - 12g_1g_0\mu\sigma + g_1^2\mu^2 + 12g_0^2\sigma^2) (-g_1^2\lambda + g_1g_0\mu - g_0^2\sigma)},$$

$$k_1 = \frac{\sqrt{-\frac{\mu^2 - 4\lambda\sigma}{8g_1^2\lambda\sigma - 12g_1g_0\mu\sigma + g_1^2\mu^2 + 12g_0^2\sigma^2}} g_1}{u_0},$$

$$k_2 = -\sqrt{-\frac{\mu^2 - 4\lambda\sigma}{8g_1^2\lambda\sigma - 12g_1g_0\mu\sigma + g_1^2\mu^2 + 12g_0^2\sigma^2}} g_1$$

$$u_{21}(x, t) = g_0 + g_1 \left[-\frac{\mu}{2\sigma} + \frac{\sqrt{(\mu^2 - 4\lambda\sigma)}}{2\sigma} \tanh_A \left(\frac{\sqrt{(\mu^2 - 4\lambda\sigma)}}{2} \xi \right) \right], \tag{114}$$

S3: for $\lambda\sigma > 0$ and $\mu = 0$, it is obtained

$$g_0 = g_0, \quad g_1 = g_1,$$

$$b_1 = 6 \frac{\sigma (u_0 k_1 - k_2) (u_0 k_1 + k_2) g_0}{3k_2^2 \sigma g_0^2 - g_1^2 \lambda + 2k_2^2 g_1^2 \lambda},$$

$$b_2 = -3 \frac{(u_0 k_1 + k_2) (u_0 k_1 - k_2) \sigma}{3k_2^2 \sigma g_0^2 - g_1^2 \lambda + 2k_2^2 g_1^2 \lambda},$$

$$k_1 = k_1, \quad k_2 = k_2,$$

$$\delta = \frac{\sqrt{-\frac{(3+3k_2^2)(u_0 k_1 - k_2)(u_0 k_1 + k_2)}{\sigma(3k_2^2 \sigma g_0^2 - g_1^2 \lambda + 2k_2^2 g_1^2 \lambda)}} g_1}{\text{Ln}(A) u_0 k_1^2}.$$

$$u_{22}(\xi) = g_0 + g_1 \left[-\frac{\mu}{2\sigma} + \frac{\sqrt{(\mu^2 - 4\lambda\sigma)}}{2\sigma} \coth_A \left(\frac{\sqrt{(\mu^2 - 4\lambda\sigma)}}{2} \xi \right) \right], \tag{115}$$

$$u_{23}(x, t) = g_0 + g_1 \left[-\frac{\mu}{2\sigma} + \frac{\sqrt{(\mu^2 - 4\lambda\sigma)}}{2\sigma} \tanh_A \left(\sqrt{(\mu^2 - 4\lambda\sigma)} \xi \right) \pm i \frac{\sqrt{pq(\mu^2 - 4\lambda\sigma)}}{2\sigma} \text{sech}_A \left(\sqrt{(\mu^2 - 4\lambda\sigma)} \xi \right) \right], \tag{116}$$

$$u_{31}(x, t) = g_0 + g_1 \sqrt{\frac{\lambda}{\sigma}} \tan_A \left(\sqrt{\lambda\sigma} \xi \right), \tag{119}$$

$$u_{24}(x, t) = g_0 + g_1 \left[-\frac{\mu}{2\sigma} - \frac{\sqrt{(\mu^2 - 4\lambda\sigma)}}{2\sigma} \coth_A \left(\sqrt{(\mu^2 - 4\lambda\sigma)} \xi \right) \pm \frac{\sqrt{pq(\mu^2 - 4\lambda\sigma)}}{2\sigma} \text{csch}_A \left(\sqrt{(\mu^2 - 4\lambda\sigma)} \xi \right) \right], \tag{117}$$

$$u_{32}(x, t) = g_0 - g_1 \sqrt{\frac{\lambda}{\sigma}} \cot_A \left(\sqrt{\lambda\sigma\xi} \right), \tag{120}$$

$$u_{33}(x, t) = g_0 + g_1 \left[\sqrt{\frac{\lambda}{\sigma}} \tan_A \left(\sqrt{2\lambda\sigma\xi} \right) \pm \sqrt{pq\frac{\lambda}{\sigma}} \sec_A \left(\sqrt{2\lambda\sigma\xi} \right) \right], \tag{121}$$

$$u_{34}(x, t) = g_0 + g_1 \left[-\sqrt{\frac{\lambda}{\sigma}} \cot_A \left(\sqrt{2\lambda\sigma\xi} \right) \pm \sqrt{pq\frac{\lambda}{\sigma}} \csc_A \left(\sqrt{2\lambda\sigma\xi} \right) \right], \tag{122}$$

$$u_{35}(x, t) = g_0 + g_1 \left[\frac{1}{2} \sqrt{\frac{\lambda}{\sigma}} \left(\tan_A \left(\frac{\sqrt{\lambda\sigma}}{2} \xi \right) - \sqrt{\frac{\lambda}{\sigma}} \cot_A \left(\frac{\sqrt{\lambda\sigma}}{2} \xi \right) \right) \right], \tag{123}$$

S4: for $\lambda\sigma < 0$ and $\mu = 0$, yields to

$$g_0 = \frac{1}{3} \sqrt{\frac{-3\lambda(-1+2u_0^2k_1^2)}{\sigma}} g_1, \quad g_1 = g_1,$$

$$b_1 = -\frac{2}{3} \frac{u_0\delta^2k_1^3(Ln(A))^2\sigma^2\sqrt{-3\frac{\lambda(-1+2u_0^2k_1^2)}{\sigma}}}{g_1(1+u_0^2k_1^2)},$$

$$b_2 = \frac{u_0^2\delta^2k_1^4(Ln(A))^2\sigma^2}{g_1^2(1+u_0^2k_1^2)},$$

$$k_1 = k_1, \quad k_2 = \pm u_0k_1$$

$$u_{41}(x, t) = \frac{1}{3} \sqrt{\frac{-3\lambda(-1+2u_0^2k_1^2)}{\sigma}} g_1 - g_1 \sqrt{\frac{-\lambda}{\sigma}} \tanh_A \left(\sqrt{-\lambda\sigma\xi} \right), \tag{124}$$

$$u_{42}(x, t) = \frac{1}{3} \sqrt{\frac{-3\lambda(-1+2u_0^2k_1^2)}{\sigma}} g_1 - g_1 \sqrt{\frac{-\lambda}{\sigma}} \coth_A \left(\sqrt{-\lambda\sigma\xi} \right), \tag{125}$$

$$u_{43}(x, t) = \frac{1}{3} \sqrt{\frac{-3\lambda(-1+2u_0^2k_1^2)}{\sigma}} g_1 - g_1 \left[\sqrt{\frac{-\lambda}{\sigma}} \tanh_A \left(\sqrt{2\lambda\sigma\xi} \right) \pm i\sqrt{pq\frac{-pq\lambda}{\sigma}} \operatorname{sech}_A \left(2\sqrt{-\lambda\sigma\xi} \right) \right], \tag{126}$$

$$u_{44}(x, t) = \frac{1}{3} \sqrt{\frac{-3\lambda(-1+2u_0^2k_1^2)}{\sigma}} g_1 - g_1 \left[\sqrt{\frac{-\lambda}{\sigma}} \coth_A \left(2\sqrt{-\lambda\sigma\xi} \right) \pm \sqrt{-pq\frac{\lambda}{\sigma}} \operatorname{csch}_A \left(2\sqrt{-\lambda\sigma\xi} \right) \right], \tag{127}$$

$$u_{45}(x, t) = \frac{1}{3} \sqrt{\frac{-3\lambda(-1+2u_0^2k_1^2)}{\sigma}} g_1 - g_1 \left[\frac{1}{2} \left(\sqrt{\frac{-\lambda}{\sigma}} \tanh_A \left(\frac{\sqrt{-\lambda\sigma}}{2} \xi \right) + \sqrt{\frac{-\lambda}{\sigma}} \coth_A \left(\frac{\sqrt{-\lambda\sigma}}{2} \xi \right) \right) \right]. \tag{128}$$

S5: for $\lambda = \sigma$ and $\mu = 0$, it is obtained

$$g_0 = g_0, \quad g_1 = g_1,$$

$$b_1 = \frac{6(u_0k_1 - k_2)(u_0k_1 + k_2)g_0}{-g_1^2 + 3k_2^2g_0^2 + 2k_2^2g_1^2},$$

$$b_2 = -\frac{3(u_0k_1 - k_2)(u_0k_1 + k_2)}{-g_1^2 + 3k_2^2g_0^2 + 2k_2^2g_1^2}, \quad k_1 = k_1, \quad k_2 = k_2$$

$$\delta = \frac{\sqrt{\frac{(3+3k_2^2)(u_0k_1-k_2)(u_0k_1+k_2)}{-g_1^2+3k_2^2g_0^2+2k_2^2g_1^2}} g_1}{Ln(A)\sigma u_0k_1^2},$$

$$u_{51}(x, t) = g_0 + g_1 \tan_A(\lambda\xi), \tag{129}$$

$$u_{52}(x, t) = g_0 - g_1 \cot_A(\lambda\xi), \tag{130}$$

$$u_{53}(x, t) = g_0 + g_1 \left[\tan_A(2\lambda\xi) \pm \sqrt{pq} \sec_A(2\lambda\xi) \right], \tag{131}$$

$$u_{54}(x, t) = g_0 - g_1 \left[\cot_A(2\lambda\xi) \pm \sqrt{pq} \csc_A(2\lambda\xi) \right], \tag{132}$$

$$u_{55}(x, t) = g_0 + g_1 \left[\frac{1}{2} \left(\tan_A\left(\frac{\lambda}{2}\xi\right) - \cot_A\left(\frac{\lambda}{2}\xi\right) \right) \right], \tag{133}$$

S6: for $\lambda = -\sigma$ and $\mu = 0$, it is obtained the set of result

$$g_0 = \frac{1}{3} \frac{\sqrt{3 - 6u_0^2 k_1^2} g_1}{u_0 k_1}, \quad g_1 = g_1,$$

$$b_1 = -\frac{2}{3} \frac{u_0 \delta^2 k_1^3 (Ln(A))^2 \sigma^2 \sqrt{3 - 6u_0^2 k_1^2}}{g_1 (1 + u_0^2 k_1^2)},$$

$$b_2 = \frac{u_0^2 \delta^2 k_1^4 (Ln(A))^2 \sigma^2}{g_1^2 (1 + u_0^2 k_1^2)}, \quad k_1 = k_1, \quad k_2 = \pm u_0 k_1,$$

$$\delta = \frac{\sqrt{\frac{(3+3k_2^2)(u_0 k_1 - k_2)(u_0 k_1 + k_2)}{-g_1^2 + 3k_2^2 g_0^2 + 2k_2^2 g_1^2}} g_1}{Ln(A) \sigma u_0 k_1^2}$$

$$u_{61}(x, t) = \frac{1}{3} \frac{\sqrt{3 - 6u_0^2 k_1^2} g_1}{u_0 k_1} - g_1 \tanh_A(\lambda \xi), \tag{134}$$

$$u_{62}(x, t) = \frac{1}{3} \frac{\sqrt{3 - 6u_0^2 k_1^2} g_1}{u_0 k_1} - g_1 \coth_A(\lambda \xi), \tag{135}$$

$$u_{63}(x, t) = \frac{1}{3} \frac{\sqrt{3 - 6u_0^2 k_1^2} g_1}{u_0 k_1} - g_1 [\tanh_A(2\lambda \xi) \pm i \sqrt{pq} \operatorname{sech}_A(2\lambda \xi)], \tag{136}$$

$$u_{64}(x, t) = \frac{1}{3} \frac{\sqrt{3 - 6u_0^2 k_1^2} g_1}{u_0 k_1} - g_1 [\coth_A(2\lambda \xi) \pm \sqrt{pq} \operatorname{csch}_A(2\lambda \xi)], \tag{137}$$

$$u_{65}(x, t) = \frac{1}{3} \frac{\sqrt{3 - 6u_0^2 k_1^2} g_1}{u_0 k_1} - g_1 \left[\frac{1}{2} \left(\tanh_A\left(\frac{\lambda}{2} \xi\right) + \coth_A\left(\frac{\lambda}{2} \xi\right) \right) \right]. \tag{138}$$

S7: for $\mu^2 = 4\lambda\sigma$, it is obtained the following result

$$g_0 = g_0, \quad g_1 = g_1,$$

$$b_1 = -\frac{2(u_0 k_1 - k_2)(u_0 k_1 + k_2) \left(-3g_0 \sigma g_1^2 \lambda + 3g_0^2 \sigma g_1 \sqrt{\lambda \sigma} - g_0^3 \sigma^2 + \sqrt{\lambda \sigma} g_1^3 \lambda \right)}{k_2^2 \left(-g_1^2 \lambda + 2g_1 g_0 \sqrt{\lambda \sigma} - g_0^2 \sigma \right)^2},$$

$$b_2 = \frac{(u_0 k_1 - k_2)(u_0 k_1 + k_2) \sigma}{k_2^2 \left(-g_1^2 \lambda + 2g_1 g_0 \sqrt{\lambda \sigma} - g_0^2 \sigma \right)},$$

$$k_1 = k_1, \quad k_2 = k_2, \quad \delta = \frac{\sqrt{\frac{(k_2^2 + 1)(u_0 k_1 - k_2)(u_0 k_1 + k_2)}{\sigma \left(-g_1^2 \lambda + 2g_1 g_0 \sqrt{\lambda \sigma} - g_0^2 \sigma \right)}} g_1}{Ln(A) u_0 k_1^2 k_2},$$

$$u_{71}(x, t) = g_0 - g_1 \frac{2\lambda(\mu \xi Ln(A) + 2)}{\mu^2 \xi Ln(A)}, \tag{139}$$

S10: for $\mu = \lambda = 0$, it is obtained the following results

$$g_0 = g_0, \quad g_1 = g_1,$$

$$b_1 = 2 \frac{(u_0 k_1 - k_2)(u_0 k_1 + k_2)}{k_2^2 g_0}, \quad b_2 = -b_1, \quad k_1 = k_1, \quad k_2 = k_2,$$

$$\delta = \frac{\sqrt{-(1 + k_2^2)(u_0 k_1 - k_2)(u_0 k_1 + k_2)} g_1}{Ln(A) \sigma u_0 k_2 k_1^2 g_0}$$

$$u_{101}(x, t) = g_0 + g_1 \frac{-1}{\sigma \xi Ln(A)}, \tag{140}$$

S11: for $\mu \neq 0$, and $\lambda = 0$, it is obtained the following results

RI: $g_0 = g_0, \quad g_1 = g_1, \quad b_1 = \frac{6\sigma(u_0 k_1 - k_2)(u_0 k_1 + k_2) g_0}{3k_2^2 \sigma g_0^2 - g_1^2 \lambda + 2k_2^2 g_1^2 \lambda},$

$$b_2 = -\frac{3\sigma(u_0 k_1 - k_2)(u_0 k_1 + k_2)}{3k_2^2 \sigma g_0^2 - g_1^2 \lambda + 2k_2^2 g_1^2 \lambda}, \quad k_1 = k_1, \quad k_2 = k_2,$$

$$\delta = \frac{\sqrt{\frac{-3(1+k_2^2)(u_0 k_1 - k_2)(u_0 k_1 + k_2)}{\sigma(3k_2^2 \sigma g_0^2 - g_1^2 \lambda + 2k_2^2 g_1^2 \lambda)}} g_1}{Ln(A) u_0 k_1^2},$$

$$u_{111}(x, t) = g_0 + g_1 \left[\frac{p\mu}{\sigma(\cosh_A(\mu \xi) - \sinh_A(\mu \xi) - p)} \right]. \tag{141}$$

R 2: $g_0 = \frac{1}{3} \frac{\sqrt{\frac{-3\lambda(-1+2u_0^2 k_1^2)}{\sigma}} g_1}{u_0 k_1}, \quad g_1 = g_1,$

$$b_1 = -\frac{2}{3} \frac{u_0 \delta^2 k_1^3 (Ln(A))^2 \sigma^2 \sqrt{-3 \frac{\lambda(-1+2u_0^2 k_1^2)}{\sigma}}}{g_1 (1 + u_0^2 k_1^2)}, \quad b_2 = \frac{u_0^2 \delta^2 k_1^4 (Ln(A))^2 \sigma^2}{g_1^2 (1 + u_0^2 k_1^2)},$$

$$k_1 = k_1, \quad k_2 = \pm u_0 k_1.$$

$$u_{112}(x, t) = \frac{1}{3} \frac{\sqrt{\frac{-3\lambda(-1+2u_0^2 k_1^2)}{\sigma}} g_1}{u_0 k_1} + g_1 \left[\frac{p\mu}{\sigma(\cosh_A(\mu \xi) - \sinh_A(\mu \xi) - p)} \right], \tag{142}$$

S12: for $\mu = k, \sigma = mk(m \neq 0)$, and $\lambda = 0$, it is obtained the following result

$$g_0 = g_0, \quad g_1 = g_1,$$

$$b_1 = \frac{12(u_0 k_1 - k_2)(u_0 k_1 + k_2)(-g_1 + 2g_0 m)m}{12k_2^2 g_0^2 m^2 + k_2^2 g_1^2 + g_1^2 - 12k_2^2 g_1 g_0 m},$$

$$b_2 = -\frac{12m^2(u_0k_1-k_2)(u_0k_1+k_2)}{12k_2^2g_0^2m^2+k_2^2g_1^2+g_1^2-12k_2^2g_1g_0m}, \quad k_1 = k_1, \quad k_2 = k_2,$$

$$\delta = \frac{2\sqrt{\frac{(3k_2^2+1)(u_0k_1-k_2)(u_0k_1+k_2)}{12k_2^2g_0^2m^2+k_2^2g_1^2+g_1^2-12k_2^2g_1g_0m}g_1}}{\ln(A)u_0k_1^2k}$$

$$u_{121}(x, t) = g_0 - g_1 \frac{pA^{k\xi}}{q - mpA^{k\xi}}, \tag{143}$$

where $u(x, t) = U(\xi)$, $\xi = \frac{k_1}{\alpha}t^\alpha + \frac{k_2}{\alpha}x^\alpha$, and $p, q > 0$. Therefore, in this paper ξ_0 is considered as zero value. The details of the generalized hyperbolic and triangular functions are given in [42]. It is observed that, for cases (8)–(10) none solutions have been obtained.

4.2 On solving the nonlinear differential governing low-pass electrical transmission lines by using the New Sub-ODE equation

The initial step is to use the balance principle which between the higher order derivative and the higher order nonlinear term. So, it is obtained $3s + 2p = 4s \Rightarrow s = 2p$. Consequently, Eq. (107) read

$$U(\xi) = \mu F^{2p}(\xi), \tag{144}$$

Inserting Eqs.(46) and (144) into Eq. (107) gives the set of system of equation in terms of $F^{jp}(\xi)$. Setting the obtained system of algebraic equation to zero and making used MAPLE it is revealed the following set of results:

Result 1:

$$A = 0, B = 0, C = \frac{63}{4} \frac{b_1^2}{(-192b_2+7b_1^2)p^2\delta^2}, D = 0, E = E,$$

$$\mu = \frac{1}{18} \frac{(-192b_2+7b_1^2)p^2\delta^2E}{b_1b_2}, k_1 = \frac{2}{3}i\sqrt{3}, k_2 = 8\sqrt{\frac{3b_2}{-192b_2+7b_1^2}}u_0.$$

Hence, it is recovered three types of solutions to Eq. (1).

Case 1. If $A = 0, B = 0, D = 0$, bright type is obtained

$$u_{2,1,1}(x, t) = \mu \left[\varepsilon \sqrt{-\frac{C}{E}} \operatorname{sech}(p\sqrt{C}\xi) \right]^{\frac{1}{2}}, \quad C > 0, \quad E < 0, \quad \varepsilon \pm 1, \tag{145}$$

a periodic solution

$$u_{2,1,2}(x, t) = \mu \left[\varepsilon \sqrt{-\frac{C}{E}} \sec(p\sqrt{-C}\xi) \right]^{\frac{1}{2}}, \tag{146}$$

$$C < 0, \quad E > 0, \quad \varepsilon \pm 1,$$

and a rational solution

$$u_{2,1,3} = \mu \left[\frac{\varepsilon}{p\sqrt{E}\xi} \right]^{\frac{1}{2p}}, \quad C = 0, \tag{147}$$

$$E > 0, \quad \varepsilon \pm 1.$$

Result 2:

$$A = \frac{3969}{64} \frac{b_1^4}{(54b_2+7b_1^2)^2E\delta^4p^4}, B = 0, C = \frac{63}{4} \frac{b_1^2}{(54b_2+7b_1^2)p^2\delta^2}, D = 0, E = E,$$

$$\mu = \frac{4}{27} \frac{(54b_2+7b_1^2)p^2\delta^2E}{b_1b_2}, k_1 = \frac{2}{3}i\sqrt{3}, k_2 = 8\sqrt{\frac{3b_2}{-192b_2+7b_1^2}}u_0.$$

The corresponding solutions give:

Case 2. By setting the conditions $B = 0, D = 0, A = \frac{C^2}{4E}$, it is gained dark soliton-like solution of Eq. (1):

$$u_{2,2,1} = \mu \left[\varepsilon \sqrt{-\frac{C}{2E}} \tanh\left(p\sqrt{\frac{-C}{2}}\xi\right) \right]^{\frac{1}{2}}, \tag{148}$$

$$C < 0, \quad E > 0, \quad \varepsilon \pm 1,$$

and a periodic solution

$$u_{2,2,2} = \left[\varepsilon \sqrt{\frac{C}{2E}} \tan\left(p\sqrt{\frac{C}{2}}\xi\right) \right]^{\frac{1}{2}}, \tag{149}$$

$$C > 0, \quad E > 0, \quad \varepsilon \pm 1.$$

Case 3. By setting the conditions $B = 0, D = 0$, we deduce three forms of Jacobian elliptic functions solutions of Eq. (1):

$$u_{2,3,1} = \mu \left[\varepsilon \sqrt{\frac{-Cm^2}{E(2m^2-1)}} \operatorname{cn}\left(p\sqrt{\frac{C}{2m^2-1}}\xi\right) \right]^{\frac{1}{2}}, \tag{150}$$

$$C > 0, \quad A = \frac{C^2m^2(m^2-1)}{E(2m^2-1)^2}, \quad \varepsilon \pm 1,$$

$$u_{2,3,2} = \mu \left[\varepsilon \sqrt{\frac{-C}{E(2-m^2)}} \operatorname{dn}\left(p\sqrt{\frac{C}{2-m^2}}\xi\right) \right]^{\frac{1}{2}}, \tag{151}$$

$$C > 0, \quad A = \frac{C^2(1-m^2)}{E(2-m^2)^2}, \quad \varepsilon \pm 1,$$

and

$$u_{2,3,3} = \mu \left[\varepsilon \sqrt{\frac{-Cm^2}{E(1+m^2)}} \operatorname{sn}\left(p\sqrt{\frac{-C}{1+m^2}}\xi\right) \right]^{\frac{1}{2}}, \tag{152}$$

$$C < 0, \quad A = \frac{C^2m^2}{E(1+m^2)^2}, \quad \varepsilon \pm 1.$$

Case 4: Assuming $B = D = 0$ and $E \neq 0$, it is revealed Weierstrass elliptic function solutions to set of Eq. (5),

$$u_{2,4,1} = \mu \left[\frac{\wp(p\xi, g_2, g_3)}{E} - \frac{C}{3E} \right]^{\frac{1}{4}}, \tag{153}$$

where $g_2 = \frac{4C^2-12AE}{3}, g_3 = \frac{4C(-2C^2+9AE)}{27}$.

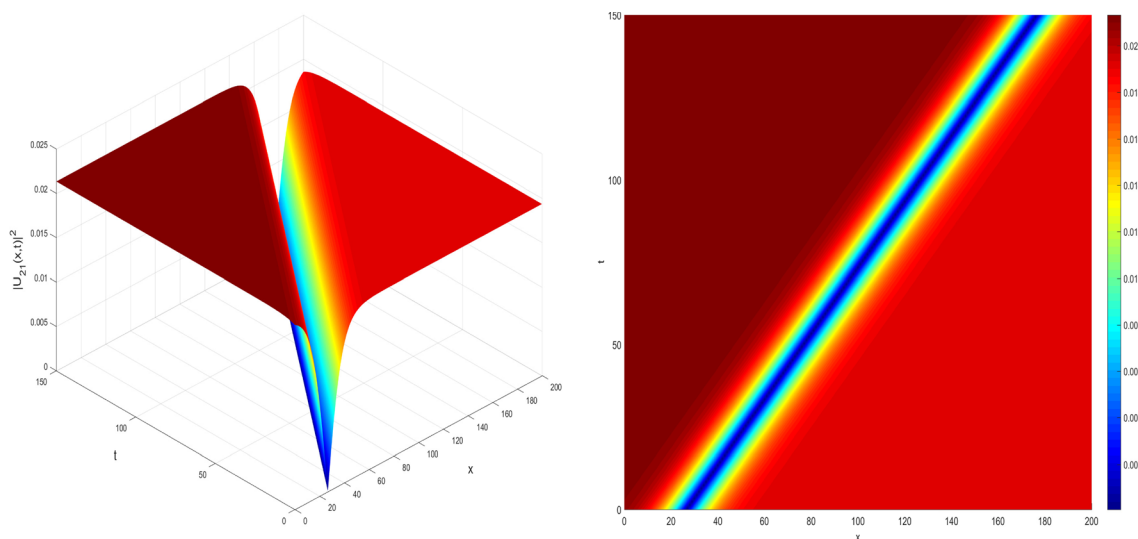


Fig. 1 Spatiotemporal plot evolution and contour plot of dark solitons $|u_{21}(x,t)|^2$ at $\alpha = 1, A_1 = e, k_1 = -k_2 = 3.840, g_0 = 0.001, g_1 = 0.018, \lambda = -0.312, \sigma = -0.0185$

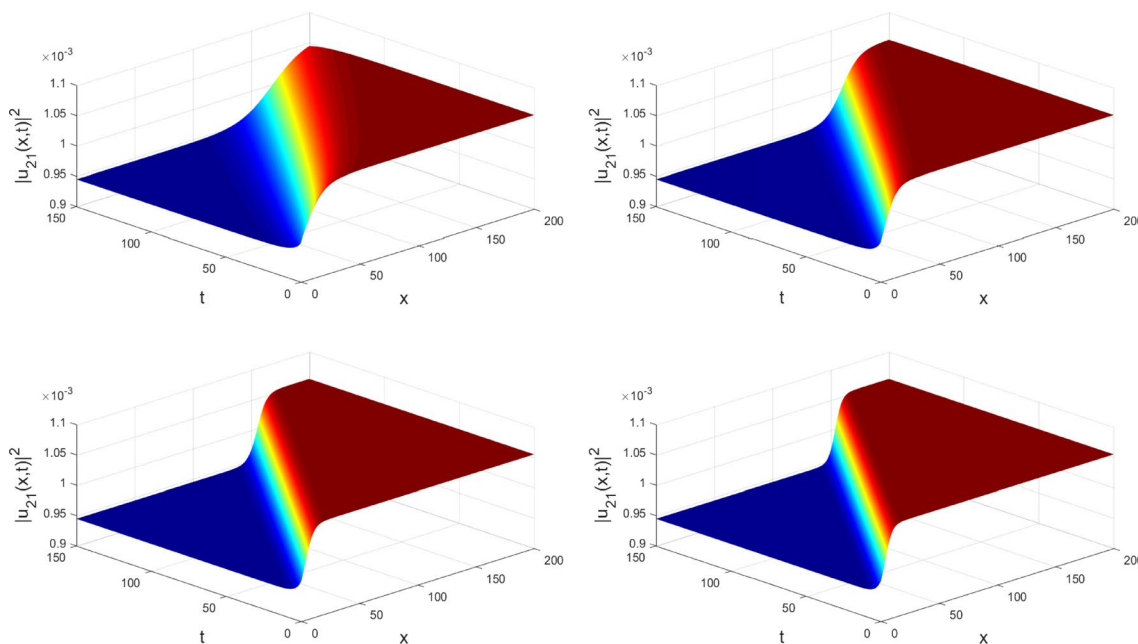


Fig. 2 Spatiotemporal plot evolution of kink-like solitons $|u_{21}(x,t)|^2$ at $\alpha = 0.75, \alpha = 0.85, \alpha = 0.95$ and $\alpha = 1, A = e, k_1 = -k_2 = 25.840, g_0 = 0.001, g_1 = -0.18, \mu = -0.015, \lambda = -0.0312, \sigma = -2.000185$ respectively

$$u_{2,4,2} = \mu \left[\frac{3A}{3\wp(p\xi, g_2, g_3) - C} \right]^{\frac{1}{2}}, \tag{154}$$

where $g_2 = \frac{4C^2 - 12AE}{3}, g_3 = \frac{4C(-2C^2 + 9AE)}{27}$.

$$u_{2,4,3} = \mu \left[\frac{6\sqrt{A}\wp(p\xi, g_2, g_3) + C\sqrt{A}}{3\wp'(p\xi, g_2, g_3)} \right]^{\frac{1}{2}}, \tag{155}$$

where $\wp'(p\xi, g_2, g_3) = \frac{d\wp(p\xi, g_2, g_3)}{d\xi}, g_2 = \frac{C^2}{12} + AE, g_3 = \frac{C(36AE - C^2)}{216}$.

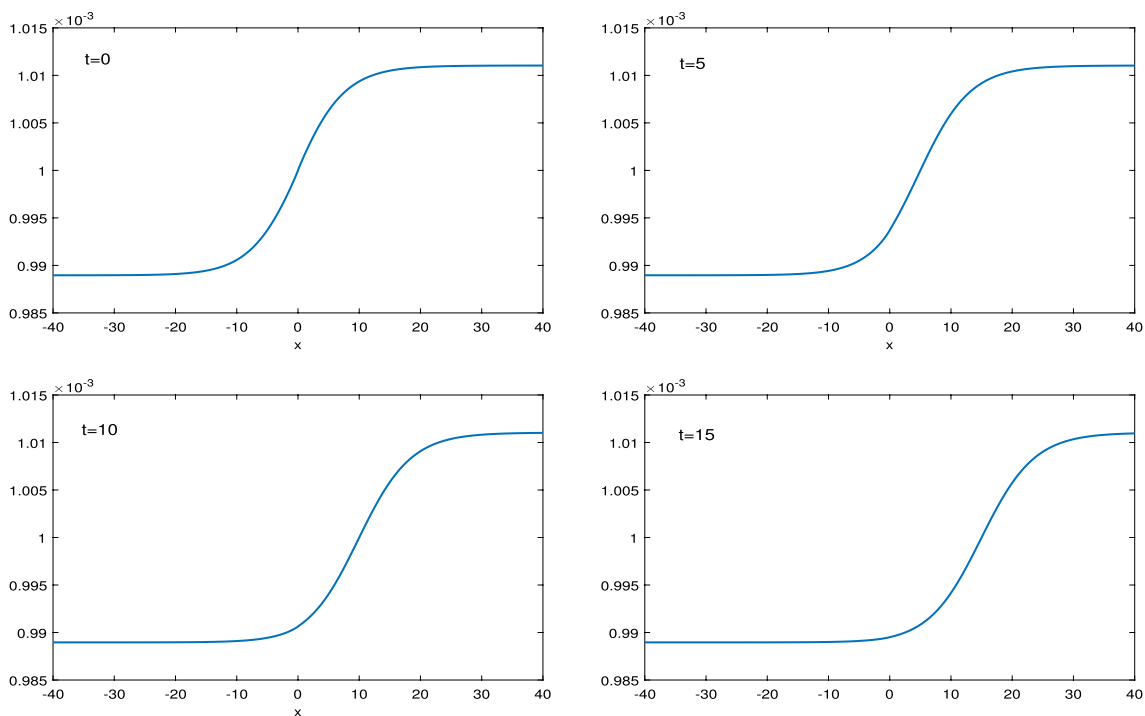


Fig. 3 Spatiotemporal plot evolution of 2D of kink-like solitons $|u_{23}(x,t)|^2$ at $\alpha = 0.95$, $A = e$, $k_1 = -k_2 = 20.840$, $g_0 = -0.001, g_1 = 0.18$, $\mu = -0.015$, $\lambda = -0.0312$, $\sigma = -10.000185$

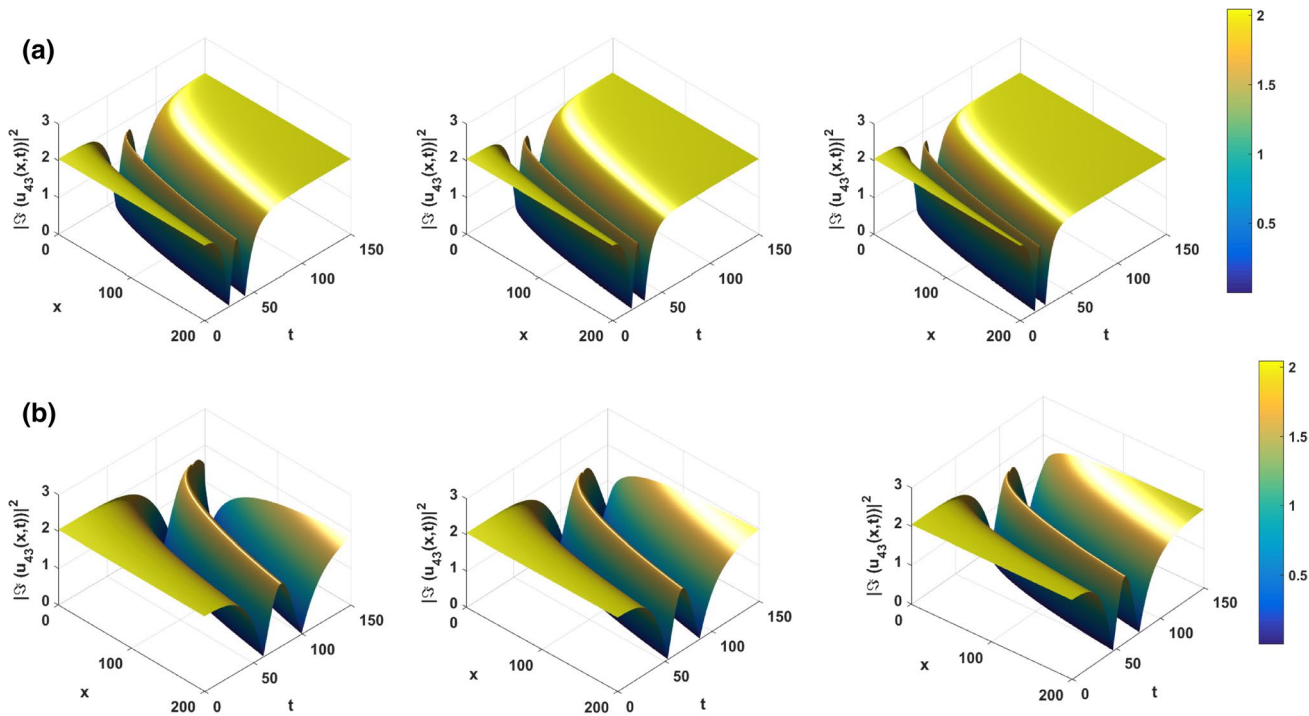


Fig. 4 Spatiotemporal plot evolution of the W-shape bright soliton of $|S u_{43}(x,t)|^2$ for **a** [$\alpha = 0.52, \alpha = 0.54, \alpha = 0.56$, **b** [$\alpha = 0.45, \alpha = 0.46, \alpha = 0.47$] at $A = e$, $k_1 = 10.75$, $k_2 = 2.15$, $u_0 = 0.2$, $g_0 = 3.33$, $g_0 = 0.75$, $p = q = 1$, $\mu = 0$, $\lambda = -0.5$, $\sigma = 0.02$, $p = 0.8$, $q = 0.5$

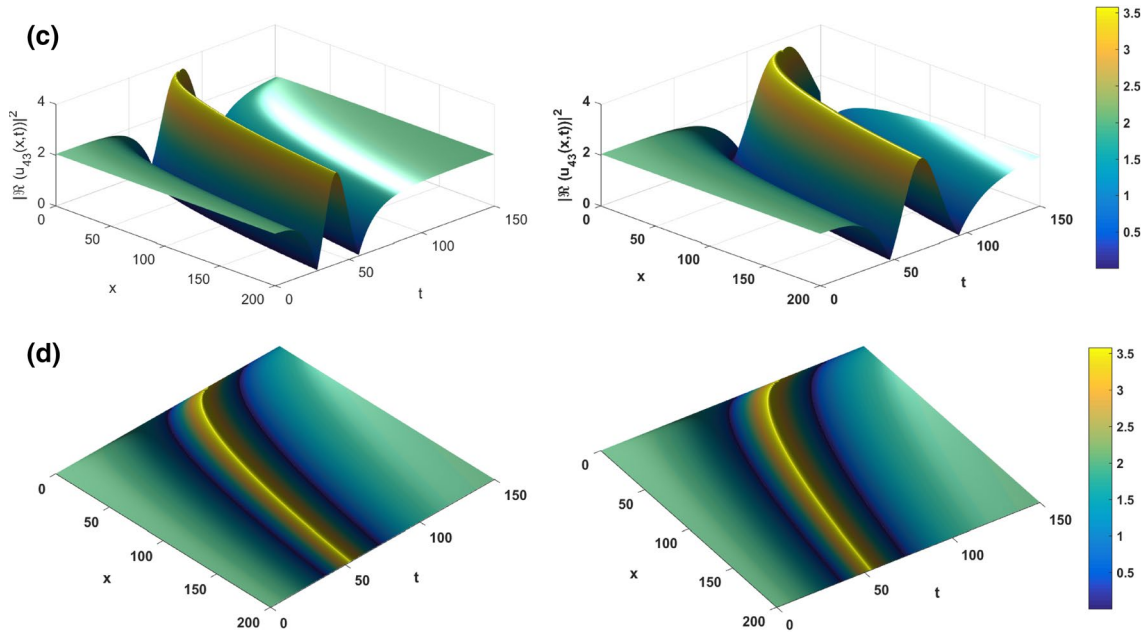


Fig. 5 Spatiotemporal plot evolution and Contour plot evolution of the W-shape bright soliton of $|\Im u_{43}(x,t)|^2$ for **c** [$\alpha = 0.5, \alpha = 0.47$], **d** [$\alpha = 0.48, \alpha = 0.49$] at $A = e, k_1 = 10.75, k_2 = 2.15, u_0 = 0.2, g_0 = 3.33, g_0 = 0.75, p = q = 1, \mu = 0, \lambda = -0.5, \sigma = 0.02, p = 0.8, q = 0.75$

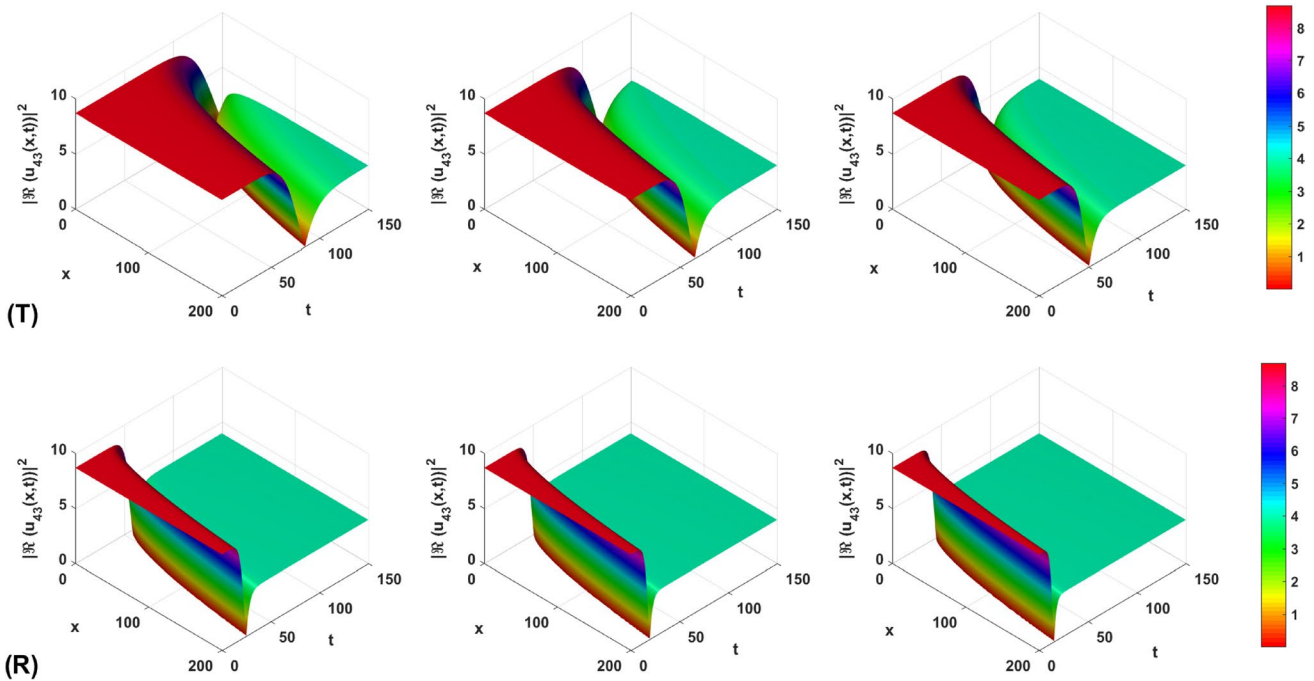


Fig. 6 Spatiotemporal plot evolution of the dark soliton of $|\Re u_{43}(x,t)|^2$ for **T** [$\alpha = 0.45, \alpha = 0.47, \alpha = 0.49$], **R** [$\alpha = 0.55, \alpha = 0.57, \alpha = 0.59$] at $A = e, k_1 = 10.75, k_2 = 2.15, u_0 = 0.2, g_0 = 3.33, g_0 = 0.75, p = 0.71, q = 0.95, \mu = 0, \lambda = -0.5, \sigma = 0.02$

$$u_{2.4.4} = \mu \left[\frac{3\sqrt{E^{-1}}\wp'(p\xi, g_2, g_3)}{6\wp(p\xi, g_2, g_3) + C} \right]^{\frac{1}{2}}, \tag{156}$$

where $A = \frac{5C^2}{26E}, g_2 = \frac{2C^2}{9}, g_3 = \frac{C^3}{54}$,

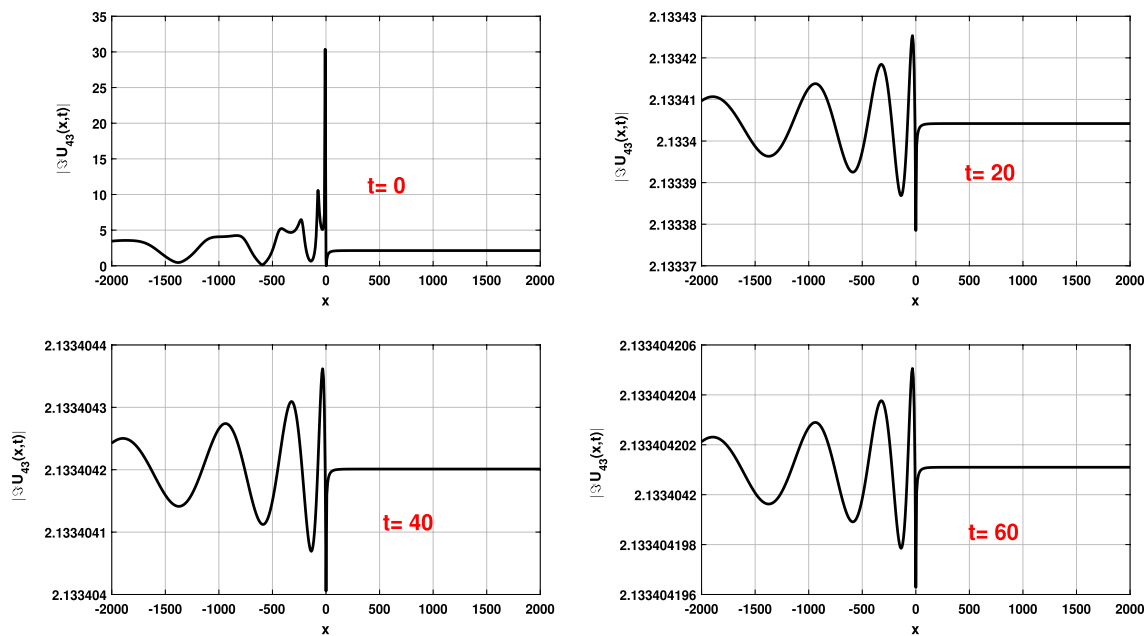


Fig. 7 Plot evolution of $|\Im u_{43}(x, t)|^2$ for $\alpha = 0.48, A = e, k_1 = 20.75, k_2 = 2.15, u_0 = 0.2, g_0 = 3.33, g_0 = 0.75, p = 0.71, q = 0.95, \mu = 0, \lambda = -0.5, \sigma = 0.02$

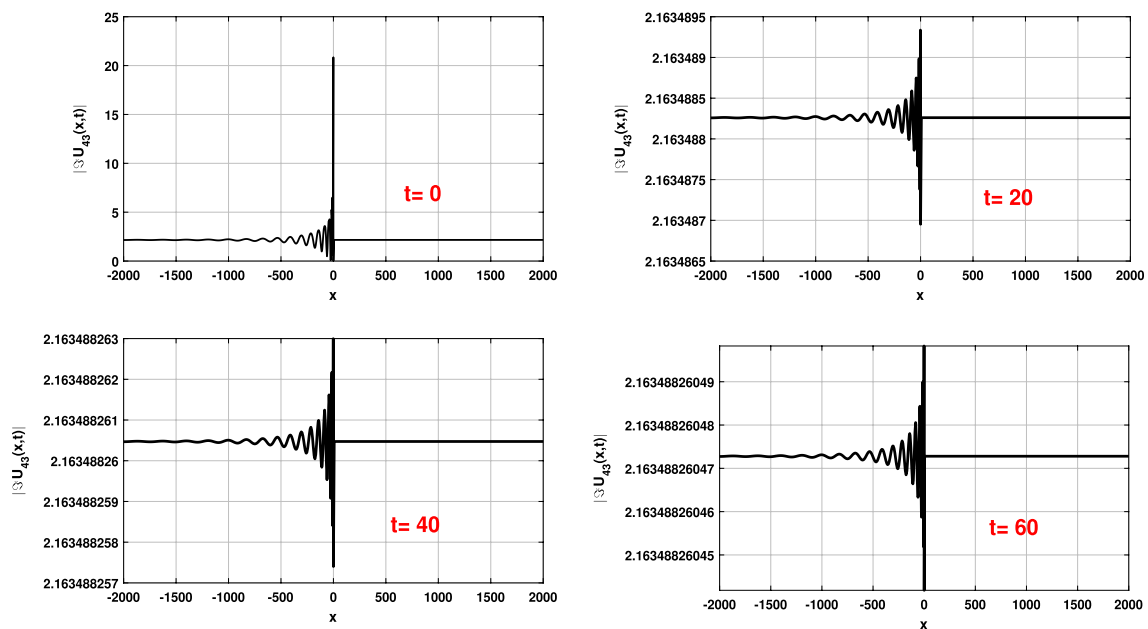


Fig. 8 Plot evolution of breather corresponding to $|\Im u_{43}(x, t)|^2$ for $\alpha = 0.48, A = e, k_1 = 25.75, k_2 = 18.54, u_0 = 0.72, g_0 = 3.33, g_0 = 0.75, p = 0.8, q = 0.4, \mu = 0, \lambda = -0.5, \sigma = 0.02$

$$u_{2,4,5} = \mu \left[\sqrt{\frac{5C^2}{36E} \frac{6\wp(p\xi, g_2, g_3) + C}{3\wp'(p\xi, g_2, g_3)}} \right]^{\frac{1}{2}}, \tag{157}$$

while g_2 and g_3 are the invariants of the Weierstrass elliptic function and $\xi = \frac{k_1}{\alpha}t^\alpha + \frac{k_2}{\alpha}x^\alpha$.

5 Physical interpretation

Figure 1 is the spatiotemporal plot evolution of the dark soliton of $|u_{21}(x, t)|^2$ and Figs. 2 and 3 are the plot evolution of anti-kink like solution $|u_{23}(x, t)|^2$. Furthermore, Figs. 4

Fig. 9 Plot evolution of of the bright soliton $|\mathfrak{S}u_{43}(x, t)|^2$ for $\alpha = 0.48, A = e, k_1 = 25.75, k_2 = -18.54, u_0 = -0.72, g_0 = 3.33, g_0 = 0.75, p = 0.8, q = 0.4, \mu = 0, \lambda = -0.5, \sigma = 0.02$

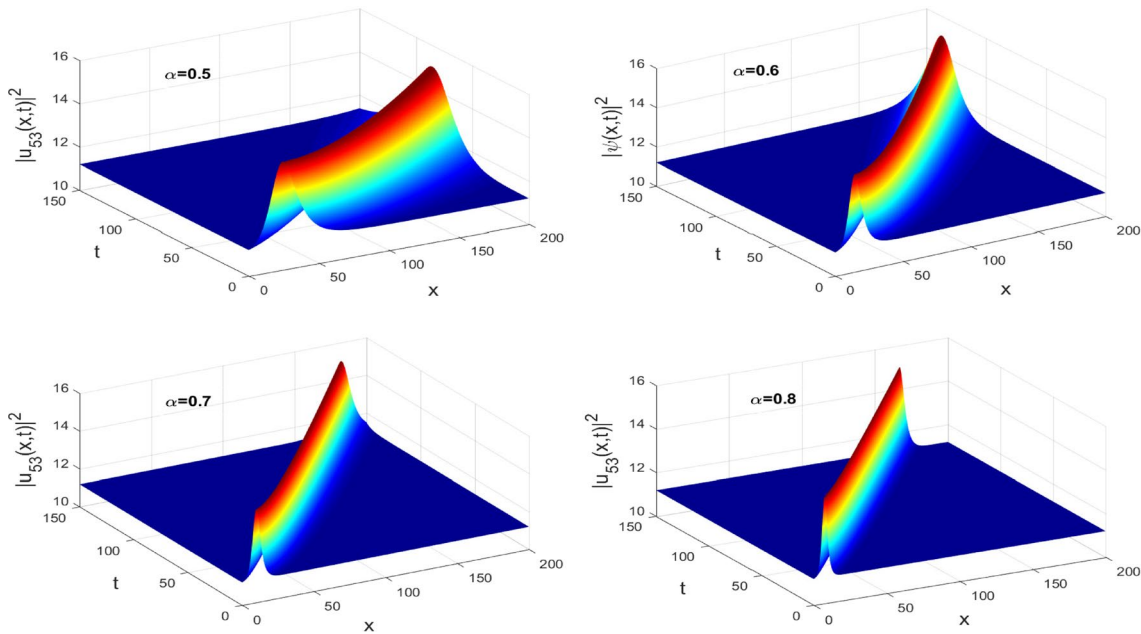
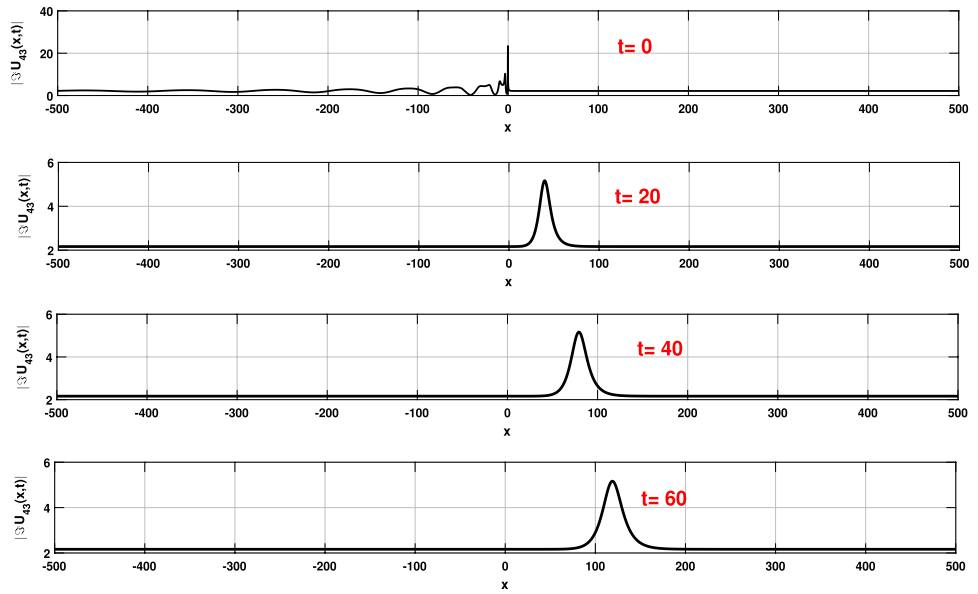


Fig. 10 Spatiotemporal Plot evolution of bright $|u_{53}(x, t)|^2$ at $A = e, k_1 = -k_2 = 20.40, g_0 = -5.001, g_1 = -10.18, \lambda = -0.002$

and 5 are the spatiotemporal plot evolution of the W-shape bright solutions of $|\mathfrak{S}u_{43}(x, t)|^2$. Moreover, by varying the fractional order parameter, Fig. 6 gives the profile of dark soliton with the effect of the latter. Besides, by considering the parameters of the line $k_1 = 25.75, k_2 = 18.54$ and $\alpha = 0.48$, we obtain the breather (see Fig. 7) which propagates at different times. This behavior appears to be new in the electrical transmission line. In Figs. 7 and 8, we obtain the same behavior. However, in Fig. 9 we manage to

reverse the behavior of the breather type over time by taking $k_2 = -18.54$. The soliton obtained is bright as a solution which propagates along the line, this exhibits the behavior of modulated waves in a nonlinear electrical transmission line. In addition, Fig. 10 depicts the 3D bright solitons under the effect of the fractional derivative order. It is pointed out the deformation of the shape during the propagation of the latter. Figure 11 gives the normal shape of the dark soliton at $\alpha = 0.1$.

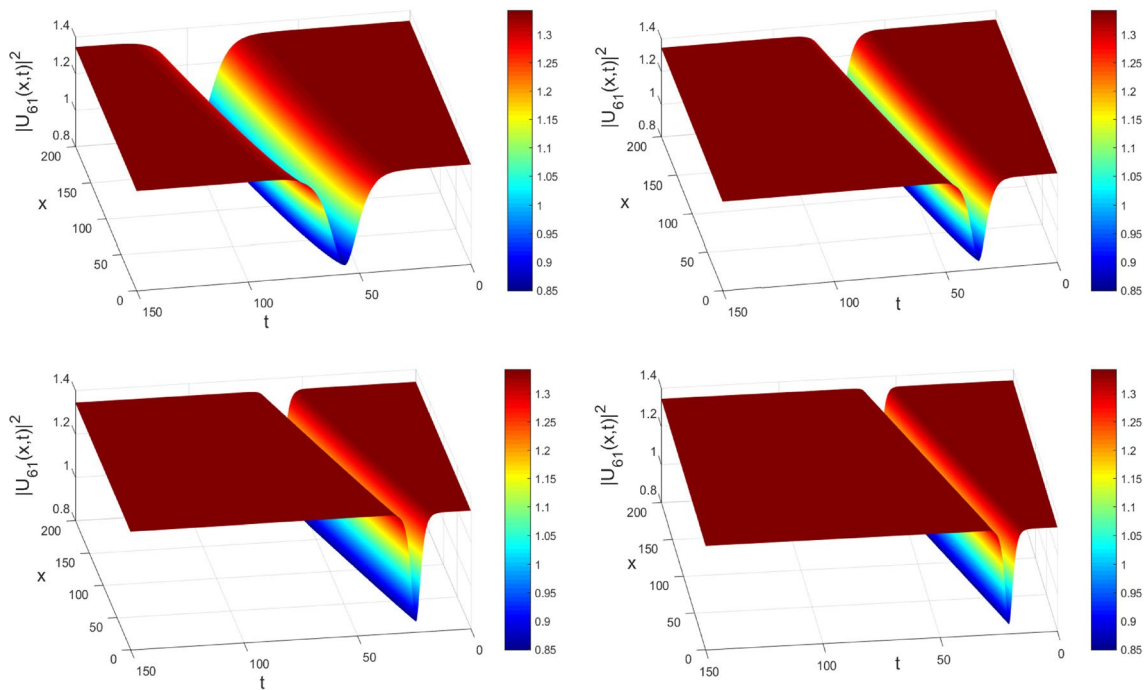


Fig. 11 Spatiotemporal plot of dark solitons $|u_{61}(x,t)|^2$ at $\alpha = 0.85$, $\alpha = 0.90$, $\alpha = 0.95$, $\alpha = 1$, respectively and $g_1 = -1.04$, $A = e$, $k_1 = -4.84$, $k_2 = -0.90 u_0 = 5.125$, $\sigma = -1.185$

The results obtained are more general than those reported by Hubert Malwe et al. [41]. It is observed that, fractional order α has the effects on the width and on the amplitude of the obtained bright and dark soliton solutions (see Figs. 1, 2, 3, 4, 5, 6, 7, 8, 9, 10). Furthermore, dark and bright solitons obtained will be helpful to explain natural phenomena and the other solutions could be probably used in diverse applications in science and engineering.

Without doubt, it could be predicted that the derivative order affects the shape of the traveling-wave in the electrical transmission line. Otherwise, the obtained results of the nonlinear fractional differential equation governing wave propagating in the low-pass electrical transmission lines are essential to explain the phenomenon of the data transmission in telecommunication, as the latter depicts the natural event such as propagation with a finite speed and vibration.

On the other hand, these obtained results can help to explain internal waves in the ocean, as it is well known that soliton are virtually hazardous for offshore engineering building such as gas and oil pipelines and shipping decks. The best important effect of solitons generation is the tidal energy conversion from barotropic to baroclinic component over large-scale oceanic bottom obstructions (shelf breaks, sea mounts, canyons and ridges). Otherwise, dark and bright solitary waves are omnipresent everywhere strong tides happen in the quarter of irregular topography. Solitons are frequently important lineaments discovered in optical and radar satellite imagery of coastal water. In this case, solitary waves

can travel over several thousand kilometers and carry both load and impulse. However, during their propagation, a considerable velocity shear causes turbulence and mixing. The obtained mixing, frequently offer background nutritious into the water column, thus enrich the local region and changing the biology inside.

Finally, it emerges that using the extended direct algebraic method, we obtain a diversity of solutions such as dark [Eq. (114)], trigonometric function solutions Eqs. (109)–(113), singular solitons and combined solutions [Eqs. (116)–(118)]. The virtue of this method lies in obtaining the W-shape bright soliton which is well known in nonlinear optical fibers. Otherwise, it is gained jacobian elliptic function solutions and Weierstrass elliptic function solutions by applying the Sub-equation method [see Eqs. (153)–(157)]. On the other hand, by setting $C = \mu^2 - 4\lambda\sigma$ and $E = \sigma$ and assuming $g_0 = 0$ and $g_1 = 0$, Eqs. (114) and (148) are the same.

6 Conclusion and remarks

This paper secures W-shape bright soliton and diverse traveling waves solutions to the nonlinear differential equation governing wave propagation in low-pass electrical transmission line with conformable derivatives by adopting the new extended direct algebraic method and sub-ODE method. From the new extended direct algebraic method it is pointed

out W-shape bright, dark solitary waves, kink-like soliton solutions, periodic solutions and rational solutions compare to Hubert Malwe et al. [41] and Rezazadeh et al. [42]. It is worth to mention also the virtue of the relevant results in communication system and data encoding during thousand kilometers of communication via the optical fibers. More recently, soliton perversion has been involved in experimental devices to facilitate a conception of an inhomogeneous system of coupled nonlinear waveguides [58]. Furthermore, the used of the sub-ODE method added new types of solutions called the Weierstrass elliptic function. This paper offers a plethora of traveling waves which include the results obtained in Refs. [1, 3–5]. By choosing the appropriate values of the conformable derivative order, the behaviors of the obtained results have been illustrated graphically in 3D and 2D and these soliton solutions are identically to the results obtained in nonlinear differential equation which describe the propagation of long waves in shallow water [56, 57].

References

- Aminikhah, H., Sheikhan, A.R., Rezazadeh, H.: Sub-equation method for the fractional regularized long-wave equations with conformable fractional derivatives. *Sci. Iran.* **3**, 1048–1054 (2016)
- Korkmaz, A., Hepson, O.E., Hosseini, K., Rezazadeh, H., Eslami, M.: Sine-Gordon expansion method for exact solutions to conformable time fractional equations in RLW-class. *J. King Saud Univ.-Sci.* **32**, 567–574 (2020)
- Houwe, A., Sabi'u, J., Hammouch, Z., Doka, S.Y.: Solitary pulses of the conformable derivative nonlinear differential equation governing wave propagation in low-pass electrical transmission line. *Phys. Scr.* **95**, 1–15 (2020)
- Hammouch, Z., Mekkaoui, T.: Travelling-wave solutions for some fractional partial differential equation by means of generalized trigonometry functions. *Int. J. Appl. Math. Res.* **1**, 206–212 (2012)
- Sabi'u, J., Jibril, A., Gadu, A.M.: New exact solution for the (3+1) conformable space-time fractional modified Korteweg-de-Vries equations via Sine–Cosine Method. *J. Taibah Univ. Sci.* **13**, 91–95 (2019)
- Owolabi, K.M., Hammouch, Z.: Mathematical modeling and analysis of two-variable system with noninteger-order derivative. *Chaos* **29**, 013145–15 (2019)
- Khan, H., Jarad, F., Abdeljawad, T., Khan, A.: A singular ABC-fractional differential equation with p-Laplacian operator. *Chaos, Solitons Fractals* **129**, 56–61 (2019)
- Singh, J., Kumar, D., Hammouch, Z., Atangana, A.: A fractional epidemiological model for computer viruses pertaining to a new fractional derivative. *Appl. Math. Comput.* **316**, 504–515 (2018)
- Yang, X.J., Machado, J.A.T., Nieto, J.J.: A new family of the local fractional PDEs. *Fundam. Inf.* **151**, 63–75 (2017)
- Rezazadeh, H., Inc, M., Baleanu, D.: New solitary wave solutions for variants of (3 + 1)-dimensional Wazwaz–Benjamin–Bona–Mahony equations. *Front. Phys.* **8**, 1–11 (2020)
- Vahidi, J., Masood Zekavatmand, S., Rezazadeh, H., Inc, M., Akinlar, M.A., Chu, Y.M.: New solitary wave solutions to the coupled Maccari's system. *Results Phys.* **21**, 1–11 (2021)
- Bansal, M.K., Kumar, D.: On the integral operators pertaining to a family of incomplete I-functions. *AIMS Math.* **5**, 1247–1259 (2020)
- Hashemi, M.S., Inc, M., Yusuf, A.: On three-dimensional variable order time fractional chaotic system with nonsingular kernel. *Chaos Solitons Fractals.* **133**, 1–8 (2020)
- Inc, M., Kilic, B.: Classification of travelling wave solutions for the time-fractional fifth-order KdV-like equation. *Waves Random Complex Media* **24**, 393–403 (2014)
- Kilic, B., Inc, M.: The first integral method for the time fractional Kaup–Boussinesq system with time dependent coefficient. *Appl. Math. Comput.* **254**, 70–74 (2015)
- Prakash, A., Goyal, M., Baskonus, H.M., Gupta, S.: A reliable hybrid numerical method for a time dependent vibration model of arbitrary order. *AIMS Math.* **5**, 979–1000 (2020)
- Atangana, A.: Fractional discretization. The Africanish tortoise walk. *Chaos Solitons Fractals* **130**, 109399 (2020)
- Kumar, D., Singh, J., Baleanu, D.: Modified Kawahara equation within a fractional derivative with non-singular Kernel. *Therm. sci.* **22**, 789–796 (2018)
- Atangana, A., Alkahtani, B.S.T.: Analysis of the Kelleri–Segel model with a fractional derivative without singular kernel. *Entropy* **17**, 4439–4453 (2015)
- Orkun, T., Senol, M., Kurt, A., Özkanc, O.: New solutions of fractional Drinfeld–Sokolov–Wilson system in shallow water waves. *Ocean Eng.* **161**, 62–68 (2018)
- Rezazadeh, H., Khodadad, F.S., Manafian, J.: New structure for exact solutions nonlinear time fractional Sharma–Tasso–Olver equation via conformable fraction derivative. *Appl. Appl. Math. Int. J.* **12**, 405–414 (2017)
- Rezazadeh, H., Korkmaz, A., Eslami, M., Vahidi, J., Asghari, R.: Traveling wave solution of conformable fractional generalized reaction Dufing model by generalized projective Riccati equation method. *Opt. Quantum Electron.* **50**, 1–13 (2018)
- Samko, S.G., Kilbas, A.A., Marichev, O.I.: *Fractional Integrals and Derivatives Theory and Applications*. Gordon and Breach, New York (1993)
- Igor, P.: *Fractional Differential Equations*, 1st edn. Academic Press (1998)
- Abdon, A., Dumitru, B., Alsaedi, A.: New properties of conformable derivative. *Open Math.* **13**, 8891–898 (2015)
- Sousa, J.V.D.C., Oliveira, E.: A new truncated M-fractional derivative type unifying some fractional derivative types with classical properties. *Int. J. Anal. Appl.* **16**, 83–96 (2018)
- Costa, A., Alfred Osborne, R., Donald, T., Resio, S., Alessio Chrivi, E., Saggese, E., Bellomo, K., Chuck Long, E.: Soliton turbulence in shallow water ocean surface waves. *Phys. Rev. Lett.* **113**, 108501–5 (2014)
- Ekici, M., Mirzazadeh, M., Sonmezoglu, A., Biswas, A.: Optical solitons with anti-cubic nonlinearity by extended trial equation method. *Optik* **136**, 368–373 (2017)
- Rezazadeh, H., Tariq, H., Eslami, M., Mirzazadeh, M., Zhou, Q.: New exact solutions of nonlinear conformable time-fractional Phi-4 equation. *Chin. J. Phys.* **56**, 2805–2816 (2018)
- Ali, A., Seadawy, A.R., Lu, D.: Soliton solutions of the nonlinear Schrödinger equation with the dual power law nonlinearity and resonant nonlinear Schrödinger equation and their modulation instability analysis. *Optik* **145**, 79–88 (2017)
- Zayed, E.M.E., Alurrfi, K.A.E.: New extended auxiliary equation method and its applications to nonlinear Schrödinger-type equations. *Optik* **127**, 9131–9151 (2016)
- Mirzazadeh, M., Alqahtani, R.T., Biswas, A.: Optical soliton perturbation with quadratic-cubic nonlinearity by Riccati–Bernoulli sub-ODE method and Kudryashov's scheme. *Optik* **145**, 74–78 (2017)

33. Gabshi, M.A., Krishnan, E.V., Alquran, A., Al-Khaled, K.: Jacobi elliptic function solutions of a nonlinear Schrödinger equation in metamaterials. *Nonlinear Stud.* **3**, 469–480 (2017)
34. Jawad, A.J.M., Mirzazadeh, M., Zhou, Q., Biswas, A.: Optical solitons with anti-cubic nonlinearity using three integration schemes. *Superlattices Microstruct.* **105**, 1–10 (2017)
35. Seadawy, A.R.: Stability analysis of traveling wave solutions for generalized coupled nonlinear KdV equations. *Appl. Math. Inf. Sci.* **1**, 209–14 (2016)
36. Qin, Z., Liu, L., Liu, Y., Yu, H., Yao, P., Wei, C., Zhang, H.: Exact optical solitons in metamaterials with cubic quintic nonlinearity and third-order dispersion. *Nonlinear Dyn.* **3**, 1365–1371 (2015)
37. Eslami, M., Rezazadeh, H.: The first integral method for Wu-Zhang system with conformable time-fractional derivative. *Calcolo* **3**, 475–85 (2016)
38. Tchier, F., Inc, M., Korpınar, Z., Baleanu, D.: Solution of the time fractional reaction-diffusion equations with residual power series method. *Adv. Mech. Eng.* **10**, 11–10 (2016)
39. Hammouch, Z., Mekkaoui, T., Agarwal, P.: Optical solitons for the Calogero–Bogoyavlenskii–Schiff equation in $(2 + 1)$ dimensions with time-fractional conformable derivative. *Eur. Phys. J. Plus* **248**, 1–6 (2018)
40. Houwe, A., Boudoue Hubert, M., Savaissoub, N., Jerome, D., Justin, M., Betchewe, G., Doka, Timoleon, S.Y., Crepin, K., Khang, S., Biswas, A., Ekici, M., Adesanya, S., Seithuti Moshokoah, S.P.S., Belic, M.: Optical solitons for higher-order nonlinear Schrödinger equation with three exotic integration architectures. *Optik* **179**, 861–866 (2019)
41. Hubert Malwe, B., Betchewe, G., Doka, S.Y., Crepin Kofane, T.: Travelling wave solutions and soliton solutions for the nonlinear transmission line using the generalized Riccati equation mapping method. *Nonlinear Dyn.* **84**, 171–177 (2016)
42. Rezazadeh, H., Mehdi Mirhosseini-Alizamini, S., Eslami, M., Abbagari, S.: New optical solitons of nonlinear conformable fractional Schrödinger–Hirota equation. *Optik* **172**, 545–553 (2018)
43. Akinyemi, L., Rezazadeh, H., Yao, S.W., Ali Akbar, M., Mostafa Khater, M.A., Jhangeer, A., Inc, M., Ahmad, H.: Nonlinear dispersion in parabolic law medium and its optical solitons. *Results Phys.* **26**, 1–9 (2021)
44. Ali Akbar, M., Akinyemi, L., Yao, S.W., Jhangeer, A., Rezazadeh, H., Mostafa Khater, M.A., Ahmad, H., Inc, M.: Soliton solutions to the Boussinesq equation through sine-Gordon method and Kudryashov method. *Results Phys.* **25**, 1–10 (2021)
45. Ahmad, H., Tufail Khan, A., Ahmad, I., Predrag Stanimirovi, S., Chu, Y.M.: A new analyzing technique for nonlinear time fractional Cauchy reaction–diffusion model equations. *Results Phys.* **19**, 1–8 (2020)
46. Ahmad, H., Akgül, A., Tufail Khan, A., Predrag Stanimirovic, S., Chu, Y.M.: New perspective on the conventional solutions of the nonlinear time-fractional partial differential equations. *Hindawi* **2020**, 1–10 (2020)
47. Ahmad, H., Tufail Khan, A.: Variational iteration algorithm-I with an auxiliary parameter for wave-like vibration equations. *J. Low Freq. Noise, Vibr. Active Control* **38**, 1113–1124 (2019)
48. Ahmad, H., Tufail Khan, A., Predrag Stanimirovic, S., Chu, Y.M., Ahmad, I.: Modified variational iteration algorithm-II: convergence and applications to diffusion models. *Hindawi* **2020**, 1–14 (2020)
49. Ahmad, I., Ahmad, H., Inc, M., Yao, S.W., Almohsen, B.: Application of local meshless method for the solution of two term time fractional-order multi-dimensional PDE arising in heat and mass transfer. *Therm. Sci.* **24**, 95–105 (2020)
50. Inc, M., Nawaz Khan, M., Ahmad, I., Yao, S.W., Ahmad, H., Thounthong, P.: Analysing time-fractional exotic options via efficient local meshless method. *Results Phys.* **19**, 1–6 (2020)
51. Zayed, E.M.E., Alngar, M.E.M., Al-Nowehy, A.G.: On solving the nonlinear Schrödinger equation with an anti-cubic nonlinearity in presence of Hamiltonian perturbation terms. *Optik* **178**, 488–508 (2019)
52. Li, Z.: Periodic wave solutions of a generalized KdV–mKdV equation with higher-order nonlinear terms. *Z. Naturforsch.* **56a**, 649–657 (2010)
53. Chen, H.T., Zhang, H.Q.: New double periodic and multiple soliton solutions of the generalized $(2+1)$ -dimensional Boussinesq equation. *Chaos Soliton Fractals* **20**, 4765–769 (2004)
54. Wazwaz, A.M.: New solitary wave solutions to the modified forms of Degasperis–Procesi and Camassa–Holm equations. *Appl. Math. Comput.* **186**, 130–141 (2007)
55. Wazwaz, A.M.: The tanh–coth method for new compactons and solitons solutions for the $K(n, n)$ and the $K(n + 1, n + 1)$ equations. *Appl. Math. Comput.* **188**, 1930–1940 (2007)
56. Ibrahim, R.W., Meshram, C., Hadid, S.B., Momani, S.: Analytic solutions of the generalized water wave dynamical equations based on time-space symmetric differential operator. *J. Ocean Eng. Sci.* **5**, 186–195 (2020)
57. Lu, D., Seadawy, A.R., Ali, A.: Dispersive analytical wave solutions of three nonlinear dynamical water waves models via modified mathematical method. *Results Phys.* **13**, 102–177 (2019)
58. Burioni, R., Cassi, D., Sodano, P., Trombettoni, A., Vezzani, A.: Topological filters and high-pass/low-pass devices for solitons in inhomogeneous networks. *Phys. Rev. E* **73**, 066624 (2006)

Publisher's Note Springer Nature remains neutral with regard to jurisdictional claims in published maps and institutional affiliations.